Report No. FHWA-RD-76-120

URBAN STORM RUNOFF INLET HYDROGRAPH STUDY

Vol. 5. Soil-Cover-Moisture Complex: Analysis of Parametric Infiltration Models for Highway Sideslopes

March 1976
Final Report

Prepared for
FEDERAL HIGHWAY ADMINISTRATION
Offices of Research & Development
Washington, D.C. 20590

NOTICE

This document is disseminated under the sponsorship of the Department of Transportation in the interest of information exchange. The United States Government assumes no liability for its contents or use thereof.

The contents of this report reflect the views of the Utah Water Research Laboratory, which is responsible for the facts and accuracy of the data presented herein. The contents do not necessarily reflect the official views or policy of the Department of Transportation. This report does not constitute a standard, specification, or regulation.

The United States Government does not endorse products or manufacturers. Trade or manufacturers' names appear herein only because they are considered essential to the object of this document.

TECHNICAL REPORT STANDARD TITLE PAGE

1. Report No. FHWA-RD-76-120	2. Government Assession No.	3. Recipient's Catalog No.
4. Title and Subtitle URBAN STORM RUNOFF INLET HYDROGRAPH STUDY Vol. 5. Soil-Cover-Moisture Complex: Analysis of Parametric Infiltration Models for Highway Sideslopes		5. Report Date March 1976 6. Performing Organization Code
7. Author(s) C. L. Chen		8. Performing Organization Report No. PRWG 106-5
9. Performing Organization Name and Address Utah Water Research Laboratory Utah State University Logan, Utah 84322		10. Work Unit No. 11. Contract or Grant No. DOT-FH-11-7806
12. Sponsoring Agency Name and Address Offices of Research and Development Federal Highway Administration U.S. Department of Transportation Washington, D.C. 20590		13. Type of Report and Period Covered Final Report 14. Sponsoring Agency Code

15. Supplementary Notes

FHWA contract manager: D. C. Woo

16. Abstract

The main objective of this study is to develop an accurate design method for computing inlet hydrographs of surface runoff, with average recurrence intervals of 10, 25, and 50 years, from typical urban highway by flood routing technique.

The boundary-value problem of one-dimensional infiltration resulting from rainfall is formulated and solved numerically on a digital computer. The numerical solutions of this idealized mathematical model is used as a basic testing tool in the subsequent analysis of various parametric infiltration models including the Green-Ampt, Kostiakov, Philip, Horton, and Holtan equations. The time of ponding is shown to be the most important parameter in a parametric infiltration model and can be expressed in terms of other parameters in the model as well as the rainfall intensity. The values of all the model parameters are determined to be fairly constant for a soil having the same initial and upper boundary (soil surface) conditions. Use of the Green-Ampt, Kostiakov, and Philip type models for the prediction of the infiltration rate before and after ponding is proved to be satifactory. For engineering practice, the standard infiltration-capacity curves for soil-cover-moisture complexes representing urban highway sideslopes are empirically developed based on the unique selection of the Soil Conservation Service runoff curve number. Validity of typical standard curves so developed were experimentally examined in the Utah Water Research Laboratory stormflow experiment facility.

This volume is the fifth in a series. The others in the series are:

Vol. No.	FHWA No.	Short Title	NTIS (PB) No. (if available)
1	76-116	Computer Analysis of Highway Runoff	(not yet available)
2	76-117	Laboratory Studies of Sheet Flows	(not yet available)
3	76-118	Hydrologic Data for Highway Watersheds	(not yet available)
4	76-119	Synthetic Storms for Urban Highways	(not yet available)

17. Key Words	18. Distribution Statement
Algebraic equations, Highway, Hydrologic soil groups, Hydrology, Infiltration, Infiltration capacity, Infiltration rate, Laboratory studies, Mathematical models, Parametric models, Plant cover, Rain infiltration, Runoff curve number, Sideslopes, Soils, Soil classifications, Soil moisture, Standard curve, Turf, Urban.	No restriction. This document is available to the public through the National Technical Information Service, Springfield, Virginia 22161

19. Security Classif. (of this report)	20. Security Classif. (of this page)	21. No. of Pages	22. Price
Unclassified	Unclassified	185	

PREFACE

The work described in this report was performed under contract DOT-FH-11-7806, entitled ''Urban Storm Runoff Inlet Hydrograph Study'' between the Federal Highway Administration and Utah State University. This research contract aimed at the development of an accurate design method for computing inlet hydrographs of surface runoff under intense rainstorms on urban highways. One of the major tasks of this research project was the determination of the infiltration-capacity curves or the infiltration relationships as related to soil-cover-moisture complexes representing highway sideslopes. The results obtained from this study were finally integrated into the general surface-runoff model that was formulated in the analytical phase of the research project.

The research was conducted under the general supervision of Dr. Cheng-lung Chen, Professor of Civil and Environmental Engineering at Utah State University. During this study, Dr. Musa N. Nima, Post Doctoral Fellow at Utah Water Research Laboratory, helped review literature on factors affecting infiltration and existing soil classifications. Dr. George C. Shih, Research Engineer at Utah Water Research Laboratory, also helped write a computer program for solving numerically the boundary-value problem of rain infiltration.

The contract was monitored by Dr. D. C. Woo, Contract Manager, Environmental Design and Control Division, Federal Highway Administration. The author is indebted to Dr. Woo for his ideas contributed during the initial phase, and guidance throughout this study. Numerous detailed discussions about the research were held with Dr. Woo during all phases of the study. He also gave many critical reviews and comments of the results during the course of work.

Special acknowledgments are due Dr. Lyman S. Willardson, Professor of Agricultural and Irrigation Engineering, Dr. Roland W. Jeppson, Professor of Civil and Environmental Engineering, Dr. Richard H. Hawkins, Associate Professor of Forest Science, all at Utah State University for their reviews of and comments on the entire manuscript and their valuable suggestions.

TABLE OF CONTENTS

TABLE OF CONTENTS (Continued)

TABLE OF CONTENTS (Continued)

LIST OF FIGURES

LIST OF FIGURES (Continued)

LIST OF FIGURES (Continued)

LIST OF TABLES

LIST OF ABBREVIATIONS AND SYMBOLS

A	=	parameter
a	=	constant; parameter
AMC	=	antecedent soil moisture condition
B	=	total or partial area of the test bed under rainfall projected on the horizontal plane
b	=	constant
C	=	constant
CN	=	runoff curve number
D	=	soil moisture diffusivity
D_{max}	=	maximum effective diffusivity
$D(\theta)$	=	soil moisture diffusivity as a function of soil moisture content
F	=	cumulative infiltration
f	=	infiltration rate or infiltration capacity
$f(t)$	=	infiltration rate or infiltration capacity as a function of time
f_{∞}	=	final infiltration rate
$\hat{f}_{\infty}$	=	least squares estimate of final infiltration rate
h	=	ponding depth of water on the soil surface or average depth of surface detention
$h(t)$	=	ponding depth of water on the soil surface as a function of time
I_a	=	initial abstraction
k	=	parameter
K_o	=	initial hydraulic conductivity
K_s	=	saturated hydraulic conductivity
$K(\theta)$	=	hydraulic conductivity as a function of soil moisture content

$K^{j}_{i+1/2}$ = hydraulic conductivity at a point halfway between grid points i and i + 1 at time level j

L = distance below the soil surface, defined by Equation 37

L_f = coordinate of the saturation front

L_p = L value at the time of ponding

L_w = soil depth at the wetting front

$L_f(t)$ = coordinate of the saturation front as a function of time

m = number of data points

n = exponent; parameter; number of discharge-measuring flumes

P = water storage potential of soil above the first impeding stratum

Q = actual direct runoff

Q_f = discharge measured by discharge-measuring flume

q_t = outflowing discharge per unit width from the test bed

R = accumulated storm rainfall

r = rainfall intensity

$\bar{r}$ = time-average rainfall intensity

R_e = potential runoff of effective storm rainfall

r(t) = rainfall intensity as a function of time

$\bar{r}(t)$ = time-average rainfall intensity as a function of time

S = sorptivity of soil; potential infiltration

$\hat{S}$ = least squares estimate of potential infiltration

S_a = available storage in the surface layer (i.e., ''A'' horizon in agricultural soils)

S_f = water storage in discharge-measuring flume

SCS = Soil Conservation Service

t = time

t_o = parameter

t_p = time of ponding

USDA = U.S. Department of Agriculture

UWRL = Utah Water Research Laboratory

z = vertical coordinate positive upward

α = parameter

β = correction factor for hydraulic conductivity and capillary potential distributions

Δt = time interval

Δz = vertical distance grid interval

λ = constant

ψ_o = initial soil capillary potential or tension

$\psi(\theta)$ = soil capillary potential or tension as a function of soil moisture content

ψ_i^j = soil capillary potential or tension at grid point i and time level j

τ = integration variable for time

θ = soil moisture content

θ_o = initial soil moisture content

θ_s = soil moisture content at saturation

θ_i^j = soil moisture content at grid point i and time level j

θ_1^n = soil moisture content on the soil surface at time level n when ponding occurs

INTRODUCTION

An urban highway sideslope may be either bare, paved, or grassed. A sideslope exposed with bare soil is normally seen only during its construction or shortly after its construction prior to grass growth. Regardless of whether or not the soil surface of a sideslope is covered with grass, infiltration plays a significant role in the rainfall-runoff process which is reflected in the total runoff from an urban highway watershed. The successful modeling of surface runoff from such a small watershed thus hinges greatly on how accurately one can evaluate the infiltration amount or rate during and after a rainstorm. For example, a poor estimate on the infiltration capacity for a given soil-cover-moisture complex of a sideslope may result in unrealistically low or high flow rates computed for a drainage inlet by means of one of existing surface runoff models. In view of the fact that the sideslopes may have various soil strata including topsoils and subsoils, several species of grass, and different degrees of antecedent moisture content, among many other factors which may influence infiltration, development of a general infiltration model which accounts for all pertinent variables is a formidable task. No attempt was made to develop such a general model. Instead, existing parametric (algebraic) infiltration equations were used to formulate ''standard'' infiltration-capacity curves for soil-cover-moisture complexes representing highway sideslopes. It is noted that the standard curves may also provide a basis for classifying or grouping soil-cover-moisture complexes as related to their final infiltration capacity (Musgrave, 1955; Musgrave and Holtan, 1964). Therefore, time-varying infiltration characteristics of a given soil-cover-moisture complex on a highway sideslope can be expressed in terms of a unique infiltration capacity curve which, after being described mathematically, can be integrated into a general surface runoff model for inlet hydrograph computations.

Following a brief literature review on rain infiltration, a mathematical model of the one-dimensional infiltration is formulated and solved numerically. The primary objective of formulating and solving such an idealized mathematical model is to use its numerical solution as a basic testing tool in the subsequent analyses of various parametric infiltration models. It was felt that this mathematical tool was necessary in the validation of the parametric infiltration models for lack of reliable experimental data available in the present study. Laboratory observations were made of the effects of various properties of soil, rain, and grass and different bed slopes on the infiltration capacity using a computer-controlled rainstorm simulator. Conclusive results were not obtained because of instrumentation failure in some data acquisition systems.

A method was developed to relate the standard infiltration-capacity curves for given soil-cover-moisture complexes to the corresponding Soil Conservation Service (SCS) runoff curve numbers (CN) for hydrologic soil-cover-moisture complexes. The parameters in the infiltration model were

related to the runoff CN so that given a CN value, the corresponding infiltration model parameters could be evaluated from such relationships and hence the standard infiltration-capacity curve constructed. The practical use of this method is evident because some easily applicable relationships between the infiltration parameter values and runoff CN are readily obtained or estimated from the SCS hydrologic groups of given soil-cover-moisture complexes.

LITERATURE REVIEW

Rain infiltration is a process of major importance in the hydrologic cycle. The importance of rain infiltration has been recognized for several decades, as is evidenced by the detailed studies of Wollny in Germany as early as 1874 (Baver, 1938). In the United States, extensive research on infiltration was undertaken during the 1930's when soil and water conservation became a matter of national concern. Hydrologists, interested in the prediction of surface runoff from watersheds, sought quantitative estimates of water intake rates of soils over a wide range of cover and soil conditions.

Ramser (1927) began his pioneering studies on small mixed-cover watersheds ranging in size from 1.12 to 1.25 acres. His prime objective was to determine the values of C, the coefficient in the so-called rational formula (Mulvaney, 1851; Kuichling, 1889; Lloyd-Davis, 1906) for computing the maximum rate of runoff from an agricultural watershed. Ramser's (1927) data were the first to show on the basis of direct field measurements that there were many interdependent factors influencing runoff from watersheds, such as the size and shape of the watershed, surface slope, nature and amount of vegetation, character of the soil regarding permeability, drainage channels, evaporation, storage and underground conditions, and the duration and intensity of rainfall. Hydrologists are still trying to determine the full significance of most of the factors influencing runoff. Among them, infiltration that is the entry into soil of water through its soil-atmosphere interface (Rose, 1966), plays one of the most important roles in the rainfall-runoff process. Historical developments in infiltration studies including concepts, factors affecting infiltration, characteristics, and modeling are reviewed herein. For convenience, all the previous findings and results are presented without elaborating justification of their accuracies.

Early Concepts on Infiltration and its Mechanism

Horton (1933, 1940) defined infiltration capacity as the maximum rate at which the soil, when in a given condition, can absorb falling rain. The term ''capacity'' in this connection has no relation to total volume absorbed but is a limiting infiltration rate. Oppostion to using this confusing terminology has been seen in later publications with different names being used such as infiltration rate (Richards, 1952), potential infiltration rate (Smith, 1944), and infiltrability (Hillel, 1971; Swartzendruber and Hillel, 1973). Horton (1933, 1940) also stated that the rate of infiltration is the actual rate at which the rainfall can be absorbed into a given soil under a given condition. Fletcher (1949) considered infiltration as the total amount of water entering the soil from the time of its addition to the end of the first hour. Richards (1952)

also defined the infiltration rate of soil as the maximum rate at which a soil, in a given condition at a given time, can absorb water applied in excess to the soil surface, either as rainfall or shallow impounded water. Quantitatively, infiltration rate, defined as the volume of water passing into the soil per unit area per unit time, has the dimension of velocity.

Turner (1963), Musgrave and Holtan (1964), and Hermanson (1970) among many other previous investigators considered infiltration as a three-step sequence: (1) surface entry, (2) transmission through the soil, and (3) depletion of storage capacity in the soil. They have found that after saturation, the rate of infiltration is limited to the lowest transmission rate encountered in the saturated profile by the infiltrating water, and that if the surface entry rate is slower than transmission capacity of any horizon, infiltration is limited to the surface entry rate throughout an entire storm.

Colman and Bodman (1944) distinguished five zones in the soil during infiltration: (1) saturated zone (a zone reaching a depth of about 1.5 cm), (2) transition zone (a zone of about 5 cm in which a rapid decrease in moisture occurs), (3) transmission zone (a zone in which moisture content is nearly constant), (4) wetting zone (a zone of fairly rapid change in moisture content), and (5) wetting front (a zone of very steep moisture gradient which shows a visible limit of moisture penetration into the soil).

Factors Affecting Infiltration

Factors affecting infiltration have been studied by Baver (1933), Lewis and Powers (1938), Horton (1940), Fletcher (1949), Diebold (1951), Musgrave (1955), Miller and Gardner (1962), Lull (1964), Musgrave and Holtan (1964), Powell and Beasley (1967), Gifford (1968), and Hermanson (1970) among many other investigators. An extensive review of previous investigations reveals that all the studies reported have considered many common factors that affect infiltration and hence runoff. Some of the most common factors are soil properties (including grain size and its distribution, porosity, compactness, etc.), plant cover, slope, degree of aggregation of soil, antecedent soil moisture, and rainfall intensity and duration. In the following paragraphs, some of these factors are reviewed in terms of previous investigators' findings and results.

Effect of antecedent moisture

The rate of infiltration into a soil is at a maximum when a soil is fairly dry, for after water is added, the pore space becomes full of water and the infiltration rate of additional water declines to a low but uniform level. Neal (1938), in a laboratory study of the effects of degree of slope, surface conditions, and rainfall intensity on infiltration, found that initial soil moisture content had a greater effect on the rate

of infiltration during the first 20 minutes of simulated rainfall than any other factors. Other workers (Arend and Horton, 1943; Free et al., 1940) obtained similar results in field measurements with infiltrometers. Hansen (1955) in the study of surface irrigation, has concluded that in spite of the fact that the rate of entry in moist soils is less than in drier soils, the wetting front advances more rapidly when the soil is wet than when it is dry. Powell and Beasley (1967) have also found that the antecedent soil moisture has it greatest effect on infiltration when the soil is bare. This is expected, since the beating action of rain and sorting of particles to fill the pores is greatest where the soil is bare. Meeuwig (1970) concluded that the initial moisture content exerts a significant effect on the amount of water retained. Retained water decreases about 0.1 inch for each 0.05 inch in initial moisture content of the surface 2 inches of soil. These findings are, in general, in agreement with previous studies conducted by Brakensiek and Frevert (1961), Jamison and Thornton (1961), and Thames and Ursic (1960). Green (1962) found a significant effect of antecedent moisture content on infiltration under field conditions. In addition, he found that the rate of advance of the wetting front is proportional to the antecedent moisture level, and concluded from field infiltration rates measured on two different soils that in some cases, antecedent moisture differences in a given soil may influence infiltration rates as much as tillage, surface sealing, or profile differences between soils.

Effect of soil texture and structure

Horton (1933) recognized maximum and minimum infiltration rates of a soil. The maximum infiltration rate for a given rain occurs at the beginning of the rain. He has indicated that the infiltration rate decreases rapidly because of changes in the structure of the surface soil and increases in soil moisture, and then gradually approaches to a somewhat stable minimum. Powell and Beasley (1967) have reasoned that when the soil is dry, the high initial infiltration rate is primarily the result of the filling of the pore spaces larger than capillary size. Once these pores are filled, the infiltration is due mainly to the advance of water by capillary potential.

Musgrave and Holtan (1964) indicated that the soil characteristics affecting infiltration most were largely ones in relation with pore size and pore-size distribution as well as their relative stability during storms. In sands the pores are relatively stable, while soils with appreciable amounts of clay are subject during a storm to the disintegration of the surface crumbs or aggregates which in their dry state may provide relatively large pores but swell appreciably upon wetting. During a storm, sands may slowly rearrange themselves into a more dense mix than formerly, whereas in silts and clays a breakdown of soil crumbs and a melting of aggregates take place upon the impact of raindrops, causing the very small particles of silt and clay to move across the surface and penetrate previously existing pores, thus clogging them and greatly reducing infiltration. The degree of swelling that occurs in soil also is affected by the content and kind of clay minerals present.

For certain soils which develop large cracks or sun checks when dry, it seems more convenient to treat infiltration as the disappearance of water below the general ground surface. This results in including, as part of infiltration capacity, the rate at which surface water runs into open cracks. The effect of this inclusion produces relatively high infiltration-capacity rates at the beginning of the storm, decreasing sharply when the cracks are filled or become closed (Horner, 1944).

Rauzi and Fly (1968) have found that the ability to absorb rainfall may have been impaired, even on highly permeable sand range sites, where poor structure (i.e., poor arrangement of the soil particles with respect to functions as determined by the capacity of the soil to hold water and the movement of water through soils) has been developed either by excessive trampling by livestock, by sealing of surface pores through splash erosion, or by deposition of wind or water carrying sediments. Unfavorable surface soil conditions markedly reduce water intake rates. In addition, they have found that soils with compact or blocky clay subsoils and clay or clayey soils affected by alkali, clay soils having good structure and no alkali, clay soils of poor structure, and alkali or saline-alkali soils all have low intake rate. Clay soils with good structure take water at rates three to four times that of alkali soils or dense clay with poor structure. Range-soil groups with equal amounts of vegetal covers do not necessarily have similar water intake rates. Differences are usually traceable to good or poor structure. The rate of water intake on soils with good structure is always greater than that on soils with poor structure with equal vegetal cover. The subsurface texture and structure influence the downward movement of water after the surface layer is saturated. For instance, prismatic and subangular blocky structure with vertical cleavage in the subsoil is conductive to water movement, whereas coarse blocky or angular blocky structure with greater horizontal than vertical cleavages retards downward movements of water.

A major factor among many soil properties influencing infiltration is the degree that the surface soil is compacted. Modification of pore sizes and pore-size distribution occurs in the field. Under wet conditions, for example, one pass of a tractor has been known to reduce noncapillary pore space by half and infiltration rate by 80 percent (Steinbrenner, 1955) and in another instance, two passes with a tractor reduced infiltration rate from 1.4 to 0.6 in./hr (Doneen and Henderson, 1953). When a soil is compacted, its total porosity is decreased, the major reduction being in noncapillary porosity. The converse is found in tillage when, at least for a short time, the soil is opened up and large pores are provided.

Duley and Kelley (1939) tested intake rates on different soil types, such as clay loams, silty clay loams, silty loams, and sandy loams. Their subsoil varies from deep, uniform sandy materials and uniform silty subsoils to heavy clay and clay pan subsoils. The amount of water absorbed by these different soils is given in Table 1. The results shown are for bare cultivated soils on a 4 percent slope for a 1.5 hour period of water application. After this water had been applied, the plots were allowed to stand until the following day when a second application of water was made.

Table 1. Effect of soil types on total intake of water and infiltration rate on bare cultivated soil with a slope of 4 percent (after Duley and Kelley, 1939).

Soil Type	Total intake of water in 90 minutes (inches)		Infiltration rate at end of 90 minutes (inches/hour)	
	1st day	2nd day	1st day	2nd day
Pawnee clay loam	1.20	0.76	0.50	0.33
Lancaster sandy loam	1.71	0.61	0.68	0.32
Knox silt loam	1.05	0.58	0.38	0.21
Butler silt loam	1.32	0.57	0.38	0.25
Dickinson sandy loam	1.37	0.48	0.40	0.24
Marshal silt loam (eroded phase)	1.08	0.43	0.42	0.21
Marshal silt loam (heavy subsoil)	2.43	0.38	0.28	0.21
Butler silt clay loam	1.24	0.37	0.30	0.16

The total intake of water and the final infiltration rates on cultivated bare land show much less variations among the different soil types than anticipated. In spite of the fact that the soils tested varied greatly in texture of the surface soil and in profile characteristics, the amount of water taken into the soil in a given time was strikingly similar for all soils, and the infiltration rates were finally reduced almost to a common level. The difference between the first day tests and second day tests is probably due mainly to antecedent moisture content.

Meeuwig (1970) has found that water retention (catchment at the surface plus infiltration) decreases with increasing bulk density. However, this relation is strongly affected by the coarseness of the soil. When a large proportion of the soil is composed of particles and aggregates larger than 0.5 mm, the effect of bulk density is minimal, but when the soil is fine and poorly aggregated, water retention decreases sharply as bulk density increases.

Many experiments have shown that pore sizes and pore-size distribution are greatly affected by the content of soil organic matter because both the sizes of soil aggregates and their stability in water are related to the amount of soil organic matter. Organic matter is conducive to the formation of relatively large stable aggregates. This is not only true in silts and clays, but also in most soils containing colloidal material. The addition of organic matter or its removal, as by intensive cultivation and oxidation, changes the prevailing permeability. However, these effects are more pronounced in some silts and clays than in sands.

The influence of soil texture and structure on infiltration, as described through noncapillary porosity, clay content, and organic-matter content, was also shown in a statistical study of 68 soils (Free et al., 1940), in which noncapillary porosity of the subsoil gave a correlation coefficient of 0.54; surface organic matter, 0.50; clay content of the subsoil, 0.42; and organic matter in the subsoil, 0.40. When the factors were combined in multiple correlations, the highest multiple coefficient

of 0.71 was obtained with noncapillary porosity, organic matter of both surface and subsoil, and clay content of the subsoil.

Effect of frost

Frozen ground affects infiltration. If frozen when very dry, some soils are fluffed up and frost is discontinuous, as in the honeycomb and stalactite types. A soil under this condition may be permeable as, or even more permeable than, frost-free soil. On the other hand, if the soil is frozen while saturated, concrete frost in the form of a very dense, nearly impermeable layer often results. Trimble et al. (1958) found that in the Northeast, infiltration was zero on concrete frost in the open and forest area, but was not affected where soil was traversed by large holes in which water had not frozen. Infiltration tests on concrete frost in northern Minnesota forest and grassland gave 0.09 in./hr of infiltration rate in silt-loam soils and 0.47 in./hr in sands (Stoeckeler and Weitzman, 1960).

Effect of plant cover

Musgrave and Holtan (1964) have stated that vegetation is one of the most significant factors affecting surface entry of water. Vegetation or mulch protects the soil surface from rainfall impact. Massive plant root systems such as grass in sods perforate the soil, keeping it unconsolidated and porous. The organic matter from crops promotes a crumb structure and improves permeability. On the other hand, vegetation such as a row crop gives less protection from raindrop impact, depending upon the stage of growth, and the root system perforates only small portions of the soil profile and the normal accompanying tillage may further reduce permeability. Forest litter, crop residues, and other humus materials protect the soil surface. High biotic activity in and beneath surface layers open up the soil, resulting in high entrance capacities.

Hays (1949) showed the general trend of results obtained at three latitudes in the central U.S. by comparing runoff amounts from continuous row crops, crops in 3-year rotations, and continuous grass. At the Upper Mississippi Valley Conservation Experiment Station, La Crosse, Wisconsin, for instance, it was found that average annual runoff on Fayette silt loam with a slope of 16 percent was 27.7 percent of rainfall for continuous corn (row crop); 20.6 percent for corn in rotation of corn-barley-red clover; 18.9 percent for barley in the rotation; 11.5 percent for red clover in the rotation; and 5.5 percent for protected bluegrass. Similar comparisons for the Red Plains Conservation Experiment Station, Guthrie, Oklahoma, and the Missouri Valley Loess Conservation Experiment Station, Clarinda, Iowa, were reported (Glymph and Holtan, 1969). It is evident that runoff from these plots is inversely related to the density of vegetation and the frequency of cultivation.

The density of herbaceous vegetation is closely related to infiltration, as has been attested by several studies on the western range. Packer (1951), for instance, found that the percent of the soil covered by living or dead plant parts was closely related to runoff, and therefore to infiltration. As cover density increased to about 70 percent on wheatgrass and cheatgrass areas, overland flow decreased. At densities above 70 percent, there was little further decrease. Fibrous-rooted vegetation such as wheatgrass has been found to be much more effective in controlling runoff than taprooted annual weeds (Lull, 1964).

The great influence of vegetated cover on infiltration is further evidenced by the fact that bare-soil infiltration capacity can be increased 3 to 7.5 times with good permanent forest or grass cover, but little or no increase results with poor row crops (Jens and McPherson, 1964).

Duley and Kelley (1939) considered that there might be far greater variations between the infiltration rates obtained under different surface conditions on a single soil type than on different soil types having the same surface condition. This consideration may make it necessary to study the infiltration rate characteristic of surface conditions rather than that of a specific soil type.

Although plant cover is like all other factors that affect infiltration and runoff, it is not an independent factor. Rauzi and Fly (1968) found that in general water intake rate increased with vegetal cover, and that this increase was about 1 inch per hour per 2,000 lbs per acre vegetal cover with good soil structure, and 1 inch per hour per 3,200 lbs per acre with poor soil structure. A large number of tests on the silty range site enabled the separation of rates of water intake of three major soil structure classes. The amount of vegetal cover required to increase the rate of water intake 1 inch per hour for the silty range site was between 1,000 and 5,000 lbs per acre. At the 3,000 lbs per acre level of vegetal cover, the mean water intake rates were for excellent structure, 2.40 inches per hour; for fair to good structure, 1.65 inches per hour; and for poor structure, 1.10 inches per hour. The clayey range site included soil textures of sandy clay loam, silty clay loam, and clay. Water intake increased rapidly when the vegetal cover increased to between 500 and 3,000 lbs per acre. No increase in water intake and even a slight decrease was noted with more than 4,000 lbs per acre of total cover. The rate of 1,700 lbs per acre of total cover was equivalent to an increase of 1 inch per hour of water intake on soils of good structure, but 3,750 lbs per acre was required on soils of poor structure.

If the soil surface was protected with straw in the amount of 2.5 tons per acre, the total intake of water by each soil tested was much higher than on the bare soil. The infiltration rates were also high and remained at relatively high levels throughout long periods of application, (Duley and Kelley, 1939). They also found that alfalfa gave a higher infiltration rate at the end of 90 minutes than oats, probably somewhat in proportion to the density of soil cover. The native sod absorbed water at about the same rate as the land covered with straw. However, where

the grass was clipped close to the ground and the surface litter removed, the infiltration rate dropped almost as low as on cultivated land. Apparently the soil still containing the grass roots did not cause it to absorb water rapidly.

Table 2 shows the difference in infiltration on soils of varying depth from deep to shallow, each having contrasting covers or land-use conditions. The soils are all silt loams, differing mainly in depth and content of organic matter. The Viola is a relatively shallow soil, comparatively low in organic matter content. The Muscatine is a deep, very dark colored soil, rich in organic matter content. Tama, Berwick, and Clinton are listed in the table in the approximate order of depth and organic matter content between Muscatine and Viola. The difference in land use is due mainly to plant cover. The bluegrass, of course, provides a dence surface cover highly protective against raindrop impact. The tests were made on farms where the grass was under practical grazing conditions. Corn is not noteworthy for any great protective effects, and intertillage tends to break down soil aggregation or crumb structure. Data in Table 2 are the results of replicated wet runs of the type-F infiltrometer under the 1.80 inches per hour simulated rainfall with a large drop size and an energy of impact similar to that of natural storms of this size. The results show: (1) the consistent and wide difference between the two kinds of land use (or plant cover) on each of the soils and (2) the steadily decreasing infiltration under a high protective cover such as bluegrass from the deep soil with high content of organic matter to the shallow soil with low content of organic matter. But this close relationship of infiltration to soil depth and content of organic matter is not found under the less protective corn, where surface conditions rather than soil depth and content of organic matter tend to govern intake. In other words, the differences in soil characteristics—even where they are rather large as in this case—have relatively little effect under adverse cover conditions. It is also interesting to note infiltration rates on the different soils during the last hour of this 5-hour storm during which a total of 9 inches of water was applied. As expected, the rates during the fifth hour are less than the average of the entire period. Without exception, the more protective cover on each soil is producing a greater

Table 2. Infiltration on soils of varying depth and organic matter with contrasting covers (after Holtan and Musgrave, 1947).

Silt loam soils	Total infiltration in 5 hour, inches		Difference due to land use	Infiltration rates during fifth hour	
	Bluegrass Pasture	Corn land		Bluegrass in./hr	Corn land in./hr
Muscatine	5.38	1.34	4.04	0.61	0.11
Tama	5.03	1.51	3.52	0.77	0.14
Berwick	3.48	1.21	2.27	0.34	0.12
Clinton	2.77	2.17	0.60	0.29	0.18
Viola	1.63	1.28	0.35	0.16	0.08

infiltration rate as shown in Table 2. Again it is readily seen that the soils tend to be arranged under the bluegrass in the order of their depth and content of organic matter. Under the less protective cover, however, soil differences tend to be overshadowed by what obviously happened on the soil surface, namely clogging of pores (Musgrave and Holtan, 1964).

Woodward (1943) observed that infiltration rates increased directly with plant cover density although the magnitude of the increase varied between cover types and soils. Mazruk, Kriz, and Ramig (1960) studied the rates of water entry as affected by age of perennial grass sods. In their study, two species of grass were used: Agropyron intermedium and Bromus inermis. Only the age of grass stand showed any significance in the rate of water entry in the soil. Box (1961) concluded that all vegetation improved water intake on the clay soil, but grass proved superior to brush. According to his study, under grass sod, an average of 8.9 inches of water entered the ground in 2 hours as compared with 7.5 inches under mesquite and 3.5 inches under bare soil.

There are other studies dealing with the effect of plant cover on infiltration. Some results were not very clear-cut and conclusive because other factors were also taken into consideration in their studies, whereas others analyzed data statistically without giving a due account of their results. It is not intended to elaborate a review of such studies herein, but those who are interested in the subject may refer to, for example, Bertoni, Larson, and Shrader (1958), Smith and Leopold (1942), Woodward (1943), Osborn (1952), Hanks and Anderson (1957), Meeuwig (1970), and Fletcher (1960).

In the preceding review, the kind of cover was mainly stressed, but none of the studies compared different cover densities on the same soil as it is affecting infiltration.

Effect of rainfall

Linsley, Kohler, and Paulhus (1949) have reported that rainfall intensity has little effect on the rate of infiltration when it exceeds the capacity rate. This agrees with the findings of Schreiber and Kincaid (1967), but disagrees with those of Fletcher (1960). Willis (1965) has found that the infiltration rate of a bare soil was reduced by an increase in kinetic energy of rainfall which is a function of the velocity of impact of raindrops and of the rainfall intensity. However, Duley and Kelley (1939) observed no significant difference in either total intake or infiltration rate, although there is a difference in the rate of application of water which materially exceeded the rate of intake. Local experimentation on the variation of infiltration capacity with rainfall intensity showed predominant variation for bare soil, as noted by Horner and Jens (1942), and a lesser amount of variation for sodded areas.

Duley and Kelley (1939) also found that when the rate of application of water was sufficient to give runoff, a fairly definite amount of water

entered the soil and any amount of application in excess of this intake appeared in the runoff. During the progress of their tests on cultivated plots of four soil types with different slopes and different rates of application, it became increasingly clear that rainfall and its related factors were exerting only a minor influence on the intake rate.

Duley (1939) observed that the rapid reduction in the rate of intake by cultivated soils, as rain continuously fell on the soil surface, was accompanied by the formation of a thin, compact layer at the soil surface, and that the water was able to pass through this layer very slowly. He postulated that this thin, compact surface layer was apparently the result of severe structural disturbance due in part to the beating effects of the raindrops, and in part, to an assorting action, as water flowed on the soil surface, fitting fine particles around the larger ones to form a relatively impervious seal. His data showed that this thin, compact layer had a greater effect on intake of water than the soil type, slope, moisture content, or soil profile characteristics. Later, Duley and Kelley (1939) successfully prevented the formation of this semi-impervious layer, often a few millimeters thick, by breaking down the soil structure by the impact of raindrops on the soil surface, using a cover of straw or a growing crop.

Ellison (1950) in his study of soil erosion by rainstorms has reported that raindrops working through the splash (impact plus spatter) process break down clods and crumbs of soil and compact these broken materials. The inflow of surface water made muddy by splash further seals surface cracks and pores, and tends to waterproof the soil surface. Tests on open ranges showed that with good grass cover only about a ton of soil per acre was splashed and the water intake was 2.66 inches during a 15 minute period. On other areas where there was less forage, the splash tended to increase and water intake tended to decrease with reduction in vegetal cover. Finally, on bare areas where there was no cover at all, 70 tons per acre of soil were splashed and water intake was reduced to 0.10 inches in 15 minutes.

Green (1962) has also concluded that surface sealing diminishes the effect of antecedent moisture on infiltration because the hydraulic conductivity of the immediate soil surface controls water flow into the soil and surface sealing does not allow suction gradients to control the rate of infiltration.

Duley and Domingo (1949) found that on an area affected by overflow deposits and trampling of animals, intake rate on bluegrass land was reduced to a very low point, i.e., from a normal 2.02 inches per hour down to 0.14 inches per hour under dry conditions and from a normal of 0.85 inches per hour to 0.13 inches per hour under wet conditions.

Effect of soil-surface slope

Duley and Kelley (1939) on four soils tested four different slopes, 2 percent, 4 percent, 6 percent, and 10 percent. They noted that there

was a tendency for the amount of water intake to decrease slightly with increase in slope. The greatest intake was found on the gentlest slope, particularly 2 percent slope or less. Their observations that the degree of slope has only a slight effect on infiltration were reported to be in line with earlier investigations.

Infiltration Characteristics

In the early years of his infiltration studies, Horton (1935) assumed that infiltration capacity might be satisfactorily approximated as having a constant uniform value during the first hour or two of a precipitation period. Since then the importance of the role the shape of the early segment of infiltration capacity curves plays in the calculation of runoff from a watershed, particularly a small area under intense precipitation, has been widely recognized by most investigators. Many methods have been developed to derive infiltration capacity curves from natural or artificial rainfall (Musgrave and Holtan, 1964). There have been the detention-flow-relationship method (Hydrology, SCS, 1969; Sharp and Holtan, 1940 and 1942), the time-condensation method (Holtan, 1945), and the block method (Horner and Lloyd, 1940; Sherman, 1940; Sherman and Mayer, 1941). Infiltration capacity curves so determined all have characteristically similar shapes, their values being relatively high in the beginning of precipitation, decreasing rapidly as precipitation continues, and tending to reach rather definite minimum values, for a particular precipitation period. The use of such characteristic curves represented a long advance over the earlier conception of uniform infiltration capacity.

The results of extensive research on infiltration capacity conducted by Horner and Jens (1942) indicated that: (1) Infiltration capacity varied little with surface slope; (2) it probably varied materially with soil porosity and soil moisture, possibly with soil moisture deficiency below field capacity; (3) it might change rapidly with an alteration of soil surface condition such as might occur under the puddling action of rain impact, or under erosion and in-working of fines where the soil is not protected by good vegetal cover; (4) it might be quite different for bare cultivated soils as compared with grass or other good vegetal cover; and (5) for bare soils it might vary with precipitation intensity, but under good vegetal cover it was relatively independent of intensity. From Horner and Jens' research results, basic infiltration capacity curves might be selected so that they would be satisfactorily representative of any particular combination of soil and cover under specific seasonal conditions.

Every soil and cover complex has a related characteristic curve of decreasing infiltration capacity during a precipitation period. As a rule, infiltration capacity of a given soil passes through a cycle from storm to storm. If the character of the soil and its moisture history are known for a time preceding a given rain, the infiltration capacity which it will have at the time of rain can, in general, be closely

predicted (Horton, 1935). Suffice it to say that each soil and cover complex has a unique infiltration-capacity curve, and that the values of infiltration capacity will follow a definite decay curve during a period of precipitation where rainfall intensities are in excess of infiltration capacity and adjust to a somewhat modified curve during the period of precipitation where intensities are less than infiltration capacity (Horner, 1944).

Although, for any soil, cover, and seasonal condition, the curve representing the decay of infiltration capacity appears to have a quite definite form under continuous excess rainfall, the appearance of infiltration capacity during a particular precipitation period may also vary with the initial (antecedent) soil moisture and with intermittent or varying precipitation. Adjustment of infiltration capacity to antecedent conditions and precipitation pattern must be in order. However, with the present knowledge in the mechanics of infiltration, there is no definite rule that can be followed in adjusting initial and continuing infiltration capacities for a range of soils and covers in question.

For selection of an infiltration capacity curve representative of any soil and cover condition under an average antecedent condition, the use of a standard infiltration-capacity curve is becoming quite a common practice (Musgrave and Holtan, 1964). Curves derived from analyses of a number of storms on single-practice watersheds are used in arriving at standard curves of infiltration capacity. Jens (1948) derived infiltration capacity curves for wet and normal antecedent conditions of turf areas. These curves may be accepted as reasonably representative of the infiltration capacity curve for a turfed cover for a rather wide range of clay subsoils. In view of the little artificial compaction that would occur from trampling of the surface under intensive recreational use or from walking over city lawns, representative curves for city lawns would be slightly lower than those derived by Jens (1948). For sandy loams or sands, infiltration capacity would be materially higher. Holtan and Kirkpatrick (1950) derived three typical standard infiltration curves for hay, grain, and bare soil, respectively, on certain soils of the Piedmont.

For all practical purposes, three factors (soils, vegetation, and antecedent soil moisture) may be used as bases for grouping infiltration capacity and hence the rainfall-runoff relationship within each soil-cover-moisture complex. The result should be a family of curves representing infiltration capacity and hence rainfall-runoff relationships for the various complexes (Musgrave and Holtan, 1964).

Soil. Musgrave (1955) grouped soils in accordance with their infiltration capacity, after a period of prolonged wetting. The array of these soils arranged in the order of the minimum infiltration rates was derived by Musgrave mostly from analyses of runoff hydrographs. It is tentative, subject to revision or verification by further testing. Also noted is the fact that Musgrave's grouping of soils (A, B, C, and D) is somewhat different from the SCS hydrologic soil groups (Hydrology, 1969; Ogorsky and

Mockus, 1964) to which no ranges of quantitative final infiltration values are given. A thorough review of soil classifications (see Appendix A) reveals that the SCS hydrologic soil group classification, if supplemented by the catena concept (Chiang, 1971), would probably give the most practical soil array for use as a basis in the derivations of standard infiltration capacity curves.

The SCS hydrologic soil group classification (A, B, C, and D) was based on the premise that similar soils (i.e., similar in depth, organic matter content, structure, and degree of swelling when saturated) would respond in an essentially similar manner during a rainstorm having excessive intensities. In application, it is cautioned that some of the soils in the table were classified, for example, under the D group because of a high water table that creates a drainage problem. Once these soils are effectively drained, they can be placed in an alphabetically higher group. In order to supplement and refine the SCS classification, Chiang (1971) suggested a rating table using the catena concept. The Chiang rating table allows for an intermediate class between each of the four groups classified by SCS. The rating was given according to internal drainage, depth, and texture of the soil, as well as subsurface soil conditions.

Cover. Detailed information about the vegetative cover, such as plant density and height, root density and depth, extent of plant cover, and extent and amount of litter, is seldom available. Therefore, data on the effect of vegetative cover on the infiltration capacities of various soils may rely on the land use as an index of cover conditions. The SCS (Hydrology, 1969) listed various land-use practices in the estimated order of their influence upon the infiltration capacities of various soils. The order is that indicated by analyses of hydrographs from plots and single-practice watersheds and by infiltrometer tests.

Antecedent soil moisture. The four points of soil-water equilibrium, i.e., saturation, field capacity, wilting point, and hygroscopic moisture were suggested for use in moisture classification to determine their effects on infiltration capacity (Musgrave and Holtan, 1964). Many schemes have been devised for estimating the antecedent moisture status relative to these points of equlibirium. For practical purposes, however, the index of watershed wetness used in connection with the SCS runoff estimation method (Hydrology, 1969) may be more convenient than those previously developed. The following three levels of antecedent moisture condition (AMC) were used in the SCS method:

AMC-I. Lowest runoff potential. The watershed soils are dry enough for satisfactory plowing or cultivation to take place.

AMC-II. Average runoff potential.

AMC-III. Highest runoff potential. The watershed is practically saturated from antecendent rains.

Inclusion of this index in the estimation of infiltration capacities for various soils-cover complexes will be investigated later.

Infiltration Modeling

Infiltration-capacity decay curve (or more recently called infiltrability-time curve by Swartzendruber and Hillel (1973)) of a given soil-cover-moisture complex, beginning with a very high infiltration rate, and eventually approaching a constant non-zero value asymptotically with time, has been hypothetically portrayed as a solution to a boundary-value problem of rain infiltration (Philip, 1957a and 1969b; Hanks and Bowers, 1962; Wang and Lakshminarayana, 1968; Rubin and Steinhardt, 1963; Rubin, 1966b; Braester, 1973; Bruce and Whisler, 1972; Whisler and Klute, 1965 and 1969), using a nonlinear form of the Fokker-Planck equation (Philip, 1969b) as the flow equation for water moving through a rigid, unsaturated soil, subject to various initial and boundary conditions of interest. Many of the concepts leading to the nonlinear Fokker-Planck equation were implicit in Buckingham's (1907) monograph, but Richards (1931) formerly presented the equation in 1931 (Philip, 1969b). It is now well known as, and for convenience henceforth referred to as, the Richards equation. Many natural soils contain swelling clay, which can cause movement of the soil particles as well as of the water, and produce air bubbles upon ponding on the soil surface. These phenomena have made the Richards equation more difficult to be accepted as the basic flow equation. For infiltration with counter flow of air, Peck (1965), Adrian and Franzini (1966), Morel-Seytoux and Noblanc (1973), and Morel-Seytoux and Khanji (1974) developed a method of moving strained coordinates that greatly facilitates the study of two-fluid systems. For infiltration into deforming porous media, Smiles and Rosenthal (1968) and Philip (1969a) did some work in an attempt to derive the flow equations representing the more realistic system of water and soil in which both the water and the soil particles are moving, but the full implications for such complicated infiltration models are as yet not clear. A general treatment of transport in an unsaturated soil consisting of a mixture of a solid phase, an aqueous phase, and a gaseous phase in relation to deformable soils was given by Raats and Klute (1968a, 1968b).

All of the solutions to the boundary-value problems of infiltration process will yield infiltration-capacity decay curves, but they are not generally expressible in closed form. In application, however, several algebraic (empirical) infiltration equations have been developed. Because most algebraic equations are expressed as a function either of time or of the total quantity of water infiltrated into the soil, they are judged to be in the most convenient form for use in the runoff study. The algebraic infiltration equations in their historical order of development include the Green-Ampt equation (1911), the Kostiakov equation (1932), the Horton equation (1940), the Philip equation (1957a), and the Holtan equation (1961). All of these parametric equations will be discussed at some length later in this report.

BOUNDARY-VALUE PROBLEM OF RAIN INFILTRATION AND ITS NUMERICAL SOLUTIONS

Because the solution to the boundary-value problem of rain infiltration can produce the infiltration-capacity decay curve, though not in closed form, as mentioned previously, a mathematical infiltration model consisting of the Richards equation and appropriately prescribed initial and boundary conditions was formulated in this study and solved numerically on a digital computer. The infiltration-capacity decay curve so determined did help evaluate the effect of each significant factor on infiltration capacity without resorting to very extensive laboratory experiments. Thus, it was hoped that the mathematical evaluation of the significant factors might help lead to the establishment of relationships, if any, between the significant factors and the model parameters used in each of the algebraic infiltration equations.

No analytical solution to the rain infiltration problem has been devised for actual soils with the time-varying soil-surface condition, i.e., changing from a flux condition (before ponding) to a concentration condition (after ponding). (The time of ponding is defined herein as an instant at which the soil surface becomes saturated.) For a concentration condition on the soil surface, Philip (1957a) expressed the infiltration flux in a power series expansion of time. For the same concentration condition as specified by Philip (1957a), Parlange (1971) has recently developed an alternate method to obtain an approximate (or ''quasi-analytical'') solution. Parlange (1972) applied his method to the problem with a flux condition. Knight and Philip (1973) critically studied the applicability and limitations of the Parlange method and offered a new quasi-analytical technique which, however, has affinities with Parlange's method (Philip and Knight, 1974).

In view of the difficulty in obtaining the analytical solution to the infiltration problem, almost every investigator resorted to a numerical method for various boundary conditions and solved it on a computer. For example, Hanks and Bowers (1962) obtained numerical solutions for a zero ponding-depth condition, Wang and Lakshminarayana (1968) for a saturated moisture-content condition, Rubin and Steinhardt (1963) and Rubin (1966a) for a constant water-flux condition, and Bruce and Whisler (1973) for non-constant water-flux (rainfall) condition.

Numerical solutions to various types of the boundary-value problems of infiltration have been obtained by many investigators using the implicit numerical scheme (e.g., Hanks and Bowers, 1962; Rubin and Steinhardt, 1963; Rubin, 1966b; Freeze, 1969) while other investigators have used the explicit numerical scheme for solution (e.g., Staple and Lehane, 1954; Gupta and Staple, 1964; Staple, 1966 and 1969; Wang and Lakshminarayana, 1968). Both numerical schemes have been used with

success in solving the boundary-value problem of rain infiltration although most of those solved are subject to a less restrictive boundary condition than those prescribed in the present study. Generally speaking, explicit-difference methods are less efficient but easier to program than implicit methods. In this study, partly due to a complex and variable upper-boundary condition (i.e., a change from a constant flux to constant head condition) to be imposed on the soil surface, the explicit difference method is adopted herein.

No effort was spent on development of an unsaturated flow equation of a general type for a soil containing swelling clay as well as for infiltration with counter flow of air. As mentioned previously, several investigators have already started formulating such a general flow equation (or a set of flow equations in the case with air counterflow), but no solution to such a complex problem is available as yet. Making the mathematical modeling of the natural rain infiltration problem more complicated is the fact that during heavy rainstorms, a lens of air may be trapped between the advancing wetting front and a lower layer with high resistance to flow of air due to a high water content and/or a small porosity. When air ahead of the wetting front is compressed because of no access to the atmosphere, the wetting front becomes unstable. Raats (1973) derived criteria for instability of the wetting front on the basis of a simple hydraulic model due to Green and Ampt (1911). Several investigators (e.g., Wilson and Luthin, 1963; Peck 1965; Dixon and Linden, 1972; Vachaud, Gaudet, and Kuraz, 1974) have measured large increases in air pressure during ponded infiltration in the field and laboratory experiments. The often-observed escape of air bubbles through the wetted zone may be related to the instability of the wetting front. Although the phenomenon is mathematically describable, it was decided not to pursue modeling such a natural, yet complicated, rain infiltration problem. For simplicity, the Richards equation is used as an unsaturated flow equation throughout this study.

Idealized Rain Infiltration Problem

The soil water movement under rainfall can hypothetically be described by using the concepts in continuous mechanics. The flow equation formulated on the basis of these concepts is the well-known Richards equation that can be derived by incorporating Darcy's law with the equation of continuity. An initial condition such as a constant or specified initial moisture content is given. To formulate boundary conditions requires a knowledge of the rainfall infiltration process that is briefly described as follows.

When rainfall starts, rain water falling on the soil surface causes an increase in the soil water content. If rainfall continues, the soil surface becomes saturated and eventually is ponded. However, not all events of rainfall reach this ponding stage. Some rainfall intensities which are less than the limiting infiltration rate (or the saturated hydraulic

conductivity) maintain the soil in an unsaturated condition. In other words, with small rainfall intensities, rain infiltration can continue indefinitely without ponding (Rubin and Steinhardt, 1963). On the other hand, some extremely high rainfall intensities could cause immediate ponding on the soil surface with a brief wetting stage to attain full saturation of the surface lamina of soil. In general, the rain infiltration process can be divided into two stages: The first one is before ponding and the second one is after ponding. Thus, the following two different boundary conditions on the soil surface should be specified for these two different stages: Before ponding the soil surface condition is a flux condition equal to the given rainfall rate, and after ponding it becomes a pressure head boundary condition equal to the ponded water depth.

After ponding, the saturated zone that began at the soil surface gradually proceeds downward with the saturated zone overlying the unsaturated zone. If the ponding situation continues, the interface between the saturated and unsaturated zones (henceforth called the saturation front) moves downward until the specified lower boundary such as the groundwater table or impervious layer is reached provided that air is not entrapped. When the saturation front reaches the lower boundary, the soil layer is saturated throughout. However, the lower boundary condition may not be required if the soil layer is assumed semi-infinite, as was the assumption usually adopted in the rain infiltration study. The flow equation applicable in the saturated zone is the Laplace equation that can readily be derived from the Richards equation. A boundary condition at the saturation front can be prescribed by the air entry value in terms of the soil capillary potential. If the soil air has access to the atmosphere, the pore air pressure may be assumed to remain essentially atmospheric and the soil capillary potential at the saturation front can thus be assumed equal to atmospheric pressure.

A considerable amount of knowledge and understanding on the mechanism of rain infiltration has been advanced by many investigators (e.g., Philip, 1957a, 1969b, and 1973; Rubin and Steinhardt, 1963, 1964; Rubin, Steinhardt, and Reiniger 1964; Rubin, 1966a and 1966b; Parlange, 1971 and 1972; Knight and Philip, 1973; Philip and Knight, 1974). Freeze (1969) summarized available numerical mathematical treatments for one-dimensional, vertical, saturated-unsaturated, unsteady, flow problems in soils. Remson, Hornberger, and Molz (1971) also outlined numerical techniques used in this area. The finite-difference method adopted in the present study is in essence the same explicit scheme as formulated by Richtmeyer (1957). In order to circumvent computational instability due to the use of the explicit scheme, the stability criterion of Richtmeyer (1957) was followed. This stability criterion is a restriction which makes the computation very long; however, Gupta and Staple (1964), Staple (1966, 1969), and Wang and Lakshminarayana (1968) have successfully applied explicit-difference methods in solving the rain infiltration problem.

Although a form or scheme for a finite difference equation may be arbitrary, various factors were considered when deciding on an explicit scheme. First, the programming of an explicit scheme is relatively simple,

as unknowns are solved for separately, one at a time. Second, the explicit scheme requires less computations than the implicit scheme for every time step. However, it should be cautioned that because the explicit solution of a parabolic equation is subject to a stability criterion which limits the size of the time step that can be used, a large amount of computer time will be required when an explicit scheme is used in solving the problem involving the length of time with such an order of magnitude as days and weeks. Use of an explicit scheme may be justified only on the case that the infiltration-capacity decay curve for a period of one hour or so after rainfall needs to be computed. The narrow range of interest in time would probably make the explicit scheme as efficient as, if not more efficient than, the implicit scheme in the present computation, aside from other intrinsic problems resulting from the use of the implicit scheme. Noteworthy is the convergence problem of the implicit scheme (Smith and Woolhiser, 1971). The fact that an implicit-difference equation is unconditionally stable does not necessarily guarantee a convergent solution. Convergence of the numerical scheme depends on the form of the equation, and on some parameters, which are functions of the coefficients in the differential equation and the mesh size in both time and space.

Mathematical Statement of the Problem

In the formulation of the mathematical model, the following assumptions are made:

(1) A water system in the soil will be regarded as a continuous medium.

(2) Soil will be treated as a semi-infinite, homogeneous, isotropic porous body of stable structure.

(3) The flow of the water system is assumed to be uni-directional (i.e., in the vertical or gravitational direction only) and to obey Darcy's law.

(4) The physical properties of soil, such as capillary tension, hydraulic conductivity, and moisture diffusivity are unique, single-valued, continuous functions of soil moisture content. In other words, there is no hysteresis as long as only the wetting parts of the relationships are considered.

(5) For simplicity, the initial moisture content will be assumed uniform. Note that in reality the initial moisture content is rarely uniformly distributed.

(6) Raindrops falling on the soil surface will be treated as a continuous medium of water.

(7) Pore air pressure is assumed to remain essentially atmospheric.

Based on the preceding assumptions, the mathematical description of rain infiltration is:

$$\frac{\partial\theta}{\partial t} = \frac{\partial}{\partial z}\left(K(\theta)\,\frac{\partial\psi(\theta)}{\partial z}\right) + \frac{\partial K(\theta)}{\partial z} \quad \text{(Richards Equation)} \quad . \quad . \quad (1)$$

$$\theta(z,0) = \theta_o \quad . \quad . \quad . \quad . \quad . \quad . \quad . \quad . \quad . \quad . \quad . \quad (2)$$

$$\left[K(\theta)\frac{\partial\psi(\theta)}{\partial z} + K(\theta)\right]\Bigg|_{z=0} = r(t) \qquad (0 \le t \le t_p) \quad . \quad . \quad . \quad (3)$$

$$\psi(0,t) = h(t) \qquad (t \ge t_p) \quad . \quad . \quad . \quad . \quad . \quad . \quad . \quad . \quad (4)$$

$$\left[K(\theta)\frac{\partial\psi(\theta)}{\partial z} + K(\theta)\right]\Bigg|_{z=-\infty} = K_o \quad . \quad . \quad . \quad . \quad . \quad . \quad . \quad (5)$$

where θ = soil moisture content; t = time; z = vertical coordinate positive upward; $K(\theta)$ = hydraulic conductivity; $\psi(\theta)$ = soil capillary potential; θ_o = initial moisture content; $r(t)$ = rainfall intensity; t_p = time of ponding; $h(t)$ = depth of water ponding on the soil surface ($z = 0$); and K_o = initial hydraulic conductivity corresponding to the initial moisture content, θ_o. Equation 5 is the ''hypothetical'' lower boundary condition that is needed in order to solve the problem.

At the time of ponding ($t = t_p$), the soil moisture content, $\theta(z, t)$, just becomes saturated (θ_s). In the mathematical expression, it is

$$\theta(0, t_p) = \theta_s \quad . \quad . \quad . \quad . \quad . \quad . \quad . \quad . \quad . \quad . \quad . \quad (6)$$

Equation (6) is a criterion used for the computation of t_p and is valid only if the air entry value of the soil is zero.

The mathematical model consists of Eqs. 1 through 6 and the $\psi(\theta)$- and the $K(\theta)$-relationships of the given soil. Although the preceding set of equations, Eqs. 1 through 6, is formulated in one-space dimension, z, only the rainfall intensity, r, and the ponding depth, h, may vary independently, in addition to time, t, with another space-dimension, x, in the direction of surface water flow if Eqs. 1 through 6 are coupled with a surface runoff model for the surface runoff computation.

Before ponding, it is apparent from Eq. 3 that the infiltration rate, $f(t)$, is equal to the rainfall intensity, $r(t)$. However, rain infiltration can continue indefinitely without ponding if $r \le K_s$, where K_s is the

saturated hydraulic conductivity corresponding to the moisture content at saturation, θ_s. Furthermore, if $r < K_o$, the total soil moisture content may decrease. This does not sound logical, but can readily be seen from

$$r(t) = \int_{-\infty}^{0} \frac{\partial \theta}{\partial t} \, dz + K_o \quad . \quad . \quad . \quad . \quad . \quad . \quad . \quad . \quad . \quad (7)$$

which was derived by integrating Eq. 1 with respect to z from $-\infty$ to 0 and then having its results substituted by Eq. 3 and the ''hypothetical'' lower boundary condition, Eq. 5. Consequently, if $r < K_o$, Eq. 7 yields

$$\int_{-\infty}^{0} \frac{\partial \theta}{\partial t} \, dz = r - K_o < 0 \quad . \quad . \quad . \quad . \quad . \quad . \quad . \quad . \quad . \quad (8)$$

which indicates the decrease in the total moisture content remaining in the soil. If the initial condition is specified at the static equilibrium where $K_o \to 0$, this of course happens only when $r < 0$ in./hr (i.e., equivalent to evaporation).

It is noted that before ponding, the $\psi(\theta)$ and $K(\theta)$ relationships of a given soil have no bearing on the infiltration rate, f(t), as long as

$$f(t) = r(t) \quad . \quad . \quad . \quad . \quad . \quad . \quad . \quad . \quad . \quad . \quad (9)$$

which is apparent from Eq. 7 because f(t) is evaluated by

$$f(t) = \int_{-\infty}^{0} \frac{\partial \theta}{\partial t} \, dz + K_o \quad . \quad . \quad . \quad . \quad . \quad . \quad . \quad . \quad . \quad (10)$$

Equation 10 can readily be obtained from Eq. 1 in a similar fashion deriving Eq. 7 with the help of the following definition of the infiltration rate on the soil surface:

$$f(t) = \left[K(\theta) \frac{\partial \psi(\theta)}{\partial z} + K(\theta) \right] \Bigg|_{z=0} \quad . \quad . \quad . \quad . \quad . \quad . \quad (11)$$

As soon as the soil surface starts ponding, Eq. 9 is no longer valid. The $\psi(\theta)$ and $K(\theta)$ relationships of soil properties, initial soil moisture content, θ_o, soil moisture content at saturation, θ_s, rainfall intensity, r, and ponding depth, h, all come into play with the infiltration rate, f, which must be computed by either Eq. 10 or 11. Use of Eq. 10 has a slight advantage over that of Eq. 11 because the evaluation of the θ- distribution seems to be more accurate than that of the soil capillary potential gradient, $\partial \psi(\theta)/\partial z$, at the soil surface ($z = 0$) in terms of known values at grid points.

Some investigators (Smith and Woolhiser, 1971; Smith, 1971), assuming initial water movement to be negligible, ignored the K_o term in Eq. 10 in their evaluation of f(t) after ponding. This may result in a big error if $K_o \to K_s$. Without the K_o term in Eq. 10, it can readily be shown from Eq.

1 that as t approaches infinity, $f(t)$ cannot be asymptotic to K_s. In other words, integration of Eq. 1 with respect to z as t approaches infinity gives

$$\lim_{t\to\infty} \int_{-\infty}^{0} \frac{\partial\theta}{\partial t}\, dz \to K_s - K_o \qquad (12)$$

Thus, incorporating Eq. 12 into Eq. 10 yields

$$\lim_{t\to\infty} f(t) \to K_s \qquad (13)$$

which does not seem to vary with any of the factors mentioned previously.

After ponding, the soil profile becomes fully saturated near the soil surface with the saturated zone overlying the unsaturated zone, as shown in Figure 1. As described before, the saturation front advances downward, starting at the soil surface. The flow equation (Richards equation, Eq. 1) used in the unsaturated zone can also apply in the saturated zone; however, because $\theta = \theta_s$ and K_s = constant, it can be simplified to the Laplace equation in terms of the hydraulic head, $h = \psi + z$, or ψ as

$$\frac{\partial^2\psi}{\partial z^2} = 0 \qquad (14)$$

Note that Eq. 14 is equivalent to the Darcy law having a constant vertical velocity component, $f(t)$. Integration of Eq. 14 with respect to z with the help of Eqs. 4 and 11 at the soil surface yields

$$\psi = \left(\frac{f(t) - K_s}{K_s}\right) z + h(t) \qquad (15)$$

because in the saturated zone the vertical velocity, though it does not vary with z, varies with t and hence is not constant.

At $z = 0$, Eq. 15 is identical to Eq. 4, the soil surface condition after ponding. On the other hand, at the saturation front ($z = -L_f$), ψ is zero and hence $f(t)$ can be expressed from Eq. 15 as

$$f(t) = K_s \frac{h(t) + L_f(t)}{L_f(t)} \qquad (16)$$

In application, use of Eq. 16 in the problem of the infiltration rate computation after ponding requires a knowledge of $L_f(t)$ which is, of course, unknown. The following simple method was developed to determine the $L_f(t)$. Equating Eq. 16 to Eq. 10 yields

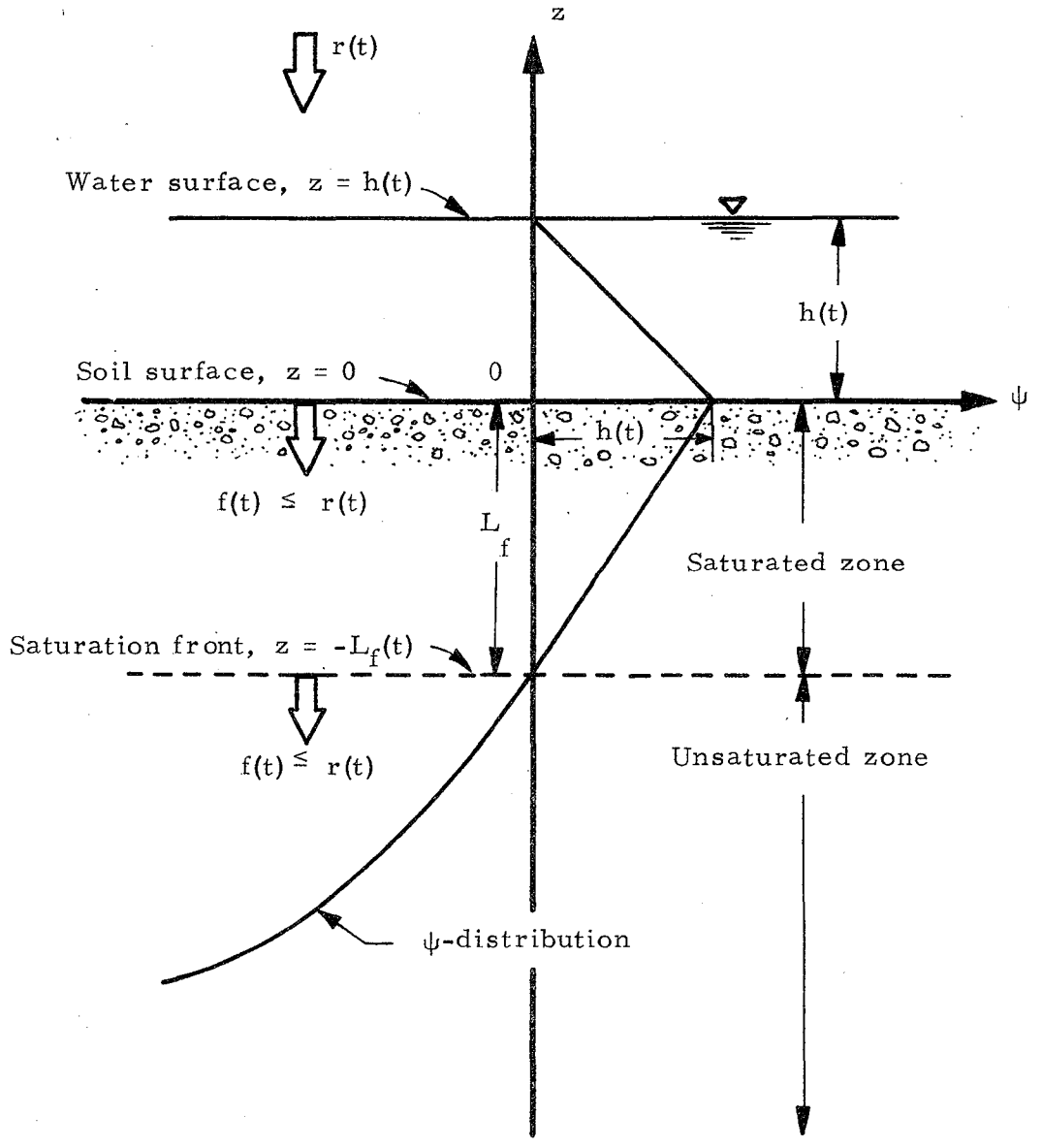

Figure 1. Definition sketch of rain infiltration after ponding.

$$L_f(t) = \frac{K_s h(t)}{\int_{-\infty}^{0} \frac{\partial \theta}{\partial t} dz + K_o - K_s} \quad . \quad . \quad . \quad . \quad . \quad . \quad (17)$$

Therefore, by knowing the total rate of change of the soil moisture content in the unsaturated zone (the first term in the denominator on the right side of Eq. 17, includes the total rate of change of θ in the saturated zone, but the total rate of change of θ in the saturated zone is assumed to be zero by implication), the $L_f(t)$ value can readily be computed. Use of Eqs. 16 and 17 at some critical points of time requires that a few comments be made here. At the time of ponding, because $h(t_p)$ and $L_f(t_p)$ are all zero, Eq. 16 becomes indeterminate. In other words, Eq. 16 is not valid at $t = t_p$ whereas Eq. 17 reduces to $L_f(t_p) = 0$. On the other hand, as $t \to \infty$, one obtains $f(t) \to K_s$ and $L_f(t) \to \infty$ from both Eqs. 16 and 17, respectively. If the $\psi(z, t)$- or $\theta(z, t)$-distributions computed are accurate, the f(t) values computed from Eqs. 10, 11, and 16, respectively, should not deviate very much from each other. However, given h(t), any error in the numerical computation of the θ value would cause errors in the computation of $L_f(t)$ by using Eq. 17, which in turn makes the f(t) calculation inaccurate by using Eq. 16. It will be shown later at some length in this report that oscillation in the computation of f(t) at the beginning of ponding is actually induced by this inaccuracy in the θ-distribution computation, and aggravated, especially, by the larger finite-difference space-step size, the higher rainfall intensity, the higher ponding depth, and/or the smaller initial moisture content. Nevertheless, the computational oscillation damps out quite quickly with the advancing saturation front as it proceeds deeper in the soil column.

After ponding, complications in the computation of the $\psi(z, t)$- or $\theta(z, t)$-distributions and hence the f(t) value have also been recognized by some investigators (Freeze, 1969; Smith and Woolhiser, 1971). Freeze imposed the upper boundary condition at the first unsaturated node while Smith and Woolhiser incorporated Eq. 15 into their implicit finite-difference scheme at the last saturated nodal point. To apply the upper boundary condition, either Eq. 3 before ponding or Eq. 4 after ponding, at the first unsaturated node is controversial because both Eqs. 3 and 4 do not accurately describe the situation at the saturation front. Use of Eq. 3 at the saturation front is only correct when $f(t) = r(t)$. This is the situation only when $t = t_p$. Smith and Woolhiser's approach in essence is similar to the one presented herein, but is taken without actually solving the location of the saturation front, L_f. Accuracy of both the present method and their approach are ultimately subjected to the accuracy of the computation of the f(t) value that can be evaluated by Eq. 10 (or Eq. 10 without K_o in Smith and Woolhiser's approach). It

would be more accurate for the explicit scheme to compute the exact location of the saturation front such as by using Eq. 17, especially when the saturation front is close to the soil surface.

Another approach proposed by Fujioka and Kitamura (1964) assumes a discontinuous propagation of pore pressure at the saturation front. Hornberger and Remson (1970) formulated two internal moving boundary conditions at the saturation front basing on that assumption. One of them appears to be very similar to that obtained by equating Eq. 11 to Eq. 16, provided that h(t) in this report can be regarded as the critical value of pressure head defined in their study. However, their other internal moving boundary condition, that ψ is equal to the critical value of pressure head, in no way corresponds to the one defined by Eq. 15, namely $\psi = 0$ at the saturation front. The difference in one of the boundary conditions prescribed at the saturation front was best explained by Hornberger and Remson as the difference in the moisture content versus pressure head relationships that the discontinuous propagation theory assumes as a first-order discontinuity while the other theory such as in this study assumes no existence of such discontinuity. Regardless of whether or not such discontinuity exists at the saturation front, the best model will probably be the one that recognizes an internal boundary (Hornberger and Remson, 1970).

Regarding the magnitude of the rainfall intensity, r(t), only those which are greater than K_s were investigated in the present report. However this limit on r(t) imposed herein can by no means be regarded as a restriction to the present mathematical model, Eqs. 1 through 5. The model can also apply to those rainfall intensities which are less than K_s. For example, particularly if $r(t) < K_o$, the total rate of change of the moisture content in the soil decreases and hence the $\psi(\theta)$- and $K(\theta)$-relationships in the drying process should be used instead.

The ponding depth of water, h(t), can be specified as large (or small) as desired. For example, Freeze (1969) set a maximum allowable limit on h(t) while Smith (1972) assumed it always zero. If a surface runoff model is incorporated with the present infiltration model for the surface runoff computation, h(t) has yet to be computed from the surface runoff model, as illustrated in Smith and Woolhiser's (1971) study. In the latter case, if the present model is adopted, h(t) is no longer given, but in fact becomes part of the solution because of its coupling with surface water. As a special case, if the soil surface under consideration is horizontal and of an infinite areal extent without specifying any upper limit in h(t), it follows from the mass continuity principle that

$$h(t) = \int_{t_p}^{t} [r(\tau) - f(\tau)]\, d\tau \qquad (18)$$

where τ is the integration variable for time, t. The differential equation in h(t) corresponding to Eq. 18 can be formulated as

$$\frac{dh}{dt} = r(t) - f(t) \qquad . \quad . \quad . \quad . \quad . \quad . \quad . \quad . \quad . \quad . \quad (19)$$

which is actually the continuity equation for flow of surface water on the horizontal surface.

Setting an arbitrarily fixed constant value on h(t) after ponding is physically impossible in reality, regardless of whether it is zero or not. In the present study, however, such a hypothetical boundary-value problem of rain infiltration was formulated so that the effect of h(t) on f(t) could be investigated.

Numerical Model

The finite-difference equation in an explicit scheme may be formulated by use of specified grid intervals in the z, t-plane. There are other numerical schemes (Richtmeyer, 1957) which can be used. In the present study, the z, t-plane is divided into a mesh of grid lines with grid or nodal points i = 1, 2, ..., m designated along z axis and j = 1, 2, ..., along t axis, as shown in Figure 2. The interval between the two distance grid lines is Δz and that between the two time grid lines is Δt. An association of any given variable with a given grid point (i, j) in the z, t-plane will be indicated by subscript, i, and superscript, j, such as θ_i^j. The soil surface will be denoted by i = 1, the wetting front by i = m, and the initial time level by j = 1. A fractional value of subscript or superscript indicates that the variable under consideration is evaluated at a point in an indicated fraction of the way between the two grid points. For instance, i + 1/2 denotes a point halfway between grid points i and i + 1.

By following the explicit finite-difference scheme of Richtmeyer (1957), Eqs. 1, 2, 3, 4, and 6 can be approximated by

$$\frac{\theta_i^{j+1} - \theta_i^j}{\Delta t} = \frac{1}{\Delta z}\left[K_{i-1/2}^j \frac{(\psi_{i-1}^j - \psi_i^j)}{\Delta z} - K_{i+1/2}^j \frac{(\psi_i^j - \psi_{i+1}^j)}{\Delta z}\right] + \frac{(K_{i-1/2}^j - K_{i+1/2}^j)}{\Delta z} \qquad \text{for } i = 2, 3, 4, \ldots \text{ and } j = 1, 2, 3, \ldots$$

$$. \quad . \quad . \quad . \quad . \quad . \quad . \quad (20)$$

$$\theta_i^1 = \theta_o \quad \text{for } i = 1, 2, 3, \ldots \qquad . \quad . \quad . \quad . \quad . \quad . \quad (21)$$

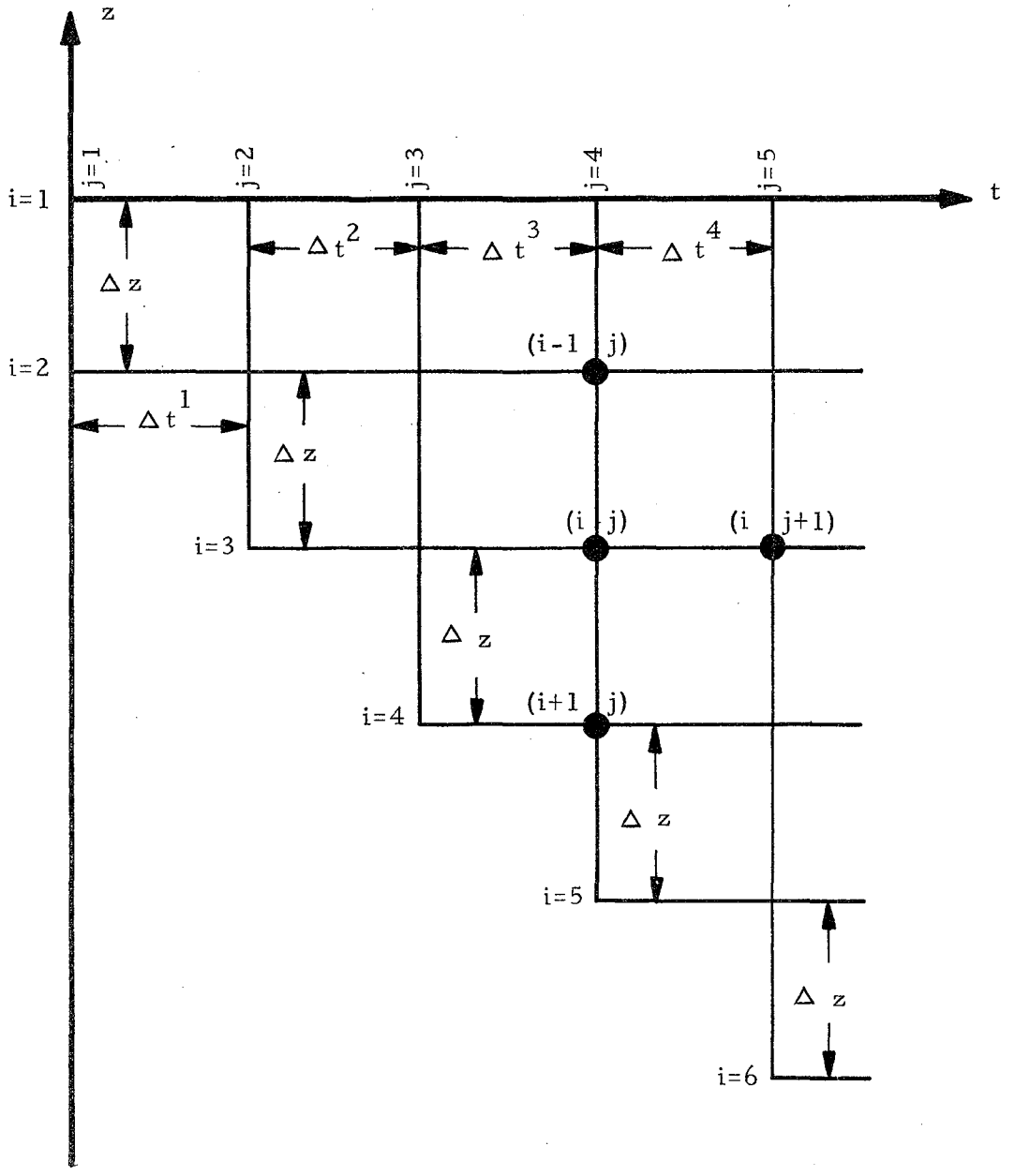

Figure 2. An explicit finite-difference scheme for semi-specified grid intervals on the z, t-plane.

$$K_{3/2}^{j+1} \frac{(\psi_1^{j+1} - \psi_2^{j+1})}{\Delta z} + K_1^{j+1} = r^{j+1} \quad \text{for } j = 1, 2, \ldots, n \qquad (22)$$

$$\psi_1^{j+1} = h^{j+1} \quad \text{for } j = n, n+1, \ldots \qquad (23)$$

$$\theta_1^n = \theta_s \qquad (24)$$

respectively. In Eq. 20, $K_{i-1/2}^j$ and $K_{i+1/2}^j$ are the hydraulic conductivities at time level j for those points halfway between grid points (i - 1) and i and halfway between grid points i and (i + 1), respectively. The hypothetical lower boundary condition at $z = -\infty$, Eq. 5, will not be utilized in the numerical computation, therefore it is not included in the numerical infiltration model that consists of Eqs. 20 through 24. At a glance, one might suspect that the proposed numerical model is a combination of explicit and implicit schemes in a sense that causes computational oscillation, but actually it is not that case. It is explicit all the way, namely unknowns are being solved for, one at a time. The numerical computation will begin with the finite-difference initial condition (Eq. 21), then proceed to determine unknowns for i = 2, 3, 4, ... at next time level by using Eq. 20, and finally end up for each time level with the solution of ψ or θ for i = 1 by means of the finite-difference boundary condition, Eq. 22 (before ponding) or 23 (after ponding), with Eq. 24 to be used as a criterion for determining the time of ponding. The fact that Rubin and Steinhardt (1963) also formulated a boundary condition similar to Eq. 22 in their linearized implicit-scheme model for rain infiltration does not necessarily mean that Eq. 22 cannot be used in the explicit-scheme model. Because Eq. 20 is valid for all i's except for i = 1 at time level (j + 1), the boundary condition such as Eq. 22 or 23 must be formulated at time level (j + 1) in order to solve for the remaining unknown at i = 1.

Finite-difference approximation of Eq. 3, as expressed by Eq. 22, has two approximate expressions of K. In Eq. 3, the first term in which K is multiplied by $\partial\psi/\partial z$ should also be designated on the same soil surface (i = 1) as the second term, but could not be done so because an approximation of $\partial\psi/\partial z$ could only be accomplished between grid points i = 1 and i = 2. This in effect forces K in the first term to be specified halfway between the two grid points. Equation 22 so formulated is somewhat different from Rubin and Steinhardt's (1963) formulation in which both K's were evaluated at i = 1, but without giving an enough account of how $\partial\psi/\partial z$ was approximated. Other investigators such as Smith and Woolhiser (1971) did more or less the same as Rubin and Steinhardt.

Ponding occurs at time level j = n, the value of which can be determined by use of Eq. 24. If Δt is invariable, ponding may or may not occur exactly at time level j = n. For convenience, in the present computation, only Δz is specified and varying Δt's are computed from the following stability criterion (Richtmeyer, 1957; Gupta and Staple, 1964):

$$\frac{D_{max}\,\Delta t}{(\Delta z)^2} \leq \lambda \qquad (25)$$

where D_{max} is the maximum effective diffusivity for a given moisture profile and λ is a constant. With a linearized form of Eq. 1 without a $\partial K/\partial z$ term, Richtmeyer (1957) obtained $\lambda = 0.5$. Since $K(\theta)$ varies with the soil depth, z, in the unsaturated zone, Eq. 1 is not linear in the present form. Despite Richtmeyer's $K = 5\theta^4$, it is questionable to use Eq. 25 as a criterion for stability of the explicit solution in the case that $K(\theta)$ varies considerably with the specified Δz. In other words, one can expect appreciable oscillation in the solution if the change in the soil moisture profile is rapid. As will be shown later, this situation actually occurred when the specified values of Δz, r, and h became too large and that of θ_o was too small. Despite this possible computational oscillation due to the preceding factors, Eq. 25 was applied to Eq. 20, for there seems no other available criterion which can be applied herein.

In general, use of Eq. 25 for all cells of the finite-difference mesh (Figure 2) at each time level permits the computation of the respective Δt values for each cell and from them the one, whichever is smaller, will be selected as a Δt for next calculation. Therefore, given a λ value which is arbitrarily chosen to be close to 0.5, the Δt can be computed from Eq. 25 as

$$\Delta t \leq \frac{\lambda(\Delta z)^2}{D_{max}} \qquad (26)$$

After the Δt is determined, the computation of the unknown θ_i^{j+1} for various i and j values by use of Eqs. 20 through 24 can proceed in the following orderly way.

For grid points other than i = 1

The values of ψ and K at grid points i - 1, i and i + 1 at time level j, as shown in Figure 2, can be used to compute the θ value at grid point i and time level j + 1 from Eq. 20. Let $(RHS)_i^j$ represent the right-hand side of Eq. 20. Then, from Eq. 20

$$\theta_i^{j+1} = \theta_i^j + (RHS)_i^j \Delta t \qquad (27)$$

Because the ψ and K values in $(RHS)_i^j$ are actually used in the computation of the θ_i^{j+1} value, any slight error in the ψ computation at time j, especially around the saturation front, would reflect in the computation of the θ_i^{j+1} value that may sometimes exceed θ_s. If this situation happens, the θ value at a grid point under consideration will then be set at θ_s and it will be assumed that the saturation front already arrived at or passed that grid point. The exact location of the saturation front can be determined by means of Eq. 17. If the saturation front so computed stays in between two grid points such as $i - 1$ and i, it would be more accurate to weigh the K value at respective grid points according to the exact location of the saturation front. A linear weighing technique can be used for this purpose. The computation of θ_i^{j+1} by means of Eq. 27 is thus straightforward.

For grid point $i = 1$ with $j \leq n$

If the ψ_2^{j+1} value was already computed by using Eq. 20 at $i = 2$, the ψ_1^{j+1} value on the upper boundary can be determined by means of Eq. 22, in which the rainfall intensity at time level $j + 1$, r^{i+1}, is also given. Because $K_{3/2}^{j+1}$, K_1^{j+1}, and ψ_1^{j+1} are all related to θ_1^{j+1} through the known physical property relationships of soil, Eq. 22 can be solved for ψ_1^{j+1} by trial and error. The iteration of the computation can proceed by first assuming $\theta_1^{j+1} \approx \theta_1^j$. Then compute $K_{3/2}^{j+1}$ and K_1^{j+1} from the known $K(\theta)$ relationship as follows: Substituting the expressions

$$\theta_{3/2}^{j+1} = (\theta_1^{j+1} + \theta_2^{j+1}) /2 \quad . \quad . \quad . \quad . \quad . \quad . \quad . \quad . \quad (28)$$

$$K_{3/2}^{j+1} = K(\theta_{3/2}^{j+1}) \quad . \quad . \quad . \quad . \quad . \quad . \quad . \quad . \quad . \quad . \quad (29)$$

$$K_1^{j+1} = K(\theta_1^{j+1}) \quad . \quad . \quad . \quad . \quad . \quad . \quad . \quad . \quad . \quad . \quad (30)$$

into Eq. 22 yields ψ_1^{j+1} for known ψ_2^{j+1}. The computed ψ_1^{j+1} value in turn will be substituted into the $\psi(\theta)$ relationship for θ_1^{j+1}. If the difference between the computed θ_1^{j+1} from the $\psi(\theta)$ relationship and the initially assumed θ_1^{j+1} is found to be within the tolerable accuracy, Eq. 22 is solved. Otherwise assume the θ_1^{j+1} value just computed in the last step and follow the foregoing computation procedure until the accuracy is met. The iteration can be accomplished in a systematic way.

For grid points in the saturated zone

The Laplace equation, Eq. 14, in the finite-difference form can be formulated to compute the ψ_i^{j+1} values for $i = 2, 3, 4, \ldots$, up to the last saturated nodal point as follows:

$$\psi_{i-1}^{j+1} - 2\psi_i^{j+1} + \psi_{i+1}^{j+1} = 0 \quad . \quad . \quad . \quad . \quad . \quad . \quad . \quad . \quad (31)$$

Since $\psi(z)$-profile is linear in the saturated zone, Eq. 15 can be used instead of Eq. 31. Recalling the upper boundary condition after ponding, Eq. 23, one can formulate Eq. 15 in the finite-difference form as

$$\psi_i^{j+1} = \left(\frac{f^{j+1} - K_s}{K_s} \right) (i - 1)\, \Delta z + \psi_1^{j+1} \quad . \quad . \quad . \quad . \quad . \quad (32)$$

where the current infiltration rate, f^{j+1}, is computed by using Eq. 10 in the finite-difference form:

$$f^{j+1} = \sum_{i=1}^{\infty} (1/2)(\theta_i^{j+1} - \theta_i^j + \theta_{i+1}^{j+1} - \theta_{i+1}^j) \frac{\Delta z}{\Delta t} + K_o \quad . \quad . \quad . \quad (33)$$

Actually, f(t) computed by using Eq. 33 corresponds more closely to $f^{j+1/2}$ than to f^{j+1}. Accordingly, the ψ value computed from Eq. 32 should be at time level (j + 1/2) rather than (j + 1) for given ponding depth, $\psi_1^{1+1/2}$, at the corresponding time level. There certainly will be a time lag, $\Delta t/2$, for ψ and f values so computed at each time level, but the computed values will in no way be affected by the time lag.

Before one computes the $\psi(z)$-profile in the saturated zone, the θ (z)-profile in the unsaturated zone must be determined. As mentioned previously, the ψ value in the saturated zone so computed could be in a significant error if the current f^{j+1} computation for the unsaturated zone by using Eq. 33 is not accurate enough. In other words, the inaccuracy in the computation of the current f^{j+1} value would result in the erroneous computation of the location of the current saturation front, L_f^{j+1} by using Eq. 17, and hence the current ψ_1^{j+1} values in the saturated zone by using Eq. 32. The apparent interaction in the computation of the ψ_1^{j+1} and f^{j+1} appearing in both Eqs. 32 and 33 may result in computational oscillation which, however, damps out quickly with the advancing saturation front.

Use of Eq. 16 in the evaluation of the infiltration rate, f(t), has a problem at the time of ponding, t_p, when both $h(t_p)$ and $L_f(t_p)$ become zero, as pointed out previously. Therefore, Eq. 16 cannot be used in the computation of f(t). Instead, Eq. 10 or, more specifically a finite-difference form thereof, Eq. 33 was used throughout the study. Use of Eq. 33 does not require the exact location of the saturation front, $L_f(t)$, for the total rate of change of the moisture content in the saturated zone is always assumed to be zero. Furthermore, because the present method requires that the moisture content in the unsaturated zone at the current time level (j + 1) be computed before proceeding to compute ψ in

the saturated zone, there should not be any technical difficulty in determining $L_f(t)$ from Eq. 17 in which f(t) is approximated by Eq. 33. Of course, the accuracy of $L_f(t)$ so determined depends on how well Eq. 33 can approximate f(t), which is in turn dependent upon the accuracy of θ for all nodal points in the unsaturated zone.

It is understood that in any numerical scheme, explicit or implicit, the roundoff error is generally caused by a combination of numerous factors including the step size in space (Δz) and time (Δt) and additional assumptions or conditions imposed in the computation. If the θ value varies rapidly with the soil depth (i.e., the cases usually associated with very large Δz, r, and h or very small θ_o, as mentioned before), determination of θ by using Eqs. 20 and 22 may not be sufficiently accurate. Since Eq. 33 was also used in the approximation of f(t) before ponding, the inaccuracy of using Eq. 33 before and after ponding manifested itself on the infiltration decay curve in the form of oscillation, as will be shown later in this report.

Soil properties $\psi(\theta)$ and $K(\theta)$ relationships

The physical properties of soil such as the $\psi(\theta)$ and $K(\theta)$ relationships are required in the solution of the numerical model, Eqs. 20 through 24. In the present study, sandy clay loam at the Hullinger Farm near Vernal, Utah, was selected and tested. The $\psi(\theta)$ and $K(\theta)$ relationships as determined by Nimah and Hanks (1973) were used. The moisture diffusivity, $D(\theta)$, was determined by using its definition

$$D(\theta) = K(\theta) \frac{d\psi(\theta)}{d\theta} \quad . \quad . \quad . \quad . \quad . \quad . \quad . \quad . \quad . \quad . \quad (34)$$

For illustration, these soil property relationships are shown in Figures 3 through 5 and also tabulated in Table 3. It can readily be seen from Figure 5 and Table 3 that the shape of the $D(\theta)$ relationship is quite irregular. In the modeling, it is thus much easier and more reliable to use the $\psi(\theta)$ relationship than the $D(\theta)$ relationship.

The aforementioned procedures of computation and the functional relationships of soil properties for Vernal sandy clay loam are programmed in Fortran V and executed in the UNIVAC 1108 computer for validation of the present finite-difference model.

Computer Results

Many computer runs were conducted for the purpose of examining the validity and performance characteristics of the present numerical model. Computer results for a typical run are shown in Figure 6, in which the θ-profiles, the ψ-distributions in the saturated zone, and the ponding

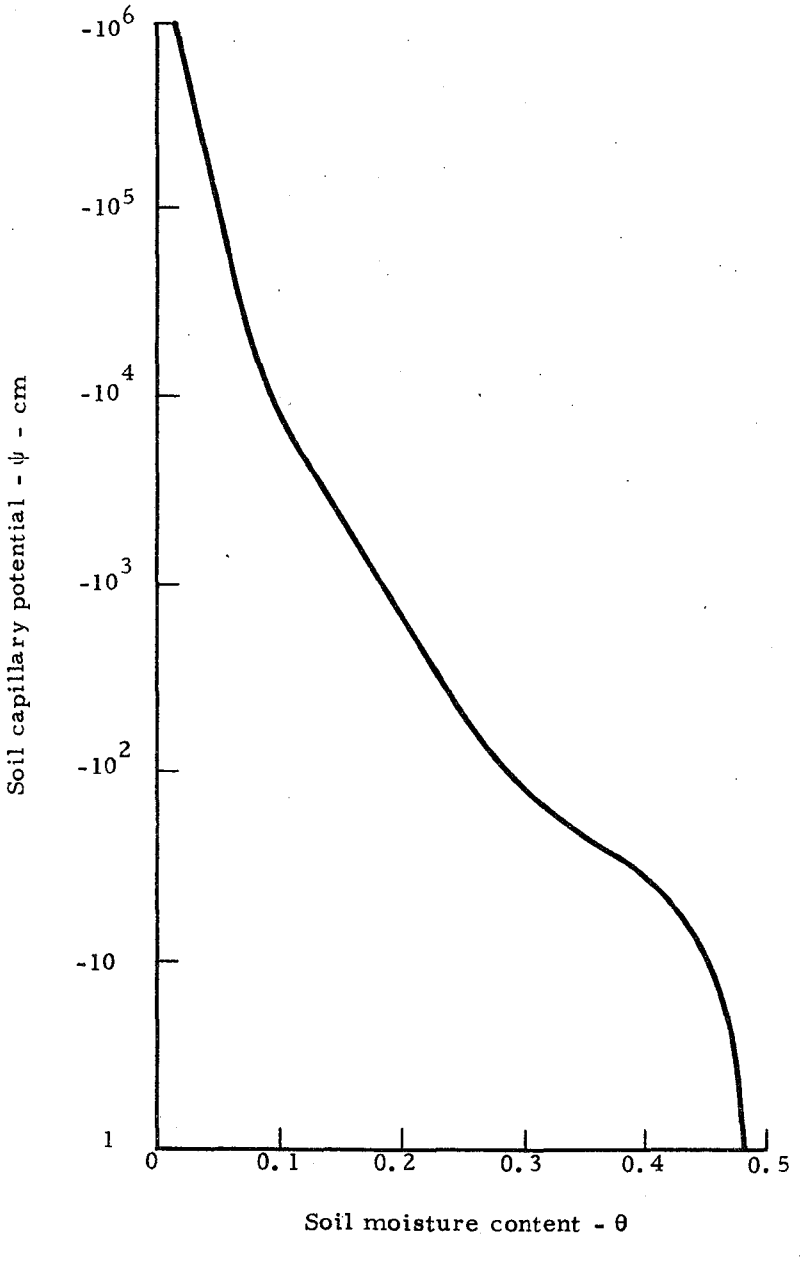

Figure 3. Functional relationship between soil capillary potential (ψ) and soil moisture content (θ) for Vernal sandy clay loam.

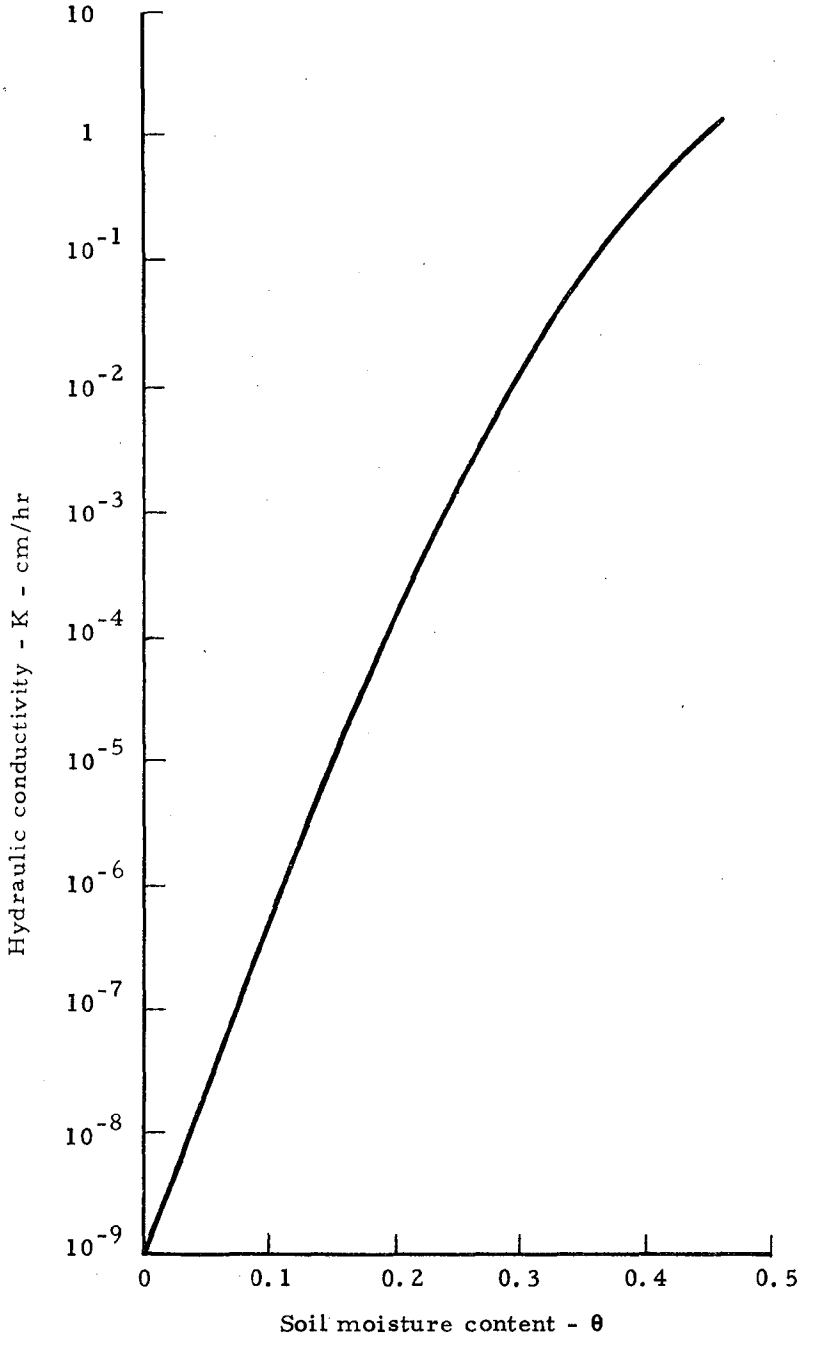

Figure 4. Functional relationship between hydraulic conductivity (K) and soil moisture content (θ) for Vernal sandy clay loam.

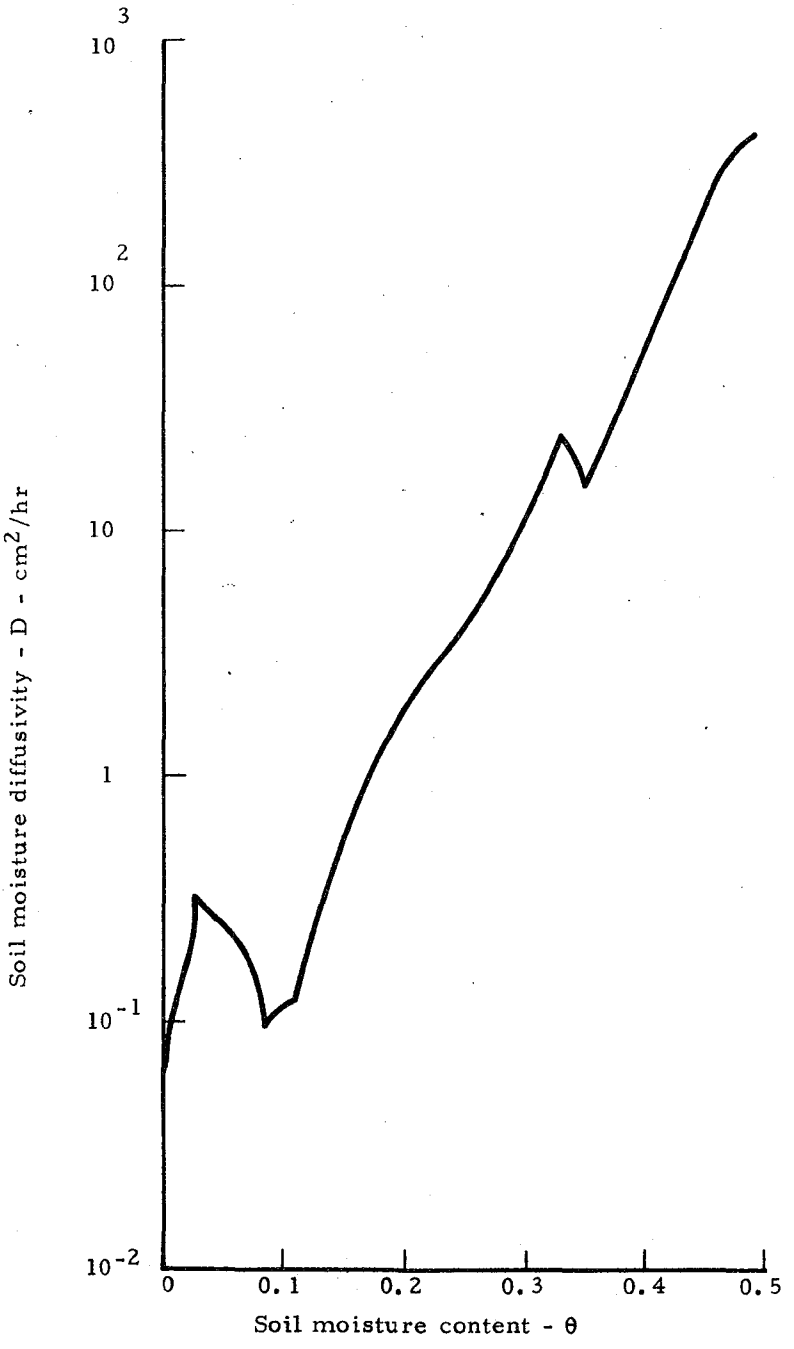

Figure 5. Functional relationship between soil moisture diffusivity (D) and soil moisture content (θ) for Vernal sandy clay loam.

Table 3. Physical properties of Vernal sandy clay loam used in the computation.

θ	$\psi(\theta)$ cm	K(θ) cm/hr	D(θ) cm^2/hr
0	-2.0×10^{6}	1.0×10^{-9}	7.00×10^{-2}
.01	-1.3×10^{6}	2.0×10^{-9}	1.15×10^{-1}
.02	-8.5×10^{5}	3.4×10^{-9}	1.50×10^{-1}
.03	$-42. \times 10^{5}$	1.0×10^{-8}	3.15×10^{-1}
.04	-2.2×10^{5}	1.7×10^{-8}	2.59×10^{-1}
.05	-1.2×10^{5}	3.0×10^{-8}	2.43×10^{-1}
.06	-5.8×10^{4}	5.4×10^{-8}	2.29×10^{-1}
.07	-3.0×10^{4}	9.2×10^{-8}	1.98×10^{-1}
.08	-1.5×10^{4}	1.6×10^{-7}	1.52×10^{-1}
.09	-1.1×10^{4}	2.7×10^{-7}	9.45×10^{-2}
.10	-8.0×10^{3}	4.8×10^{-7}	1.15×10^{-1}
.11	-6.2×10^{3}	7.5×10^{-7}	1.16×10^{-1}
.12	-4.9×10^{3}	1.5×10^{-7}	1.65×10^{-1}
.13	-4.0×10^{3}	2.5×10^{-6}	2.38×10^{-1}
.14	-3.0×10^{3}	4.5×10^{-6}	3.71×10^{-1}
.15	-2.4×10^{3}	8.7×10^{-6}	5.00×10^{-1}
.16	-1.9×10^{3}	1.4×10^{-5}	6.30×10^{-1}
.17	-1.5×10^{3}	2.5×10^{-5}	9.13×10^{-1}
.18	-1.1×10^{3}	4.5×10^{-5}	1.30
.19	-8.7×10^{3}	7.5×10^{-5}	1.69
.20	-6.7×10^{2}	1.1×10^{-4}	1.87
.21	-5.3×10^{2}	1.7×10^{-4}	2.21
.22	-4.1×10^{2}	2.7×10^{-4}	2.83
.23	-3.2×10^{2}	4.0×10^{-4}	3.20
.24	-2.5×10^{2}	6.1×10^{-4}	3.66
.25	-2.0×10^{2}	9.5×10^{-4}	4.04
.26	-1.7×10^{2}	1.5×10^{-3}	4.87
.27	-1.4×10^{2}	2.4×10^{-3}	6.00
.28	-1.2×10^{2}	3.5×10^{-3}	6.30
.29	-9.9×10	5.5×10^{-3}	8.25
.30	-8.5×10	9.0×10^{-3}	1.12×10
.31	-7.4×10	1.4×10^{-2}	1.40×10
.32	-6.5×10	2.1×10^{-2}	1.89×10
.33	-5.6×10	2.8×10^{-2}	2.38×10
.34	-4.8×10	3.5×10^{-2}	2.00×10
.35	-4.5×10	4.6×10^{-2}	1.55×10
.36	-4.1×10	6.0×10^{-2}	2.13×10
.37	-3.8×10	7.9×10^{-2}	2.71×10
.38	-3.4×10	1.0×10^{-1}	3.17×10
.39	-3.1×10	1.3×10^{-1}	4.62×10
.40	-2.7×10	1.7×10^{-1}	5.94×10
.41	-2.4×10	2.3×10^{-1}	7.30×10
.42	-2.1×10	3.1×10^{-1}	1.08×10^{2}
.43	-1.7×10	4.1×10^{-1}	1.56×10^{2}
.44	-1.3×10	5.4×10^{-1}	1.89×10^{2}
.45	-1.0×10	6.9×10^{-1}	2.20×10^{2}
.46	-7.0	8.8×10^{-1}	3.07×10^{2}
.47	-3.2	1.0	3.60×10^{2}
.48	0	1.3	4.13×10^{2}

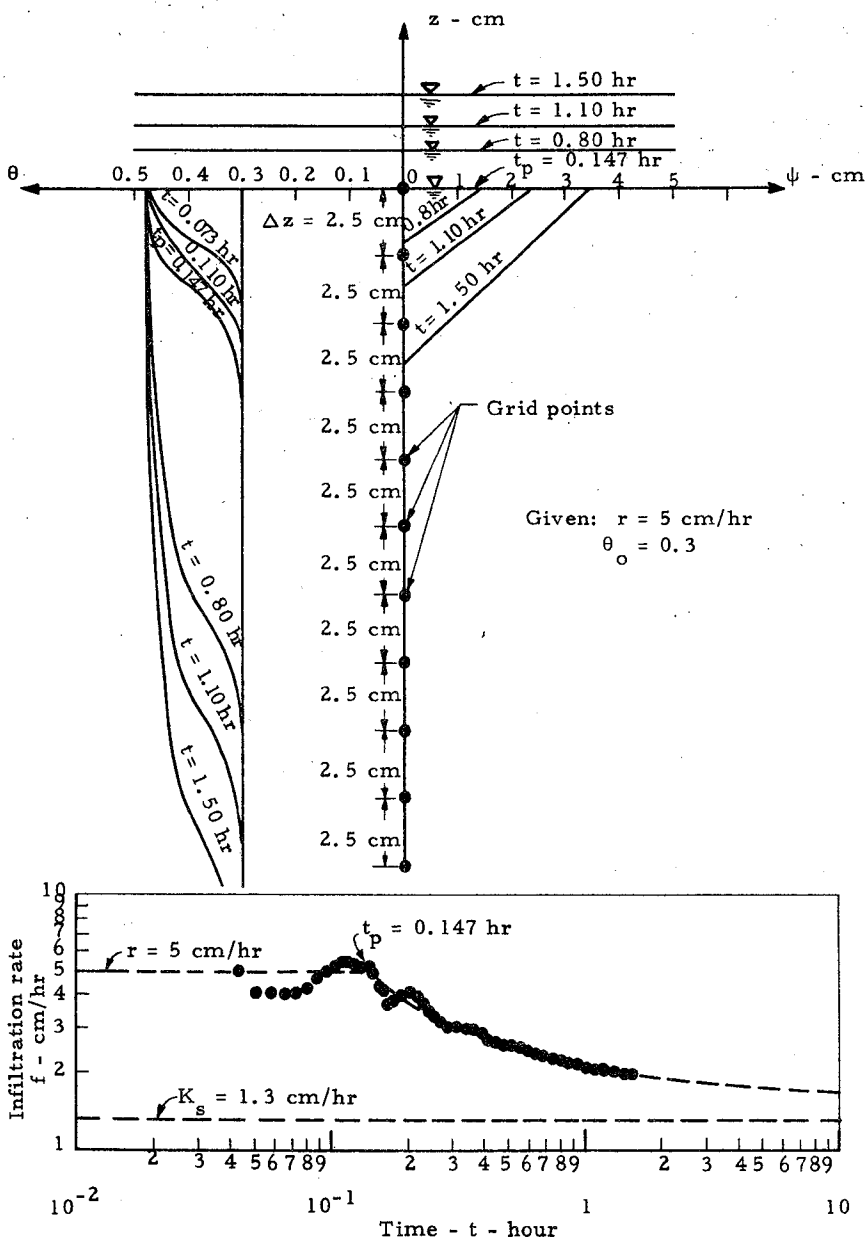

Figure 6. Typical computer solutions for rain infiltration.

depth variations are all plotted on ordinary scale, but the infiltration decay curve is drawn on log-log scale. In this typical problem, the initial moisture content, θ_o, of Vernal sandy clay loam is specified arbitrarily at 0.30 and the given rainfall intensity, r, is 5 cm/hr. For simplicity, the soil surface is assumed horizontal so that Eq. 18 is applied to the computation of the ponding depth, h. As expected, computational oscillation is significantly large at the beginning of the computation, but quickly damps out after t_p = 0.147 hours. The computed infiltration rate (marked by dots) is compatible with the ''theoretical'' curve (marked by a broken line) that consists of the 5 cm/hr line from Eq. 3 before ponding and, of course, an unknown decay curve after ponding. A theoretical decay curve after ponding cannot be exactly plotted. The broken curve after ponding plotted in Figure 6 is merely a line connecting those computed points which do not seemingly fluctuate or, in the more strict sense, a best-fit line of the computed points.

The oscillation also manifests itself on the saturation front depth (L_f) versus time curve and the ponding depth versus time relationship, as shown in Figure 7. For illustration of the significance of oscillation at early stage, they are also plotted on log-log scale. It is conceivable that oscillation in the computer results appears in the computation of all the f(t), L_f(t), and h(t) values because of their interrelated roles through Eqs. 16, 17, and 18.

The validity of the present numerical model and the accompanying computational oscillation due to the adopted numerical scheme were further investigated by solving a hypothetical problem which was so formulated that the performance characteristics and the related or interrelated roles of variables in the model could manifest themselves in the solution. For example, the magnitude of the infiltration rate after ponding depends largely on the ponding depth and this dependence varies with infiltration time (Philip, 1958). However, the ponding depth that changes with time cannot be determined unless surface flow conditions are known. Only for water on the horizontal soil surface, can the ponding depth be computed by using Eq. 18. Therefore, for convenience, the ponding depth was hypothetically assumed constant immediately after ponding. The hypothetical ponding depth imposed is similar to a physical situation under which an infiltrometer operates after a brief intake of irrigated water to the saturation point.

Each of the possible factors which may affect the accuracy of the numerical model was tested and its computer results are briefly discussed in the following.

Effect of space-step size (Δz)

The computed infiltration decay curves depicted in Figure 8 are the computer results of a hypothetical immediate-ponding rain infiltration problem with the rainfall intensity (r) of 200 cm/hr and the assumed ponding depth (h) of 4 cm after ponding, using various space-step (Δz)

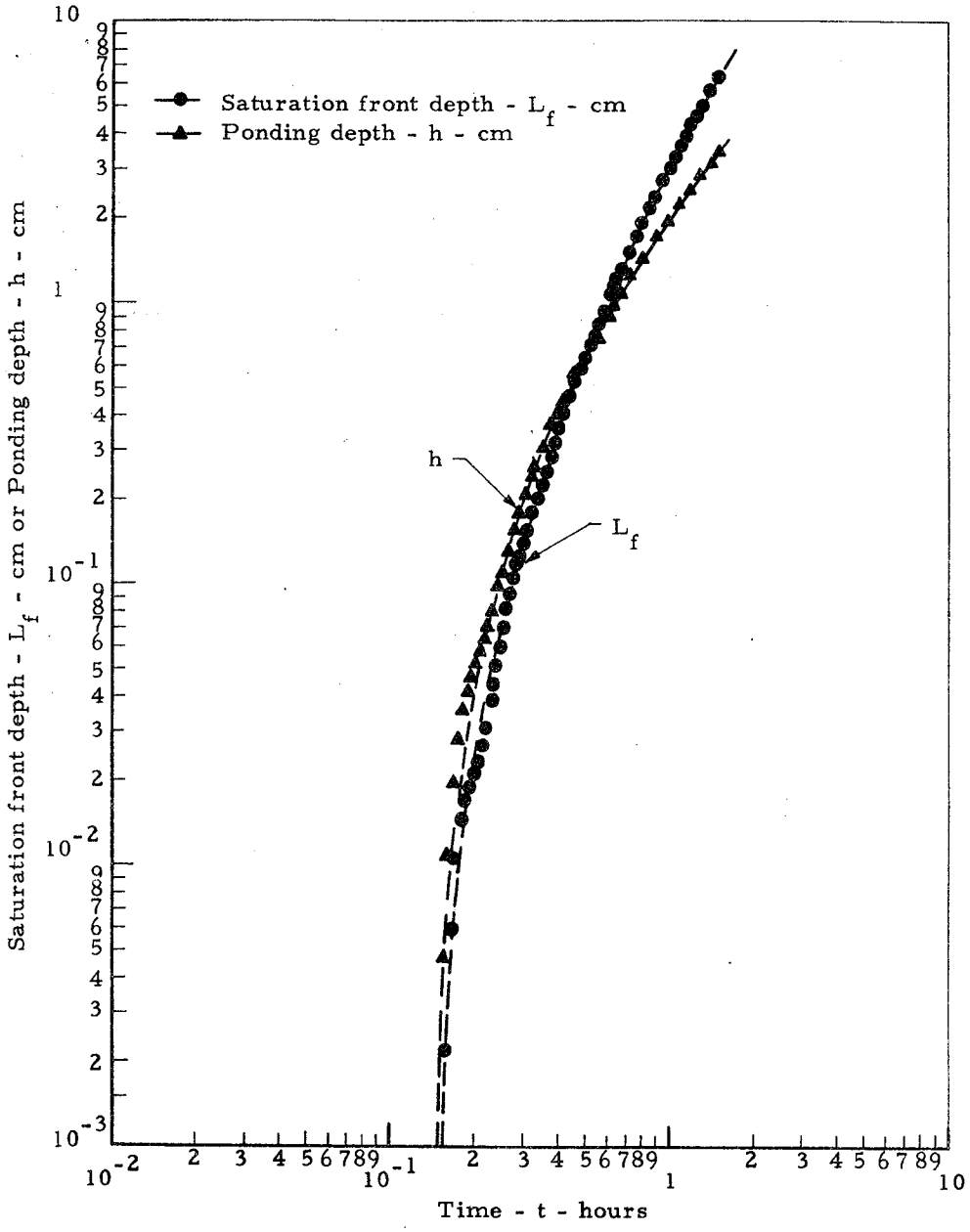

Figure 7. Saturation front depth (L_f) versus time (t) and ponding depth (h) versus time (t) relationships.

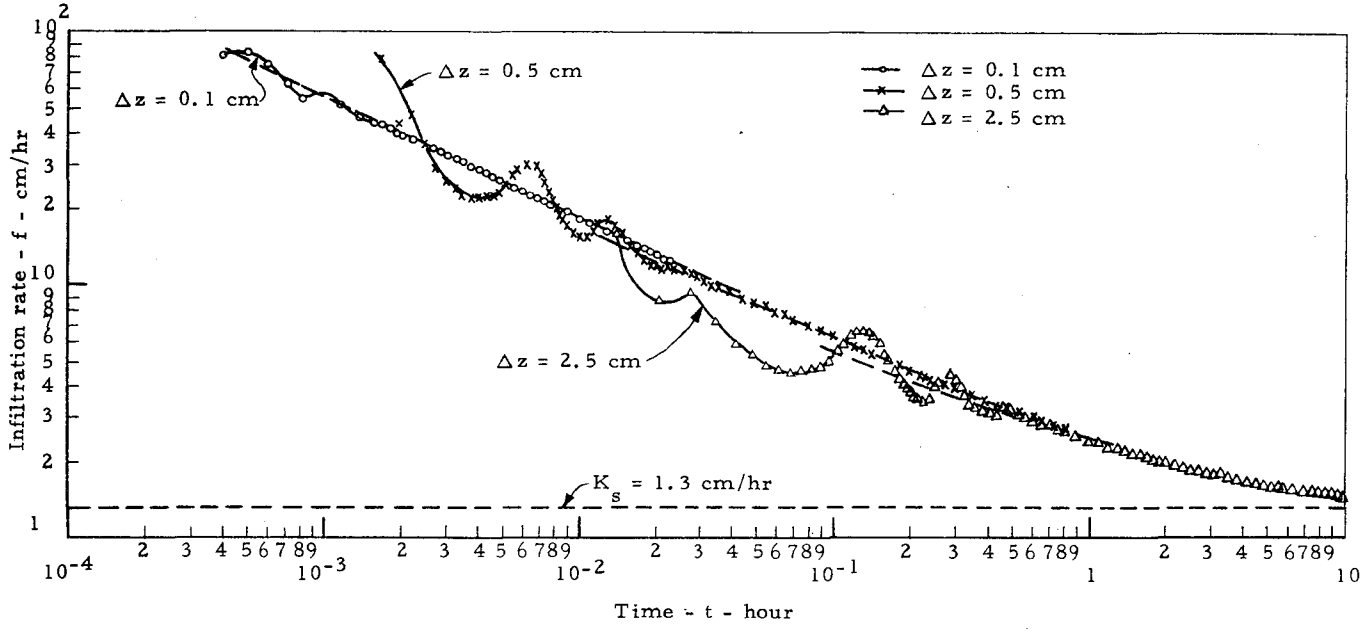

Figure 8. Examples of the effect of space-step (Δz) size on computed infiltration rate (f) under a hypothetical immediate ponding situation.

size. The infiltration decay curves are plotted on log-log paper in order to assure a complete functional relationship between f and t with a broad range of both the infiltration rate and time scale, including especially the portion of the high infiltration rate shortly after ponding. The computed f before ponding and t_p are not shown in Figure 8 because the imposed rainfall intensity is so high that even with the first Δt tried, the boundary condition before ponding, Eq. 22, was never used in the computation. Three different space-step sizes such as 0.1, 0.5, and 2.5 cm were tested. It can readily be seen from Figure 8 that the smallest space-step size yields the best results. As the Δz size increases, oscillation is magnified and prolonged. A best-fit line connecting the computed points for each Δz size can be drawn as marked in broken line (Figure 8). It appears that the best-fit line for $\Delta z = 0.1$ cm merges in the best-fit line for $\Delta z = 0.5$ cm which subsequently merges in the best-fit line for $\Delta z = 2.5$ cm and so forth, in essence becoming one single best-fit infiltration decay curve. In other words, if the infiltration rate computation could be reversed, starting at $t = \infty$, a larger Δz could cause the earlier occurrence in oscillation and an eventual breakdown. From the accuracy point of view, it is apparently more accurate to use the smaller Δz in the computation. Despite a large Δz used, a divergence problem did not seem to occur on many computer runs tested herein. Because the finite-difference computation with a very small Δz is time consuming and expensive, use of a small Δz cannot be justified unless one is only interested in the accuracy of the solution. In view of the necessity of considering both accuracy and efficiency involved in a particular computer run, the range of interest associated with the computation of the infiltration rate versus time must be taken into account in the selection of a suitable Δz size.

Figure 8 demonstrates the differences in the range of the computed infiltration rate for the three different Δz sizes used in the computation, given the various lengths of computer time (e.g., UNIVAC 1108 CPU time 95 seconds for $\Delta z = 0.1$ cm up to $t = 0.02$ hours, 155 seconds for $\Delta z = 0.5$ cm up to $t = 0.8$ hours, and 64 seconds for $\Delta z = 2.5$ cm up to $t = 10$ hours). Computer output for each Δz size used is labeled in different symbols. An inspection of Figure 8 reveals that using a Δz size of either 0.1, 0.5, or 2.5 cm could yield approximately the same infiltration decay curve at about half an hour after ponding. However, in terms of computer time involved in the computation, use of $\Delta z = 2.5$ cm would be more than twenty times less expensive than that of $\Delta z = 0.5$ cm as far as that range of the infiltration rate (i.e., $t > 0.5$ hours) is concerned. In another case, if one is interested in the infiltration rate shortly after ponding, say $t < 0.002$ hours (or 7.2 seconds), a Δz size of 0.1 cm or less should be used. Use of a Δz size of 0.5 or 2.5 cm in the latter case is obviously not adequate.

Effect of initial moisture content (θ_o)

Different initial moisture contents were tested to determine the effect of initial moisture content on the accuracy of the present

finite-difference model. For comparison, an equal Δz size, 2.5 cm, was used and values of all variables except θ_o were kept constant in the computation of the same hypothetical conditions shown in Figure 8. Computed infiltration decay curves for θ_o equal to 0.1, 0.2, 0.3, and 0.4, by using about the equal length of computer time were depicted in different symbols, as shown in Figure 9. As anticipated, the higher the initial moisture content, the smaller the computational oscillation. When the initial moisture content is high such as 0.4, close to saturation, the infiltration rate computed by means of Eq. 33 does not appear to have a large error for $t > 0.1$ hours. As the value of θ_o decreases, computational oscillation, although damped out in the end, is amplified and prolonged. The present finite-difference model, was tested and shown to be valid up to $\theta_o = 0.01$, but it broke down for θ_o less than 0.01. The failure may be attributed to the accuracy of computation specified in interpolating the physical properties of soil for θ less than 0.01 (see Table 2). There seems no apparent difficulty in testing the upper limit of θ_o value.

Effect of ponding depth (h)

Various immediate ponding situations with the ponding depth, h, equal to 0, 4, 16, and 64 cm were tested on the same finite-difference model, as shown in Figure 10, with the Δz size this time being kept at 0.5 cm and $\theta_o = 0.2$. It can readily be seen from Figure 10 that computational oscillation is amplified and prolonged as the ponding depth increases. Especially, at h = 64 cm, the computation by using a Δz size of 0.5 cm has come near the margin of breakdown, as demonstrated by big fluctuations a, b, and c, in Figure 10. This result clearly indicates that a smaller Δz size should be used with such a big ponding depth.

Combined effect of rainfall intensity (r) and space-step size (Δz)

To test the effect of the rainfall intensity, r, on the accuracy of the present numerical model requires the proper selection of Δz sizes for the different r values under study, though a very small Δz always makes all the computations possible. As shown in Figure 11, $\Delta z = 0.1$, 0.25, 0.5, and 2.5 cm are used in the analysis of problem involving r = 50, 25, 10, and 5 cm/hr, respectively. Computed infiltration rates for different r values are marked in different symbols and compared with a best-fit infiltration decay curve (broken line) which is replotted from Figure 8 for a hypothetical immediate ponding case. Unlike the results shown in Figure 6, the computed infiltration rate in Figure 11 for each r suddenly rises at the time of ponding. There are two possibilities which may cause this rapid rise in the computed f value at the time of ponding: One is a discontinuity in the upper boundary condition imposed at the time of ponding and the other, a discontinuity in the θ-ψ relation at saturation beyond which θ cannot increase whereas ψ can (i.e., the diffusivity becomes undefined). In Figure 6 the h value that changes

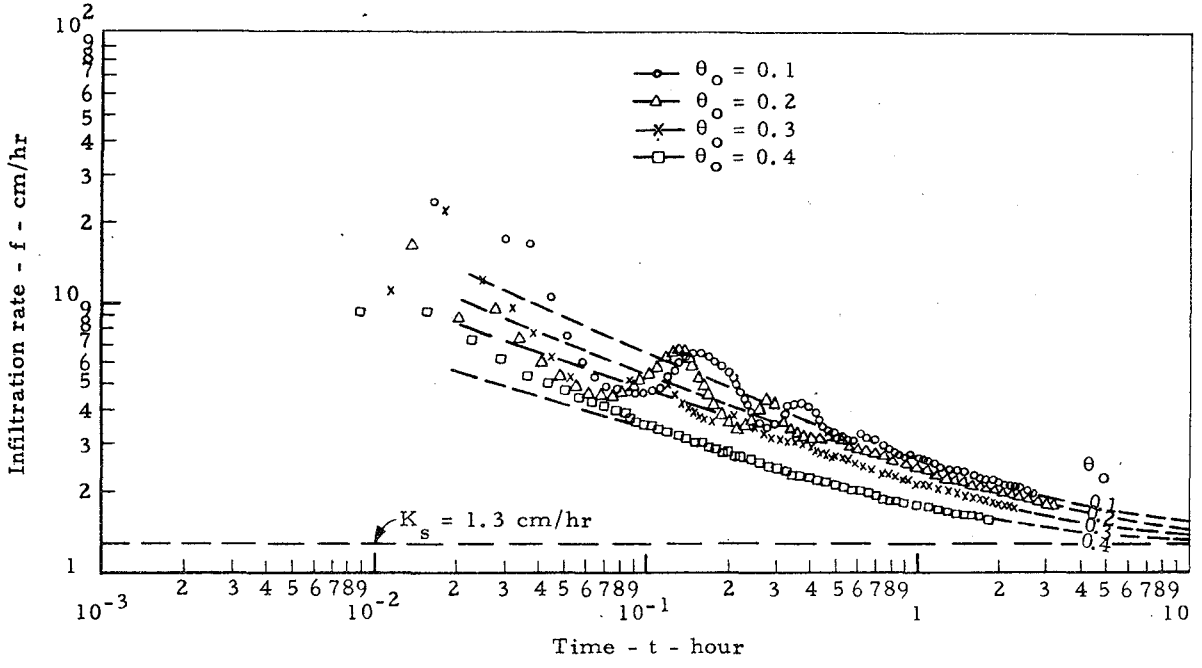

Figure 9. Examples of the effect of initial moisture content (θ_o) on computed infiltration rate (f) under a hypothetical immediate ponding situation.

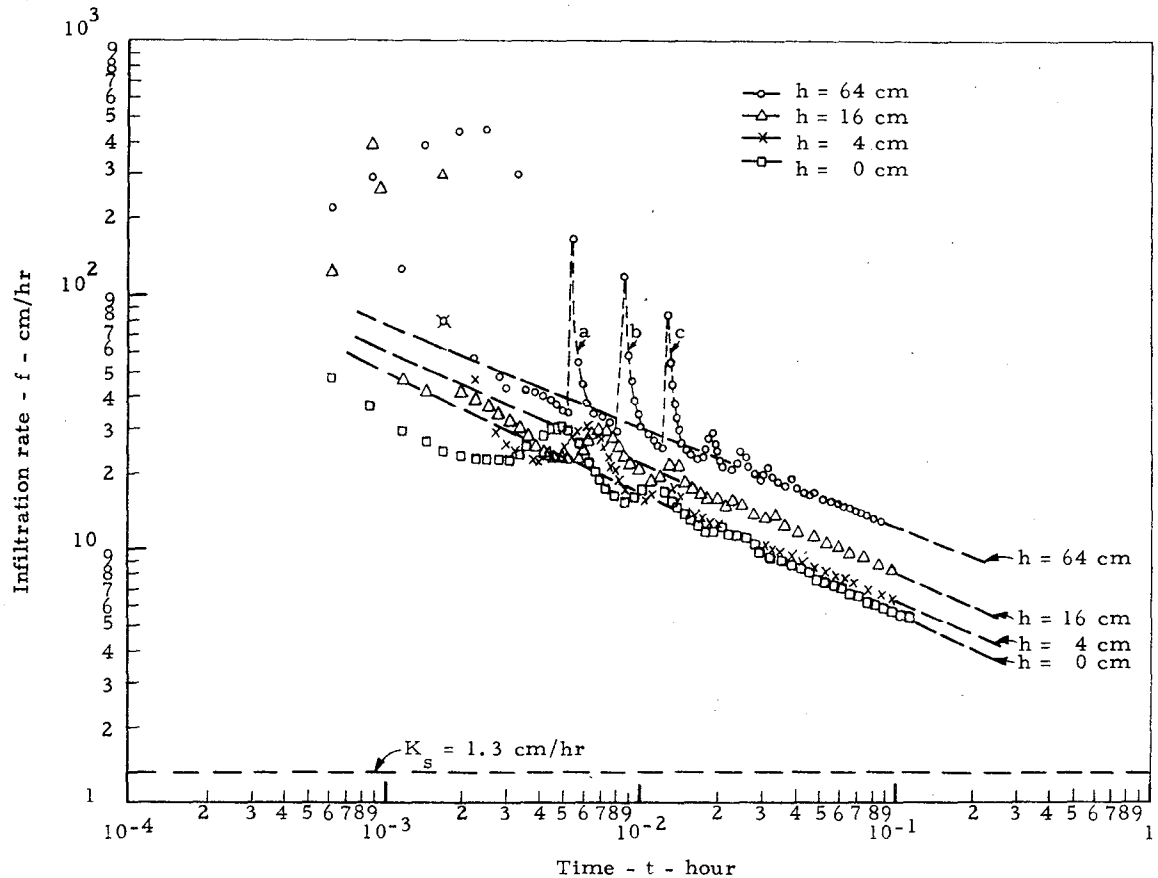

Figure 10. Examples of the effect of ponding depth (h) on computed infiltration rate (f) under various hypothetical immediate ponding situation.

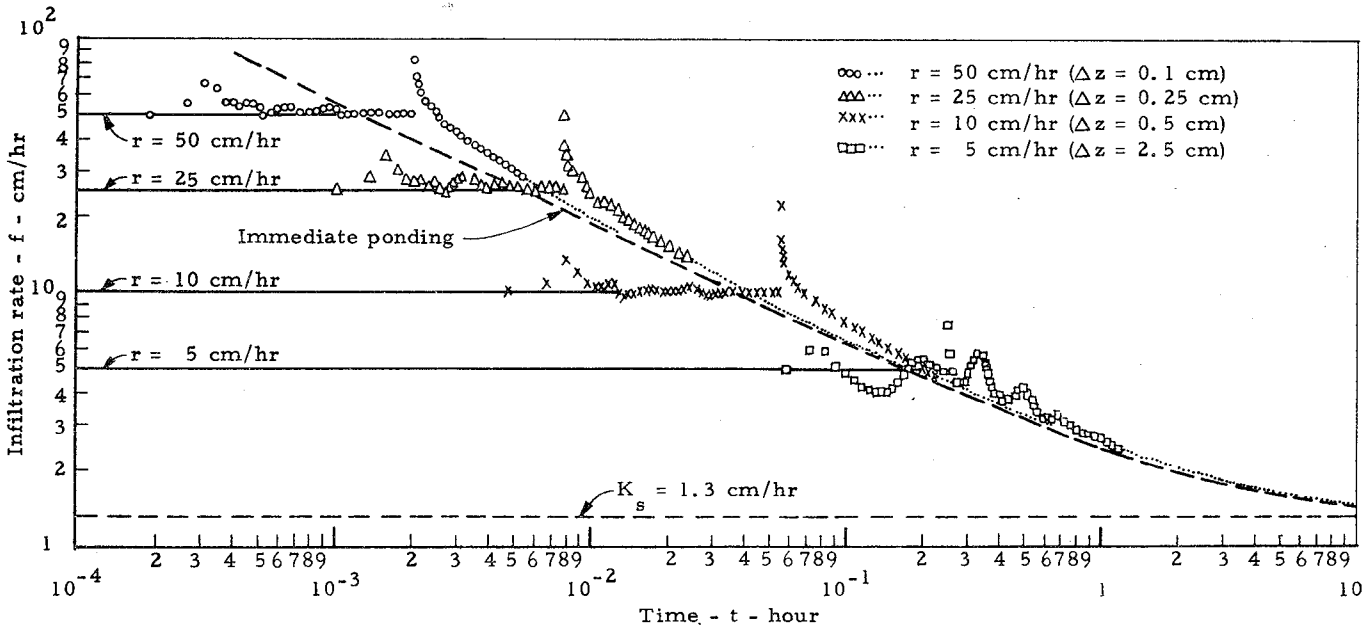

Figure 11. Examples of the combined effect of rainfall intensity (r) and space-step (Δz) size on computed infiltration rate (f).

gradually from zero was obtained from Eq. 18, while in Figure 11 the h value was fixed at 4 cm immediately after ponding. As mentioned previously, an imposition of the h value, if different from zero, after ponding could become a source of computational oscillation at the time of ponding. Nevertheless, if computational oscillation damps out before ponding starts, such as the cases for all r's except r = 5 cm/hr in Figure 11, the discontinuity in the upper boundary condition can only cause a big single rise in the computed f at the time of ponding. On the other hand, if computational oscillation has not damped out yet before ponding starts, such as the case of r = 5 cm/hr, the computational oscillation continues for a while even after ponding. It is not surprising to see from Figure 11 that all the computed infiltration decay curves for the various r values become asymptotic at large t to the best-fit infiltration decay curve for a hypothetical immediate ponding case.

The idealized rain infiltration process was modeled by using the Richards equations and appropriately prescribed initial and boundary conditions. The computed infiltration rate by means of an explicit finite-difference scheme exhibits oscillation at the beginning of computation. However, a few computer experiments did show that the computational oscillation was improved by the proper selection of a space-step (Δz) size while still maintaining the efficiency and accuracy of the computation. Error analysis showed that no divergence problem occurred on the computed infiltration rate if the space-step size (Δz) was suitably selected. A best-fit infiltration decay curve connecting the computed points can be drawn for every r greater than K_s as shown in Figures 8 through 11. This curve will be used to represent the ''theoretical'' solution of the rain infiltration problem and compared with results to be obtained from existing algebraic infiltration equations. Comparisons of various parametric infiltration models with this ''theoretical'' solution will be made in the following section.

PARAMETRIC MODELS OF RAIN INFILTRATION

The boundary-value problem of rain infiltration, as formulated in the previous section, is an idealized mathematical model in which the flow equation used is the Richards equation (1931). The analytical or numerical solutions of the Richards equation, linearized or nonlinear, have undoubtedly promoted our knowledge on the mechanics of soil water movement associated with the rainfall-runoff process, but in the past have met with limited application due partly to their time-consuming computations, even with the help of a modern electronic computer and partly to the unrealistic assumptions imposed on the model. Validity of the Richards equation becomes questionable when a natural soil under investigation is nonisothermal, deformable (i.e., swelling or shrinkable such as in clay) and/or produces a counter flow of air upon watering, as mentioned previously. Although the Richards equation was developed for flow through all soils, homogeneous or heterogeneous, isotropic or anisotropic, saturated or unsaturated, and with or without hysteresis, it will be much simpler and more useful in application to describe the infiltration decay characteristics by means of a small number of parameters combined in certain forms of algebraic equation than by use of the Richards equation. The algebraic infiltration equations, though mostly developed on the basis of empiricism, have increasingly gained wide recognition as modeling tools because of their simplicity. There is a problem, however, to evaluate such model parameters which are not physically based, but are essential to the virtual usefulness in the model. This and other related problems concerning the validity of existing algebraic infiltration equations are discussed herein.

Many algebraic infiltration equations have been published in the literature. Among them there are the Green-Ampt equation (Green and Ampt, 1911), the Kostiakov equation (Kostiakov, 1932), the Horton equation (Horton, 1940), the Philip equation (Philip, 1957a), the Holtan equation (Holtan, 1961). The major obstacle that has prevented more effective use of the algebraic infiltration equations is the difficulty in the evaluation of their parameter values. Several recent studies for validating some of the algebraic infiltration equations in their application to the rain infiltration process include the work of Holtan (1971), Onstad, Olson, and Stone (1972), Smith (1972), Talsma and Parlange (1972), Papadakis and Preul (1973), and Bauer (1974) among many others. In order to have the algebraic infiltration equations widely accepted as predictive models in the subsurface runoff computation, reappraisal on the methods for determining their parameter values is necessary. All the algebraic infiltration equations will thus be appraised in terms of theoretical concepts behind their developments, physical interpretations, if any, of the parameters involved, and the accuracy in the prediction of the infiltration rate.

All the algebraic infiltration equations were developed for computing the infiltration capacity under a particular condition. The term infiltration rate used in this study is defined in a broad sense as the infiltration flux or velocity at any instant rather than as the maximum infiltration flux. If the infiltration capacity is defined as the maximum infiltration flux resulting when water at the atmospheric pressure is made freely available at the soil surface, the infiltration rate for water application (rainfall or irrigation) intensities less than the infiltration capacity becomes equal to the application intensity before water ponding on the soil surface, and greater than or equal to the infiltration capacity after water starts ponding, depending upon whether or not there is a non-zero water depth on the soil surface. Unless the time of ponding that separates the above two distinctive infiltration stages under rainfall can also be predicted, the algebraic infiltration equations originally formulated for the maximum infiltration flux are hardly applicable to the case of rain infiltration. Few attempts have been made to overcome this difficulty, however. For example, Mein and Larson (1971 and 1973) have extended the Green-Ampt equation to the rain infiltration rate computation, while Smith (1970) has used the modified Kostiakov equation to evaluate the time of ponding parametrically. Both approaches are nevertheless limited to the case wherein the ponding depth of water on the soil surface is assumed negligibly small. It appears that a more general approach needs to be developed to remove this and other limitations without loss of simplicity which is demanded in principle by any algebraic infiltration equation. The present section is thus specifically directed to investigate the feasibility of developing such a general approach.

Formulation of Parametric Infiltration Models

If the rainfall intensity is greater than the final limiting infiltration rate (or the saturated hydraulic conductivity), the rain infiltration process in general can be divided into two stages: One is before ponding and another after ponding. Therefore, a parametric infiltration model, if formulated, must consist of both stages. As mentioned previously, before ponding the infiltration rate is equal to the rainfall intensity and after ponding it is greater than or equal to the infiltration capacity. Mathematically the parametric infiltration model can be expressed as

$$f = r(t) \qquad \text{for } 0 \leq t \leq t_p \qquad . \quad . \quad . \quad . \quad . \quad . \quad (35)$$

$$f = f(t) \qquad \text{for } t \geq t_p \qquad . \quad . \quad . \quad . \quad . \quad . \quad . \quad (36)$$

where f = infiltration rate, $r(t)$ = rainfall intensity which may or may not vary with time, t = time, t_p = time of ponding, $f(t)$ = infiltration function which is an explicit function of time. It should be noted that the $f(t)$ expression in Eq. 36 can be any form of the algebraic infiltration equations except the Green-Ampt equation that is expressed implicitly

as a function of f and t. Evidently, in addition to the parameters in f(t) that must be evaluated, the time of ponding, t_p, must be determined before the parametric infiltration model, Eqs. 35 and 36, can apply. Each of the available algebraic infiltration equations to be used in Eq. 36 is briefly discussed as follows.

The Green-Ampt equation

This is one of the algebraic infiltration equations in which the parameters are made of physical properties of the soil-water system. The Green-Ampt equation, also called the ''delta-function'' solution by Philip (1969b), has been independently derived and studied by several other workers (Rode, 1965). The primary assumption imposed in the derivation of the Green-Ampt equation is that the soil surface is ponded by a pool of non-zero-depth water. Philip derived the average volumetric moisture content and hydraulic conductivity basing on an additional assumption that either similarity is preserved on the moisture profiles (Philip, 1957b) or the moisture diffusivity is the Dirac-delta function of the moisture content around the saturation point near the soil surface (Philip, 1954). Mein and Larson (1971 and 1973) on the other hand evaluated the average suction at the wetting front from the soil suction-hydraulic conductivity relationship rather than integrating the suction over the soil depth. It is in fact the same as the Philip assumption that similarity on the moisture profiles, with Mein and Larson's assumed shape (i.e., linear), is preserved. Talsma and Parlange (1972) however derived the delta-function solution from an integral method recently developed by Parlange (1971). Although the Green-Ampt equation and its solutions give no information about details of the moisture profiles, they do offer estimates of integral properties such as the infiltration rate, f(t), and the cumulative infiltration, F(t). A more generalized Green-Ampt equation can be formulated in the following way.

The infiltration rate, f(t), can be mathematically expressed in two integro-differential forms, Eqs. 10 and 11. Both expressions were used in the solution of the boundary-value problem of rain infiltration. Let L be the distance below the soil surface (z = 0) at which non-zero depth of water is ponded, and be defined by

$$\int_{-L_w}^{0} (\theta - \theta_o)\, dz = (\theta_s - \theta_o)\, L(t) \qquad \text{for } t \geq t_p \quad . \quad . \quad . \quad (37)$$

where L_w = soil depth at the wetting front; θ_o = initial volumetric moisture content; and θ_s = saturated volumetric moisture content. The L(t) value that varies with $L_w(t)$ and $\theta(z,t)$, as defined in Eq. 37, has such a physical meaning that the shaded areas in Figure 12a are equal. With this definition of L, Eq. 10 reduces to

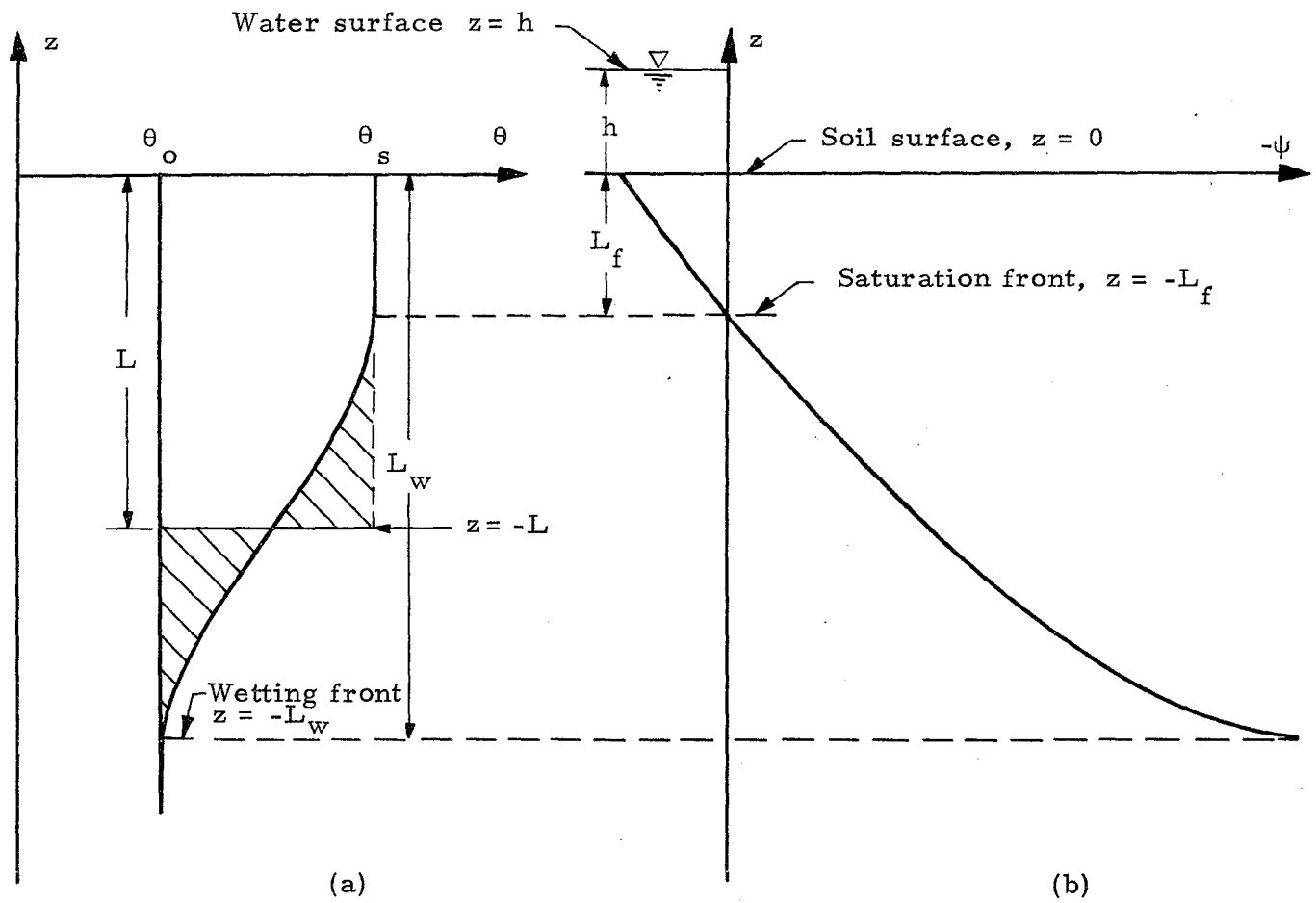

Figure 12. Definition sketch of rain infiltration after ponding with (a) soil moisture profiles and (b) soil capillary potential profiles.

$$f = (\theta_s - \theta_o) \frac{dL}{dt} + K_o \qquad \text{for } t \geq 0 \quad . \quad . \quad . \quad . \quad . \quad . \quad (38)$$

To express Eq. 11 in terms of L requires additional assumptions. Since the expression of the infiltration rate, as shown in Eq. 11, is essentially that of Darcy's velocity, w(z,t), at the soil surface (z = 0), one may assume that

$$f = \frac{1}{L} \int_{-L_w}^{0} [-w(z,t)]\, dz \qquad \text{for } t \geq t_p \quad . \quad . \quad . \quad . \quad (39)$$

where

$$w(z,t) = -K(z,t) \frac{\partial \psi(z,t)}{\partial z} - K(z,t) \quad . \quad . \quad . \quad . \quad . \quad . \quad (40)$$

We cannot integrate Eq. 39 by simply substituting Eq. 40 into Eq. 39 unless K-distribution is known. For the K(z)-distribution having very sharp peak around the θ_s [i.e., the tendency for soil diffusivity to have very large values around the θ_s-Dirac-delta function distribution (Philip, 1969)], it may be justified to assume that

$$\overline{K(z,t)} = \frac{1}{L} \int_{-L_w}^{0} K(z,t)\, dz \approx K_s \quad . \quad . \quad . \quad . \quad . \quad . \quad . \quad (41)$$

$$\overline{K(z,t)\frac{\partial \psi(z,t)}{\partial z}} = \frac{1}{L} \int_{-L_w}^{0} K(z,t)\frac{\partial \psi(z,t)}{\partial z}\, dz$$

$$= \beta\, \overline{K(z,t)}\ \overline{\frac{\partial \psi(z,t)}{\partial z}} \quad . \quad . \quad . \quad . \quad . \quad (42)$$

where β is the correction factor for K(z)- and $\psi(z)$-distributions and

$$\overline{\frac{\partial \psi(z,t)}{\partial z}} = \frac{1}{L} \int_{-L_w}^{0} \frac{\partial \psi(z,t)}{\partial z}\, dz = \frac{h(t) - \psi_o}{L} \quad . \quad . \quad . \quad (43)$$

where the bar over the variables represents average values over L_w times the ratio of L_w to L ($L_w \geq L$); h(t) = ponding water depth; and ψ_o = initial soil capillary potential, equal to $\psi(-L_w,t)$, negative

in value. Substituting Eqs. 41, 42, and 43 into Eq. 39 yields

$$f = \beta K_s \frac{h - \psi_o}{L} + K_s \qquad \text{for } t \geq t_p \quad . \quad . \quad . \quad . \quad . \quad (44)$$

It is noted that Nielsen, Biggar, and Erb (1973) treated spatial variation in soil properties over an areal extent by expressing average hydraulic conductivity as a function of average soil water content.

In particular, at the saturation front ($z = - L_f$), where the saturated and unsaturated zones meet and $\psi = 0$, as shown in Figure 12b, one can derive Eq. 16 or

$$f = K_s \frac{h}{L_f} + K_s \qquad . \quad . \quad . \quad . \quad . \quad . \quad . \quad . \quad . \quad . \quad (45)$$

A comparison of Eqs. 44 and 45 reveals that the correction factor, β, cannot become unity unless $L = L_f$ and $\psi_o = 0$. Equating Eqs. 38 and 44 gives

$$(\theta_s - \theta_o) \frac{dL}{dt} = \beta K_s \frac{h - \psi_o}{L} + K_s - K_o \qquad \text{for } t \geq t_p . \quad . \quad (46)$$

If h and β are constant, Eq. 46 becomes a first-order, nonlinear ordinary differential equation in L(t) and has the solution

$$t = t_p + \frac{\theta_s - \theta_o}{K_s - K_o} (L - L_p) - \beta K_s \frac{(h - \psi_o)(\theta_s - \theta_o)}{(K_s - K_o)^2} \log_e \left[\frac{(K_s - K_o)L + K_s(h - \psi_o)}{(K_s - K_o)L_p + \beta K_s (h - \psi_o)} \right] \qquad \text{for } t \geq t_p \quad . \quad . \quad . \quad (47)$$

where L_p is the L value at $t = t_p$. Because L in Eq. 47 is not expressed as an explicit function of t, the value of L for given t must be determined numerically, for instance, by the Newton-Raphson method. After L is computed, the value of L will be substituted either into Eq. 38 or 44 for the computation of the f value. Note that use of Eq. 44 has a slight advantage over that of Eq. 38 because any error involved in the evaluation of dL/dt in Eq. 38 can be avoided. However, use of either Eq. 38 or 44 requires the prior computation of the values of t_p and L_p.

Determination of the t_p and L_p values. Before ponding ($t \leq t_p$), the cumulative infiltration, F(t), is rt for constant rainfall intensity, r. Thus, from Eq. 38, after integration and rearrangement, one obtains at $t = t_p$

$$L_p = \left(\frac{r - K_o}{\theta_s - \theta_o} \right) t_p \quad . \quad . \quad . \quad . \quad . \quad . \quad . \quad . \quad . \quad (48)$$

and from Eq. 44, at $t = t_p$

$$L_p = \frac{\beta K_s (h - \psi_o)}{(r - K_s)} \quad . \quad . \quad . \quad . \quad . \quad . \quad . \quad . \quad . \quad . \quad (49)$$

Equating Eqs. 48 and 49 yields

$$t_p = \beta K_s \frac{(\theta_s - \theta_o)(h - \psi_o)}{(r - K_o)(r - K_s)} \quad . \quad . \quad . \quad . \quad . \quad . \quad . \quad . \quad . \quad (50)$$

The values of L_p and t_p can be determined from Eqs. 49 and 50 respectively. Like Eq. 47, the β value must be evaluated or given first in order for Eqs. 49 and 50 to be useful.

Evaluation of the β value. As defined in Eq. 42, the β value depends on the $K(z)$- and $\psi(z)$-distributions, which are, of course, unknown. However, if one knows the K-ψ relationship for the soil, the β value can be readily evaluated from Eq. 42 and the K-ψ relation. It is understood that the K-ψ relation is hysteritic, but will be assumed unique herein as long as the wetting process is only considered. Several forms of the K-ψ relation have been assumed by different investigators in an attempt to best fit the field or experimental data. Because the soil after ponding (for $h > 0$) has both the saturated and unsaturated zones, all the forms of the K-ψ relation must be modified to include $K = K_s$ for $\psi \geq 0$.

The simplest of the available K-ψ relations is a linear relationship between K and ψ, proposed by Richards (1931).

$$K = a\psi + K_s \qquad \text{for } \psi \leq 0 \quad . \quad . \quad . \quad . \quad . \quad . \quad . \quad (51a)$$

$$K = K_s \qquad \text{for } \psi \geq 0 \quad . \quad . \quad . \quad . \quad . \quad . \quad . \quad (51b)$$

where ''a'' is simply a constant.

Raats (1971) and Braester (1973) among others used an exponential form in K and ψ.

$$K = K_s e^{a\psi} \qquad \text{for } \psi \leq 0 \quad . \quad . \quad . \quad . \quad . \quad . \quad . \quad (52a)$$

$$K = K_s \qquad \text{for } \psi \geq 0 \quad . \quad . \quad . \quad . \quad . \quad . \quad . \quad (52b)$$

It should be noted that Eqs. 51 and 52 have only one parameter, a, needed to be determined from the K-ψ data.

Several researchers proposed multi-parameter models which should fit the K-ψ data better than the one-parameter model. For example, Gardner's (1958) original three-parameter model for $\psi < 0$ may be extended to include $\psi = 0$ so that

$$K = \frac{a}{(-\psi)^n + b} \qquad \text{for } \psi \leq 0 \qquad (53a)$$

$$K = K_s \qquad \text{for } \psi \geq 0 \qquad (53b)$$

where a, b, and n are all constants. However, the necessity of having $K = K_s$ at $\psi = 0$ results in the loss of freedom for Eq. 53a to choose the a value other than bK_s. Conversely, if $K = K_s$ at $\psi = 0$ is merely considered as a data point in the K-ψ relationship, the values of a, b, and n in Eq. 53a can be determined by using a least squares optimization procedure. After that, one should take the value of K_s equal to a/b. In view of the difficulty in integrating Eq. 53a with respect to ψ upon substitution of Eq. 53a into Eq. 42 for the evaluation of the β value, the following compatible form similar to Eq. 53a is proposed herein:

$$K = \frac{a}{(-\psi + b)^n} \qquad \text{for } \psi \leq 0 \qquad (54a)$$

$$K = K_s \qquad \text{for } \psi \geq 0 \qquad (54b)$$

By the same token, the values of a, b, and n in Eq. 54a can be estimated by using a least squares optimization technique, and hence the value of K_s may be taken to be equal to a/b^n.

The values of a, b, and n determined from Eqs. 53 and 54 are not all dimensionless. In order to make these dimensionally different parameters consistent (i.e., dimensionless), some investigators proposed dimensionless forms of Eq. 53 with the same number of parameters used in Eq. 53. Of them, Wei (1971) has used the most general one that is nevertheless not adopted in this study due to the same reason as given for Eq. 53.

Substituting Eqs. 51, 52, and 54 into Eq. 42 yields

$$\beta = 1 - \frac{a\psi_o^2}{2K_s(h - \psi_o)} \qquad (55)$$

$$\beta = \frac{1}{(h - \psi_o)} \left[h + \frac{1}{a} (1 - e^{a\psi_o}) \right] \quad . \quad . \quad . \quad . \quad . \quad . \quad (56)$$

and

$$\beta = \frac{1}{(h - \psi_o)} \left[h + \frac{1}{(1 - n)} b^2 (-\psi_o + b)^{1-n} - \frac{b}{(1 - n)} \right] . \quad (57)$$

respectively. Especially for $h = 0$, Eqs. 55, 56, and 57 reduce to

$$\beta = \frac{1}{2} \left(1 + \frac{K_o}{K_s} \right) \quad . \quad . \quad . \quad . \quad . \quad . \quad . \quad . \quad . \quad . \quad (58)$$

$$\beta = \frac{1}{a\psi_o} \left(e^{a\psi_o} - 1 \right) \quad . \quad . \quad . \quad . \quad . \quad . \quad . \quad . \quad . \quad . \quad (59)$$

and

$$\beta = \frac{1}{\psi_o} \left[\frac{b}{1 - n} - \frac{b^n}{1 - n} (-\psi_o + b)^{1-n} \right] \quad . \quad . \quad . \quad . \quad . \quad (60)$$

respectively. For soils having spacial variation in soil properties over an areal extent, one may use the average hydraulic conductivity as a function of average soil capillary potential, $\bar{K}(\bar{\psi})$, in the foregoing analysis.

As pointed out previously, the Green-Ampt approach does not give information about details of the moisture profiles. However, the role of the β factor playing in the determination of L, L_p, and t_p, respectively, from Eqs. 47, 49, and 50 should not be ignored. The β factor, as defined in Eq. 42, can be regarded as a gross measure of the effect of moisture profiles on the infiltration process of a Green-Ampt type. Consequently, to assume $\beta = 1$ and $K_o = 0$ in Eq. 46 by some investigators may result in an erroneous solution of L from Eq. 47 and hence of f from Eq. 44.

The Kostiakov equation

This is strictly an empirical formula, which was developed independently by Lewis (1937). Kostiakov (1932) expressed the infiltration capacity, f, as a negative power function of time, t:

$$f = At^{-\alpha} \qquad (0 < \alpha < 1) \qquad \text{for } t \geq t_p \quad . \quad . \quad . \quad . \quad (61)$$

where A and α are parameters. Despite simplicity in its form, the applicable range of time for Eq. 61 is rather limited, as pointed out by Philip (1957b). In other words, in order to fit the whole range of t, the value of α and hence of A must vary with t, which in essence detracts from its usefulness. Conversely, if the values of α and A are kept constant, Eq. 61 provides an infinite initial f, but asserts f_∞ to approach zero as t increases, rather than a constant non-zero f_∞ (= K_s). However, this awkwardness in the form of Eq. 61 can be remedied by assuming the form

$$f = f_\infty + A(t - t_o)^{-\alpha} \qquad \text{for } t \geq t_p \qquad . \quad . \quad . \quad . \quad . \qquad (62)$$

as generalized by Smith (1970) and Smith and Chery (1973) (henceforth called the modified Kostiakov equation). In Eq. 62, t_o is another parameter, in addition to A and α, needs to be determined from soil data. The form of Eq. 62 is simple, but the values of A, α, and t_o cannot be predicted in advance. Furthermore, there is no provision or criterion for predicting when ponding occurs under rainfall (i.e., the time of ponding, t_p). Smith (1970) has attempted to express t_p as a negative power function of the rainfall intensity, r, using the numerical solutions obtained from the boundary-value problem of rain infiltration for six soils. His strictly empirical formulation of t_p, though the values of A, α, and t_o may already be given or determined from experiments, hardly makes Eq. 62 useful under conditions other than those tested. The usefulness of an algebraic infiltration equation must lie in the validity and applicability of its simple expression over a wide range of conditions imposed or given. Whether and how Eq. 62 can be applied to the computation of t_p is investigated herein.

A review of Smith's (1970) results reveals that the values of A and α for soil under various rainfall intensities tested are fairly constant. This finding suggests the possibility of applying Eq. 62 to a soil under the same initial moisture content, θ_o, and the same soil surface condition, h, but under various rainfall intensities, say r_1, r_2, and so forth, as shown in Figure 13. Therefore, with the same θ_o and h values, one may have

$$f = f_\infty + A(t - t_{o1})^{-\alpha} \qquad \text{for } t \geq t_{p1} \qquad . \quad . \quad . \quad . \quad . \qquad (63)$$

$$f = f_\infty + A(t - t_{o2})^{-\alpha} \qquad \text{for } t \geq t_{p2} \qquad . \quad . \quad . \quad . \quad . \qquad (64)$$

where t_{o1} and t_{o2} are parameters corresponding to r_1 and r_2, respectively; and t_{p1} and t_{p2} are the times of ponding corresponding to r_1 and r_2, respectively. Because the same soil having the identical initial and boundary conditions is subjected to two different application rates, r_1 and r_2, it may be assumed that the total cumulative infiltration, $F(\infty)$, for the soil with the same water-storage potential, though under the different rainfall intensities, must be equal. Physically, this assumption implies that the shaded areas, (1) and (2), in Figure 13, are equal, or mathematically it can be expressed as

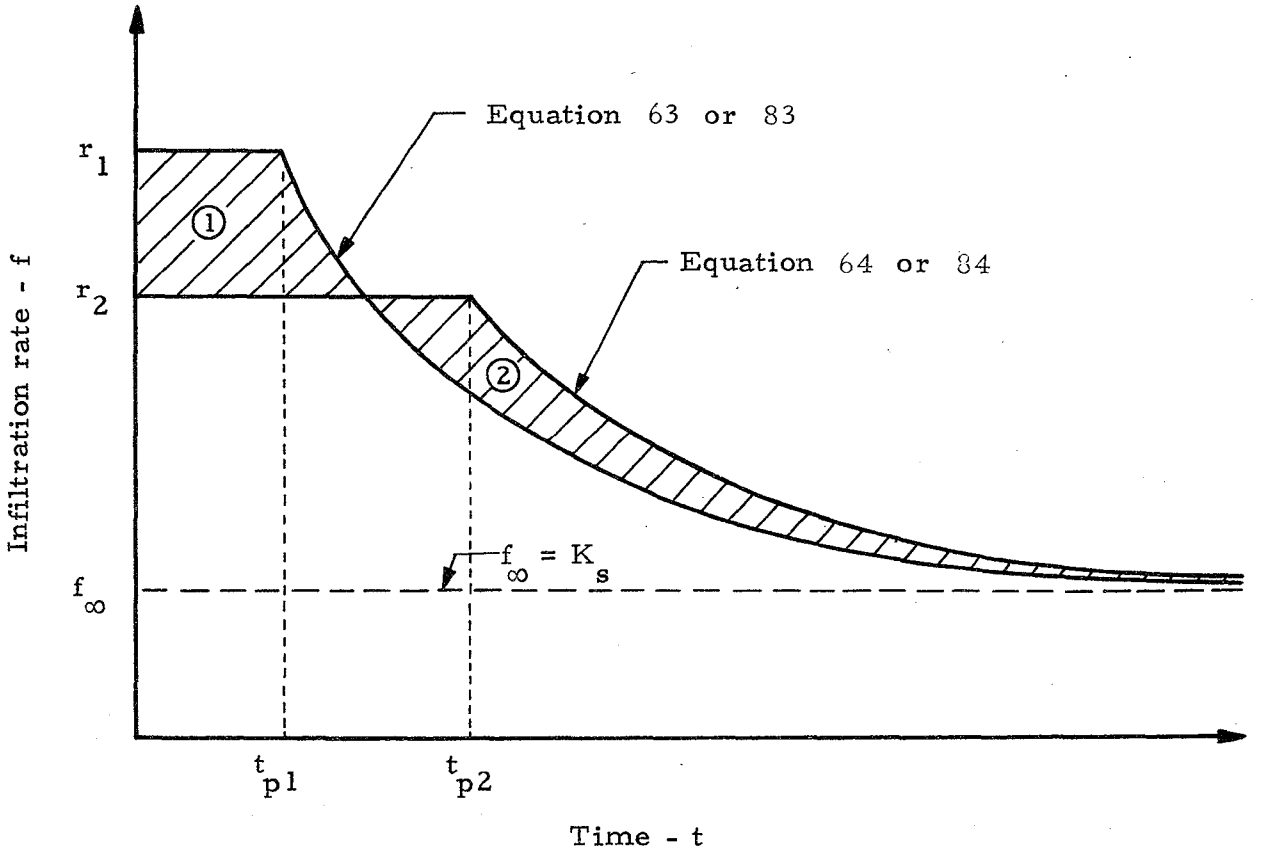

Figure 13. Schematic diagram of the infiltration rates under various rainfall intensities.

$$r_1 t_{p1} + \int_{t_{p1}}^{\infty} [f_\infty + A(t - t_{o1})^{-\alpha}]\, dt$$

$$= r_2 t_{p2} + \int_{t_{p2}}^{\infty} [f_\infty + A(t - t_{o2})^{-\alpha}]\, dt \quad . \quad . \quad . \quad . \quad . \quad (65)$$

In the evaluation of both integrations in Eq. 65, one may further assume that in the limit as t approaches infinity

$$\lim_{t\to\infty} \left[f_\infty t + \frac{A}{1 - \alpha} (t - t_{o1})^{1-\alpha} \right] = \lim_{t\to\infty} \left[f_\infty t + \frac{A}{1 - \alpha} (t - t_{o2})^{1-\alpha} \right] \quad . \quad . \quad . \quad . \quad . \quad (66)$$

It is also true from Eqs. 63 and 64 that

$$r_1 = f_\infty + A(t_{p1} - t_{o1})^{-\alpha} \quad . \quad . \quad . \quad . \quad . \quad . \quad . \quad . \quad (67)$$

$$r_2 = f_\infty + A(t_{p2} - t_{o2})^{-\alpha} \quad . \quad . \quad . \quad . \quad . \quad . \quad . \quad . \quad (68)$$

Performing the integrations in Eq. 65 and then manipulating the result with the assistance of Eqs. 66, 67, and 68 yields the relation

$$t_{o2} = \alpha t_{p2} - (\alpha t_{p1} - t_{o1}) \left(\frac{r_1 - f_\infty}{r_2 - f_\infty} \right) \quad . \quad . \quad . \quad . \quad . \quad (69)$$

Substituting Eq. 69 into 68, after rearrangements, gives

$$t_{p2} = \frac{1}{1 - \alpha} \left(\frac{A}{r_2 - f_\infty} \right)^{1/\alpha} - \left(\frac{\alpha t_{p1} - t_{o1}}{1 - \alpha} \right) \left(\frac{r_1 - f_\infty}{r_2 - f_\infty} \right) \quad . \quad . \quad (70)$$

$$t_{o2} = \frac{\alpha}{1 - \alpha} \left(\frac{A}{r_2 - f_\infty} \right)^{1/\alpha} - \left(\frac{\alpha t_{p1} - t_{o1}}{1 - \alpha} \right) \left(\frac{r_1 - f_\infty}{r_2 - f_\infty} \right) \quad . \quad . \quad (71)$$

Both Eqs. 70 and 71 satisfy Eqs. 68 and 69, or a combination of Eqs. 67 and 68; namely

$$(r_1 - f_\infty)(t_{p1} - t_{o1})^\alpha = (r_2 - f_\infty)(t_{p2} - t_{o2})^\alpha = A \quad . \quad . \quad (72)$$

Thus, if one of the algebraic infiltration equations such as Eq. 63 or 64 is known or given, the other equation corresponding to the other rainfall intensity can readily be found from Eq. 70 and 71. In view of the fact that the results can also apply in the case of immediate ponding wherein both t_{o1} and t_{p1} approach zero, Eqs. 70 and 71 can be further simplified to

$$t_{p2} = \frac{1}{1 - \alpha}\left(\frac{A}{r_2 - f_\infty}\right)^{1/\alpha} \quad . \quad . \quad . \quad . \quad . \quad . \quad . \quad . \quad . \quad (73)$$

$$t_{o2} = \frac{\alpha}{1 - \alpha}\frac{A}{r_2 - f_\infty}^{1/\alpha} \quad . \quad . \quad . \quad . \quad . \quad . \quad . \quad . \quad . \quad (74)$$

whence

$$t_{o2} = \alpha t_{p2} \quad . \quad . \quad . \quad . \quad . \quad . \quad . \quad . \quad . \quad . \quad . \quad (75)$$

or

$$t_{p2} = \frac{t_{o2}}{\alpha} \quad . \quad . \quad . \quad . \quad . \quad . \quad . \quad . \quad . \quad . \quad . \quad (76)$$

The consequence of this result, Eq. 75 or 76, is rather striking. In other words, to satisfy Eq. 75 or 76 requires from Eq. 69 the relation $t_{o1} = \alpha t_{p1}$ and so forth. Therefore, in general, once the values of A and α are specified or determined by experiments for a given soil having the same initial and upper boundary conditions, regardless of whether the ponding depth h is equal to or greater than zero, the value of t_p and t_o for any r can be computed from Eqs. 73 and 74, or

$$t_p = \frac{1}{1 - \alpha}\left(\frac{A}{r - K_s}\right)^{1/\alpha} \quad . \quad . \quad . \quad . \quad . \quad . \quad . \quad . \quad . \quad (77)$$

$$t_o = \frac{\alpha}{1 - \alpha}\left(\frac{A}{r - K_s}\right)^{1/\alpha} \quad . \quad . \quad . \quad . \quad . \quad . \quad . \quad . \quad . \quad (78)$$

A combination of Eqs. 77 and 78 leads to

$$t_o = \alpha t_p \quad . \quad . \quad . \quad . \quad . \quad . \quad . \quad . \quad . \quad . \quad . \quad (79)$$

It must be remembered, however, that Eqs. 78 and 79 are not valid if the value of t_o determined through curve-fitting becomes negative.

The term infiltration envelope was coined by Smith (1970) to describe the t_p - r relationship in the plot of a family of infiltration decay curves. In the light of Eqs. 77 and 78, the t_p - r relation may be called the upper infiltration envelope and the t_o - r relation, the lower infiltration envelope.

The Philip equation

The Philip equation (1957b), the first two terms in the infinite-series solution (i.e., not shown herein) of the boundary-value problem of rain infiltration, may be regarded as a typical form of the modified Kostiakov equation, Eq. 62, with physically-based parameters, $A = S/2$, $\alpha = 1/2$, $t_o = 0$, and $f_\infty \neq K_s$, where S is the sorptivity of the soil (Philip, 1969b). Since the sorptivity, S, is only related to the initial state of the soil, θ_o, and the imposed upper boundary condition, h (Philip, 1969b), the restrictions made on the parameter A in the derivation of Eqs. 77 and 78 are now proved to be consistent with the physical significance of Philip's S. The Philip equation is a two-parameter infiltration model, in which f_∞ may be fixed by the dynamic behavior of f at small t or taken as the value of K_s if f data are fitted over the whole range of t. Because the Philip equation does not have t_o, Eqs. 77 through 79 are not formulated in a suitable form to describe a Philip's type rain infiltration. The true expression of t_{p2} for the Philip equation can thus be obtained by eliminating t_{o1} and t_{o2} from Eqs. 70 and 71 and then combining the results. Furthermore, it can readily be shown from Eq. 72 that t_{p1} and t_{p2} have the same expression. Therefore, in general

$$t_p = \frac{1}{4} S^2 (r - K_s)^{-2} \quad . \quad . \quad . \quad . \quad . \quad . \quad . \quad . \quad . \quad (80)$$

It is also interesting to note that the exponent of the negative power function of $(r - K_s)$ in Eq. 80 is 2, which is approximately the value of Smith's (1970) formulation for four out of the six soils tested, although Smith expressed t_p as a negative power function of r only. Whether or not Smith's t_p expression should be modified in the light of Eqs. 77 and 80, as a negative power function of $(r - K_s)$ instead of r, needs to be further investigated.

The Horton equation

Horton (1940) derived, following the assumption that the rain infiltration process is of the nature of exhaustion process, the expression of the infiltration capacity, f, in terms of an inverse exponential function of time, t, as follows:

$$f = f_\infty + (f_o - f_\infty)e^{-kt} \quad . \quad . \quad . \quad . \quad . \quad . \quad . \quad . \quad . \quad (81)$$

where f_o is the initial value of f at the beginning of rain ($t = 0$) and k is a constant. Despite some investigators' questions on the suitability of the form of Eq. 81, the Horton equation was found by Horton (1940) to fit hundreds of experimental infiltration capacity curves obtained from different soils with different types of vegetal cover and in widely separated regions. Moreover, since the graph of an inverse exponential equation such as Eq. 81 can be represented over a considerable range by a hyperbola having the equation similar to the Kostiakov equation, Eq. 61, the Horton equation may be regarded as good as, if not better than, the Kostiakov equation as far as the empirical nature of the description of infiltration is concerned. One might expect, however, that for a particular soil, the longer the time range, the better the Horton equation would describe infiltration. If $f_\infty = K_s$, Eq. 81 actually becomes a two-parameter model, in which two parameters, f_o and k, are unknown and need to be determined in advance. Like the modified Kostiakov equation, Eq. 62, the following modified Horton equation can be formulated by considering that f_o may be given any assigned value, say r, and t measured from the time when $f_o = r$ occurs on the infiltration capacity curve, say t_p, without changing the form of Eq. 81 or the value of k. That is

$$f = f_\infty + (r - f_\infty)e^{-k(t-t_p)} \qquad \text{for } t \geq t_p \quad . \quad . \quad . \quad . \quad (82)$$

Hereafter Eq. 82 will be called the modified Horton equation. Note that the parameter f_o in Eq. 81 is replaced by the rainfall intensity, r, in exchange for the addition of another parameter, t_p, the time of ponding which is rather easily determined based on the same hypothesis that leads to Eq. 77.

Let the value of k be assumed to change only with the initial moisture content, θ_o, and the upper boundary condition, h. Then, for a soil with the same θ_o and h under different rainfall intensities, r_1 and r_2, Eq. 82 applies. Therefore,

$$f = f_\infty + (r_1 - f_\infty)e^{-k(t-t_{p1})} \qquad \text{for } t \geq t_{p1} \quad . \quad . \quad . \quad (83)$$

$$f = f_\infty + (r_2 - f_\infty)e^{-k(t-t_{p2})} \qquad \text{for } t \geq t_{p2} \quad . \quad . \quad . \quad (84)$$

where t_{p1} and t_{p2} are different times of ponding corresponding to r_1 and r_2, respectively. Again, as shown in Figure 13, if the total cumulative infiltration, $F(\infty)$, for any application rate is assumed to be always constant, then one can formulate similar to Eq. 65

$$r_1 t_{p1} + \int_{t_{p1}}^{\infty} [f_\infty + (r_1 - f_\infty)e^{-k(t-t_{p1})}]\, dt$$

$$= r_2 t_{p2} + \int_{t_{p2}}^{\infty} [f_\infty + (r_2 - f_\infty)e^{-k(t-t_{p2})}]\, dt \quad . \quad . \quad . \quad (85)$$

Because the integrands in Eq. 85 are exponential functions, Eq. 85 can readily be integrated, after rearrangements, to have the relation

$$t_{p2} = \left(\frac{r_1 - f_\infty}{r_2 - f_\infty}\right) t_{p1} \quad . \quad . \quad . \quad . \quad . \quad . \quad . \quad . \quad . \quad (86)$$

This result physically implies that the area enclosed between the lines $f = r$ and $f = f_\infty$ (of K_s) in the plot of infiltration decay curves (Figure 13) before ponding ($t \leq t_p$) is constant. Consequently, the infiltration envelope for a Horton type rain infiltration can be described by

$$t_p = \frac{C}{(r - K_s)} \quad . \quad . \quad . \quad . \quad . \quad . \quad . \quad . \quad . \quad . \quad . \quad (87)$$

where C is a constant with dimension in length. This is the equation of an equilateral hyperbola with a unit power in $(r - K_s)$. In application, if the values of k and t_p for a soil under a single application rate are known or determined from experiments, the values of t_p for other different application rates on the same soil under the same initial and upper boundary conditions can readily be computed from Eq. 87.

A parametric infiltration model consists of two equations, Eqs. 35 and 36, with the parameter, t_p, the time of ponding being used to separate them. For use in the second equation, Eq. 36, of the parametric infiltration model any one of the algebraic infiltration equations, as discussed previously, may be assigned. Because of the predominant role that t_p plays in the model, an effort has thus far been made to formulate the various expressions of t_p or the infiltration envelope for existing algebraic infiltration equations except for the Holtan (1961) equation. Despite the varieties in the forms of the algebraic infiltration equations used, all the expressions of t_p so developed look similar to each other. An inspection of Eqs. 50, 77, 80, and 87 developed from the Green-Ampt, modified Kostiakov, Philip, and modified Horton equations, respectively, reveals that t_p can generally be expressed as an inverse (or negative) power function of $(r - K_s)$. The power of $(r - K_s)$ varies with the different algebraic equations used. The most physically meaningful expression of t_p is Eq. 50 which is actually expressed as an inverse power function of $(r - K_o)$ $(r - K_s)$ rather than $(r - K_s)$ alone. The negative powers of

$(r - K_s)$ in Eqs. 77, 80, and 87 are $1/\alpha$, 2, and 1, respectively. Since the value of α may change from 0 to 1 exclusive, depending upon the initial and upper boundary conditions of the soil, the negative power of $(r - K_s)$ in Eq. 77 may change from 1 to ∞ accordingly. It appears that Horton's t_p, Eq. 87, yields the smallest negative power of $(r - K_s)$ while Philip's t_p, Eq. 80, perhaps gives a moderate exponent, 2, of the negative power.

Other algebraic infiltration equations

The algebraic infiltration equations discussed thus far are all expressed as an explicit function of t except the Green-Ampt equation. This is a convenient form in application as long as the rainfall intensity, r, remains constant. However, their applications would be limited if r varies with t, as in most cases in the nature. Smith (1970), after studying the numerical results of five soils tested under step-changing rainfall intensities, has found that ponding occurs at very nearly the time when accumulated volume of infiltrated water reaches a constant which is associated with the particular rate of rainfall when ponding occurs. This particular rate of rainfall when ponding occurs may be regarded as the mean rainfall intensity, $\bar{r}$, which also changes with time and will be defined as

$$\bar{r}(t) = \frac{1}{t} \int_0^t r(\tau)\, d\tau \quad . \quad . \quad . \quad . \quad . \quad . \quad . \quad . \quad . \quad (88)$$

where τ is the integration variable for t. With the definition of $\bar{r}$, the value of t_p corresponding to $\bar{r}$ can be computed from Eq. 50, 77, 80, or 87, depending on which algebraic equation one wants to adopt for describing infiltration decay curves. If the value of t_p just computed is larger than the time, t, at which $\bar{r}(t)$ was determined, the computation of $\bar{r}$ and t_p will continue until $t = t_p$. Thus, at the real time of ponding, t_p, Eq. 88 becomes

$$\bar{r}(t_p) = \frac{1}{t_p} \int_0^{t_p} r(\tau)\, d\tau \quad . \quad . \quad . \quad . \quad . \quad . \quad . \quad . \quad (89)$$

The value of $\bar{r}(t_p)$ so computed can be substituted into Eq. 50, 77, 80, or 87 for the final computation of t_p. If the Horton equation is used, the values of $\bar{r}(t_p)$ and t_p are both needed in Eq. 82.

The preceding method of computing the value of t_p for varying $r(t)$ which is assumed to be greater than K_s for $t \geq 0$ has an apparent problem when the value of $\bar{r}(t_p)$ so computed is larger than that of $r(t_p)$. This situation may occur in a hyetograph with antecedent rainfall prior to a major storm arriving, as shown in Figure 14a. This is an undesired situation in which the value of t_p so computed is not the real time of ponding because the infiltration rate for a portion of the infiltration decay curve after t_p (a-b in Figure 14a) becomes greater than $r(t)$. Therefore, if $\bar{r}(t_p) > r(t_p)$, it is suggested that we simply ignore the value of t_p just computed until a new t_p can be found.

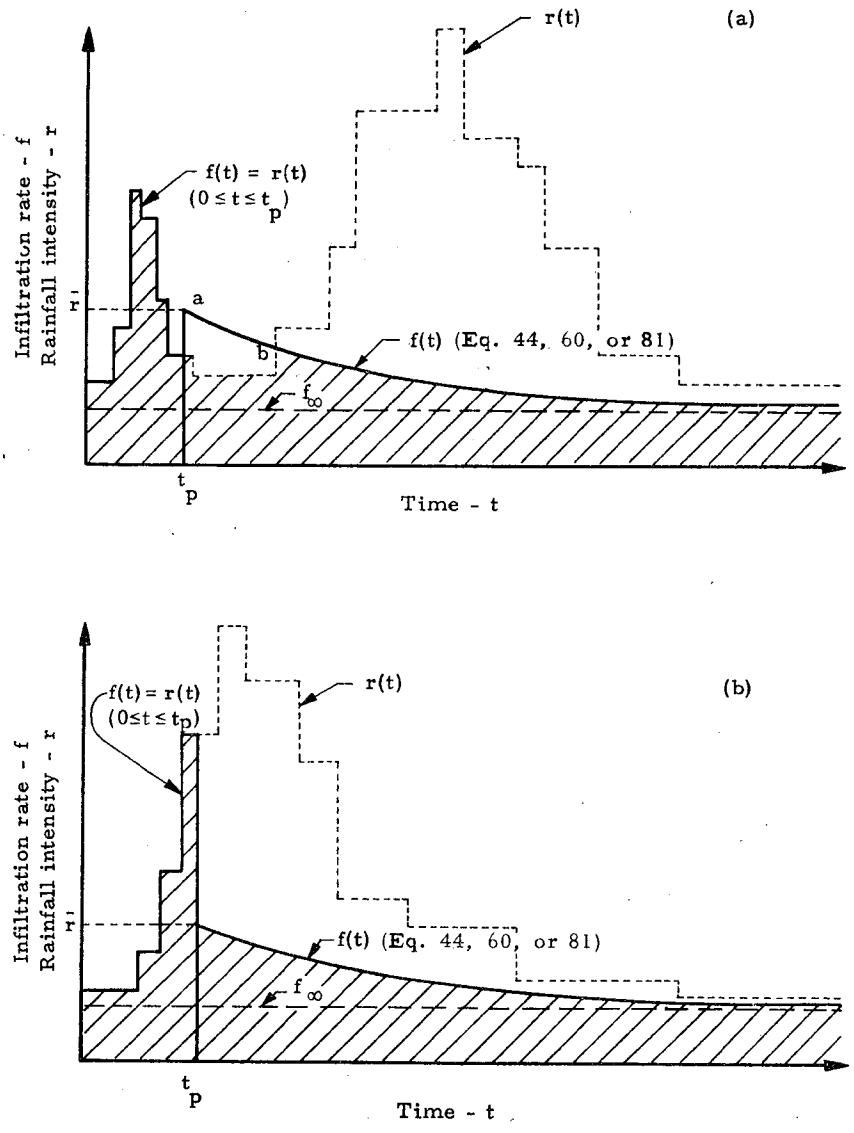

Figure 14. Schematic diagram of the time distribution of the rainfall intensity and the infiltration rate. The shaded areas are the cumulative infiltration for two different cases: (a) incorrect estimation of the time of ponding, t_p, and (b) otherwise.

If $\bar{r}(t_p) \leq r(t_p)$, such as the case illustrated in Figure 14b, the value of t_p so computed is the correct time of ponding at which the infiltration rate expression is divided into two parts, Eqs. 35 and 36. The shaded area in Figure 14b is the cumulative infiltration and before ponding, equals to

$$F(t) = \bar{r}(t)\, t = \int_0^t r(\tau)\, d\tau \qquad \text{for } 0 \leq t \leq t_p \quad . \quad . \quad (90)$$

and after ponding, equals to

$$F(t) = F(t_p) + \int_{t_p}^t f(\tau)\, d\tau \qquad \text{for } t \geq t_p \quad . \quad . \quad . \quad (91)$$

where $F(t_p) = \bar{r}(t_p)\, t_p$ is the cumulative infiltration at $t = t_p$. In view of varieties in the time distribution of the rainfall intensity, some researchers preferred the use of $F(t)$ to that of t as an independent variable in the algebraic infiltration equation (Eq. 44, 62, or 81). The Holtan equation (1961) was probably developed mainly for this purpose. Unfortunately, not all of the aforementioned algabraic infiltration equations can be transformed into the form that f is a function only of F. The development of such formulation for each of the algebraic equations is beyond the scope of the present study. Only the Holtan equation is discussed herein.

The Holtan equation

Holtan (1961) proposed the following form for infiltration capacity:

$$f = f_\infty + a(P - F)^n \qquad \text{for } t \geq t_p \quad . \quad . \quad . \quad . \quad . \quad (92)$$

where P is the water-storage potential of the soil above the first impeding stratum, and a and n are constants. It should be noted that Eq. 92 is valid for $P \geq F$ only, while Eq. 92 for $P < F$ must be imposed with a condition (Swartzendruber and Hillel, 1973),

$$f = f_\infty \qquad \text{for } t \geq t_p \quad . \quad . \quad . \quad . \quad . \quad (93)$$

Let us also assume that the parameters a, P, and n in Eq. 92 vary with the initial and upper boundary conditions only. Then, under a constant rainfall intensity, r, the cumulative infiltration, F, at $t = t_p$ is equal to rt_p, and the infiltration rate, f, is simply r. Thus, substituting $F = rt_p$ and $f = r$ into Eq. 92 yields

$$t_p = \frac{P}{r} - \frac{1}{r}\left(\frac{r - f_\infty}{a}\right)^{1/n} \quad . \quad . \quad . \quad . \quad . \quad . \quad . \quad . \quad (94)$$

The value of t_p computed from Eq. 94 apparently has a limit, P/f_∞, as r approaches f_∞, whereas that obtained from Eqs. 50, 77, 80, and 87 all gives an infinite value as r approaches f_∞. The limit, P/f_∞, depends on the value of P which according to Holtan (1961) is related to the depth of the first impeding soil stratum. The difficulty in the evaluation of P and thus the unnecessary limit, P/f_∞, of t_p as r approaches f_∞ could make the Holtan equations (Eqs. 92 through 94) unattractive among the algebraic infiltration equations, despite some investigators' claim that the Holtan equation, Eq. 92, has an advantage because F rather than t enters its formulation.

In view of varieties in $r(t)$, the advantage of using F rather than t in the right-hand side of Eq. 36 might look very unique in the past because all the algebraic infiltration equations have been formulated without the specification of t_p. If the value of t_p is specified for each of the algebraic infiltration equations to be used, as has been done in this report, there seems no need to keep track of the value of F up to the time of ponding, t_p, from which all the algebraic equations are supposedly valid. Thus, after the value of $F(t_p)$ (i.e., the subsurface water storage of initial abstraction) is determined, the advantage of using F rather than t in Eq. 36 seemingly no longer exists as far as the computation of the infiltration capacity using the algebraic infiltration equation is concerned. Furthermore, the value of $F(t_p)$ which varies with $r(t)$, as shown in Figure 14b, cannot be used as a basis for determining the time of ponding unless it is a constant, which seems unlikely.

For a varying $r(t)$, the method described in this section for determining the value of $\bar{r}(t_p)$ can also be applied to the Holtan equation.

Evaluation of Parameters for Various Infiltration Models

Each of the algebraic infiltration equations formulated by Green and Ampt (1911), Kostiakov (1932), Horton (1941), Philip (1957b), and Holtan (1961), or modified forms thereof, has merit in application, if adequately used. However, to make the algebraic infiltration equations suitable for the prediction of the infiltration rate during rainfall requires the accurate evaluation of the parameters in the equations. Some equations such as the Green-Ampt equation and the Philip equation have physically-based parameters which can readily be evaluated from known soil properties as well as given initial and boundary conditions, whereas other equations which have empirically-determined parameters can apply only when soil properties and initial and boundary conditions under consideration are similar. The most useful parameter in the infiltration model that consists of Eqs. 35 and 36 appears to be the time of ponding, t_p. In the following, other parameters in the parametric infiltration model including one of the algebraic infiltration equations are evaluated in terms of the accuracy of the predicted infiltration rate. To verify the attainment of the accuracy desired in connection with existing experimental data, the infiltration rate computed from each of the parametric infiltration models

is compared with the numerical solutions (henceforth called ''theoretical'' solutions) obtained from the boundary-value problem of rain infiltration. The comparisons are made simply for determining which of the algebraic infiltration equations will be in the most suitable form for rain infiltration modeling from the viewpoint of an idealized situation. The result, of course, does not imply precise duplication of actual situations in which soil surface sealing under raindrop impact, soil variability, etc. may be more important. For convenience, the same sandy clay loam at Hullinger Farm near Vernal, Utah, as characterized in the previous section is used herein.

Green-Ampt type model

The K-ψ relationship for unsaturated Vernal sandy clay loam can be best described by using an empirical formula of a type of Eq. 54a rather than Eq. 51a or 52a. The method of least squares was used in the determination of the a, b, and n values. This can be accomplished in a systematic way as follows: Taking logarithm of both sides of Eq. 54a yields

$$\log K = \log a - n \log (-\psi + b) \quad . \quad . \quad . \quad . \quad . \quad . \quad . \quad (95)$$

which is linear in $\log K$ and $\log (-\psi + b)$ for a given value of b. Because the value of b is unknown, an optimization technique similar to the method of steepest descent for optimizing an unconstrained problem was incorporated with the method of least squares. The optimization problem formulated herein is equivalent to the one to find the a, b, and n values for minimizing the expression

$$Q(a,b,n) = \sum_{j=1}^{m} [\log K_j - \log a + n \log (-\psi_j + b)]^2 \quad . \quad . \quad (96)$$

with the ''m'' number of data points (K_j, ψ_j) for $j = 1, 2, \ldots, m$. For Vernal sandy clay loam, the a, b, and n values so computed are 25.5 cm/hr, 2.54 cm, and 1.80 (dimensionless), respectively. Note that with these values, the value of K at $\psi = 0$ becomes $a/b^n = 4.78$ cm/hr, which is not equal to $K_s = 1.3$ cm/hr. This discrepancy in the value of K at $\psi = 0$ from the actual K_s value would result in the possible inaccuracy in the evaluation of the β value by means of Eq. 57.

The β value, for example, for $\theta_o = 0.2$ (or $\psi_o = -6.7 \times 10^2$ cm) and $h = 4$ cm was found to be 0.0106 from Eq. 57. This β value can be substituted into Eqs. 50 and 49 for the computation of the t_p and L_p values, respectively, in response to a given rainfall intensity, r. The values of β, t_p, and L_p so computed are substituted into Eq. 47 for the solution of L with respect to time, t, which in turn is used to compute the infiltration rate, f, through Eq. 44. Because L in Eq. 57 is not an explicit function of t, the Newton-Raphson method was applied to obtain the value of L for given t. The computed f's for $r = 5$

and 10 cm/hr are plotted in Figure 15 and compared with the theoretical solutions (in solid lines).

An inspection of Figure 15 reveals that the Green-Ampt type model with physically-based parameter values slightly underestimates the infiltration rate, though in general it closely maintains the same patterns of the infiltration capacity curves as do the theoretical solutions. As indicated previously, the main source of this discrepancy in the results may be attributed to the inaccuracy in the evaluation of a, b, and n from Eq. 54a and hence of β from Eq. 57. In other words, there is still a question of the suitability and representative accuracy of the K-ψ relationship by use of Eq. 54a.

To investigate the adequacy of the β value, different values of β are arbitrarily assigned and the infiltration rate computed accordingly. For comparison, the computed f's for $\beta = 0.02$ and $\beta = 0.05$ are shown in Figure 15. It appears that f for a β value between 0.02 and 0.05 will fit best to the theoretical solutions.

Regarding the β value and the subsequent computation of the f value, care must be taken to avoid confusion resulting from the extreme values of β. If the K-ψ relationship of the soil is characterized correctly by Eq. 54a, there is only one possible β value for given initial and boundary conditions. Different decay curves for different β values, as shown in Figure 15, are not intended to demonstrate that any arbitrary β value can be assumed. If the soil properties and initial and boundary conditions vary, the β value will change accordingly. It can readily be seen from Eqs. 55, 56, and 57 (or Eqs. 58, 59, and 60) that as $\psi_o \to 0$ or $K_o \to K_s$, the value of β approaches unity in the limit. Conversely, as $\psi_o \to -\infty$ or $K_o \to 0$, the value of β approaches zero in the limit for Eqs. 56 and 57 and 1/2 in the limit for Eq. 58. Apparently the β value ranges from 0 or 1/2 for initially dry soils to unity for initially moist soils. The difference in the β value certainly reflects in the computation of the t_p, L_p, L, and f values. The effect of the β value on the infiltration rate should be investigated further, especially near the extreme values of β such as $K_o \to K_s$ where Eq. 47 starts to breakdown.

The parameters in the Green-Ampt model can all be physically based and their values readily determined from the soil properties such as the K-ψ relationship, the initial condition, θ_o (or ψ_o), and the boundary condition, h, as demonstrated above. Therefore, the Green-Ampt model, if the β value so computed is accurate, calculates the infiltration rate without going through the curve-fitting process to determine the parameter values in advance. However, if the infiltration rate so computed deviates too far from the true value, it is always possible to readjust the β value to fit the actual data. In view of the latter flexibility in the modeling, the Green-Ampt model may be regarded as a one-parameter (at most) representation of the dynamics of rain infiltration.

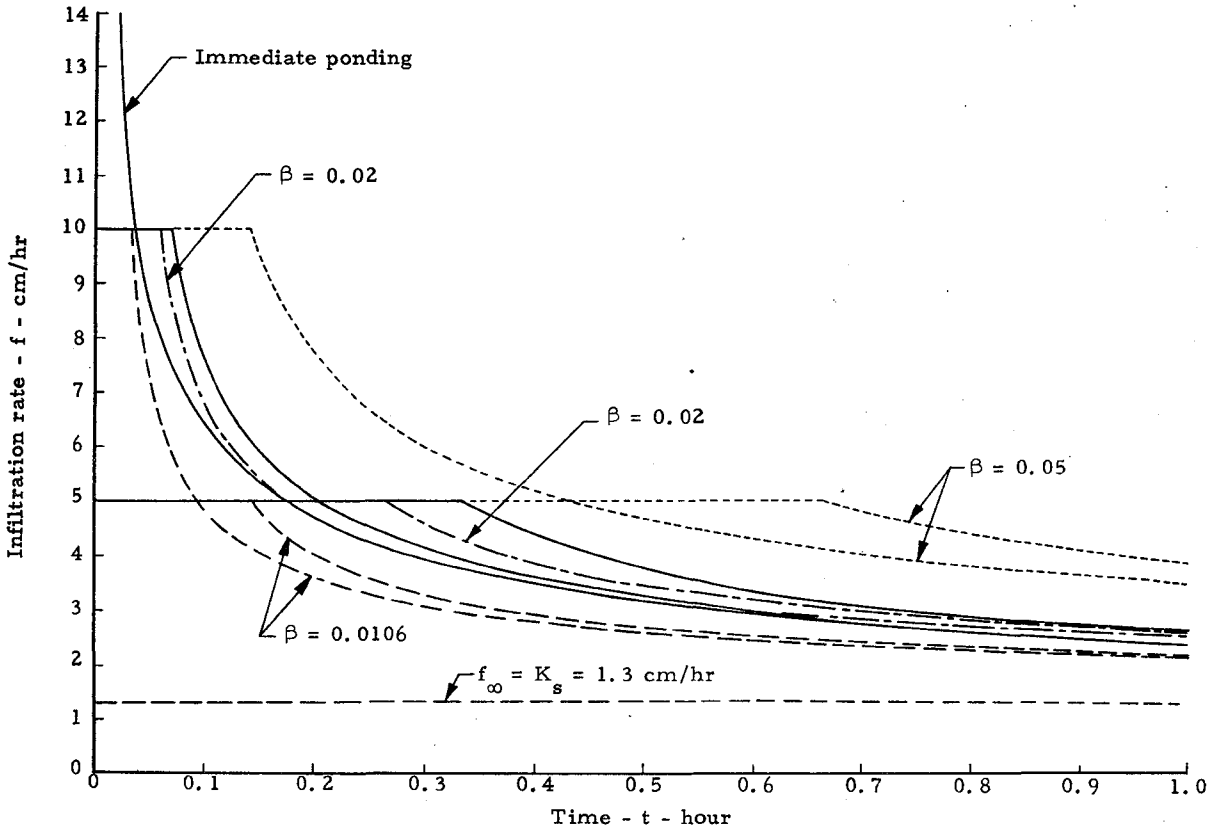

Figure 15. Comparison of the Green-Ampt type infiltration model (in broken lines) with the numerical solutions (in solid lines) obtained from the boundary-value problem of rain infiltration. All curves are asymptotic to line $f = f_\infty$ (= K_s).

Kostiakov type model

This model is built entirely based on the assumption that the values of A and α in Eq. 62 do not change under the same soil conditions (including the soil properties and initial and boundary conditions). Thus, in order to make the model applicable, it is necessary to determine these parameter values for each of the possible different soil conditions encountered in the field. However, this drawback does not seem to constitute a major problem to the user because the ranges of the initial and boundary conditions of a soil under investigation are not expected to vary drastically in the field. A few on-site infiltration tests may be sufficient to formulate the functional relationships of A and α with respect to θ_o and h.

The values of A, α, and t_o were determined by using again the method of least squares with the help of an optimization technique similar to the method of steepest descent for minimizing the expression

$$Q(A,\alpha,t_o) = \sum_{j=1}^{m} [\log (f_j - f_\infty) - \log A + \alpha \log (t_j - t_o)]^2 \quad . \quad . \quad . \quad . \quad (97)$$

with the ''m'' number of data points (f_j, t_j) for $j = 1, 2, \ldots, m$. The A, α, and t_o values so determined for an immediate ponding case of Vernal sandy clay loam having $\theta_o = 0.2$ and $h = 4$ cm are 1.07, 0.672, and -0.00380 hours, respectively. (Note that t_o can have a negative value.) The time of ponding, t_p, and the parameter, t_o, for different rainfall intensities can then be determined by substituting the computed values of A and α into Eqs. 77 and 78. The infiltration rate after ponding can thus be calculated by means of Eq. 62. The computer results for $r = 5$ and 10 cm/hr are plotted in broken lines, as shown in Figure 16, and again compared with the theoretical solutions (in solid lines). Apparently there is an overestimate in the value of t_p and hence t_o. A plot of the computer results on log-log scale reveals that the A and α values obtained for an immediate ponding case are not accurate enough to describe the infiltration rate at small t. To compensate for this inaccuracy, the values of t_p and t_o are computed from Eqs. 70 and 71, respectively, by using the same values of A, α, t_{p1} (=0.0000784 hours), and t_{o1} (= -0.00380 hours) except the value of the reference rainfall intensity, r_1 being adjusted to 50 cm/hr for matching the theoretical t_p. The computed infiltration capacity curves for $r = 5$ and 10 cm/hr, plotted in dots in Figure 16, follow closely the theoretical solutions. This in a sense proves that the assumption for the Kostiakov type model to have the same value of A and α under different rainfall intensities is valid as long as a soil under study has the same initial and boundary conditions.

Among the six soils Smith (1970) tested in his study of a Kostiakov type infiltration model, the one best confirming the preceding assumption

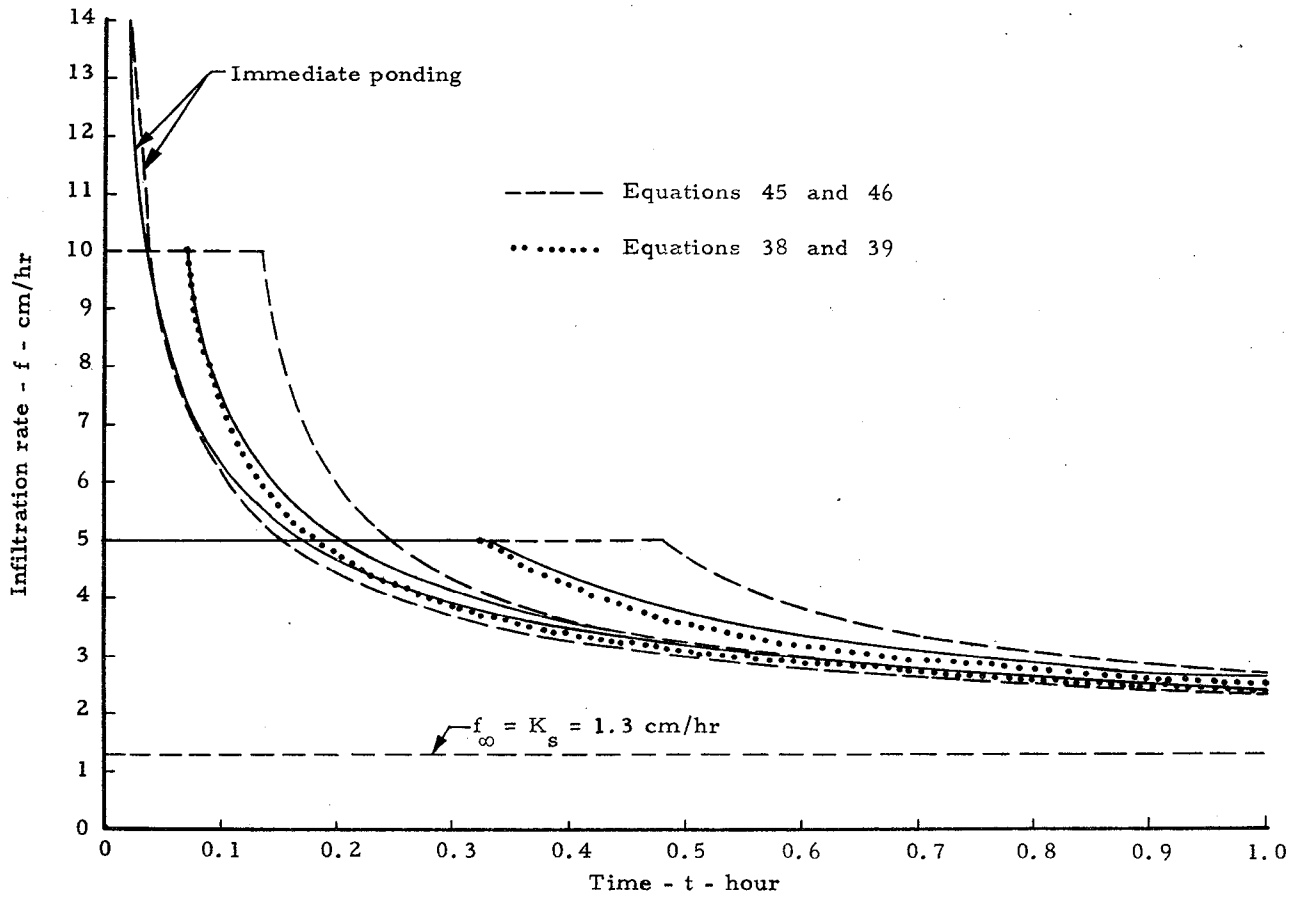

Figure 16. Comparison of the Kostiakov type infiltration model (in broken lines and dots) with the numerical solutions (in solid lines) obtained from the boundary-value problem of rain infiltration. All curves are asymptotic to line $f = f_\infty$ ($= K_s$).

is Muren clay. By using the parameters given in Smith's (1970) Table 2, the values of t_p and t_o are recomputed either from Eqs. 77 and 78 or from Eqs. 70 and 71 for appropriately assumed values of A and α. Because Smith's t_p and t_o values which satisfy Eq. 79 most closely for Muren clay are those at $r = 0.1481$ and 0.1693 cm/min, the values of A and α are assumed to be the average of both, namely, $A = 0.224$ and $\alpha = 0.5335$. The values of t_p and t_o for various r are computed based on these assumed values of A and α, and for comparison are shown in Table 4. Except for extreme low and high rainfall intensities, the values of t_p and t_o computed both from Eqs. 77 and 78 and from Eqs. 70 and 71 agree quite well with Smith's results. Simth's results on other five soils were not further analyzed because of the difficulty in selecting the correct A and α values for each of soils under study as well as uncertainty in the differences of the initial conditions that were not specified in his table. Nevertheless, a simple computation and comparison presented in Figure 16 and Table 4 clearly indicates that the assumptions made in the derivation of either Eqs. 77 and 78 or Eqs. 70 and 71, or both, for evaluating the parameters, t_p and t_o, are justified.

Philip type model

This infiltration model may be considered as a special case of the Kostiakov type model with physically-based parameters, f_∞ and S. If the values of f_∞ and S are both unknown, Philip's equation is a two-parameter model. However, if the value of f_∞ may be taken as K_s, then the infiltration rate data over the whole range of time can be fitted. Although the sorptivity of the soil, S, which varies with the initial and boundary conditions of the soil, can be calculated by use of the method suggested by Philip (1957b, 1958a, and 1969b), it would be more convenient to evaluate S statistically after the value of f_∞ is set at K_s. The method of least squares may be used for this purpose. The value of S so determined for an immediate ponding case of Vernal sandy clay loam is 2.66 cm/(hr)$^{1/2}$ and the time of ponding, t_p, computed by means of Eq. 80 is in fact the same as the time at which $f = r$. Therefore, the infiltration envelope, Eq. 80, and the infiltration capacity curve for such a Philip type model becomes synonymous. In Figure 17, the Philip infiltration model for $S = 2.66$ cm/(hr)$^{1/2}$ is plotted in broken lines and compared with the theoretical solutions (in solid lines). To account for the general effect of the S value on the shape of the infiltration capacity curve, the infiltration rate for other S values are also plotted in dotted lines in the same figure for comparison. If the initial and boundary conditions change, the value of S varies accordingly and the infiltration capacity curve so modeled, though being still asymptotic to line $f = f_\infty$, reflects its changes in response to the corresponding variation in the initial and boundary conditions.

The advantage of using the Philip type model lies in its simplicity; namely, only one parameter, S, needs to be determined either physically as suggested by Philip, or statistically, as proposed herein. Its

Table 4. Theoretically computed t_p and t_o values of the Kostiakov infiltration model for Muren clay in comparison with Smith's (1970) results.

Final Infiltration Rate, f_∞ (cm/min)	Rainfall Intensity r (cm/min)	Smith's Parameters in Eq. 62				Use of Eqs. 77 and 78*		Use of Eqs. 70 and 71+	
		A	α	t_p (min)	t_o (min)	t_p (min)	t_o (min)	t_p (min)	t_o (min)
0.0095	0.0847	0.225	0.529	15.64	7.7	16.6	8.85	16.5	8.78
0.0095	0.1270	0.216	0.518	7.04	3.8	7.18	3.83	7.14	3.79
0.0095	0.1481	0.223	0.532	5.21	2.78	5.28	2.82	5.24	2.78
0.0095	0.1693	0.225	0.535	4.02	2.13	4.05	2.16	4.02	2.13
0.0095	0.1905	0.231	0.542	3.19	1.62	3.18	1.70	3.15	1.67
0.0095	0.2138	0.242	0.558	2.61	1.2	2.54	1.36	2.52	1.33

*Computed on the basis of assumed A = 0.224 and α = 0.5335.
+Computed in reference to the values of t_p and t_o at r = 0.1693 cm/hr in addition to the assumed A = 0.224 and α = 0.5335.

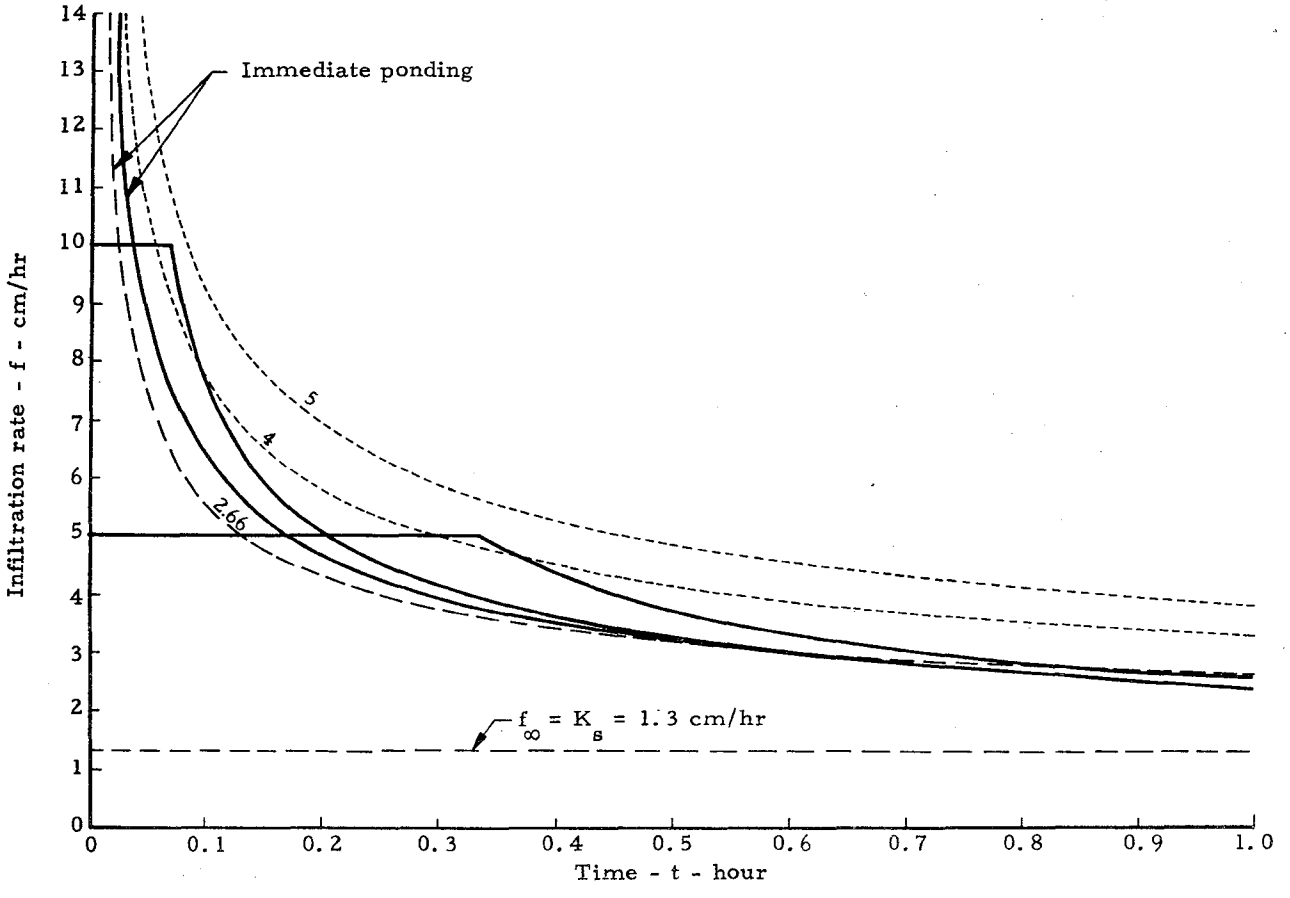

Figure 17. Comparison of the Philip type infiltration model (in broken lines) with the numerical solutions (in solid lines) obtained from the boundary-value problem of rain infiltration. Infiltration decay curves for the value of S other than 2.66 cm/(hr)$^{\frac{1}{2}}$ are plotted in dotted lines. Numerals on each curve denotes values of S in cm/(hr)$^{\frac{1}{2}}$. All curves are asymptotic to line $f = f_\infty$ ($= K_s$).

deficiency is, of course, evident from Eq. 80 and Figure 17 in that the infiltration envelope associated with the time of ponding, t_p, is exactly the same as the infiltration capacity curve. Aside from this deficiency, generally speaking, the form of the Philip type model is much simpler than those of both the Green-Ampt type and Kostiakov type models, but still give comparable, if not better, accuracy in the infiltration rate computation.

Horton type model

The Horton equation, Eq. 81, is a three-parameter model in which the values of f_o, k, and t_p need to be determined if the final infiltration rate, f_∞, is assumed to be K_s. In a similar manner, the method of least squares with the help of an optimization technique, as mentioned before, can be applied to estimating the best-fit values of f_o, k, and t_p by minimizing the expression

$$Q(f_o,k,t_p) = \sum_{j=1}^{m} [\log_e (f_j - f_\infty) - \log_e (f_o - f_\infty) + k(t_j - t_p)]^2 \quad . \quad . \quad . \quad . \quad (98)$$

with the ''m'' number of data points (f_j, t_j) for j = 1, 2, ..., m. The values of f_o, k, and t_p so determined unfortunately differ significantly from the number of data points chosen in the analysis, although the majority of data points used are identical. This discrepancy is probably due mainly to the failure of simulating the extremely large infiltration rate at small t with the Horton type model. In the case of immediate ponding on Vernal sandy clay loam, for example, use of 40 data points gives f_o = 6.45 cm/hr, k = 1.48, and t_p = 0.0341 hr, while use of 30 data points yields f_o = 5.42 cm/hr, k = 1.26, and t_p = 0.0510 hr. Based on these parameter values, the values of C in Eq. 87 for 40 and 30 data points are found to be 0.176 and 0.210 cm, respectively. The time of ponding, t_p, for various rainfall intensities is computed from Eq. 87 and the infiltration rate, f, after ponding from the modified Horton equation, Eq. 82. In Figure 18 the computed results for r = ∞, 10, and 5 cm/hr are plotted in broken lines with different symbols denoting the differences in the numbers of data points used and then compared with the corresponding theoretical solutions (in solid lines).

The comparison clearly indicates that regardless of the number of data points used in the analysis, the accuracy of the Horton type model depends to a large extent on the value of f_o, i.e., the initial infiltration rate. If the value of f_o so determined is close to the rainfall intensity under investigation, such as r = 5 cm/hr in Figure 18, the infiltration rate computed from the Horton type model does not seem to deviate from the theoretical line except at the initial stage of infiltration. However, if the rainfall intensity under study such as r = 10 cm/hr in Figure 18 is far away from the computed f_o value, use of the Horton type model in the prediction of the infiltration rate after ponding does not appear to be very accurate. Of course, one may increase or decrease

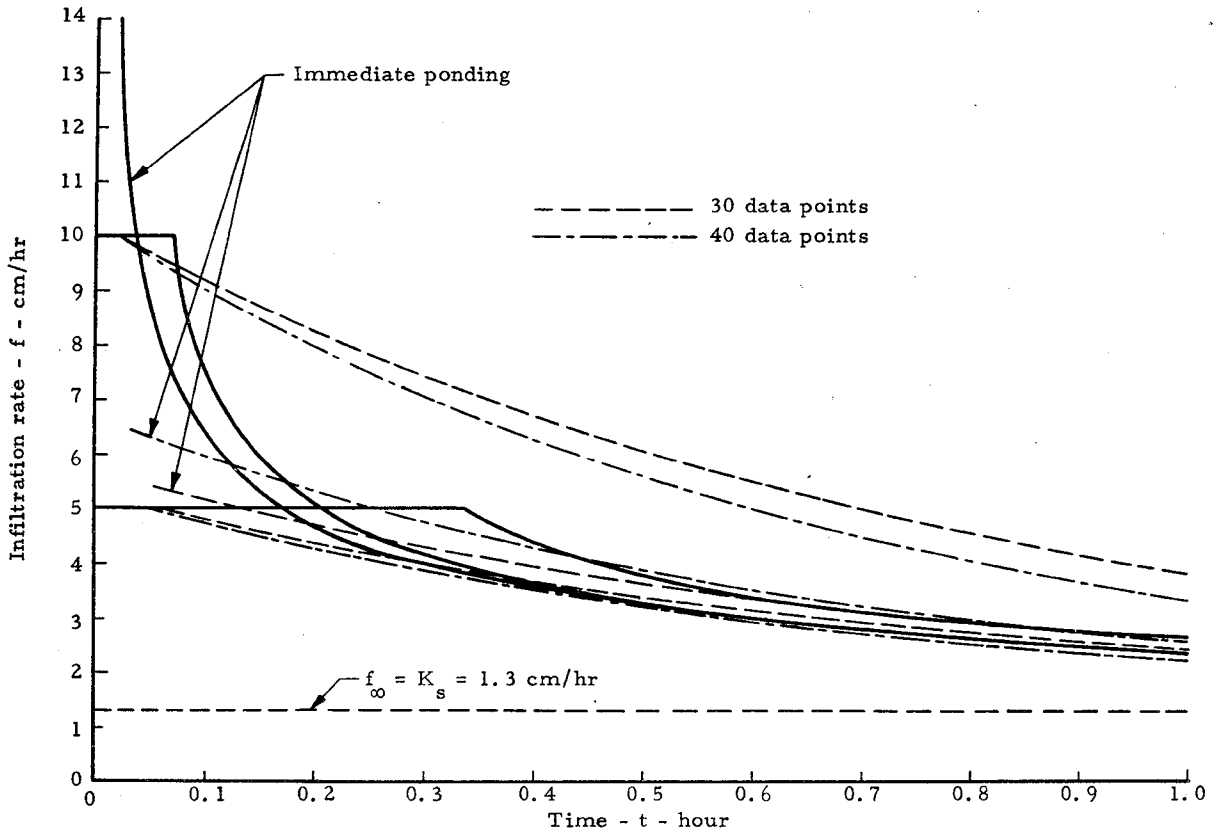

Figure 18. Comparison of the Horton type infiltration model (in broken lines) with the numerical solutions (in solid lines) obtained from the boundary-value problem of rain infiltration. All curves are asymptotic to line $f = f_\infty$ ($= K_s$).

the value of k with respect to r in order to best fit the measured or computed infiltration decay curve. The change in the value of k for different rainfall intensities in essence contradicts Horton's (1940, p. 402) original thought on the application of his equation to the runoff analysis as well as the assumptions made in the derivation of Eqs. 87 and 88. In other words, if the value of k needs to be varied for different r's, the applicability of the Horton type model in the actual field becomes extremely limited.

Holtan type model

If $f_\infty = K_s$ is given, the Holtan equation, Eq. 92, is a three-parameter infiltration model, in which the values of a, P, and n must be determined from known data. Again, the method of least squares with an optimization technique can be applied to estimating the optimum values of a, P, and n by minimizing the expression

$$Q(a,P,n) = \sum_{j=1}^{m} [\log (f_j - f_\infty) - \log a - n \log (P - F_j)]^2 \quad . \quad . \quad . \quad . \quad (99)$$

with the "m" number of data points (f_j, F_j) for $j = 1, 2, \ldots, m$. Because the value of P so determined is in no way related to the depth of the first impeding soil stratum, there was the difficulty of obtaining the optimum values of a, P, and n for the Holtan type model. As a matter of fact, in the case of immediate ponding on Vernal sandy clay loam, the extreme values for optimum a, P, and n were obtained by using the optimization technique. The values obtained are $a \to 0$, $P = 135$ cm, and $n = 42$, which causes the computation of f beyond the allowable range of the computer capacity by means of Eq. 92. The maximum data value of F_j used in the computation should not exceed the value of P. In the present case, the maximum F_j used is 18.1 cm which corresponds to the cumulative infiltration at $t_j = 9.13$ hours.

Although one cannot find the optimum values of a, P, and n for the Holtan type model, it is possible to optimize the a and n values for any given P value. The best fitted values of a and n in Eq. 92 for r equal to ∞ and 5 cm/hr for arbitrarily assigned $P = 20$ and 40 cm were computed by using the numerical solutions. The results for $P = 20$ and 40 cm are plotted in broken lines and dotted lines, respectively, in Figure 19 and then compared with the theoretical solutions (in solid lines). The time of ponding, t_p, computed from Eq. 94 for $r = 10$ cm/hr unfortunately becomes negative so that it cannot be drawn in. An inspection of Figure 19 reveals that the larger the magnitude of P, the closer the Holtan type model approaches the theoretical lines. Apparently, the optimum value of P is at infinity which through the method of least squares would give the unrealistic optimum values of a and n; namely, $a \to 0$ and $n \to \infty$. Consequently, unless the infiltration capacity curve can be simulated by use of the realistic optimum values of a, P, and n, the application of the Holtan type model to the runoff study does not look very promising.

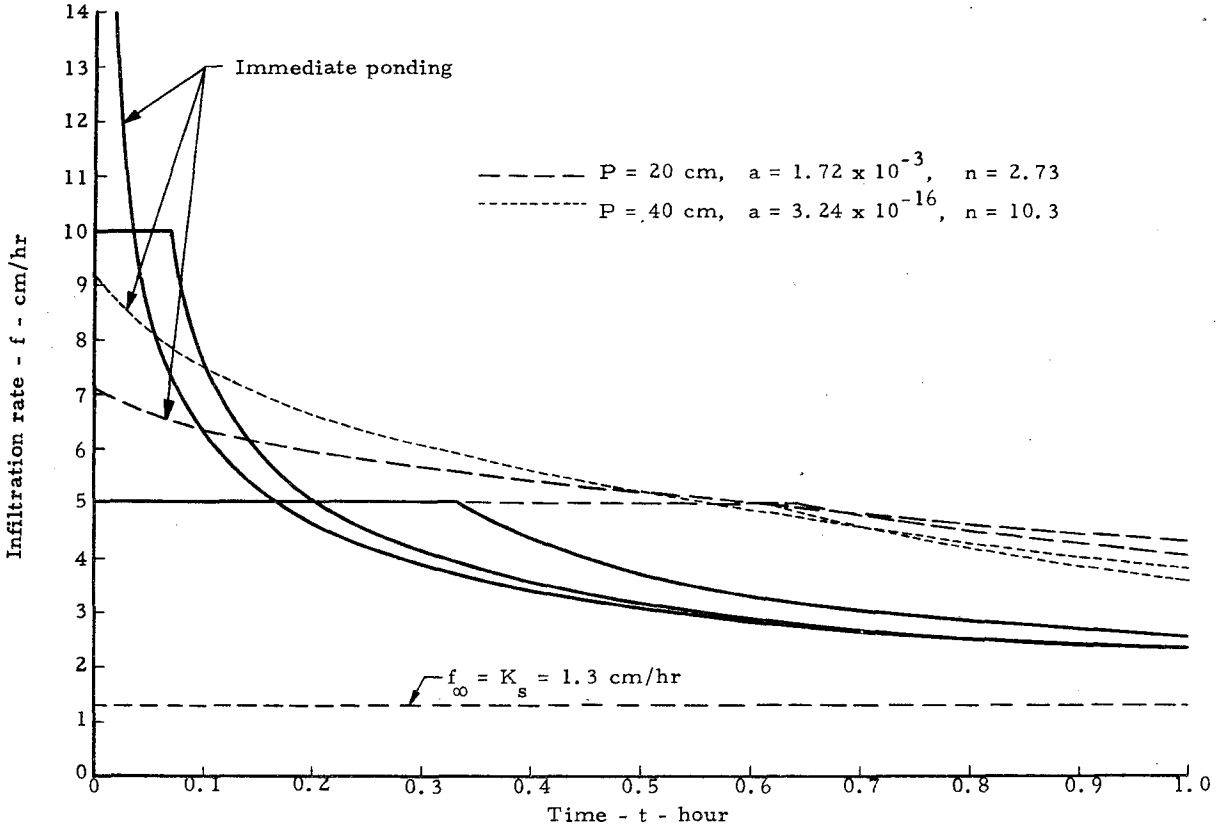

Figure 19. Comparison of the Holtan type infiltration model (in broken and dotted lines) with the numerical solutions (in solid lines) obtained from the boundary-value problem of rain infiltration. All curves are asymptotic to line $f = f_\infty$ ($= K_s$).

Application of Parametric Infiltration Models

All the infiltration models developed for a constant r can be applied to the case in which r varies with t, provided that the mean rainfall intensity, $\bar{r}$, defined in Eq. 88 is substituted for r in each of the models. The time of ponding, t_p, in response to a varying $r(t)$ can be found by the method discussed in connection with Figure 14. For example, a hypothetical storm with varying $r(t)$, such as shown in Figure 20, is assumed and the corresponding infiltration rates are computed by using different types of infiltration model. Because the infiltration rate before ponding is exactly equal to the rainfall intensity, $r(t)$ as expressed in Eq. 35, a comparison of the various models can be accomplished by comparing only the infiltration rates after ponding. Thus, the time of ponding, t_p, is the most important parameter needed to be determined before each of the infiltration models becomes applicable. In the following analysis, only the applicability of the Green-Ampt, Kostiakov, and Philip type models is studied because of the difficulty in use of the Horton and Holtan type models in the rain infiltration process, as explained previously.

Consider a storm with hyetograph, as shown in Figure 20, acting on Vernal sandy clay loam. The numerical solution of the infiltration rate obtained from the boundary-value problem of rain infiltration, Eq. 10, is shown in dots. The theoretical solution before ponding follows closely with the given $r(t)$ despite its stepwise increments. The sudden rise in the theoretical f value, more than the given $r(t)$, before ponding is probably caused by the discontinuity in the soil surface condition (h = 4 cm, arbitrary) hypothetically imposed at the time of ponding, as reasoned before. The following parameters of the various infiltration models for the same initial moisture content, $\theta_o = 0.2$, and the same upper boundary condition after ponding, h = 4 cm, are used in the computation of t_p and f.

1. Green-Ampt type model: $\beta = 0.025$, $K_s = 1.3$ cm/hr, $\psi_o = -670$ cm, $\theta_s = 0.48$, and $K_o = 0.00011$ cm/hr.

2. Kostiakov type model: $\alpha = 0.672$, $A = 1.07$, $f_\infty = 1.3$ cm/hr, and $t_o = -0.0038$ hr.

3. Philip type model: $S = 2.66$ cm/(hr)$^{1/2}$ and $f_\infty = 1.3$ cm/hr.

The time of ponding for varying $r(t)$ so determined is actually the point of intersection of the infiltration envelope and the mean rainfall intensity distribution curve, as marked by circles in Figure 21. The mean rainfall intensity distribution curve (Eq. 88) shown in Figure 21 corresponds to the hyetograph given in Figure 20, while the infiltration envelopes for the Green-Ampt, Kostiakov, and Philip type models are expressed by Eqs. 50, 70 (or 77), and 80, respectively. As long as the initial and boundary conditions of the soil under study do not change throughout the entire process, the infiltration envelope for each model

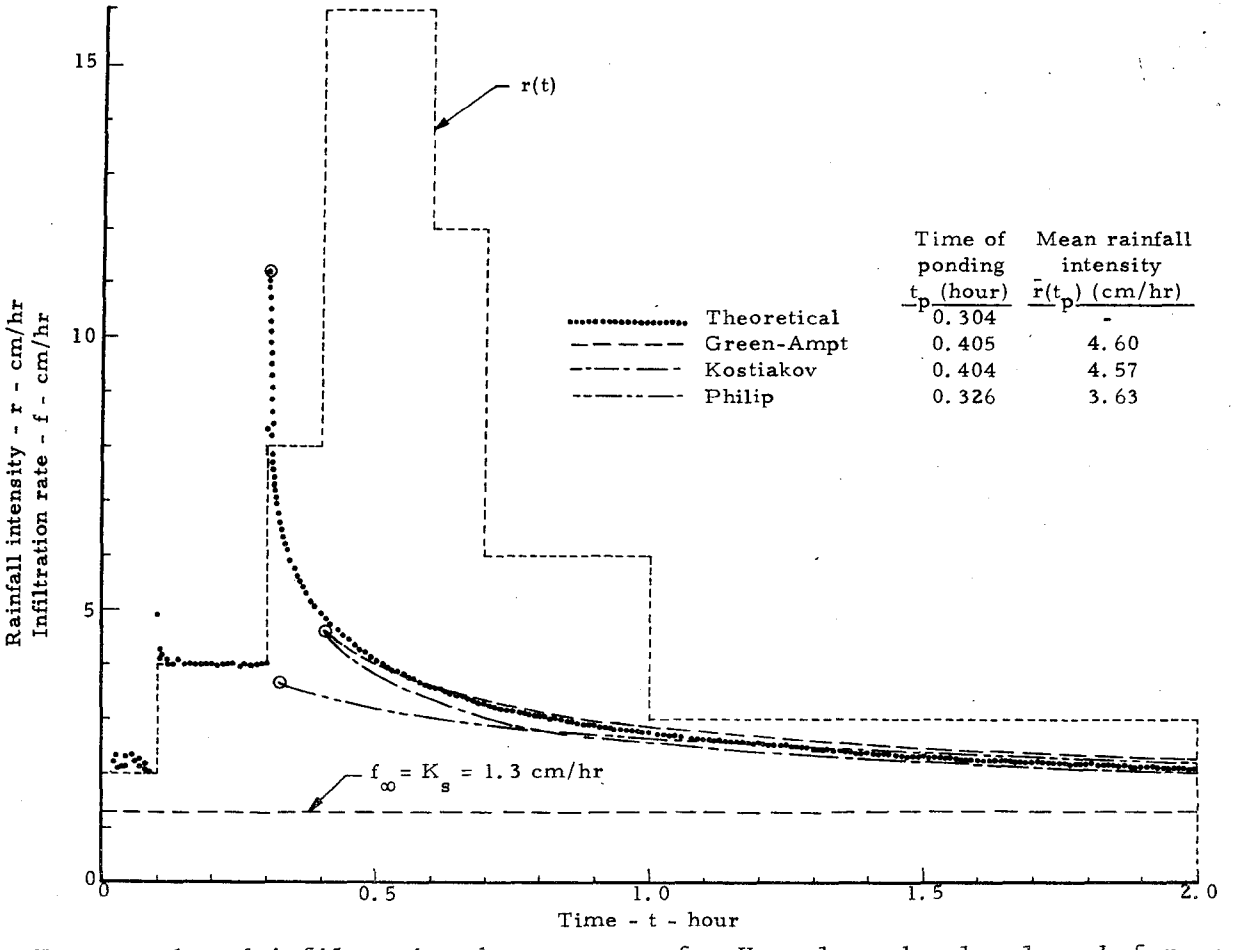

Figure 20. Hyetograph and infiltration decay curves for Vernal sandy clay loam before and after ponding. Circles are different locations at the time of ponding derived from the theoretical, Green-Ampt, Kostiakov, and Philip type models, respectively.

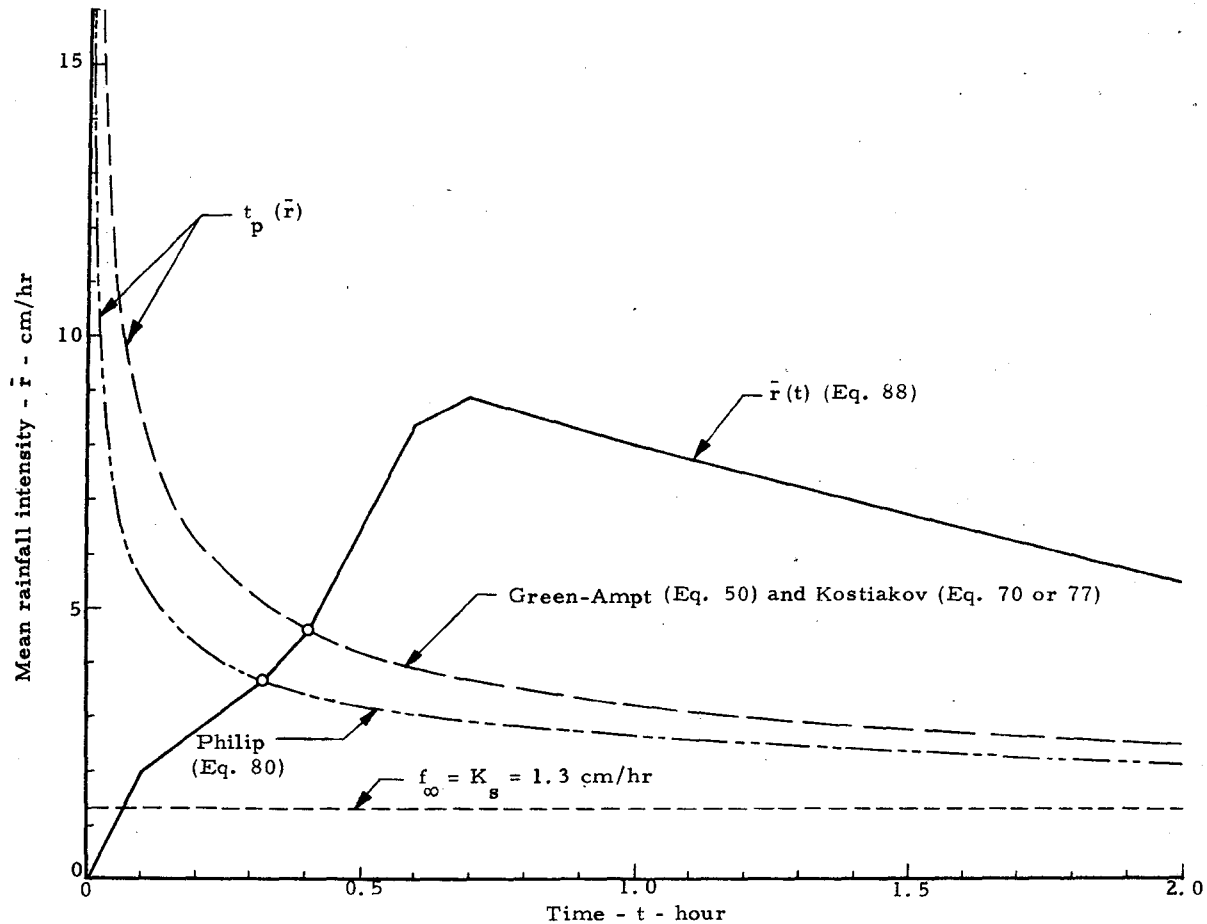

Figure 21. Infiltration envelopes for Vernal sandy clay loam and mean rainfall intensity distribution curve for a storm given in Figure 20. Intersections marked by circles are different locations at the time of ponding for the Green-Ampt, Kostiakov, and Philip type models, respectively.

is unique. Note that the infiltration envelopes for the Green-Ampt and Kostiakov type models, Eqs. 50 and 70, in the present case are collapsed to one, as shown in Figure 21. The value of t_p and that of the corresponding $\bar{r}$ for each model are computed by means of an iteration method and compared with the theoretical solution. The computed results for t_p and $\bar{r}$ are tabulated in Figure 20 for comparison.

The infiltration capacity curves for the Green-Ampt, Kostiakov, and Philip type models are computed by use of Eqs. 44, 62, and 80, respectively, and shown in Figure 20. A comparison of the computed results for the three parametric infiltration models indicates that the infiltration capacity curves obtained from the parametric infiltration models agree surprisingly well with the theoretical solution except for a short period of time after ponding in which Philip's model underestimates. Despite the fact that the Philip type model has only one parameter, S, to be evaluated, the infiltration capacity curve so determined for Philip's model is deemed accurate enough for many practical purposes. Of course, in application, the major problem facing the use of the Philip type model lies in the evaluation of the physically-based parameter, S. If the value of S is physically determined, as suggested by Philip (1958b) in his conclusion of a series of papers regarding infiltration dynamics: (with the writer's notation)

$$S = [2K_o (h - \psi_o)(\theta_s - \theta_o)]^{1/2} \quad . \quad . \quad . \quad . \quad . \quad . \quad . \quad (100)$$

substituting the known values of K_o, h, ψ_o, θ_s, and θ_o into Eq. 100 yields $S = 0.204$ cm/(hr)$^{1/2}$ which is one order of magnitude less than the statistically-determined 2.66 cm/(hr)$^{1/2}$, as used in this report. Therefore, as long as the value of S is constant for a soil with the same initial and boundary conditions, it would be more accurate to evaluate the parameter S statistically than physically, e.g., by Eq. 100.

In application, the methods described herein to compute the values of t_p and other parameters for any given hyetograph are important in any surface runoff study. Knowing how to evaluate t_p, the significant role the amount of water stored in the soil before ponding (initial abstraction) plays in the hydrologic process can thus be more accurately evaluated than before. However, it must be remembered that not all hyetographs can produce surface runoff. For example, if there is no point of intersection between the infiltration envelope and the mean rainfall intensity distribution curve, there is no surface runoff. On the other hand, in the case that there is more than one point of intersection, the situation involved is more complicated than the one just described and is not treated further herein because it is beyond the scope of the present study.

Within the realm of idealized situations in rain infiltration, it has been demonstrated that the Holtan type model is difficult to apply to the present case wherein the water-storage potential of the soil above the first impeding stratum is not specified. The values of the parameters in all the parametric infiltration models are assumed to be constant

for a soil having the same initial and boundary conditions. This assumption has been verified by using the numerical solutions obtained from the boundary-value problem of rain infiltration for all types of models except for the Horton type. Use of the Green-Ampt, Kostiakov, and Philip type models for the prediction of the infiltration rate before and after ponding has proved to be very satisfactory for many practical purposes, not only under a constant rainfall intensity but also under a time-varying storm. The Green-Ampt and Philip type models have physically-based parameters, the values of which can readily be determined from the known or given soil properties as well as the initial and boundary conditions. However, in the case where the Green-Ampt and Philip type models with the physically-determined parameters fail to compute the infiltration rate within the desired accuracy, it has also been shown that such parameter values can be optimized by means of a least squares optimization procedure. If this is the case, the Green-Ampt and Philip type models with empirically determined parameters can no longer be considered superior to the modified Kostiakov type model because of inherent limitations and deficiency in the form of the Green-Ampt and Philip type models. In other words, the Green-Ampt type model cannot compute the infiltration rate as an explicit function of time and the Philip type model, though it may be regarded as a special form of the Kostiakov type model, has the infiltration envelope the same expression as the infiltration capacity curve. The modified Kostiakov type model is thus believed to be in the most suitable form for infiltration computation for a soil-cover-moisture complex.

SOIL-COVER-MOISTURE COMPLEX ANALYSIS OF INFILTRATION CAPACITY

From the theoretical aspects of rain infiltration, as analyzed through the formulation of the boundary-value problem and the response characteristics of various parametric infiltration models, it becomes clear that every soil-cover-moisture complex has a different rainfall-related infiltration characteristic. A unique infiltration decay curve is followed during a period of precipitation where intensities are in excess of infiltration capacity. From the practical point of view, however, it is unnecessary to solve the boundary-value problem of rain infiltration as a means to obtain the infiltration capacity decay curve for each of such soil-cover-moisture complexes, aside from some technical difficulties in the method of solution which have yet to be overcome. There are many possible ways in which the system involving real soil, i.e., a composition of air, water, and soil particles under rain will respond quite differently from what the Richards equation can theoretically describe. For instance, the Richards equation does not correctly account for the real field situations under which the soil undergoes sealing and/or sorting process, under raindrop impact, deforming (swelling, shrinking, or cracking) processes upon watering or drying, producing a counter flow of air originally partially trapped by the infiltrating water, and instability of the soil moisture movement due to entrapped air at the wetting front. In addition, to make a complete theoretical treatment of the problem even more unattainable is the fact that variabilities in space and time with regard to soil and plant cover properties as well as initial (antecedent) moisture distributions in the field makes the solution of the Richards equation non-representative of the space- and time-averaging infilration capacity decay curve for the soil-cover-moisture complex under study. Therefore, the practical, if not the best, way to develop a reasonably representative infiltration-capacity decay curve for the complex of a large areal extent appears to be the use of a parametric infiltration model with physically or empirically determined parameters.

The Modified SCS Method for Computation of Infiltration Capacity

The major problem of applying any parametric infiltration model to the actual field conditions has been in the difficulty of evaluating the parameters of the model. As critically analyzed in the preceding section, in order for the model to be useful under various rainfalls, the values of the parameters should remain unchanged for a given soil under the same initial and (post-ponding) boundary conditions—equivalent to those for a given soil-cover-moisture complex. A method used in the U.S. Department of Agriculture Soil Conservation Service (USDA SCS, 1969) for computing direct storm runoff from soil-cover-moisture complexes can be incorporated in one of the parametric infiltration models to develop the standard infiltration capacity curve for a given soil-cover-moisture complex. The

SCS method involves the selection of a runoff curve number (CN) for each soil-cover-moisture complex. The CN for the hydrologic soil-cover-moisture complex is functionally related to the potential infiltration, S, in inches as

$$CN = \frac{1000}{S + 10} \quad . \quad . \quad . \quad . \quad . \quad . \quad . \quad . \quad . \quad . \quad . \quad (101)$$

or

$$S = \frac{1000}{CN} - 10 \quad . \quad . \quad . \quad . \quad . \quad . \quad . \quad . \quad . \quad . \quad . \quad (102)$$

One of the primary assumptions in the SCS method is

$$\frac{F}{S} = \frac{Q}{R_e} \quad . \quad . \quad . \quad . \quad . \quad . \quad . \quad . \quad . \quad . \quad . \quad (103)$$

in which F = actual cumulative infiltration excluding the initial abstraction, I_a, in inches, Q = actual direct runoff in inches, and R_e = potential runoff or effective storm rainfall (i.e., accumulated storm rainfall, R, minus the initial abstraction, in inches), namely

$$R_e = R - I_a \quad . \quad . \quad . \quad . \quad . \quad . \quad . \quad . \quad . \quad . \quad . \quad (104)$$

Also, by continuity

$$R_e = F + Q \quad . \quad . \quad . \quad . \quad . \quad . \quad . \quad . \quad . \quad . \quad . \quad (105)$$

From Eqs. 104 and 105, immediately

$$R = I_a + F + Q \quad . \quad . \quad . \quad . \quad . \quad . \quad . \quad . \quad . \quad . \quad . \quad (106)$$

or

$$F = R - I_a - Q \quad . \quad . \quad . \quad . \quad . \quad . \quad . \quad . \quad . \quad . \quad . \quad (107)$$

Substituting Eqs. 104 and 107 into Eq. 103 for R_e and F, respectively, yields

$$Q = \frac{(R - I_a)^2}{R - I_a + S} \qquad \text{for } R \geq I_a \quad . \quad . \quad . \quad . \quad . \quad . \quad (108)$$

or

$$F = \left(\frac{R - I_a}{R - I_a + S} \right) S \qquad \text{for } R \geq I_a \quad . \quad . \quad . \quad . \quad . \quad . \quad (109)$$

Equation 109 is the expression of the actual cumulative infiltration excluding I_a, as defined previously. The limitation, $R \geq I_a$, imposed in Eqs. 108 and 109 is necessary because both Q and F are not defined outside of the limitation.

The initial abstraction, I_a, consists mainly of interception and surface and subsurface storage, all of which occur before runoff begins. To remove the necessity for estimating these variables, the relation between I_a and S (which includes I_a) was roughly developed by the SCS (1969) through rainfall-runoff data for experimental small watersheds less than 10 acres in size as

$$I_a = 0.2\ S \quad . \quad . \quad . \quad . \quad . \quad . \quad . \quad . \quad . \quad . \quad . \quad (110)$$

Although Eq. 110 has a large standard error of estimate, it was assumed valid in the SCS method for lack of any better relationship.

On substitution of I_a from Eq. 110 into Eq. 109, the expression of F reduces to

$$F = \left(\frac{R - 0.2\ S}{R + 0.8\ S} \right) S \qquad \text{for } R \geq 0.2\ S \quad . \quad . \quad . \quad . \quad . \quad . \quad (111)$$

If the accumulated storm rainfall, $R(t)$, at any time, t, is known or computed from Eq. 88, i.e.,

$$R(t) = \int_0^t r(t)\, d\tau = \bar{r}\,(t)\ t \quad . \quad . \quad . \quad . \quad . \quad . \quad . \quad (112)$$

then Eq. 111 can be used to compute the corresponding F. Substituting Eq. 112 for the expression of R into Eq. 111 and then differentiating the result with respect to t yields

$$f = \frac{S^2 r(t)}{[\bar{r}(t)t + 0.8\ S]^2} \qquad \text{for } t \geq t_p \quad . \quad . \quad . \quad . \quad . \quad (113)$$

At $t = t_p$, if I_a consists only of infiltration before runoff starts, then from Eqs. 110 and 112,

$$\bar{r}(t_p)t_p = R(t_p) = 0.2\ S \quad . \quad . \quad . \quad . \quad . \quad . \quad . \quad . \quad . \quad (114)$$

On substitution of Eq. 114 for R at $t = t_p$, Eqs. 111 and 113 yield $F = 0$ and $f = r(t_p)$, respectively. Equation 113 is the general expression of the infiltration capacity curve for the given soil-cover-moisture complex under study.

The SCS method provides a guideline for the estimation of runoff curve numbers (CN) for various complexes, as shown in Table 5. The corresponding S can be computed from Eq. 102 or can be read directly from Table 6, which also provides adjustments of CN under three antecedent soil moisture conditions (AMC). For convenience, Eq. 113 can be further arranged into the following dimensionless form and plotted, as shown in Figure 22.

$$\frac{f}{r} = \frac{1}{[\bar{r}(t)t/S + 0.8]^2} \qquad \text{for } \frac{t}{t_p} \geq 1 \quad . \quad . \quad . \quad . \quad (115)$$

or

$$\frac{f}{r} = \frac{1}{(R/S + 0.8)^2} \qquad \text{for } \frac{R}{S} \geq 0.2 \quad . \quad . \quad . \quad . \quad (116)$$

The time of ponding, t_p, corresponding to this infiltration capacity curve (Eq. 115 or 116) is immediately evident from Eq. 114:

$$t_p = \frac{0.2\ S}{\bar{r}} \quad . \quad . \quad . \quad . \quad . \quad . \quad . \quad . \quad . \quad . \quad . \quad (117)$$

The foregoing result in which the dimensionless infiltration capacity, f/r, is unique for a specified value of the dimensionless parameter, R/S, is hardly convincing in the light of so many variables involved in the infiltration process. Although the S (or CN) value may be regarded as an index measuring combined hydrologic effects of the variables on infiltration for a given soil-cover-moisture complex, Eq. 113 does not seem to be a valid expression, when it is compared with the wide variety of actual infiltration decay curves. The following deficiencies are noted in Eq. 113:

Table 5. Runoff curve numbers (CN) for hydrologic soil-cover complexes (after USDA SCS, 1969). (Antecedent moisture condition II and $I_a = 0.2\ S$)

Land Use	Cover: Treatment or practice	Cover: Hydrologic condition	Hydrologic Soil group			
			A	B	C	D
Fallow	Straight row	--	77	86	91	94
Row Crops	Straight row	Poor	72	81	88	91
	Straight row	Good	67	78	85	89
	Contoured	Poor	70	79	84	88
	Contoured	Good	65	75	82	86
	Contoured and terraced	Poor	66	74	80	82
	Contoured and terraced	Good	62	71	78	81
Small grain	Straight row	Poor	65	76	84	88
	Straight row	Good	63	75	83	87
	Contoured	Poor	63	74	82	85
	Contoured	Good	61	73	81	84
	Contoured and terraced	Poor	61	72	79	82
	Contoured and terraced	Good	59	70	78	81
Closed-seeded legumes[a] or rotation meadow	Straight row	Poor	66	77	85	89
	Straight row	Good	58	72	81	85
	Contoured	Poor	64	75	83	85
	Contoured	Good	55	69	78	83
	Contoured and terraced	Poor	63	73	80	83
	Contoured and terraced	Good	51	67	76	80
Pasture or range		Poor	68	79	86	89
		Fair	49	69	79	84
		Good	39	61	74	80
	Contoured	Poor	47	67	81	88
	Contoured	Fair	25	59	75	83
	Contoured	Good	6	35	70	79
Meadow (permanent)		Good	30	58	71	78
Woods (farm woodlots)		Poor	45	66	77	83
		Fair	36	60	73	79
		Good	25	55	70	77
Farmsteads		--	59	74	82	86
Roads (dirt)[b]		--	72	82	87	89
(hard surface)[b]		--	74	84	90	92

[a]Close-drilled or broadcast.
[b]Including right-of-way.

Table 6. Runoff curve numbers (CN) and corresponding S values under various antecedent moisture conditions (AMC) for the case $I_a = 0.2$ S (after USDA SCS, 1969).

CN for AMC II	CN for AMC I	CN for AMC III	S values* (inches)	CN for AMC II	CN for AMC I	CN for AMC III	S values* (inches)
100	100	100	0	60	40	78	6.67
99	97	100	.101	59	39	77	6.95
98	94	99	.204	58	38	76	7.24
97	91	99	.309	57	37	75	7.54
96	89	99	.417	56	36	75	7.86
95	87	98	.526	55	35	74	8.18
94	85	98	.638	54	34	73	8.52
93	83	98	.753	53	33	72	8.87
92	81	97	.870	52	32	71	9.23
91	80	97	.989	51	31	70	9.61
90	78	96	1.11	50	31	70	10.0
89	76	96	1.24	49	30	69	10.4
88	75	95	1.36	48	29	68	10.8
87	73	95	1.49	47	28	67	11.3
86	72	94	1.63	46	27	66	11.7
85	70	94	1.76	45	26	65	12.2
84	68	93	1.90	44	25	64	12.7
83	67	93	2.05	43	25	63	13.2
82	66	92	2.20	42	24	62	13.8
81	64	92	2.34	41	23	61	14.4
80	63	91	2.50	40	22	60	15.0
79	62	91	2.66	39	21	59	15.6
78	60	90	2.82	38	21	58	16.3
77	59	89	2.99	37	20	57	17.0
76	58	89	3.16	36	19	56	17.8
75	57	88	3.33	35	18	55	18.6
74	55	88	3.51	34	18	54	19.4
73	54	87	3.70	33	17	53	20.3
72	53	86	3.89	32	16	52	21.2
71	52	86	4.08	31	16	51	22.2
70	51	85	4.28	30	15	50	23.3
69	50	84	4.49				
68	48	84	4.70	25	12	43	30.0
67	47	83	4.92	20	9	37	40.0
66	46	82	5.15	15	6	30	56.7
65	45	82	5.38	10	4	22	90.0
64	44	81	5.62	5	2	13	190.0
63	43	80	5.87	0	0	0	infinity
62	42	79	6.13				
61	41	78	6.39				

*Corresponding to CN for AMC II.

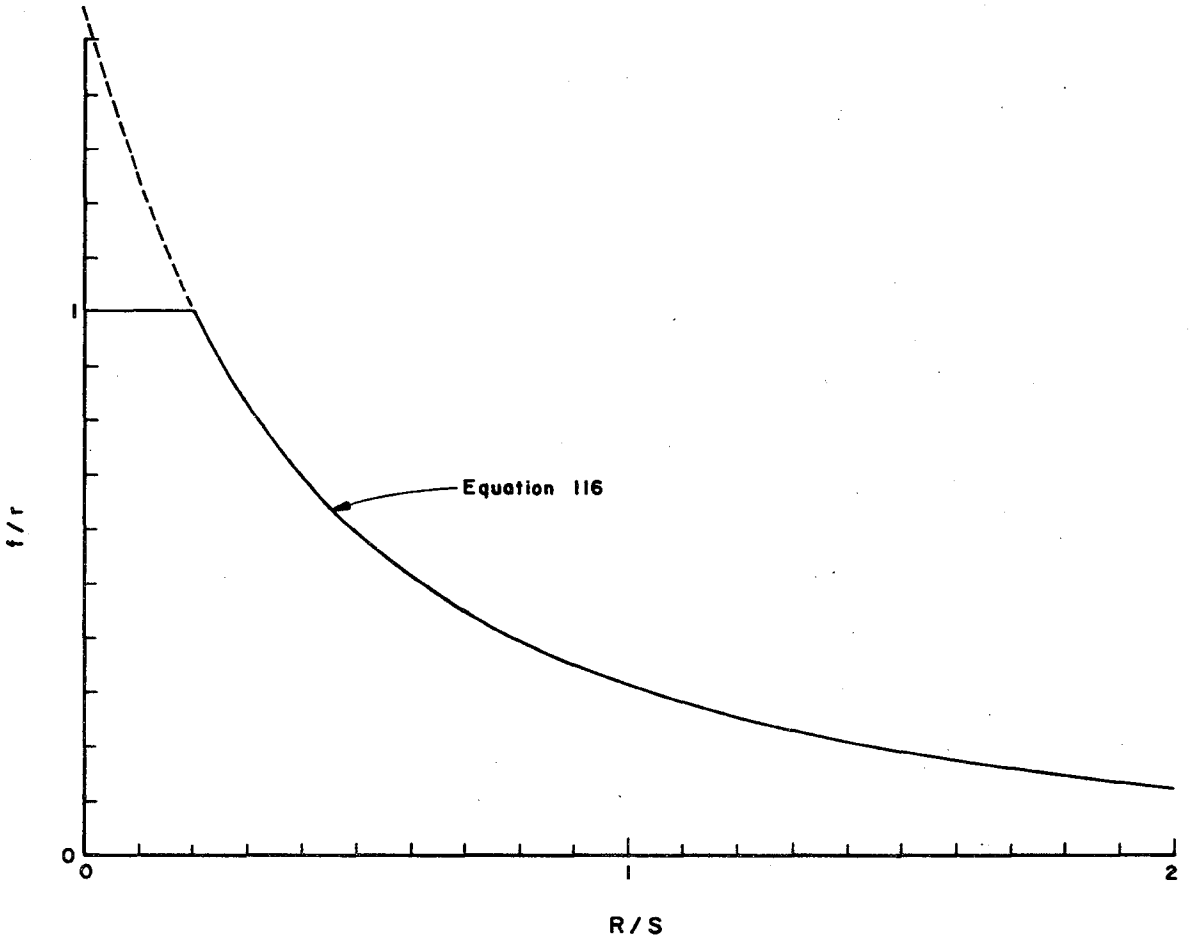

Figure 22. Dimensionless infiltration-capacity curve for a given soil-cover-moisture complex with known S under rainfall R(t) or intensity r(t).

(1) For a given soil-cover-moisture complex, if the potential infiltration, S, that is a specified value in the SCS method can be interpreted as the water-storage potential of the soil above the first impeding stratum (Holtan, 1961), Eq. 113 fails to describe the case in which the infiltration rate after prolonged wetting approaches to a constant f_∞.

(2) The denominator on the right-hand side of Eq. 113 has an exponent equal to 2, which is apparently too high for Eq. 113 to be properly fit to any of available infiltration decay curves.

Due mainly to these deficiencies, Eq. 113 should be modified to best fit the available field data. Since the Holtan (1961) type parametric infiltration model, Eq. 92, has a term, P, which is similarly defined as S, applicability of Eq. 92 based on the selection of a runoff curve number for each soil-cover-moisture complex will be examined.

Modified Holtan Type Infiltration Model

For convenience, Holtan's (1961) algebraic equation, Eq. 92, is rewritten as (Glymph et al., 1969 and 1971; Holtan, 1971):

$$f = f_\infty + aS_a^n \quad \text{for } t \geq t_p \quad . \quad . \quad . \quad . \quad . \quad . \quad . \quad . \quad (118)$$

in which S_a is the available storage in the surface layer (the ''A'' horizon in agricultural soils) in inches water equivalent; a is the infiltration capacity in inches per hour per unit of available storage (called a land use parameter or a coefficient of pore-space continuity, estimated as the product of vegetative density at plant maturity and stage of growth in percent from Table 7); and n is thought to be a function of soil texture, measured to be about equal to 1.4 for silt loams. The constant rate of infiltration, f_∞, after prolonged wetting is associated with capillary flow or with an impeding stratum (the ''B'' horizon). (See Appendix B for definitions of A- and B- horizons.) Musgrave (1955) arranged four infiltration groups in order of final infiltration rates for four hydrologic soil groups A, B, C, and D as follows:

Soil	Final Infiltration Rates (f_∞)
Group A	0.45 ~ 0.30 in./hr
Group B	0.30 ~ 0.15 in./hr
Group C	0.15 ~ 0.05 in./hr
Group D	0.05 ~ 0.00 in./hr

The upper limit of f_∞ in group A seems to be unrealistic, since the f_∞ value in some soils exceeds this limit.

Table 7. Tentative estimates of vegetative parameter "a" in the Holtan equation (after Holtan, 1971).

Land Use or Cover	Condition & Basal Area Rating*			
Fallow	After Row Crop	0.10	After Sod	0.30
Row Crops	Poor	0.10	Good	0.20
Small Grains	"	0.20	"	0.30
Hay (Legumes)	"	0.20	"	0.40
Pasture (Bunch Grass)	"	0.20	"	0.40
Hay (Sod)	"	0.40	"	0.60
Temporary Pasture (Sod)	"	0.40	"	0.60
Permanent Pasture (Sod)	"	0.80	"	1.00
Woods and Forests	"	0.80	"	1.00

*Adjustments needed for "weeds" and "grazing."

By comparison between Eqs. 92 and 118, it immediately follows that

$$S_a = S - F \qquad . \quad . \quad . \quad . \quad . \quad . \quad . \quad . \quad . \quad . \quad . \quad (119)$$

Substituting Eq. 111 into Eq. 119 yields

$$S_a = \frac{S^2}{R + 0.8\,S} \qquad . \quad . \quad . \quad . \quad . \quad . \quad . \quad . \quad . \quad . \quad . \quad (120)$$

This is the exact expression of Holtan's S_a in terms of S and R, derived on the premise that one S (or CN) value can be assigned to each hydrologic soil-cover-moisture complex. The adaptability of Eq. 120 is apparent because at $t = t_p$, $S_a = S$ resulting from $R(t_p) = 0.2\,S$ (Eq. 114), and S_a approaches zero as $t \to \infty$ [i.e., $R(t) \to \infty$ by definition, see Eq. 112]. The infiltration capacity curve equivalent to Eq. 113 expressed in terms of this S_a and S can thus be derived from Eqs. 120 and 113:

$$f = \left(\frac{S_a}{S}\right)^2 r \qquad \text{for } t \geq t_p \qquad . \quad . \quad . \quad . \quad . \quad . \quad . \quad (121)$$

which again has the same deficiencies as Eq. 113.

For modifying Eq. 121, Holtan's equation (Eq. 118), after its S_a being substituted by Eq. 120, can be expressed as

$$f = f_\infty + a\left(\frac{S}{R/S + 0.8}\right)^n \qquad \text{for } t \geq t_p \qquad . \quad . \quad . \quad . \quad (122)$$

At a glance, Eq. 122 looks better than Eq. 121, but there again are inherent problems of applying Eq. 122 to actual field conditions. It is noted that for a given soil-cover-moisture complex the values of the parameters S, a, and n, are more or less fixed (viz., "S" from Tables 5 and 6, "a" from Table 7, and n = 1.4 for silt loams). There seems no way for Eq. 122 to be modified or adjusted in accordance with the infiltration capacity curve, measured in the field. Even though one may assume that the vegetative parameter, a, or the soil-texture parameter, n, is still adjustable, the infiltration rate f in Eq. 122 cannot be set equal to any given rainfall intensity, r, at the time of ponding ($t = t_p$). Any attempt to modify Eq. 122 further in order to remedy the preceding deficiencies may result in an expression similar to the modified Kostiakov infiltration equation that is another type of model analyzed herein.

Modified Kostiakov Type Infiltration Model

The modified Kostiakov equation, Eq. 62, is indeed a two-parameter model, as mentioned previously, because f_∞ is supposedly known for a given soil and t_p and t_o have been shown to be related to the two parameters, A and α, by Eqs. 77 and 78, respectively. If one accepts the same premise that one S (or CN) value can be assigned to each hydrologic soil-cover-moisture complex, another type of the modified Kostiakov equation containing the parameter S can be formulated.

A plot of Eq. 117 for a given S indicates that a realistic form of the upper infiltration envelope should include the final infiltration rate, f_∞. Accordingly, Eq. 117 is modified to

$$t_p = \frac{CS}{\bar{r} - f_\infty} \qquad (123)$$

in which C is the coefficient assumed to be 0.2 in the SCS method. Adoption of Eq. 117 implies the hypothesis that the time, t_p, at which surface ponding occurs under rain is the time at which the cumulative rain infiltration is equal to the cumulative flooded infiltration (i.e., the case for immediate ponding). Equation 117, or a modified form thereof (Eq. 123), is another major assumption in the SCS method in addition to formerly assumed Eq. 103. This is the basic difference in the assumptions involved in the derivation of Eq. 117 or 123 from that of Eq. 77. In other words, Eq. 77 has been derived based on the assumption that the final or total cumulative rain infiltration for the soil with the same water-storage potential is always constant, regardless of application rates (see Figure 13). With the latter hypothesis, the values of Kostiakov's model parameters A and α under various rainfall intensities have been assumed to be constant. A question may arise as to how the Kostiakov equation, Eq. 62, can be modified so that it will still be valid under the new hypothesis or infiltration envelope (Eq. 123). Integrating Eq. 62 from 0 to t_p and then

equating the result to the initial abstraction (Eq. 110) that is constant for a given S yields the expression of the parameter A. Unfortunately, the parameter A so obtained is not a constant, but varies with several other parameters in the Kostiakov equation. For simplicity, however, if the parameter t_o is assumed as being related to t_p through Eq. 79, then the expression of the parameter A is simplified to

$$A = [CS(1 - \alpha)]^{\alpha} (\bar{r} - f_{\infty})^{1-\alpha} \quad . \quad . \quad . \quad . \quad . \quad . \quad . \quad (124)$$

which is the same result as obtained by equating Eq. 123 to Eq. 77. Equation 124 clearly indicates that assigned an S value for a given soil-cover-moisture complex, the value of the parameter A in the Kostiakov equation cannot be uniquely determined by the S value alone. Aside from $\bar{r}$ and f_{∞}, the value of the parameter α, ranging from 0 to 1 exclusive, obviously controls the A value. The relationship between the parameters A and α will become more clear if the parameter A is expressed in terms of t_p by substituting the expression of CS from Eq. 123 into Eq. 124 as follows:

$$A = [(1 - \alpha)t_p]^{\alpha} (\bar{r} - f_{\infty}) \quad . \quad . \quad . \quad . \quad . \quad . \quad . \quad . \quad (125)$$

Substituting Eqs. 79 and 125 into Eq. 62 yields

$$f = f_{\infty} + \left[\frac{1 - \alpha}{(t/t_p) - \alpha}\right]^{\alpha} (\bar{r} - f_{\infty}) \quad \text{for } t \geq t_p \quad . \quad . \quad (126a)$$

or in a dimensionless form,

$$\frac{f - f_{\infty}}{\bar{r} - f_{\infty}} = \left[\frac{1 - \alpha}{(t/t_p) - \alpha}\right]^{\alpha} \quad \text{for } \frac{t}{t_p} \geq 1 \quad . \quad . \quad . \quad . \quad (126b)$$

Equation 126 is the modified two-parameter Kostiakov infiltration equation, expressed in terms of t_p and α.

For illustration, Eq. 126a for CN = 90 (i.e., S = 1.11 in.), $\bar{r}$ = 10 in./hr, and various α values are plotted, as shown in Figure 23. A family of curves for the other set of CN (or S) and $\bar{r}$ values can be similarly drawn. The relative importance of the roles which the parameters, t_p and α, play in the infiltration capacity curves can readily be seen from Figure 23. In general, for a given soil-cover-moisture complex, the value of S is fixed and that of t_p is subsequently determined by Eq. 123, depending upon the $\bar{r}$ and f_{∞} values. Once the t_p value is calculated, the pattern or shape of the infiltration capacity curve depends solely on the α value which must be determined from other means. Whether

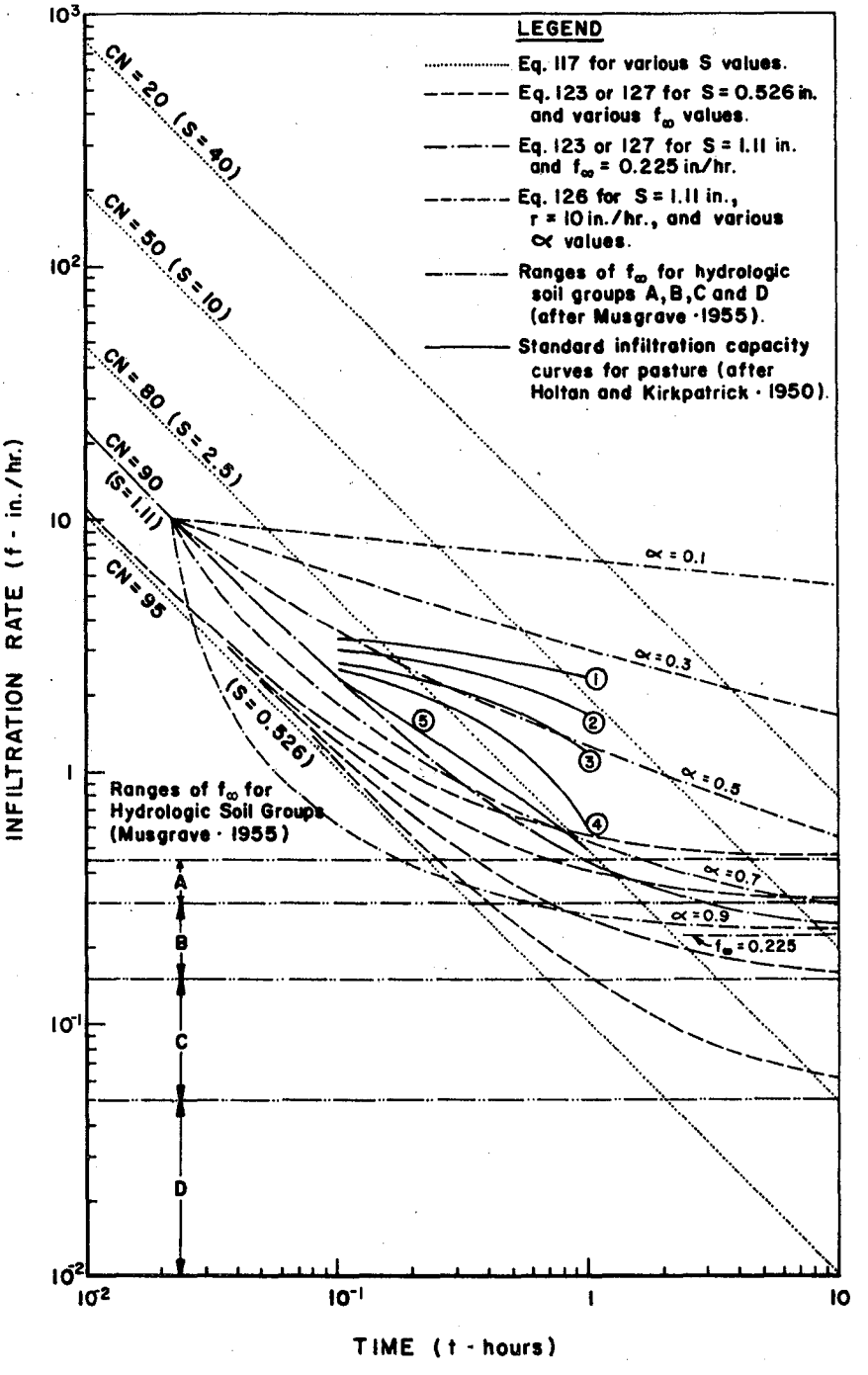

Figure 23. The modified Kostiakov-type infiltration capacity curves (Equation 126a).

or not the α value is another measure of the soil-cover-moisture complex should be investigated in the future.

It appears that the importance of the α value is only secondary to the S because without α Eq. 123 can be used to approximate the infiltration capacity curve as follows:

$$f = f_\infty + \frac{CS}{t} \quad . \quad . \quad . \quad . \quad . \quad . \quad . \quad . \quad . \quad . \quad . \quad (127)$$

in which the coefficient C can still be assumed to be the same 0.2 as made previously. Equation 127 is plotted in Figure 23, along with Eq. 126a, for comparison. It can readily be seen from Figure 23 that Eq. 127 approximates Eq. 126a for $\alpha = 0.5$ at the beginning (viz., $t = t_p$) and tends to describe Eq. 126a with the α value close to unity as t goes to infinity. The comparison can be made more clear if Eq. 126b and a dimensionless form of Eq. 127 or

$$\frac{f - f_\infty}{\bar{r} - f_\infty} = \frac{t_p}{t} \quad . \quad . \quad . \quad . \quad . \quad . \quad . \quad . \quad . \quad . \quad . \quad (128)$$

are plotted on log-log paper, as shown in Figure 24. Therefore, if the α value is unknown or unspecified for a given soil-cover-moisture complex, Eq. 127 or 128 may be used to approximate the desired infiltration capacity curve for the complex.

Standard Infiltration-Capacity Curves

Standard infiltration-capacity curves, as derived from analyses of a number of storms on single-practice watersheds, provide a basis for classifying or grouping soil-cover-moisture complexes (Musgrave and Holtan, 1964). In reverse, therefore, each soil-cover-moisture complex should have a unique standard infiltration-capacity curve, the segment of which can be used to subtract an actual or design hyetograph for routing a given rainstorm. However, to develop standard infiltration-capacity curves for all the various soil-cover-moisture complexes representing on highway sideslopes is a formidable task. For lack of data from known sources of information, it was impossible in the present study to develop the standard curves for all possible combinations of the complexes. While achieving this as a final goal, our continuing efforts and the present investigation is primarily directed to laying groundwork for future studies by analyzing a relatively few soil-cover-moisture complexes which are assumed to represent the same standard infiltration-capacity curves as those on standard highway sideslopes under similar field conditions.

A review of literature reveals that the single major source of experimental data which may lead to the construction of the standard

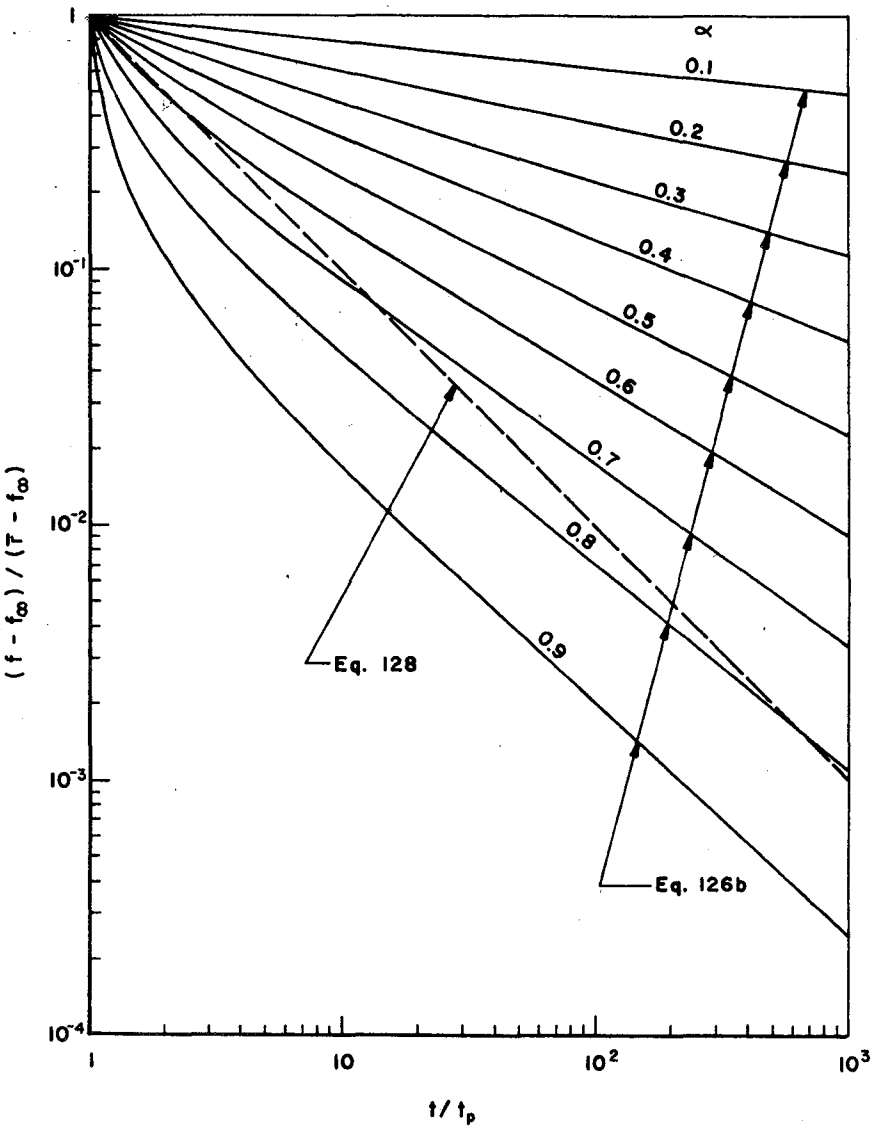

Figure 24. The normalized, modified Kostiakov infiltration (Equation 126b) compared with the simplified infiltration equation (Equation 128).

infiltration-capacity curves is the early work of Holtan and his associates (Holtan and Musgrave, 1947; Sharp, Holtan, and Musgrave, 1949; Holtan and Kirkpatrick, 1950; Musgrave, 1955; and Musgrave and Holtan, 1964). Holtan and Kirkpatrick (1950) have developed typical mass-infiltration curves for various plant covers and soil surface conditions, basing on data from Cecil, Madison, and Durham soils (all classified under hydrologic soil group B), but none of them appears to be under the same field conditions as those found on urban highway sideslopes which are planted with various species of grass. The nearest true mass-infiltration curves which can be selected to represent the overall field situations are probably ones determined for permanent pasture with various ages of growth and the degrees of grazing. From these mass curves, the corresponding standard infiltration-capacity curves have been computed and plotted as shown in Figure 25. Five standard infiltration-capacity curves in solid lines, numbered from 1 to 5 in the numerical order, show respectively those for old permanent pasture, 4-8-year-old permanent pasture, 3-4-year-old permanent pasture lightly grazed, permanent pasture moderately grazed, and permanent pasture heavily grazed. The differences in the standard curves are mainly caused by the differences in the maturity and treatment of grass and its ability to protect the soil surface from surface sealing due to raindrop impact under continuous entry of water. In other words, for each soil-moisture complex under the same antecedent moisture conditions, the infiltration capacity is highly related to the density of the plant cover. A comparison of the five standard curves indicates that the more mature or less grazed is the permanent pasture, the higher the infiltration capacity and vice versa. As a matter of fact, this result is consistent with Holtan and Musgrave's (1947) findings, as shown in Table 2. For comparison, these five standard curves labeled 1 to 5 in circles as shown in Figure 25 are plotted in Figure 23 and labeled in a similar manner.

For the same good Bluegrass cover on Bogota (group C), Alma (group C), Elco (group B), and Drury (group B) soils in a small watershed near Edwardsville, Illinois, Sharp, Holtan, and Musgrave (1949) investigated the effects of antecedent soil moisture conditions and topsoil thickness on the infiltration capacity. From the average mass-infiltration curves, the infiltration-capacity curves are computed and plotted in Figure 25 for comparison with standard infiltration curves. It can readily be seen from Figure 25 that the effect of topsoil thickness (curves L and M) is smaller than that of antecedent soil moisture content (curves I, II, and III) on the infiltration-capacity curve. However, this trend, viz., the increasing infiltration under the same protective Bluegrass cover from the deep topsoil to the shallow topsoil matter, is contradictory to Holtan and Musgrave's (1947) earlier findings in which the trend was exactly reversed (see Table 2). In the light of this inconsistency in the experimental results, the effect of topsoil thickness on the infiltration capacity, if any, can be either assumed to be negligibly small or merged in that of subsoil properties, and hence will be ignored from the present analysis. Antecedent soil moisture condition on the other hand is one of the most predominant factors affecting the infiltration capacity and thus requires additional supporting data for estimating the general trend of its effects.

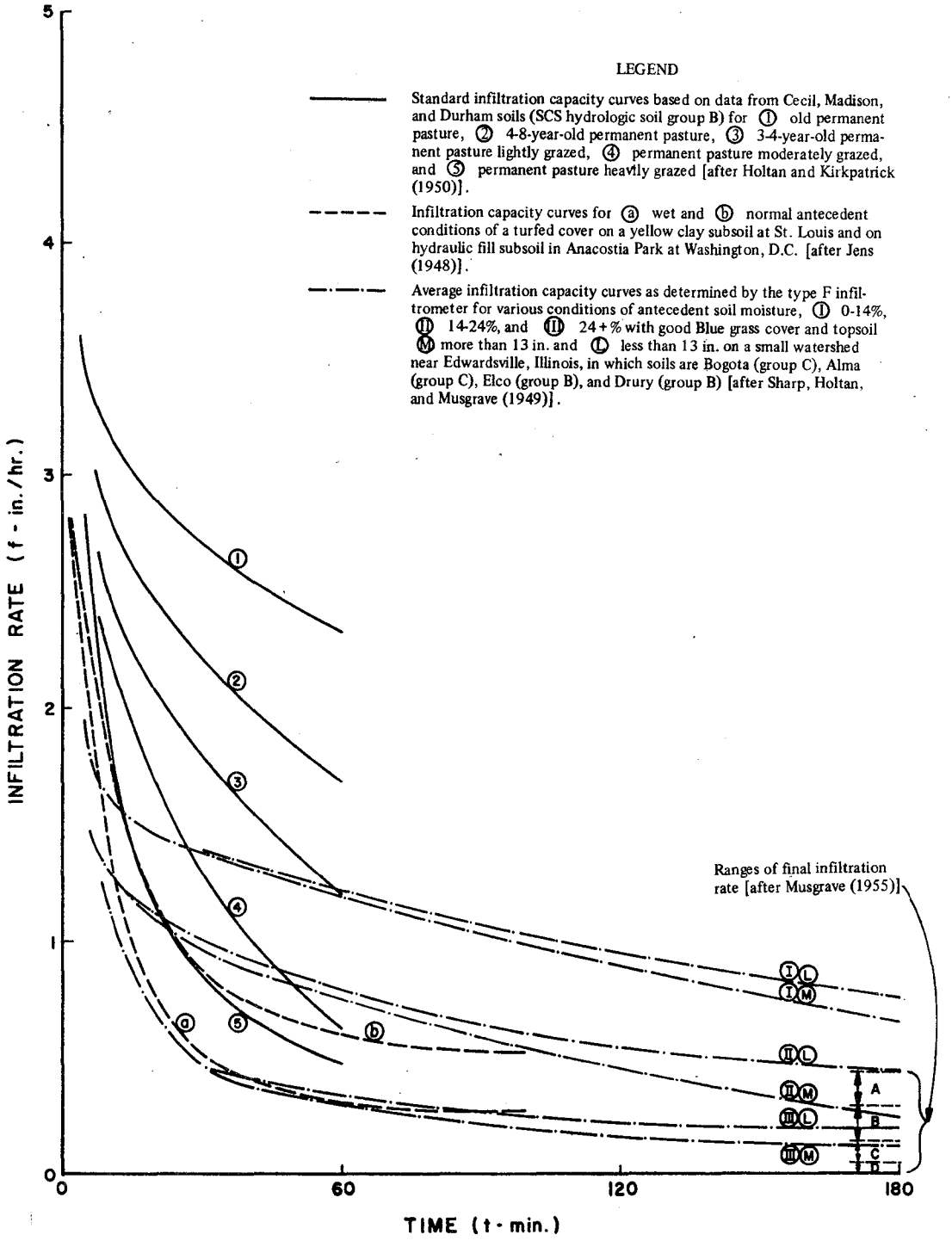

Figure 25. Standard infiltration-capacity curves for pasture, city lawn grass, and bluegrass on soils with various antecedent soil moisture conditions.

The theoretical trend of the effect of initial moisture content on the infiltration capacity was already demonstrated in Figure 9 for Vernal sandy clay loam. A similar trend was observed by Sherman (1940) on soils in Macoupin Creek Basin above Kane, Illinois, as shown in Figure 26. Also Jens (1948), after a series of tests both at St. Louis for city lawn grass on a yellow clay subsoil and at Washington D.C. for city lawn grass on hydraulic fill subsoil consisting of mud dredged from the Potomac River, found that the infiltration capacities for these two turfed areas were very nearly identical for similar antecedent soil moisture conditions, as shown in Figure 25 (curves a and b). A comparison of the infiltration-capacity curves in Figure 25 for similar antecedent soil moisture conditions from Jens (1948) and Sharp et al. (1949) reveals that despite large differences in soil properties for their soils under investigation a segment of each of the infiltration capacity curves compared coincides with each other at the early stage of infiltration with the better coincidence resulting from the wetter conditions. This implies that the large differences in soil characteristics have relatively little effect under wet or above normal soil moisture conditions.

The preceding comparisons are rather interesting because for a given soil-cover-moisture complex it may be concluded that plant cover and antecedent soil moisture conditions predominantly control the infiltration capacity, especially at the early stage of infiltration. Of course, when infiltration time becomes longer, the inherent soil characteristics have more influence on the infiltration capacity in that the infiltration rate eventually becomes the saturated hydraulic conductivity as time approaches infinity. The relative significance or insignificance of the three factors (viz., soil, plant cover, and antecedent moisture conditions) with respect to the infiltration time, as described above, again justifies the general use of the modified Kostiakov infiltration equation, Eq. 126, or a simplified form thereof, Eq. 127, for each soil-cover-moisture complex, provided that the model parameters such as S (or t_p), α, and f_∞ can accurately be evaluated.

The hydrologic soil group classification (USDA SCS, 1969), along with a rating table developed on the basis of the catena concept (Chiang, 1971), as appended to this report, help in selection of the f_∞ value for a given soil, using Musgrave's (1955) minimum infiltration-rate classification criteria. The value of S for a given soil-cover-moisture complex can then be determined from Tables 5 and 6. Where Eq. 126 is to be used, this will leave only one unknown parameter, α, yet to be determined from other means. If Eq. 127 will be used to describe the standard infiltration-capacity curve for the given soil-cover-moisture complex, the parameter, α, no longer enters the formulation. The determination of the α value is very difficult, even by trial and error. For many practical purposes, however, the α value in Eq. 126 may be assumed to be 0.5 as a first approximation.

For general use in design, it is assumed that the standard infiltration-capacity curves for the various soils of agricultural land with grass cover, used as meadow or pasture, at different stages of maturity and

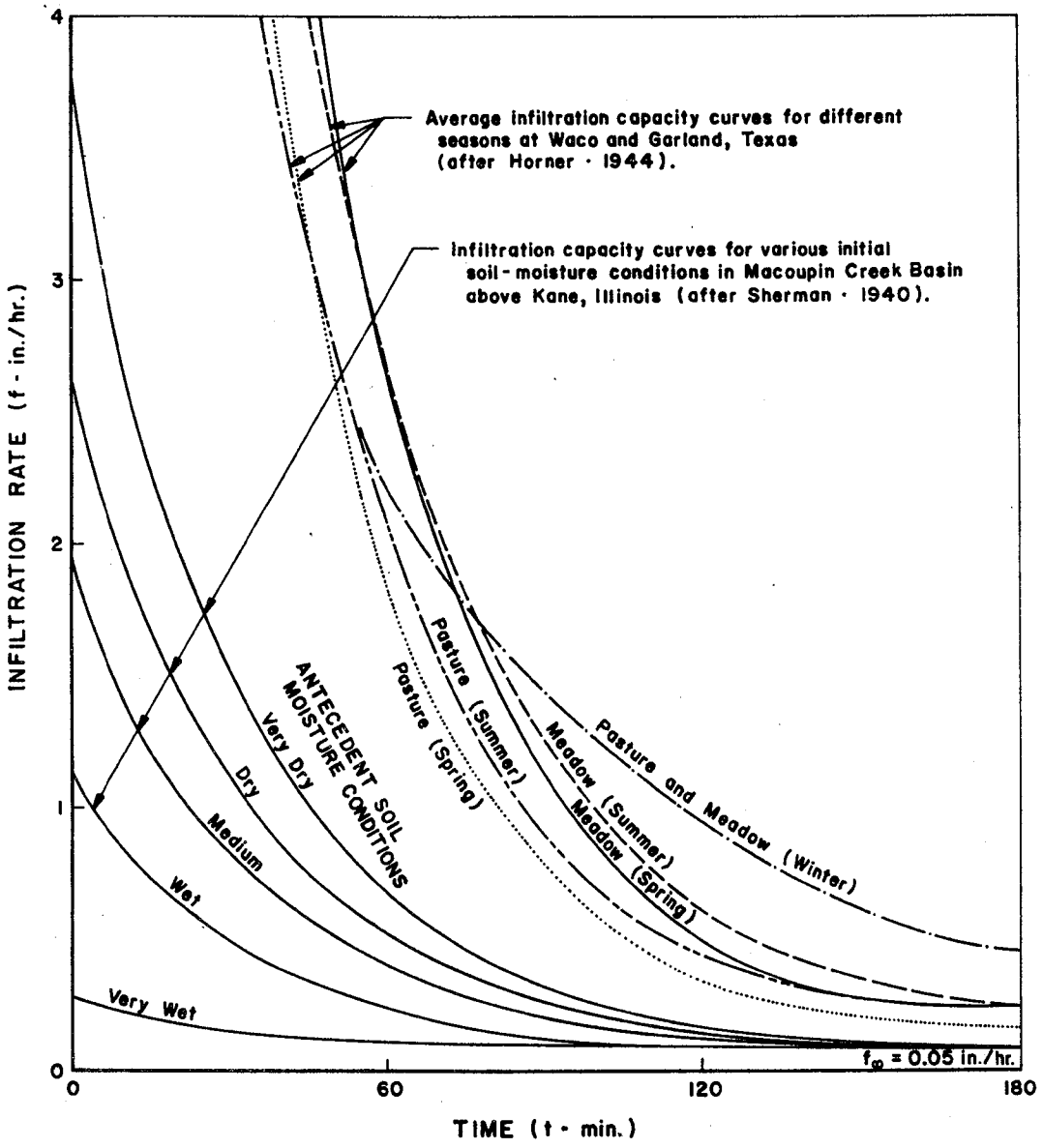

Figure 26. Standard infiltration-capacity curves as affected by seasonal changes and various antecedent (initial) soil moisture conditions.

grazing, as marked numerically in Figure 25, are generally applicable to urban highway sideslopes under similar grass cover and antecedent moisture conditions. In Figure 25, although the five standard infiltration-capacity curves for permanent pasture were obtained based on data from Cecil, Madison, and Durham soils which are all classified as hydrologic soil group B by Soil Conservation Service (USDA SCS, 1969), the exact value of f_∞ is unknown except in general terms by its range (Musgrave, 1955). For estimating the f_∞ value at the same time that S is evaluated for each of the five standard curves, the method of least squares is applied to Eq. 127 by minimizing the expression

$$Q(f_\infty, S) = \sum_{j=1}^{m} (f_j t_j - f_\infty t_j - CS)^2 \quad . \quad . \quad . \quad . \quad . \quad . \quad (129)$$

for the ''m'' number of measured or observed data points (f_j, t_j), $j = 1, 2, \ldots, m$ picked off the curve. The least squares estimates of f_∞ and S, $\hat{f}_\infty$ and $\hat{S}$, can thus be expressed

$$\hat{f}_\infty = \frac{m\Sigma_j f_j t_j^2 - \Sigma_j f_j t_j \Sigma_j t_j}{m\Sigma_j t_j^2 - (\Sigma_j t_j)^2} \quad . \quad . \quad . \quad . \quad . \quad . \quad . \quad (130)$$

$$\hat{S} = \frac{1}{mC} (\Sigma_j f_j t_j - \hat{f}_\infty \Sigma_j t_j) \quad . \quad . \quad . \quad . \quad . \quad . \quad . \quad (131)$$

When the values of $\hat{f}_\infty$ and $\hat{S}$ for each of the five standard infiltration curves were calculated by means of Eqs. 130 and 131, it was found that the best estimates of the first three curves, as marked (1), (2), and (3) in Figure 25, yielded extremely high values of f_∞, respectively 2.11, 1.42, and 0.92 in./hr, which are far above Musgrave's (1955) specified range, 0.15 to 0.30 in./hr, for the hydrologic soil group B. The standard infiltration curves with unnecessarily high estimated values of f_∞ are judged to be erroneously fit by use of Eq. 127. For curve-fitting of such standard infiltration curves, general equation, Eq. 126, with freedom in varying the α value should be applied instead. Nevertheless, for lack of an optimization method to best fit Eq. 126 to the standard infiltration curves, no attempt was made to estimate the α values for such standard infiltration curves in the present study.

Three basic standard infiltration-capacity curves are adequately fit by Eq. 127 as follows:

(I) The standard infiltration-capacity curve for permanent pasture moderately grazed (Holtan and Kirkpatrick, 1950), as marked (4) in

Figure 25, is best fit by Eq. 127 with the least squares estimates of f_∞ and S equal to 0.274 in./hr and 2.16 in., respectively.

(II) The standard infiltration-capacity curve for permanent pasture heavily grazed (Holtan and Kirkpatrick, 1950), as marked (5) in Figure 25, which coincides over a large segment of the curve for a turfed cover (Jens, 1948) on a yellow clay subsoil at St. Louis and Washington, D.C. under normal antecedent moisture conditions, is best fit by Eq. 127 with the least squares estimates of f_∞ and S equal to 0.188 in./hr and 1.53 in., respectively.

(III) A major portion of Jens' (1948) curve for a turfed cover on the same soil as above under wet antecedent moisture conditions coincides to the curve for good Kentucky Bluegrass cover on Bogota (group C), Alma (group C), Elco (group B), and Drury (group B) soils with topsoil less than 13 in. under 24 percent or more antecedent moisture conditions (Sharp, Holtan, and Musgrave, 1949) which is best fit by Eq. 127 with the least squares estimates of f_∞ and S (Eq. 127) equal to 0.145 in./hr and 0.84 in., respectively.

For further illustration, these three basic standard infiltration-capacity curves (Eq. 127) with the best estimates of f_∞ and S are plotted in Figure 27 and compared with previous investigators' data. An inspection of Figure 27 reveals that all the data points plotted fit well with Eq. 127 except for few Jens' (1948) data points in the later stage of infiltration. The deviation of Jens' (1948) data points from the corresponding best-fit curve may be attributed to the difference in the standard f_∞ for hydrologic soil group B from that for the actual soil.

From the practical point of view, if one can accept the plot of Eq. 127 with S = 1.53 in. and f = 0.188 in./hr as the standard infiltration-capacity curve for a basic soil-cover-moisture complex (i.e., hydrologic soil group B, grass or turf cover equivalent to permanent pasture on agricultural land, and AMC II) as representing the highway sideslopes, the standard infiltration curves for other hydrologic soil-cover-moisture complexes representing the highway sideslopes can be developed by interpolating or extrapolating runoff curve numbers from Tables 5 and 6 and hence the S values through the conversion formula, Eq. 102. In other words, the runoff curve number (CN) corresponding to S = 1.53 in. for the basic complex which is approximately equal to 87, is used to interpolate or extrapolate runoff curve numbers for other complexes.

Assuming that in Table 5 the runoff curve numbers for pasture (not contoured) and meadow (permanent) are listed in the decreasing order toward poorer hydrologic performance for each hydrologic soil group, one may draw by extrapolation a curve for the estimated runoff curve numbers for grassed highway sideslopes, as shown in Figure 28, with CN = 87 assigned to that for hydrologic soil group B and AMC II. Then, the runoff curve numbers for AMC I and AMC III corresponding to CN = 87 for AMC II are read from Table 6 to be 73 and 95, respectively. For comparison,

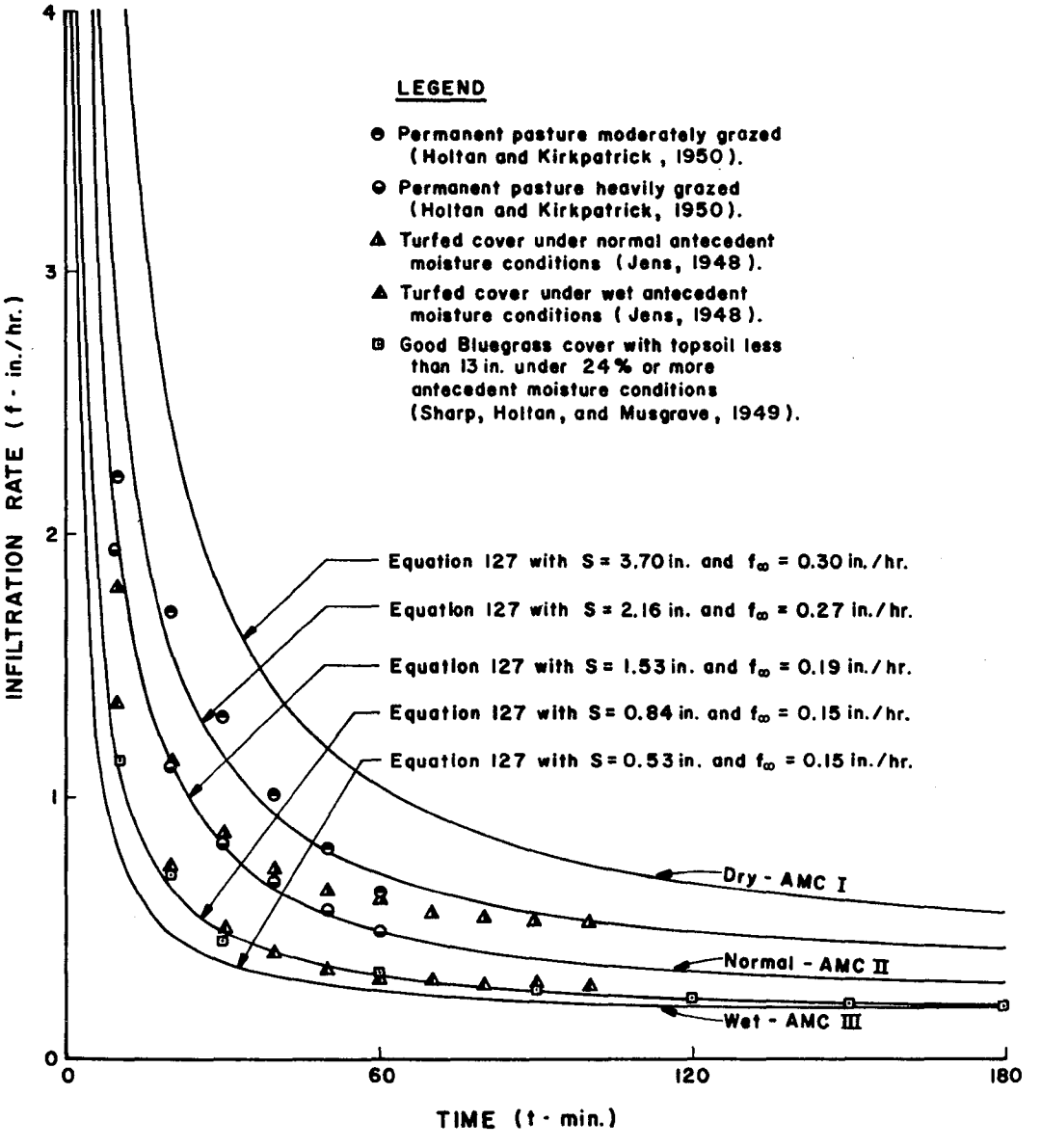

Figure 27. Hypothesized standard infiltration-capacity curves for group B subsoils with topsoil less than 13 in., covered with grass under dry, normal, and wet antecedent moisture conditions.

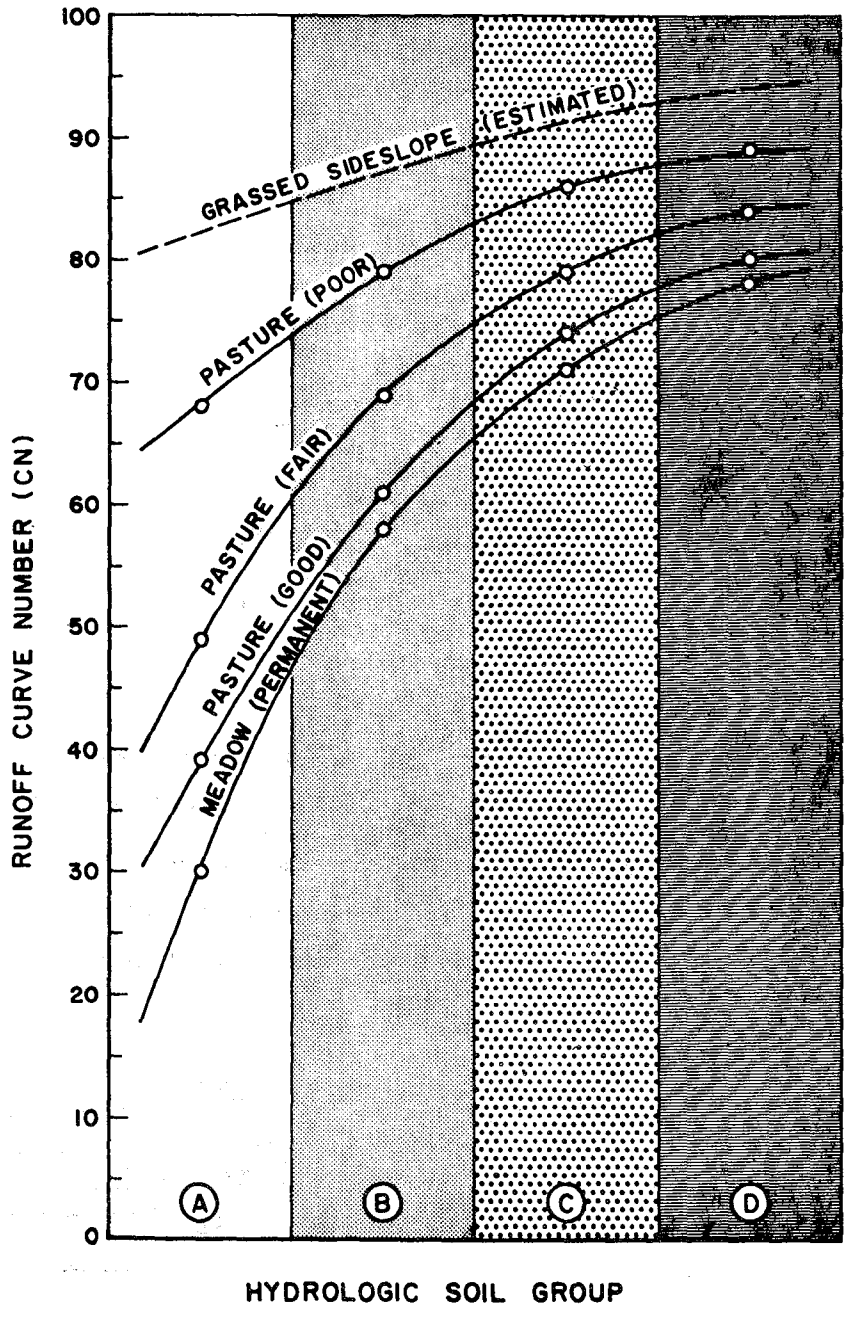

Figure 28. Type of plotting used in estimating runoff curve numbers for urban highway sideslopes. Data points for pasture and meadow are obtained from Table 5 [after USDA SCS (1969)].

Eq. 127 with CN = 73 (i.e., S = 3.70 in.) and CN = 95 (i.e., S = 0.53 in.) for hydrologic soil group B are also plotted in Figure 27. The latter two curves, along with the one formerly plotted for CN = 87, constitute a family of the standard infiltration-capacity curves for a grassed highway sideslope having hydrologic soil group B under AMC I, II, and III, respectively. Similarly, the standard infiltration-capacity curves for other hydrologic soil groups can be formulated.

For convenience in engineering application, runoff curve numbers for highway soil-cover-moisture complexes are tabulated in Table 8. Should the rating table based on the catena concept (Chiang, 1971) be used as the refined SCS classification for hydrologic soil groups, runoff curve numbers for groups +B, +C, and +D can be interpolated from Table 8. Finally the corresponding values of S can be computed from Eq. 102 and then incorporated with the estimated values of f_∞ (Musgrave, 1955) for the construction of the desired standard infiltration-capacity curves.

Unless the ground is frozen during winter, seasonal changes of the standard infiltration-capacity curves are closely related to the average antecedent soil moisture conditions of the seasons, as exemplified in a watershed at Waco and Garland, Texas (Horner, 1944) (Figure 26). The standard infiltration-capacity curves for pasture and meadow in this watershed vary with seasons in such a manner similar to the order of antecedent moisture conditions with the soils in winter judged to be the driest of the three seasons investigated. However, since the ground can be frozen upon frost, the above general trend of the seasonal variations in the infiltration capacity may or may not be valid, depending on the degree of saturation at the time of frost, as already discussed in the LITERATURE REVIEW section.

The curve numbers for AMC I and AMC III corresponding to a given CN for AMC II may be computed by using the relationships for CN which are formulated by substituting Eq. 101 into the linear relationships between the potential infiltration, S, for AMC II and that for AMC I or AMC III (USDA SCS, 1969). The relationships developed by Sobhani (1975) are

$$CN_I = \frac{CN_{II}}{2.334 - 0.01334\ CN_{II}} \qquad (132)$$

Table 8. Estimated runoff curve numbers (CN) for highway soil-cover-moisture complexes.

AMC	Hydrologic Soil Group			
	A	B	C	D
I	66	73	80	85
II	82	87	91	94
III	92	95	97	98

$$CN_{III} = \frac{CN_{II}}{0.4036 + 0.005964\ CN_{II}} \quad . \quad . \quad . \quad . \quad . \quad . \quad . \quad . \quad (133)$$

Application of Eq. 126 to the formulation of the standard infiltration-capacity curve for a given soil-cover-moisture complex has an intrinsic problem of estimating the α value, although the $\bar{r}$ value may be assumed given for a specific storm. In the first approximation, the α value may be assumed to be 0.5. For examining the adequacy of Eq. 126, the standard infiltration-capacity curves for a soil-cover-moisture complex, say hydrologic soil group B under AMC II, are formulated by using Eq. 126 with $\alpha = 0.5$ for various $\bar{r}$ values as shown in Figure 29, and then compared with that formulated from Eq. 127. Figure 29 shows that the standard infiltration-capacity curves formulated by use of Eq. 126 simulate more closely the real situations in the field.

The differences in the assumptions underlying the Kostiakov equation (Eq. 62) and the modified Kostiakov equation (Eq. 126) are summarized here. Note that both equations are a general type of the two-parameter infiltration model in which two unknown parameters must be specified prior to its application. The common unknown parameter of both equations is α which according to Eq. 79 is the ratio of t_o and t_p. Another unknown parameter in Eq. 62 is A and that in Eq. 126 is t_p (or S). Equation 79 is the basic formula relating t_o to t_p and is required in the derivation of both Eqs. 77 and 124. Since the concept of runoff curve number is adopted in the description of a hydrologic soil-cover-moisture complex, an additional assumption, Eq. 123, is required in the derivation of Eq. 124. However, use of both Eqs. 79 and 123 in the formulation of Eq. 126 constitutes an apparent contradiction in the hypotheses imposed on Eqs. 79 and 123. This is inevitable in view of the necessity of formulating a two-parameter model which is simpler than a three-parameter model; otherwise, a three-parameter model should have been formulated with the premise that t_o will be treated as another unknown parameter in addition to α and t_p (or S). The latter approach would probably make the resulting infiltration equations too complicated to be handled and is of course beyond the scope of the present study.

The SCS method has been applied to reduce the number of parameters needed in formulating some existing parametric infiltration models. The final modes of the standard infiltration capacity models so developed are of a modified Kostiakov type, Eq. 126 or Eq. 127, containing primarily the potential infiltration, S, as related to CN through Eq. 101 or 102. Consequently, the same criticisms as those applied to the SCS method regarding the accuracy of the method are also considered valid herein. It has been shown by Hawkins (1973, 1975) that uncertainty in the value of CN exerts the most serious effect on the accuracy of the estimated runoff, Q. The smaller the CN value, the larger is the error in Q and hence in F. The successful application of the SCS method in the field thus bears on the accurate selection of the CN value. Since the estimated CN values

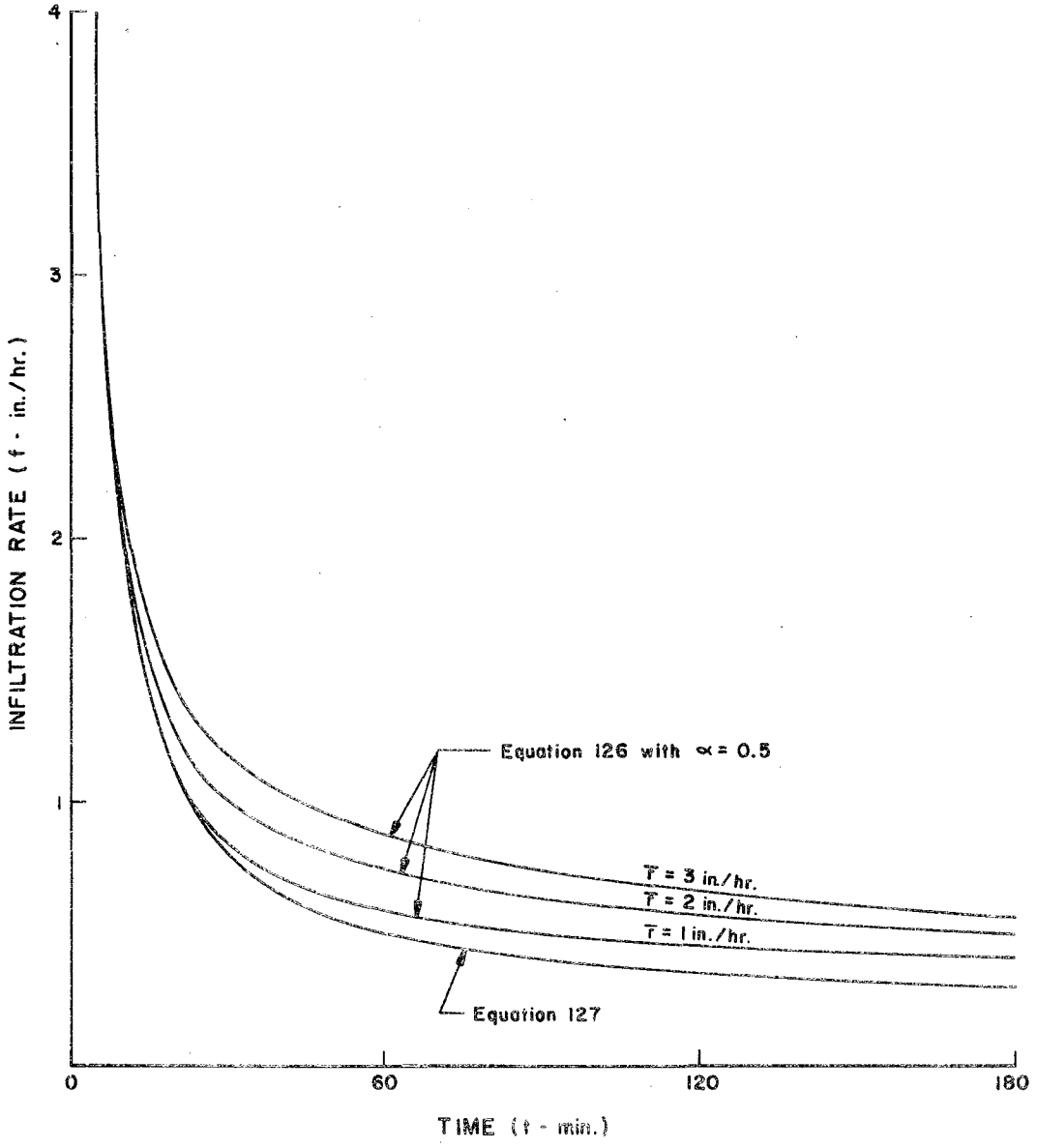

Figure 29. Standard infiltration-capacity curves formulated from Equation 126 with $\alpha = 0.5$ for various $\bar{r}$ values as compared with that from Equation 127.

for highway soil-cover-moisture complexes are quite high (Table 8), use of Eq. 126 or 127 in the construction of the standard infiltration-capacity curves is believed to be accurate enough for practical purposes.

LABORATORY OBSERVATIONS OF RAIN INFILTRATION

The standard infiltration-capacity curves for some possible combinations of subsoil groups, grass covers, and antecedent moisture conditions to represent hydrologic behavior of various urban highway sideslopes have been developed quantitatively. The standard curves so developed were used in conjunction with a surface-runoff model formulated in another phase of the research (Chen, 1975a) as a submodel of subsurface abstractions for routing a storm from a grassed sideslope. Whether or not the standard curves so developed adequately describe the overall infiltration capacities of the grassed sideslopes in the nation's interstate highway system must be experimentally examined. A stormflow experiment facility has thus been developed at the Utah Water Research Laboratory (UWRL) in an attempt to measure the infiltration capacity for a range of simulated sideslopes under various controlled storm conditions. Unfortunately, satisfactory accuracy in the measured results was not achieved in most of infiltration experiments, partly because of instrumental failures in some data acquisition systems, especially flow-depth measuring devices, and partly because of the uneven soil surface that creates inherent instability and channelization in flow, when tilted to slopes as steep as 1.5:1. These and other related problems, along with a description of the stormflow experiment facility consisting of a computer-controlled rainstorm simulator, a forcibly-drained tilting test bed, a computer, a console for manual control, and a sunlight simulator for plant growth, have been reported in detail in a separate report (Chen, 1975b). For simplicity in presentation, most of those data which were already reported, except for those related to infiltration aspects, will not be recapitulated herein.

Acquisition of Soil-and-Turf Samples for Experiments

To simulate an urban or suburban highway sideslope as closely as possible in the laboratory, one needs to know some special characteristics of the sideslope which are different from the agricultural grassland. It is noted that (1) the sideslope is composed of disturbed soils; (2) topsoil is needed to grow fine turf; (3) only fine turf species are used; (4) fertilizer is applied, whenever and wherever needed; and (5) the height of turf is maintained at 4 to 6 inches. Four kinds of subsoil representing four major different drainage conditions were artificially made in accordance with the SCS classification of hydrologic soil groups A (well drained), B (average or modestly drained), C (poorly drained), and D (very poorly drained). Six species of fine turf such as Bermuda grass (Cynodon dactylon), Crested wheat grass (Agropyron dactylon), Fescue grass (Festuca elation var arundinacea), Kentucky Bluegrass (Poa pratensis), Red Top grass (Agrostis palustris; Agrostis alba), and Rye grass (Lolinum perenne; Lolinum multiflorum) are most commonly used on the urban and suburban highway sideslopes. However, not all of the six turf species are suitable

for all types of subsoil or in all climates. There is a definite relationship between subsoil types and turf species. The following subsoil-turf combinations provided by the Federal Highway Administration approximately represent those found on the major urban and suburban highway sideslope sections in the country.

Subsoil Types	Turf Species
SCS Group A	Bermuda grass
	Crested Wheat grass
SCS Group B	Kentucky Bluegrass
	Fescue grass
	Rye grass
SCS Group C	Red Top grass
	Rye grass
SCS Group D	Red Top grass

Among the six species of turf specified, only Bermuda grass and Kentucky Bluegrass which could be sodded were tested. Time did not permit tests to be performed on all combinations of grasses and soils. Physical properties and geometric dimensions of subsoil, topsoil, and sodded turf used in the present tests were reported elsewhere (Chen, 1975b), but for convenience are briefly described below.

Soil

Subsoils to represent SCS hydrologic soil groups A, B, C, and D were simulated by mixing a washed sand with a locally available heavy soil. The mixing ratio of the soil mixture for each soil group was determined by trial and error according to the overall saturated permeability of soils in central Utah (SCS, 1972) rather than Musgrave's (1955) classification, in which the ranges of final infiltration rates specified for the four groups are too narrow to be readily reproducible in laboratory experiments. In view of the small variance possible in the control of the rainfall intensity and the continuing settlement of soils during experiments, maintaining Musgrave's (1955) ranges of final infiltration rates were not practical. Furthermore, if topsoil has a rate of transmission lower than that of subsoil and a surface-entry rate is higher than the transmission rates of both topsoil and subsoil, infiltration will be limited to the transmission rate of topsoil and thus the transmission rate of subsoil will never be at its capacity. In this case, the range of final infiltration rates for subsoil is no longer a controlling parameter in the formulation of the standard infiltration-capacity curve. It must be kept in mind, however, that this does not eliminate the possibility that topsoil penetrated with deep interconnected grass root systems can have a rate of transmission greater than that of any subsoil. For the present experiments, the ranges of final infiltration rates were tentatively set as follows (SCS, 1972):

Subsoil	Final Infiltration Rates
Group A	5 in./hr or higher
Group B	5 ~ 0.8 in./hr
Group C	0.8 ~ 0.2 in./hr
Group D	0.2 in./hr or smaller

Subsoil was placed in layers, not exceeding 1 in. in uncompacted depth, properly moistened, and compacted to an unknown bulk density (which was measured after settlement had taken place) by using a roller before the next layer was placed. Each layer of soil was spread uniformly and raked to uniform thickness prior to compacting. As the compaction of each layer progressed, continuous leveling and manipulating was made to assure uniform density. The thickness of subsoil was kept from 6 to 8 inches for a total of 1-foot soil layer to be tested. Locally available topsoil was next spread to 4- to 6-in. thickness over the subsoil after the subsoil reached the desired thickness. Compaction of the topsoil layer was treated in a similar way as the subsoil layer.

The final infiltration rate varies with the compaction of soil. Since bulk density varies with structural condition of the soil, particularly that related to packing, it is often used as a measure of soil structure or degree of compaction. Shown in Figure 30 are the relationships between the soil bulk density and the final infiltration rate for the four subsoils and single topsoil. Bulk density of soil samples taken from the test bed after an extended period of experiment (see Figure 30) indicates that a great deal of consolidation in topsoil took place over the extended period of experimental time. The consolidation of topsoil not only changed infiltration, but also caused the soil surface to be uneven to such an extent that flow depth measurements by using just a few manometer tubes became extremely difficult. This is probably one of the major reasons that satisfactory results could not be obtained from the infiltration tests.

The differences in other phases of physical properties of the subsoils and topsoil can be demonstrated by plotting the functional relationship between the soil moisture content and capillary potential. For example, moisture contents by weight at 1/3, 2/3, and 15 atmospheric suction pressures were measured and their functional relationships plotted for the subsoils and topsoil, as shown in Figure 31.

Turf

Kentucky Bluegrass sod was locally available so that it was tested first. Bermuda grass sod was obtained from California through a nursery farm in Las Vegas, Nevada. Bermuda grass sod tested was Hybrid Bermuda grass because Common Bermuda grass sod could not be obtained. It was noticed that Hybrid Bermuda grass had a deeper root system than Kentucky Bluegrass. Nevertheless, both are good, solid, dense turfs which can prevent erosion. No erosion from the turf surfaces was observed during experiments, even on slopes as steep as 1.5:1.

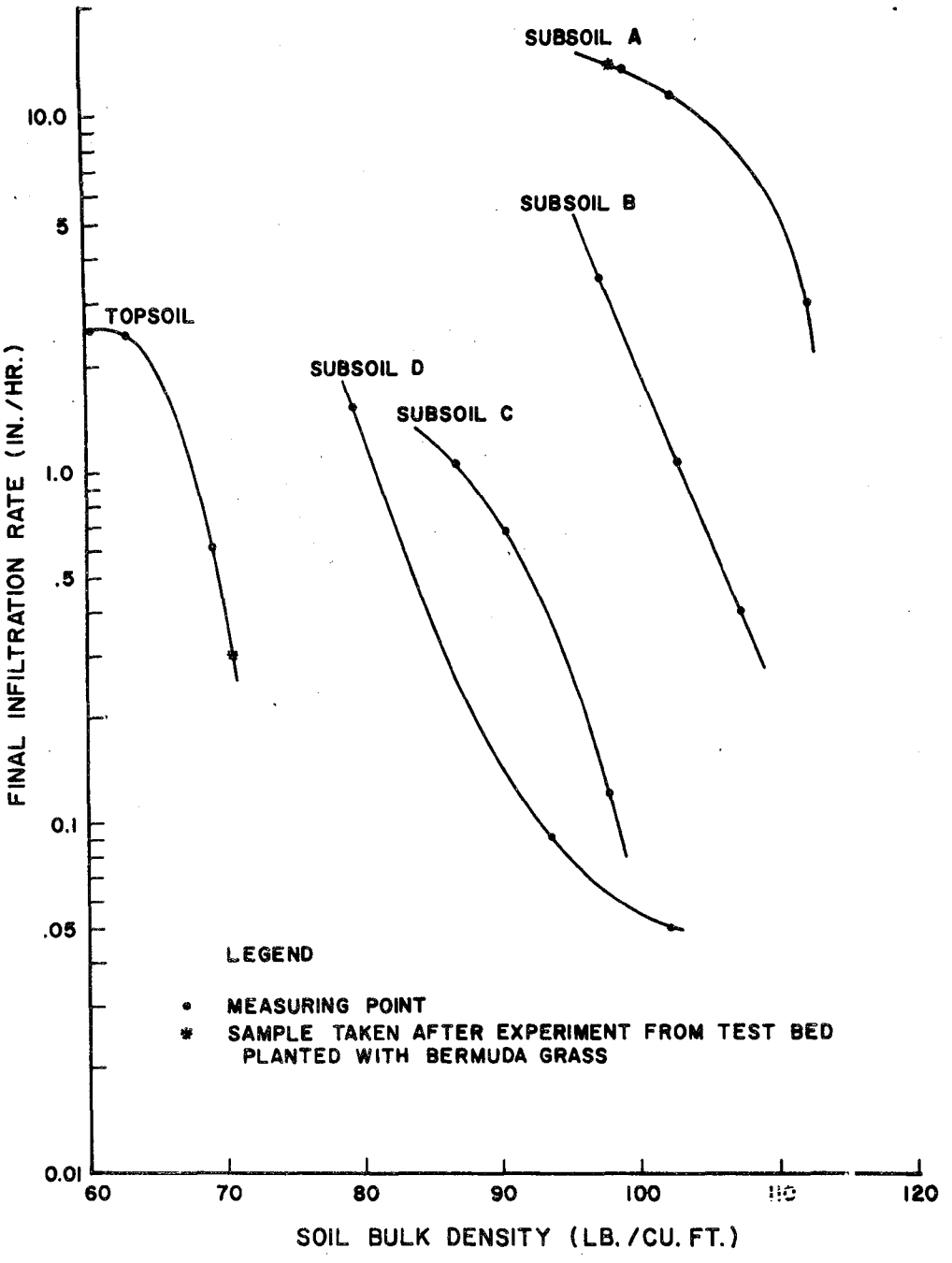

Figure 30. Soil bulk density as a measure of degree of compaction as related to final infiltration rate for four subsoils and topsoil.

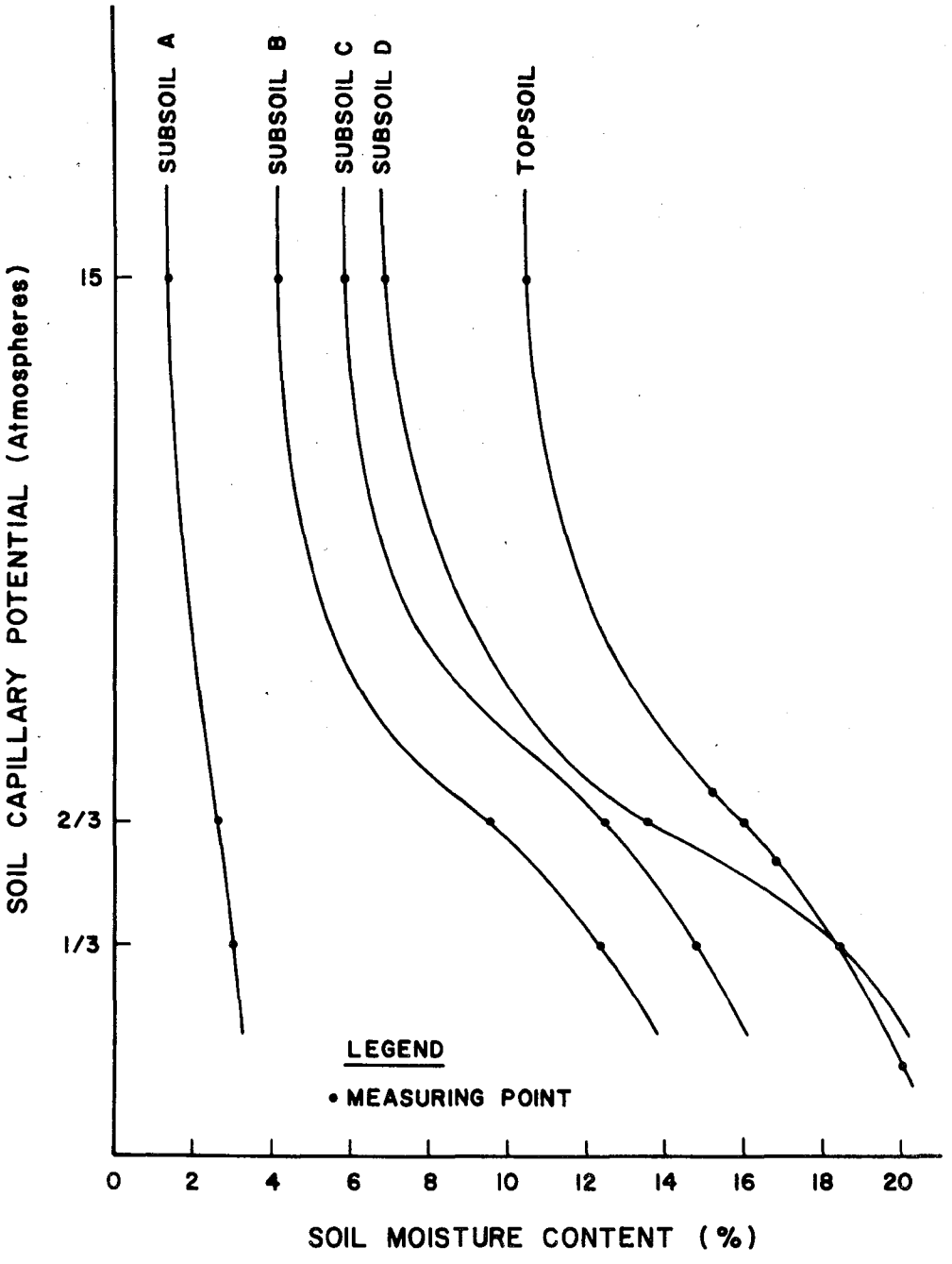

Figure 31. Functional relationships between soil moisture content and soil capillary potential for four subsoils and topsoil tested.

The thickness of sodded turf acquired from a nursery farm was practically nonuniform. It was almost impossible to make the turf surface perfectly level and even. This nonuniformity in the soil surface did become the major source of errors in the flow depth measurement.

Before testing was started, approximately two weeks were allowed for sodded turf to establish its own root system deep into the topsoil and, possibly further into the subsoil. In this establishment period an adequate amount of water and liquid fertilizer was applied to the turf in order to keep its optimum growing condition under the sunlight simulator.

Experiments began in the third week after turf was sodded. It was found from experience that no more than one infiltration test could be conducted each day because the average initial soil moisture content had to be reestablished before any further experiment. With the present facility including use of both soil profile suction pump and sunlight simulator, excess gravitational water in the soil could not be removed faster than within a half day by means of forced drainage (suction pump) and evapotranspiration (sunlight simulator). It was desired that the initial soil moisture content be at field capacity or less before a test. However, time did not permit the initial soil moisture content to be reduced to a value near the wilting point. To attain such a dry antecedent moisture condition would probably require more than a week of moisture-redistribution time.

Tall turf tends to become prone by its own weight, even though there is no external force acting on it. This may or may not change the infiltration capacity, depending upon how much the surface of the soil is sealed by prone turf that prevents or retards the entry of water into the soil. For avoiding analyzing such effects on infiltration, turf was cut shorter than specified 4 to 6 inches. Thus, average turf height was maintained approximately at 3 inches during experiments.

Noteworthy is a difference in physical appearance between naturally grown turf on a sideslope and sodded turf on the test bed. Turf in the natural environment grows in the vertical direction, regardless of the angle of inclination which the sideslope has, while sodded turf on the test bed was always perpendicular to the soil surface. Whether or not this physical appearance being different from the natural one influenced the infiltration capacity should be investigated in the future. This can be done by direct seeding on the test bed for each slope tested.

To sod rather than seed grass directly on the test bed has several advantages, as mentioned previously, but also has disadvantages which should be carefully examined. For example, topsoil which came with 1-inch thick sod would not be the same type of topsoil used in the test; this in effect would add one more unknown factor in the analysis. Therefore, if time and situation permitted, it would be more advisable to seed grass directly on the test bed rather than use sod.

Experimental Procedures

Four bed slopes for each turf were tested. The slopes tested were 0.5 percent (0.005), 6:1 (0.164), 3:1 (0.316), and 1.5:1 (0.555). For each slope, two uniform severe storms (viz., 31-in./hr constant heavy rainfall, and 10-in./hr constant medium rainfall), two typical storms (viz., 10-year 60-minute rainfall intensity and 50-year 60-minute rainfall intensity), one stationary severe maximum storm recorded, and one moving severe maximum storm recorded at most intensive rainfall stations in Kentucky Bluegrass and Bermuda grass zones (Chen, 1975c) were tested. All the storms tested were programmed and controlled by an EAI 640 computer. Unfortunately, because of the instrumentation problem (Chen, 1975b), not all of the runs performed are usable. Those which appeared to be in errors are not reported herein.

The test bed was tilted to a desired slope by operating first the two hydraulic cylinders and next a hand-operated hydraulic jack. Although both hydraulic cylinders connected to an oil reservoir in parallel were designed to support the total load equally, a slight discrepancy in the telescoped length between them (even within the manufacture's tolerance) compelled us to use a hand-operated hydraulic jack for more precise leveling.

Before an experiment was started, the rainstorm simulator, having one hundred 2 ft x 2 ft modules, was filled with city supply water and then positioned properly over the test bed. Water was also introduced into the discharge-measuring flumes and depth-measuring manometer tubes to have the reference levels or zero readings of both discharge and depth sensors checked by a portable voltmeter (Digitec Digital Multimeter S/N 3164) or a computer (EAI 640). These reference levels were used in the analysis of experimental results when the computer output data in the form of voltage were reduced to the usable units, such as cfs and inches, through the calibration curves or functional relationships. Once the rainstorm simulator was properly set, the control program that produces a desired storm was executed on the EAI 640 computer, which in turn read the flow-depth, soil-moisture, and discharge sensors and punched out on paper tape the measured data according to pre-set time intervals. The output data from the EAI 640 computer can be directly analyzed through a hybrid computer (EAI PACER 400 system).

Immediately after an experiment, the sunlight simulator was pulled over the turf surface and the growth lamps were turned on for 12 to 16 hours per day before the next experiment was started. Meanwhile, the vacuum pump was turned on to a suction of about 5 psi to remove excess gravitational water from the bottom of the soil layer. The operation of the vacuum pump continued until there was no excess water dripping at the bottom of the soil layer.

Analysis of Experimental Results

Accuracy of the measurements of the flow variables such as the discharge and depth were already discussed in another report (Chen, 1975b). The major source of error was found to be the flow depth measurement. Use of helical wound resistance wires and manometer tubes in the flow depth measurement had many inherent problems which could not be improved or modified without resorting to the development of a new type of depth-measuring device. Because of the inaccuracy in the flow depth measurement, most infiltration tests performed in this study were found unsatisfactory. Only a few which showed a reasonable trend in infiltration decay characteristics are presented herein.

Determination of infiltration rate

Consider a rainstorm with intensity, r, falling on a test bed which is tilted to a slope with the angle of inclination, θ, as schematically shown in Figure 32. Let B be the total or partial area of the test bed under rainfall projected on the horizontal plane, L the total width of the test bed, h the average depth of surface detention, f the infiltration rate, q_t the outflowing discharge per unit width from the test bed, Q_f the discharge measured by the discharge-measuring flume, n the number of the discharge-measuring flumes (i.e., 10 in the present case), and S_f the water storage in the discharge-measuring flume. Then, by the conservation of mass (i.e., input flow rate minus output flow rate is equal to the rate of the change of surface detention or water storage in the discharge-measuring flumes), the following two continuity equations are formulated:

$$(r - f)B - q_t L = \frac{d(Bh)}{dt} \quad . \quad . \quad . \quad . \quad . \quad . \quad . \quad . \quad . \quad (134)$$

$$q_t L - nQ_f = n\frac{dS_f}{dt} \quad . \quad . \quad . \quad . \quad . \quad . \quad . \quad . \quad . \quad . \quad (135)$$

Subtracting $q_t L$ from Eqs. 134 and 135 yields

$$f = r - \frac{1}{B}\left[\frac{d(Bh)}{dt} + nQ_f + n\frac{dS_f}{dt}\right] \quad . \quad . \quad . \quad . \quad . \quad . \quad (136)$$

Particularly under a stationary storm, B is constant and Eq. 134 thus reduces to

$$f = r - \frac{dh}{dt} - \frac{n}{B}\left(Q_f + \frac{dS_f}{dt}\right) \quad . \quad . \quad . \quad . \quad . \quad . \quad . \quad . \quad (137)$$

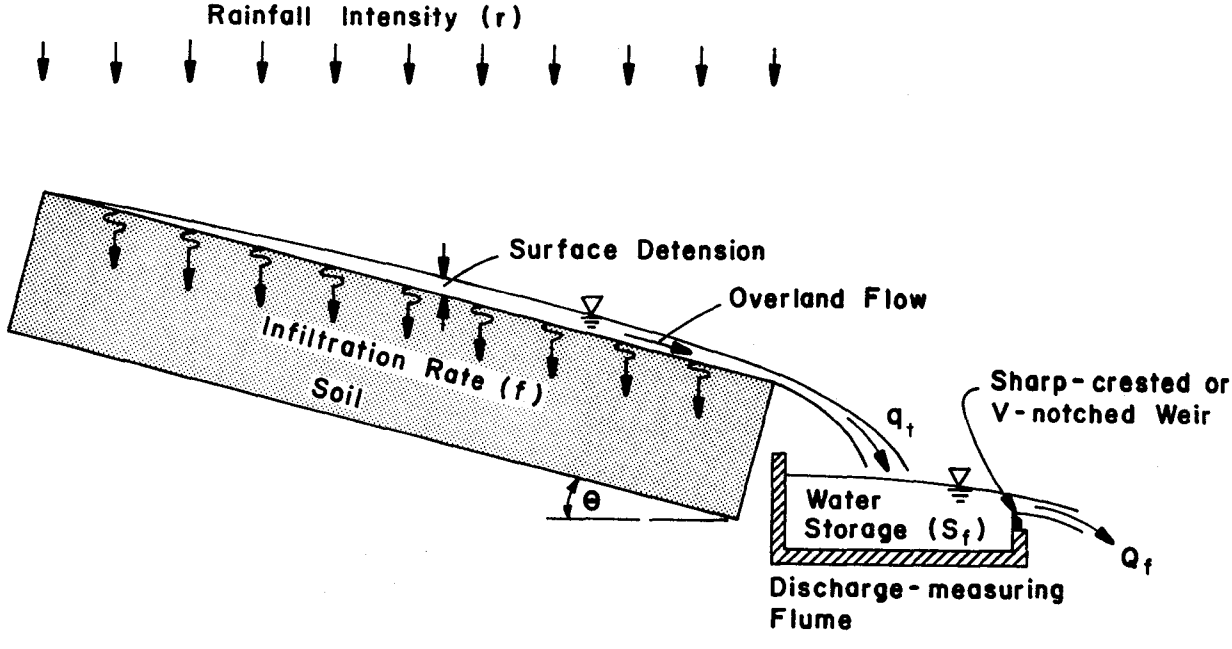

Figure 32. Schematic diagram of infiltration tests.

The amount of water storage, S_f, in the discharge-measuring flume at any time can be evaluated by measuring the corresponding water stage in the stilling well. The water stage in the stilling well was calibrated against the discharge, Q_f. All the terms on the right-hand side of Eqs. 136 and 137 are known so that f can be calculated by using one of these equations.

Note that Eqs. 136 and 137 are developed under an ideal condition which requires that overland flow is perfectly uniform across the test bed. However, in actual tests, this ideal situation never happened, although efforts had been made to improve the lateral uniformity. In view of the reality in which measured Q_f and S_f in each flume vary from each other, Eqs. 136 and 137 are modified to take this variation into account as follows:

$$f = r - \frac{1}{B}\left[\frac{d(Bh)}{dt} + \sum_{i=1}^{n} Q_{fi} + \sum_{i=1}^{n} \frac{dS_{fi}}{dt}\right] \quad . \quad . \quad . \quad . \quad (138)$$

$$f = r - \frac{dh}{dt} - \frac{1}{B}\sum_{i=1}^{n}\left(Q_{fi} + \frac{dS_{fi}}{dt}\right) \quad . \quad . \quad . \quad . \quad . \quad (139)$$

in which Q_{fi}, i = 1, 2, ..., 10 are the measured discharges in the flumes Nos. 1, 2, ..., and 10, respectively, and S_{fi}, i = 1, 2, ..., 10 are the amounts of water storage in the discharge-measuring flumes Nos. 1, 2, ..., and 10, respectively.

The most sensitive term in Eq. 138 or 139 is dh/dt which happened to be the most troublesome and inaccurate term causing a large error in the computation of f. Aside from the technical and instrumental difficulties encountered by use of the present depth-measuring device, accuracy in the depth measurement, i.e., approximately 0.01 in., automatically limited the time interval (that cannot be taken smaller than 1 minute) in order for the accuracy of f to stay within 0.1 in./hr. For example, at the equilibrium state in the rainfall-runoff process, dh/dt is supposedly near zero, yet a small error in reading, say by 0.01 in., which is of course within the accuracy of the instrument, in a time interval of 5 seconds will give a difference of 7.2 in./hr in the evaluation of f, thus resulting in a large error.

Two end points of the infiltration decay curve are obvious from Eqs. 138 and 139. Theoretically speaking, before ponding, all the terms except r on the right-hand side of Eqs. 138 and 139 are zero so that the infiltration rate is equal to the rainfall intensity (Eq. 35). By the same token, at the equilibrium state, Eqs. 138 and 139 reduce to

$$f = r - \frac{1}{B} \sum_{i=1}^{n} Q_{fi} \quad . \quad . \quad . \quad . \quad . \quad . \quad . \quad . \quad . \quad . \quad (140)$$

which is the final infiltration rate, designated as f_∞ before. However, since Eq. 138 or 139 was used in the computation of f, these two theoretical points on the infiltration decay curve were not satisfied.

It is noted that most existing methods for estimating infiltration have the average depth of surface detention, h, evaluated from detention-runoff rate relationships of overland flow. Musgrave and Holtan (1964), after analyzing many sources of experimental data from type F infiltrometer runs, provided detention-runoff rate relationships of overland flow for various bed slopes, vegetation and paved covers, and lengths of slope. Whether or not a friction-coefficient functional relationship developed in the friction tests for turf surfaces (Chen, 1975b) can be used as a detention-runoff rate relationship for turf surfaces should be investigated further. Use of the detention-runoff rate relationships would certainly eliminate the undesired errors caused by the direct measurements of flow depth.

Measured infiltration capacity curves

Only few infiltration results which show a reasonable trend of expected decay characteristics are presented herein. In addition to the instrumentation problems and inaccuracies associated with the flow depth measurement, as discussed previously, there was a problem of conducting an infiltration test on a small slope such as 0.5 percent. Because no barrier is set at the upstream end in the present facility (Figure 32), an upstream portion of overland flow on such a small slope tended to flow backward, resulting in a loss of water from the upstream end. Furthermore, all infiltration measurements on Kentucky Bluegrass are judged to be inaccurate because of incorrectly-calibrated manometer-tube problems which could not be detected in time to be adjusted before experiments on Bermuda grass (Chen, 1975b) were conducted. However, except for 0.5-percent slope, all experimental data collected are believed to be still valid and usable if the average depth of surface detention, h, can be evaluated from the detention-runoff rate relationships formulated for the turf surfaces under study. This constitutes another major task which is of course beyond the scope of the present study.

Measured infiltration capacity values for Bermuda grass on various slopes under a constant storm are plotted in Figure 33. An inspection of the measured points for various slopes under different constant rainfall intensities reveals that it is almost impossible to differentiate among them the variations in the infiltration capacity values due to changes in slope and/or rainfall intensity. For practical purposes, one may assume that after ponding, the infiltration capacity for a given soil-cover-moisture complex does not vary with the rainfall intensity and bed slope.

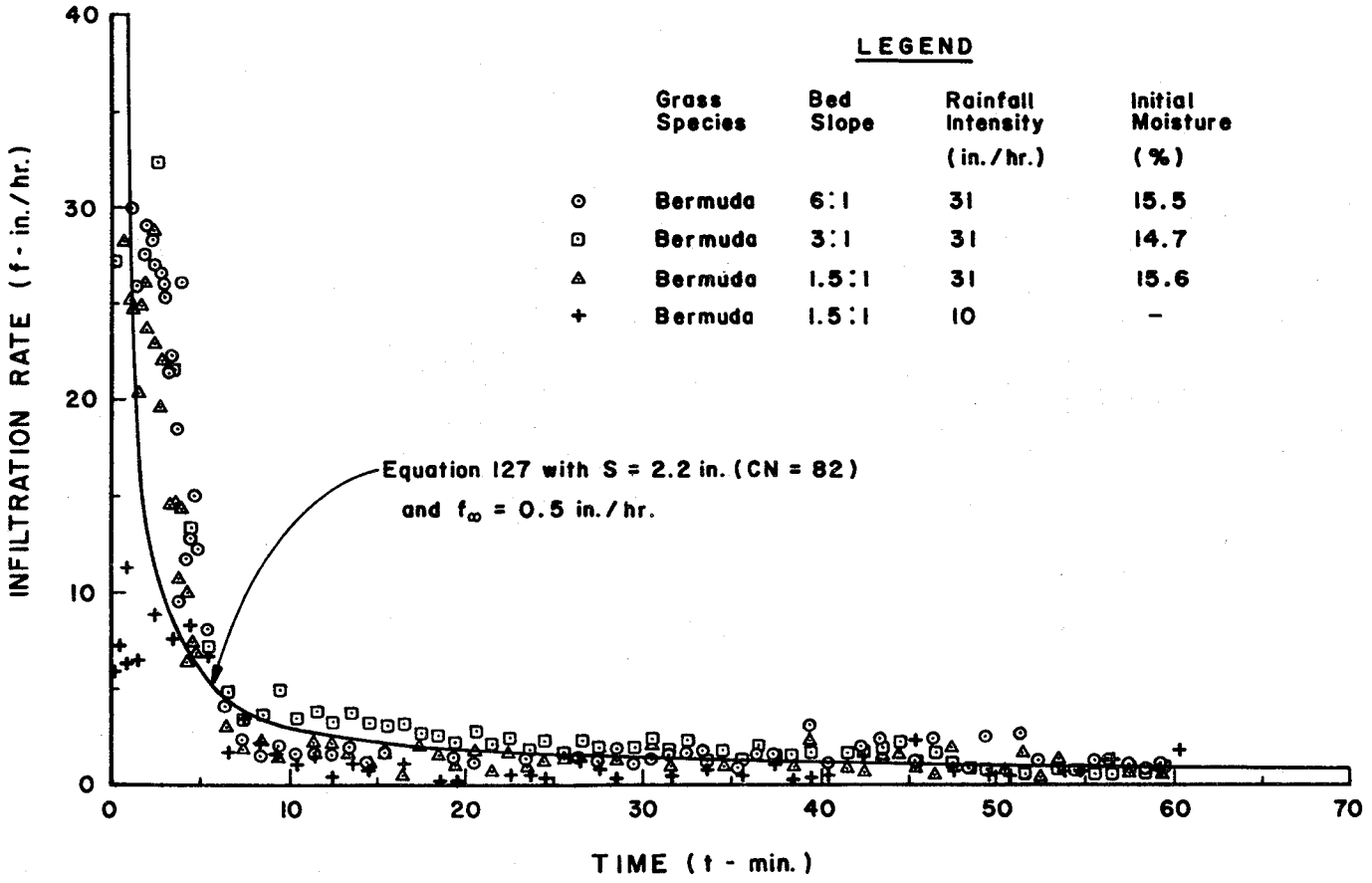

Figure 33. Measured infiltration-capacity curves for Bermuda grass on various slopes under a normal antecedent moisture condition.

Consequently, Eq. 127 with adequately chosen S and f_∞ values can be used to construct the standard infiltration-capacity curve for this typical soil-cover-moisture complex.

Typical standard infiltration-capacity curve

The judicious selection of the potential infiltration, S, and the final infiltration rate, f_∞, for this typical complex can proceed as follows. It can readily be seen from Figure 30 that after consolidation of the soil particles the f_∞ value for topsoil covered with Bermuda grass is much smaller than that for subsoil A. This is the case in which the transmission rate of topsoil is lower than that of subsoil. It is thus judged that the transmission rate of subsoil was never at its full capacity during the experiments. In this soil-cover-moisture complex the soil that controls infiltration must be topsoil, but not subsoil. Therefore, the final infiltration rate for topsoil is used in the formulation of the standard infiltration-capacity curve. Because the topsoil layer consolidated throughout the experiments, naturally its final infiltration rate also changed with time. Regrettably, no measurements were made on the magnitude of f_∞ and its variation with time during the experiments except in the final stage at which the average bulk density of topsoil, about 70 lb/cu. ft, was measured. The f_∞ value for the consolidated topsoil corresponding to this bulk density read from Figure 30 is approximately 0.3 in./hr. The f_∞ value for topsoil before consolidation took place could be much higher. In view of this time variation in f_∞, the topsoil in question can be classified as hydrologic soil group A and the average f_∞ during the experiments may be assumed to be 0.5 in./hr.

Initial moisture contents measured by soil moisture sensors in the topsoil layer, as shown in Figure 33, were about 15 percent, which is tantamount to the value at soil capillary potential (or tension) around 2/3 atmospheres according to Figure 33. However, there seems no way to know whether the tension of 2/3 atmospheres is equivalent to the normal or intermediate moisture condition (i.e., AMC II) between the wilting point and the field capacity. Richards and Weaver (1943) found the wilting point for the majority of soils investigated to occur at tensions somewhat below 15 atmospheres, while the wilting point of the soils studied by Robertson and Kohnke (1946) averaged 13.6 atmospheres. The 15-atmosphere percentage has been adopted by many soil scientists for, or in place of, the wilting point. However, there is little information concerning the tension at which moisture is held at field capacity. Richards and Weaver (1944), for example, found that the tension for the moisture equivalent was 1/3 atmosphere for a number of soils in which the moisture equivalent value varied between 8 percent and 22 percent. More recently, instead of field capacity, the 1/3-bar percentage has been used to designate the wet limit of the range of plant-available water under general field conditions. The initial moisture contents at tensions around 2/3 atmospheres are thus judged to be the normal antecedent moisture conditions (i.e., AMC II).

Runoff curve number (CN) for a highway soil-cover-moisture complex corresponding to the hydrologic soil A and AMC II is 82, as can be read from Table 8. The infiltration potential, S, corresponding to CN = 82 computed from Eq. 102 is 2.20 in. Equation 127 with S = 2.20 in. and f = 0.5 in./hr can be plotted as a standard infiltration-capacity curve for this typical complex, as shown in Figure 33, and compared with measured data points for various rainfall intensities and bed slopes. Despite scatter in the measured points, the standard curve so formulated approximately covers all the data points. It is thus concluded that standard infiltration-capacity curves for other highway soil-cover-moisture complexes, as indexed by other CN values in Table 8, can be similarly validated if additional experimental data on infiltration capacity for other initial moisture conditions, topsoils, and species of grass can be accurately obtained. Use of the modified Kostiakov type equation (Eq. 126) has been shown to improve the shape of the standard infiltration-capacity curve if the unknown model parameter α can be accurately evaluated. No attempt was made to do this, however, because the considerable scatter of data points, as shown in Figure 33, would not warrant such an improvement.

SUMMARY AND CONCLUSIONS

The boundary-value problem of one-dimensional infiltration resulting from rainfall has been solved by using the well-known Richards equation and appropriately prescribed initial and boundary conditions. This problem has been solved on a digital computer by using an explicit finite-difference scheme and the stability criterion for solution associated with such a numerical scheme. The primary objective of formulating such an idealized mathematical model was to use it as a basic testing tool in the subsequent analysis of various parametric infiltration models including Green-Ampt, Kostiakov, Philip, Horton, and Holtan equations.

A general parametric infiltration model which consists of two parts, infiltration before and after ponding, was developed. Before ponding, the infiltration rate is equal to the rainfall intensity that may or may not change with time. After ponding, one of the known algebraic infiltration equations can be used to describe the infiltration capacity curve. The time of ponding at which the two parts separate is the most important parameter in a parametric infiltration model and can be expressed in terms of other parameters in the model and the rainfall intensity. The values of the algebraic model parameters are assumed to be constant for a soil having the same initial and boundary (i.e., soil surface) conditions. This assumption has been verified by using the numerical solutions obtained from the boundary-value problem of rain infiltration for comparison with results from all of the algebraic equations except for the Horton type. The Holtan type model has been shown to be difficult to apply to a soil which does not have a uniform water-storage potential above the first impeding stratum. Use of the Green-Ampt, Kostiakov, and Philip type models for the prediction of the infiltration rate before and after ponding has been proved to be very accurate in application.

The standard infiltration-capacity curves for soil-cover-moisture complexes representing urban highway sideslopes have been empirically developed based on the unique selection of the SCS runoff curve number. For many practical purposes, the SCS method can be incorporated in one of the parametric infiltration models such as the Holtan and Kostiakov equations. An attempt was made to modify Holtan's equation based on the proper selection of the SCS runoff curve number (or potential infiltration) for a given soil-cover-moisture complex, but has failed to produce an adequate standard infiltration-capacity relationship or curve which can describe the infiltration condition at the time of ponding. In another approach, the modified Kostiakov equation containing the parameter of potential infiltration, S, was used to construct the standard infiltration-capacity curves for highway soil-cover-moisture complexes. For simplicity, however, the upper infiltration envelope (Eq. 127) can be used to describe the standard infiltration-capacity curve.

Runoff curve numbers (CN) for various highway soil-cover-moisture complexes have been estimated from the SCS data on runoff curve numbers for various agricultural land conditions including land use, treatment or practice, hydrologic conditions, hydrologic soil groups, and antecedent soil moisture conditions. The runoff curve numbers so estimated are tabulated for use in engineering practice (Table 8).

Typical standard infiltration-capacity curves so developed have been verified by using data obtained from experiments run in a stormflow experiment facility at the Utah Water Research Laboratory. Mainly because of instrumental errors and failures in some data acquisition systems, especially flow-depth measuring devices, satisfactory accuracy in the measured infiltration rates has not been able to be achieved. Nevertheless, among the few experimental results which show a reasonable trend of expected decay in the infiltration capacity, Eq. 127 with the proper selection of the S and f_∞ values has proved to be a valid expression of the standard infiltration-capacity curve which will be useful in engineering application.

RECOMMENDATIONS

The results obtained from the present study indicate the need for continuing efforts in pursuit of the formulation of a better expression for standard infiltration-capacity curves. The major areas recommended for further investigations have been pointed out throughout this report and are briefly summarized as follows:

1. Whether the standard infiltration-capacity curves developed adequately describe the overall infiltration capacities of the grassed sideslopes in the nation's interstate highway system should be experimentally examined further. The additional laboratory data will be extremely important in the verification of the standard infiltration-capacity curves for various soil-cover-moisture complexes and can be obtained at minimal unit cost since the capital investments have already been made.

2. The present flow-depth measuring device consisting of helical wound resistance wires and manometer tubes has proved to be a major source of experimental error and could not be improved or modified without resorting to the development of a new type of water depth-measuring device. The more accurate measurement of the flow depth (or the depth of surface water detention) by means of a new device will enable the more accurate determination of the infiltration rate.

As an alternative to the measurement of flow depth, it is suggested that detention-runoff rate relationships of overland flow be formulated for various bed slopes, vegetation and paved covers, and lengths of slope. Whether or not a functional relationship developed in the friction tests for turf surfaces can be used as a detention-runoff rate relationship for turf surfaces should also be investigated further.

REFERENCES

Adrian, D. D., and J. B. Franzini. 1966. Impedance to infiltration by pressure build-up ahead of the wetting front. J. Geophys. Res. 71: 5857-5862.

Arend, J. L., and R. E. Horton. 1943. Some effects of rain intensity, erosion, and sedimentation on infiltration capacity. Soil Sci. Soc. Am. Proc. 7:82-89.

Bauer, S. W. 1974. A modified Horton equation for infiltration during intermittent rainfall. Internat. Assoc. Hydrol. Sci. 19(2):219-225.

Baver, L. D. 1933. Soil erosion in Missouri. Missouri Agri. Exp. Sta. Bull. 349. 266 p.

Baver, L. D. 1938. Ewald Wollny, A pioneer in soil and water conservation research. Soil Sci. Soc. Am. Proc. 3:330-333.

Bertoni, J., W. E. Larson, and W. D. Shrader. 1958. Determination of infiltration rates on Marshall silt loam from runoff and rainfall records. Soil Sci. Soc. Am. Proc. 22:571-574.

Beutner, E. L., R. R. Gaebe, and R. E. Horton. 1940. Sprinkled-plat runoff- and infiltration-experiments on Arizona desert-soils. Trans. Am. Geophys. Union 21:550-558.

Box, T. W. 1961. Relationship between plants and soils of four range plant communities in South Texas. Ecology 42:794-810.

Braester, C. G. 1973. Linearized solution of infiltration at constant rate. Physical Aspects of Soil Water and Salts in Ecosystems. (ed. by A. Hadas, D. Swartzendruber, P. E. Rijtema, M. Fuchs, and B. Yaron), Springer-Verlag, New York, N.Y., pp. 59-63.

Brakensiek, D. L., and R. K. Frevert. 1961. Analysis and application of infiltrometer tests. Trans. Am. Soc. Agri. Engrs. 4:75-77.

Bruce, R. R., and F. D. Whisler. 1973. Infiltration of water into layered field soils. Physical Aspects of Soil, Water, and Salts in Ecosystems. (ed. by A. Hadas et al.), Springer-Verlag, Berlin-Heidelberg-New York, pp. 77-89.

Buckingham, E. 1907. Studies on the movement of soil moisture. U.S. Dept. Agr. Bur. Soils Bull. 38.

Chen, C. L. 1975a. Urban storm runoff inlet hydrograph study. Vol. 1. Computer analysis of runoff from urban highway watersheds under time- and space-varying rainstorms. Utah Water Res. Lab. Rept. PRWG106-1, Utah State University, Logan, Utah.

Chen, C. L. 1975b. Urban storm runoff inlet hydrograph study. Vol. 2. Laboratory studies of the resistance coefficient for sheet flows over natural turf surfaces. Utah Water Res. Lab. Rept. PRWG106-2, Utah State University, Logan, Utah.

Chen, C. L. 1975c. Urban storm runoff inlet hydrograph study. Vol. 4. Synthetic storms for design of urban highway drainage facilities. Utah Water Res. Lab. Rept. PRWG106-4, Utah State Univeristy, Logan, Utah.

Chiang, S. L. 1971. A runoff potential rating table for soils. J. Hydrology 13:54-62.

Colman, E. A., and G. B. Bodman. 1944. Moisture and energy conditions during downward entry of water into moist and layered soils. Soil Sci. Soc. Am. Proc. 9:3-11.

Diebold, C. H. 1951. Soil layers causing runoff from hardland wheat fields in Colorado and New Mexico. J. Soil and Water Conserv. 6:202-209.

Dixon, R. M., and D. R. Linden. 1972. Soil air pressure and water infiltration under border irrigation. Soil Sci. Soc. Am. Proc. 36:948-953.

Doneen, L. D., and D. W. Henderson. 1953. Compaction of irrigated soils by tractors. Agr. Eng. 34:94-95, 102.

Duley, F. L. 1939. Surface factors affecting the rate of intake of water by soils. Soil Sci. Soc. Am. Proc. 4:60-64.

Duley, F. L., and C. E. Domingo. 1949. Effect of grass on intake of water. Univ. of Nebraska Agri. Exp. Sta. Res. Bull. No. 159. 15 p.

Duley, F. L., and L. L. Kelley. 1939. Effect of soil type, slope, and surface conditions on intake of water. Univ. of Nebraska Agri. Exp. Sta. Res. Bull. No. 112, pp. 1-16.

Ellison, W. D. 1950. Soil erosion by rainstorms. Science 111:245-249.

Fletcher, J. E. 1949. Some properties of water solutions that influence infiltration. Trans. Am. Geophys. Union 30:548-554.

Fletcher, J. E. 1960. Some aspects of plant growth on infiltration in the Southwest. AAAS Southwestern and Rocky Mountain Division, Alpine, Texas, May 3, 1960 (Part of a Symposium on the Ecology of Water Yield).

Fletcher, J. E., and C. L. Chen. 1975. Urban storm runoff inlet hydrograph study. Vol. 3. Hydrologic data for two urban highway watersheds in the Salt Lake City area, Utah. Utah Water Res. Lab. Rept. PRWG106-3, Utah State University, Logan, Utah.

Free, G. R., G. M. Browning, and G. W. Musgrave. 1940. Relative infiltration and related physical characteristics of certain soils. U.S. Dept. Agr. Tech. Bull. 729.

Freeze, R. A. 1969. The mechanism of natural groundwater recharge and discharge, I: One-dimensional, vertical, unsteady, unsaturated flow above a recharging or discharging groundwater flow system. Water Resour. Res. 5(1):153-171.

Fujioka, Y., and T. Kitamura. 1964. Approximate solution to a vertical drainage problem. J. Geophys. Res. 69(24):5249-5255.

Gardner, W. R. 1958. Some steady-state solutions of the unsaturated moisture flow equation with application to evaporation from a water table. Soil Sci. 85(4):228-232.

Gifford, G. F. 1968. Range land watershed management, a review. Nevada Agri. Exp. Sta. Bull. No. R52. 50 p.

Glymph, L. M., and H. N. Holtan. 1969. Land treatment in agricultural watershed hydrology research. Effects of Watershed Changes on Stream Flow. (ed. by W. L. Moore and C. W. Morgan). Water Resources Symp. No. 2, Univ. of Texas Press, Austin, Texas, pp. 44-68.

Glymph, L. M., H. N. Holtan, and C. B. England. 1971. Hydrologic response of watersheds to land use management. J. Irr. Drain. Div., Proc. Am. Soc. Civil Engrs. 97(IR2):305-318.

Green, R. E. 1962. Infiltration of water into soils as influenced by antecedent moisture. Ph.D. dissertation, Iowa State Univ., Ames, Iowa.

Green, W. H., and G. A. Ampt. 1911. Studies on soil physics: 1. The flow of air and water through soils. J. Agr. Sci. 4(1):1-24.

Gupta, R. P., and W. J. Staple. 1964. Infiltration into vertical columns of soil under a small positive head. Soil Sci. Soc. Am. Proc. 28: 729-732.

Hanks, R. J., A. Klute, and E. Bresler. 1969. A numerical method for estimating infiltration, redistribution, drainage and evaporation of water from soil. Water Resour. Res. 5:1064-1069.

Hanks, R. J., and K. L. Andersen. 1957. Pasture burning and moisture conservation. Journal of Soil and Water Conservation 12:228-229.

Hanks, R. J., and S. A. Bowers. 1962. Numerical solution of the moisture flow equation for infiltration into layered soils. Soil Sci. Soc. Am. Proc. 24:530-534.

Hansen, V. E. 1955. Infiltration and soil water movement during irrigation. Soil Sci. 79:93-105.

Hawkins, R. H. 1973. Improved prediction of storm runoff in mountain watersheds. J. Irrigation and Drain. Div., Proc. Am. Soc. Civil Engrs. 99(IR4):519-523.

Hawkins, R. H. 1975. The importance of accurate curve numbers in the estimation of storm runoff. Water Resour. Bull. 11(5):887-891.

Hays, H. R. 1949. Flow pattern studies in irrigated coarse textured soil. Soil Sci. Soc. Am. Proc. 13:83-89.

Hermanson, R. E. 1970. Soil surface characteristics and rainfall-runoff-moisture relationship on coastal plain soils. Auburn Univ., Water Resources Res. Inst. Bull. No. 702.

Hillel, D. 1971. Soil and water, physical principles and processes. Academic Press, New York, N.Y., pp. 131-153.

Holtan, H. N. 1945. Time condensation in hydrograph analysis. Trans. Am. Geophys. Union 26:407-413.

Holtan, H. N. 1961. A concept for infiltration estimates in watershed engineering. U.S. Dept. Agr., Agr. Res. Service Pub. 41-51.

Holtan, H. N. 1971. A formulation for quantifying the influence of soil porosity and vegetation on infiltration. Biological Effects in the Hydrological Cycles—Terrestrial Phase. (ed. by E. J. Monke), Proc. 3rd Internat. Seminar for Hydrol. Prof., pp. 228-239.

Holtan, H. N., and G. W. Musgrave. 1947. Soil water and its disposal under corn and under bluegrass. U.S. Dept. Agr. SCS TP-68.

Holtan, H. N., and M. H. Kirkpatrick, Jr. 1950. Rainfall, infiltration, and hydraulics of flow in run-off computation. Trans. Am. Geophys. Union 31:771-779.

Hornberger, G. M., and I. Remson. 1970. A moving boundary model of a one-dimensional saturated-unsaturated, transient porous flow system. Water Resour. Res. 6(3):898-905.

Horner, W. W. 1940. Analysis of hydrologic data for small watersheds. TP-30, Soil Conservation Service, Washington, D.C.

Horner, W. W. 1944. Role of the land during flood periods. Trans. Am. Soc. Civil Engrs. 109:1269-1294.

Horner, W. W., and C. L. Lloyd. 1940. Infiltration-capacity values as determined from a study of an eighteen-month record at Edwardsville, Illinois. Trans. Am. Geophys. Union 21:522-541.

Horner, W. W., and S. W. Jens. 1942. Surface runoff determination from rainfall without using coefficients. Trans. Am. Soc. Civil Engrs. 107:1039-1091.

Horton, R. E. 1933. The role of infiltration in the hydrologic cycle. Trans. Am. Geophys. Union 14:446-460.

Horton, R. E. 1935. Surface runoff phenomena. Horton Hydrol. Lab. Paper No. 101.

Horton, R. E. 1939. Analysis of runoff-plat experiments with varying infiltration-capacity. Trans. Am. Geophys. Union 20:693-711.

Horton, R. E. 1940. An approach toward a physical interpretation of infiltration capacity. Soil Sci. Soc. Am. Proc. 5:399-417.

Horton, R. E. 1942a. A simplified method of determining the constants in the infiltration-capacity equation. Trans. Am. Geophys. Union 23:575-577.

Horton, R. E. 1942b. Simplified method of determining an infiltration-capacity curve from an infiltrometer experiment. Trans. Am. Geophys. Union 23:570-575.

Huggins, L. F., and E. J. Monke. 1966. The mathematical simulation of the hydrology of small watersheds. Tech. Rept. No. 1. Water Resour. Res. Center, Purdue Univ., Lafayette, Ind.

Jamison, V. C., and J. F. Thornton. 1961. Water intake rates of a clay pan soil from hydrograph analyses. J. Geophys. Res. 66:1855-1860.

Jens, S. W. 1948. Drainage of airport surfaces—some basic design considerations. Trans. Am. Soc. Civil Engrs. 113:785-809.

Jens, S. W., and M. B. McPherson. 1964. Hydrology of urban areas. Handbook of Applied Hydrology. (ed. by V. T. Chow), Sec. 20, McGraw-Hill Book Co., New York, N.Y.

Jensen, M. E., and R. J. Hanks. 1967. Nonsteady-state drainage from porous media. J. Irr. Drain. Div., Proc. Am. Soc. Civil Engrs. 93(IR3):209-231.

Knight, J. H., and J. R. Philip. 1973. On solving the unsaturated flow equation. 2. Critique of Parlange's method. Soil Sci. 116:407-416.

Kostiakov, A. N. 1932. On the dynamics of the coefficient of water-percolation in soils and on the necessity for studying it from a dynamic point of view for purposes of amelioration. Trans. 6th C Com. Internat. Soc. Soil Sci. Russian Part A. 17-21.

Kuichling, E. 1889. The relation between the rainfall and the discharge of sewers in populous districts. Trans. Am. Soc. Civil Engrs. 20:1-56.

Lewis, M. R. 1937. The rate of infiltration of water in irrigation practice. Trans. Am. Geophys. Union 18(2):361-368.

Lewis, M. R., and W. L. Powers. 1938. A study of factors affecting infiltration. Soil Sci. Soc. Am. Proc. 3:334-339.

Liakopoulos, A. C. 1965. Theoretical solution of the unsteady unsaturated flow problems in soils. Intern. Assoc. Sci. Hydrol. Bull. 10, pp. 5-39.

Linsley, R. K., M. A. Kohler, and J. L. H. Paulhus. 1949. Applied Hydrology. McGraw-Hill Book Co., Inc. New York, N.Y. 689 p.

Lloyd-Davis, D. E. 1906. The elimination of storm water from sewerage systems. Min. Proc. Inst. Civil Engrs. (London) 164:41-67.

Lull, H. W. 1964. Ecological and silvicultural aspects. Handbook of Applied Hydrology, (ed. by V. T. Chow). Sec. 6, McGraw-Hill Book Co., New York, N.Y.

Mazruk, A. P., W. Kriz, and R. E. Ramig. 1960. Rates of water entry into a chernozem soil as affected by age of perennial grass sods. Agronomy J. 52:35-37.

Meeuwig, R. O. 1969. Infiltration and soil erosion on Coolwater Ridge, Idaho. U.S. Dept. Agr. Forest Service Res. Note INT-103.

Meeuwig, R. O. 1970. Infiltration and soil erosion as influenced by vegetation and soil in Northern Utah. J. Range Management 23: 185-188.

Mein, R. G., and C. L. Larson. 1971. Modeling the infiltration component of the rainfall-runoff process. WRRC Bull. 43, Water Resour. Res. Center, Univ. of Minnesota, Minneapolis, Minn.

Mein, R. G., and C. L. Larson. 1973. Modeling infiltration during a steady rain. Water Resour. Res. 9(2):384-394.

Miller, D. E., and W. H. Gardner. 1962. Water infiltration into stratified soil. Soil Sci. Soc. Am. Proc. 26:115-119.

Morel-Seytoux, H. J., and A. Noblanc. 1973. Infiltration predictions by a moving strained coordinates method. Physical Aspects of Soil, Water, and Salts in Ecosystems. (ed. by A. Hadas et al.) Springer-Verlag, New York-Heidelberg-Berlin, pp. 29-42.

Morel-Seytoux, H. J., and J. Khanji. 1974. Derivation of an equation of infiltration. Water Resour. Res. 10(4):795-800.

Mulvaney, T. J. 1851. On the use of self-registering rain and flood gauges in making observations of the relations of rainfall and of flood discharges in a given catchment. Trans. Inst. Civil Engrs. Ir. (Dublin) 4(2):18.

Musgrave, GGG. W. 1955. How much of the rain enters the soil. Water, U.S. Dept. Agr. Yearbook, pp. 151-159.

Musgrave, G. W., and H. N. Holtan. 1964. Infiltration. Handbook of Applied Hydrology. (ed. by V. T. Chow), Sec. 12, McGraw-Hill Book Co., New York, N.Y.

Musgrave, G. W., and R. A. Norton. 1937. Soil and water conservation investigations at the Soil Conservation Experiment Station, Missouri Valley loess region, Clarinda, Iowa. Sta. Prog. Rept. 1931-1935 and U.S. Dept. Agr., Tech. Bull. 558, pp. 58-60.

Neal, J. H. 1938. The effect of the degree of slope and rainfall characteristics on runoff and soil erosion. Missouri Agri. Exp. Sta. Res. Bull. 280.

Nielsen, D. R., J. W. Biggar, and K. T. Erb. 1973. Spatial variability of field-measured soil-water properties. HILGARDIA 42(7):215-259.

Nimah, M. N., and R. J. Hanks. 1973. Model for estimating soil water, plant, and atmospheric interrelations: I. Description and sensitivity. Soil Sci. Soc. Am. Proc. 37:522-527.

Ogrosky, H. O., and V. Mockus. 1964. Hydrology of agricultural lands. Handbook of Applied Hydrology. (ed. by V. T. Chow). Sec. 21, McGraw-Hill Book Co., New York, N.Y.

Onstad, C. A., T. C. Olson, and L. R. Stone. 1973. An infiltration model tested with monolith moisture measurements. Soil Sci. 116(1) 13-17.

Osborn, B. 1952. Storing rainfall at the grass roots. J. Range Mangement 5:408-414.

Packer, P. E. 1951. An approach to watershed protection criteria. J. Forestry 49(9): 639:644.

Papadakis, C. N., and H. C. Preul. 1973. Infiltration and antecedent precipitation. J. Hydraul. Div., Proc. Am. Soc. Civil Engrs. 99(HY8): 1234-1245.

Parlange, J. Y. 1971. Theory of water movement in soils: 2. One-dimensional infiltration. Soil Sci. 111:170-174.

Parlange, J. Y. 1972. Theory of water movement in soils: 8. One-dimensional infiltration with constant flux at the surface. Soil Sci. 114:1-4.

Peck, A. J. 1965. Moisture profile development and air compression during water uptake by bounded porous bodies: 3. Vertical columns. Soil Sci. 100:44-51.

Philip, J. R. 1954. An infiltration equation with physical significance. Soil Sci. 77(2):153-157.

Philip, J. R. 1957a. Numerical solution of equations of the diffusion type with diffusivity concentration-dependent, II. Australian J. Phys. 10:29-42.

Philip, J. R. 1957b. The theory of infiltration: 4. Sorptivity and algebraic infiltration equations. Soil Sci. 84(3):257-264.

Philip, J. R. 1958a. The theory of infiltration: 6. Effect of water depth over soil. Soil Sci. 85(5):278-286.

Philip, J. R. 1958b. The theory of infiltration: 7. Soil Sci. 85(6): 333-337.

Philip, J. R. 1969a. Hydrostatics and hydrodynamics in swelling soils. Water Resour. Res. 5:1070-1077.

Philip, J. R. 1969b. Theory of infiltration. Advances in Hydroscience. (ed. by V. T. Chow). Vol. 5, Academic Press, New York, N.Y., pp. 215-296.

Philip, J. R. 1973. On solving the unsaturated flow equation: 1. The flux concentration relation. Soil Sci. 116:328-335.

Philip, J. R., and J. H. Knight. 1974. On solving the unsaturated flow equation: 3. New quasi-analytical technique. Soil Sci. 117:1-13.

Powell, G. M., and R. P. Beasley. 1967. Effect of erosion on water infiltration rates. Univ. of Missouri, Agri. Exp. Sta. Res. Bull. No. 922. 47 p.

Raats, P. A. C. 1971. Steady infiltration from point sources, cavities, and basins. Soil Sci. Soc. Am. Proc. 35(5):689-694.

Raats, P. A. C. 1973. Unstable wetting fronts in uniform and nonuniform soils. Soil Sci. Soc. Am. Proc. 37:681-685.

Raats, P. A. C., and A. Klute. 1968a. Transport in soils: The balance of mass. Soil Sci. Soc. Am. Proc. 32(2):161-166.

Raats, P. A. C., and A. Klute. 1968b. Transport in soils: The balance of momentum. Soil Sci. Soc. Am. Proc. 32(4):452-456.

Ramser, C. E. 1927. Runoff from small agricultural areas. J. Agr. Res. 34(9):797-823.

Rauzi, F., and C. L. Fly. 1968. Water intake on mid-continental rangelands as influenced by soil and plant cover. USDA Tech. Bull. No. 1390. 58 p.

Remson, I., G. M. Hornberger, and F. J. Molz. 1971. Numerical methods in subsurface hydrology. Wiley-Interscience, New York, N.Y., pp. 349-367.

Richards, L. A. 1931. Capillary conduction of liquids through porous mediums. Physics 1(5):318-333.

Richards, L. A. 1952. Report of the subcommittee on permeability and infiltration, committee on terminology. Soil Sci. Soc. Am. Proc. 16(1):85-88.

Richards, L. A., and L. R. Weaver. 1943. Fifteen atmosphere percentage as related to the permanent wilting percentage. Soil Sci. 56:331-339.

Richards, L. A., and L. R. Weaver. 1944. Moisture retention by some irrigated soils as related to soil-moisture tension. J. Agr. Res. 69:215-235.

Richtmeyer, R. D. 1957. Difference methods for initial-value problems. Interscience Publishers, Inc., New York, N.Y., pp. 1-16.

Robertson, L. S., and H. Kohnke. 1946. The pF at the wilting point of several Indiana soils. Soil Sci. Soc. Am. Proc. 11:50-52.

Rode, A. A. 1965. Theory of soil moisture. Vol. 1. (Translated from Russian for U.S. Dept. of Agr. and Nat. Sci. Foundation by the Israel Program for Scientific Translation in 1969).

Rose, C. W. 1966. Agricultural physics. Pergamon Press Ltd., Oxford, England. pp. 160-177.

Rubin, J. 1966a. Numerical analysis of ponded rainfall infiltration. Intern. Assoc. Sci. Hydrol., Symposium on Water in the Unsaturated Zone, Wageningen.

Rubin, J. 1966b. Theory of rainfall uptake by soils initially drier than their field capacity and its applications. Water Resour. Res. 2(4):739-749.

Rubin, J., and R. Steinhardt. 1963. Soil water relations during rain infiltration: I. Theory. Soil Sci. Soc. Am. Proc. 27:246-251.

Rubin, J., and R. Steinhardt. 1964. Soil water relations during rain infiltration: III. Water uptake at incipient ponding. Soil Sci. Soc. Am. Proc. 28:614-619.

Rubin, J., R. Steinhardt, and P. Reiniger. 1964. Soil water relations during rain infiltration: II. Moisture content profiles during rains of low intensities. Soil Sci. Soc. Am. Proc. 28:1-5.

Schreiber, H. A., and D. R. Kincaid. 1967. Regression models for predicting on-site runoff from short-duration convective storms. Water Resour. Res. 3(2):389-395.

Sharp, A. L., and H. N. Holtan. 1940. A graphical method of analysis of sprinkled-plat hydrographs. Trans. Am. Geophys. Union 21:558-570.

Sharp, A. L., and H. N. Holtan. 1942. Extension of graphic methods of analysis of sprinkled-plot hydrographs to the analysis of hydrographs of control-plots and small homogeneous watersheds. Trans. Am. Geophs. Union 23:578-593.

Sharp, A. L., H. N. Holtan, and G. W. Musgrave. 1949. Infiltration in relation to runoff on small watersheds. U.S. Dept. Agr. SCS-TP-81.

Sherman, L. K. 1940. Derivation of infiltration capacity from average loss rates. Trans. Am. Geophs. Union 21:541-550.

Sherman, L. K. 1944. Discussion of ''Role of the land during flood periods'' by W. W. Horner. Trans. Am. Soc. Civil Engrs. 109: 1295-1298.

Sherman, L. K., and L. C. Mayer. 1941. Application of the infiltration theory to engineering practice. Trans. Am. Geophys. Union 22: 666-677.

Smiles, D. E., and M. J. Rosenthal. 1968. The movement of water in swelling materials. Australian J. Soil Res. 6:237-248.

Smith, H. L., and L. B. Leopold. 1942. Infiltration studies in the Pecos River watershed, New Mexico and Texas. Soil Sci. 53:195-204.

Smith, R. E. 1972. The infiltration envelope: Results from a theoretical infiltrometer. J. Hydrol. 17:1-21.

Smith, R. E., and D. L. Chery, Jr. 1973. Rainfall excess model from soil water flow theory. J. Hydraul. Div., Proc. Am. Soc. Civil Engrs. 99(HY9):1337-1351.

Smith, R. E., and D. A. Woolhiser. 1971. Mathematical simulation of infiltrating watersheds. Hydrol. Paper No. 47. Colorado State Univ., Ft. Collins, Col.

Smith, W. E. 1944. Discussion of ''Role of the land during flood periods'' by W. W. Horner. Trans. Am. Soc. Civil Engrs. 109:1303-1310.

Sobhani, G. 1975. A review of selected small watershed design methods for possible adoption to Iranian conditions. M.S. Thesis. Utah State Univ., Logan, Utah.

Soil Conservation Service. 1972. Soil survey of Utah County, Utah, Central Part.

Staple, W. J. 1966. Infiltration and redistribution of water in vertical columns of loam soil. Soil Sci. Soc. Am. Proc. 30:553-558.

Staple, W. J. 1969. Comparison of computed and measured moisture redistribution following infiltration. Soil Sci. Soc. Am. Proc. 33:840-847.

Staple, W. J., and J. J. Lehane. 1954. Movement of moisture in unsaturated soils. Can. J. Agr. Sci. 34:329-342.

Steinbrenner, E. C. 1955. The effect of repeated tractor trips on the physical properties of forest soils. Northwest Sci. 29:155-159.

Stoeckeler, J. H., and S. Weitzman. 1960. Infiltration rates in frozen soils in Northern Minnesota. Soil Sci. Soc. Am. Proc. 24:137-139.

Swartzendruber, D., and D. Hillel. 1973. The physics of infiltration. Physical Aspects of Soil, Water, and Salts in Ecosystems (ed. by A. Hadas et al.), Springer-Verlag, New York-Heidelberg-Berlin, pp. 3-15.

Talsma, T., and J. Y. Parlange. 1972. One-dimensional vertical infiltration. Australian J. Soil Res. 10:143-150.

Thames, J. L., and S. J. Ursic. 1960. Runoff as a function of moisture and storage capacity. J. Geophys. Res. 65:651-654.

Trimble, G. R., Jr., R. S. Sartz, and R. S. Pierce. 1958. How type of frost affects infiltration. J. Soil Water Conserv. 13:81-82.

Turner, A. K. 1963. Infiltration runoff and soil classifications. J. Hydrol. 1:129-143.

U.S. Department of Agriculture, Soil Conservation Service. 1969. Hydrology, SCS National Engineering Handbook. Sec. 4.

Vachaud, G., J. P. Gaudet, and V. Kuraz. 1974. Air and water flow during ponded infiltration in a vertical bounded column of soil. J. Hydrol. 22:89-108.

Wang, F. C., and V. Lakshminarayana. 1968. Mathematical simulation of water movement through unsaturated nonhomogeneous soil. Soil Sci. Soc. Am. Proc. 32:329-334.

Wei, C. Y. 1971. Finite difference solutions of axisymmetric infiltration through partially saturated porous media. Ph.D. dissertation, Utah State Univ., Logan, Utah.

Whisler, F. D., and A. Klute. 1965. The numerical analysis of infiltration, considering hysteresis, into a vertical soil column at equilibrium under gravity. Soil Sci. Soc. Am. Proc. 29:489-494.

Whisler, F. D. and A. Klute. 1969. Analysis of infiltration into stratified soil columns. Intern. Assoc. Sci. Hydrol., Proc. Symposium on Water in the Unsaturated Zone. Wageningen, 1966. Paris, UNESCO pp. 451-470.

Whisler, F. D., and K. K. Watson. 1968. One-dimensional gravity drainage of uniform columns of porous materials. J. Hydrol. 6:277-296.

Whisler, F. D., and K. K. Watson. 1969. Analysis of infiltration into draining porous media. J. Irr. Drain. Div., Proc. Am. Soc. Civil Engrs. 95(IR4):481-491.

Willis, W. S. 1965. Use of rainfall simulator in a laboratory study of infiltration rates of bare soils. M. S. Thesis, Utah State Univ., Logan, Utah.

Wilson, L. G., and J. N. Luthin. 1963. Effect of air flow ahead of the wetting front on infiltration. Soil Sci. 96:136-143.

Woodward, L. 1943. Infiltration capacities on some plant-soil complexes on Utah range watershed-lands. Trans. Am. Geophys. Union 24:468-474.

APPENDICES

Appendix A

Soil Classifications

Introduction

Because geology has not provided the information required by soil users, the study and classification of soil has in the past been undertaken by engineers and agriculturists who have confined themselves to those soil properties and materials in which they have a special interest. The appreciation of soil made in this way has been restricted by the limited standpoint from which it has been investigated. A classification designed by one soil user has tended to be of limited value to others because it has been designed to serve a specific and limited purpose (Macvicar, 1969). On the other hand, any field classification of soils is confused by a large number of variables, some of which are permanent, though others change with time (Turner, 1963). Gibbons (1961) has commented on the seemingly impossible task of producing a universal soil classification that will show such diverse requirements as crop yields and infiltration capacities. Many soil scientists agree that such a universal classification is impossible to achieve, although some efforts are still being made with this aim.

The ultimate aim of most soil surveys of large areas has been for agriculture, and the criteria used in some of the surveys are those for growing plants. They are called ''edaphic'' surveys. Other types of classifications that still have agriculture in mind, but have less emphasis on the growing plant, are ''pedological'' surveys which attempt to describe the genesis of soil profile.

There are a number of soil classification systems. They are based mainly on the intended use of the system. In the following, these different kinds of classifications are discussed in detail.

Pedological system

This system, stemming largely from Russian soil scientists, depends on observation of the soil profile down into the C-horizon (see Appendix B for definition of the C-horizon). The system has been developed primarily with agriculture in mind, but it is not intended to serve agriculture alone. This system has the two broad divisions: Higher categories and Lower categories.

Higher categories. The Higher categories of the Pedological system are further classified into Order, Suborder, and Great Soil Group.

Under Order are the zonal, intrazonal and azonal soils. Zonal soils depend on climate and also on some local conditions, such as poor drainage.

Table A-1. Soil classification in the higher categories.*

Order	Suborder	Great Soil Group
Zonal soils	1. Soils of the cold zone	Tundra soils
	2. Light-colored soils of arid regions	Desert soils
		Red desert soils
		Sierozem
		Brown soils
		Reddish-brown soils
	3. Dark-colored soils of semiarid, subhumid, and humid grasslands	Chestnut soils
		Reddish chestnut soils
		Chernozem soils
		Prairie soils
		Reddish prairie soils
	4. Soils of the forest-grass land transition	Degraded chernozem
		Noncalcic brown, or Shantung brown soils
	5. Light-colored podzolized soils of the timbered regions	Podzol soils
		Gray wooded, or gray podzolic soils
		Brown podzolic soils
		Gray-brown podzolic soils
		Red-yellow podzolic soils
	6. Lateritic soils of forested warm-temperate and tropical regions	Reddish-brown lateritic soils
		Yellowish-brown lateritic soils
		Laterite soils
Intrazonal soils	1. Halomorphic (saline and alkali) soils of imperfectly drained arid regions and littoral deposits	Solonchak, or saline soils
		Solonetz soils
		Soloth soils
	2. Hydromorphic soils of marshes, swamps, seep areas, and flats	Humic-glei soils (includes Wiesenboden)
		Alpine meadow soils
		Bog soils
		Half-bog soils
		Low-humic-glei soils
		Planosols
		Groundwater packed soils
		Groundwater laterite soils
	3. Calcimorphic soils	Brown forest soils (Braunerde)
		Rendzina soils
Azonal soils		Lithosols
		Regosols (includes dry sands)
		Alluvial soils

*After Thorp and Smith (1949).

Azonal soils do not depend on climate zones. They include rocky soils (lithosols), dry sands (regosols), and alluvial sediments as shown in Table A-1.

The zonal soils have six Suborders, ranging from cold to tropical zones. The intrazonal soils have three Suborders: salt and alkali soils, soils of wet areas, and soils rich in calcium.

The names of the Great Soil Group shown in Table A-1 define the soils in a general way. For more details see Thorp and Smith (1949), and Kirkham (1964). Many of the Great Soil Group were originally defined by examples of Russion soils, and this method of classification has been used as the basis for hydrologic grouping in that country.

Turner (1963) following Lvovitch in a discussion of stream flow factors related relative discharge coefficients for floods or runoff per unit of precipitation with soil groups as follows:

Adopting a coefficient for solonetzes and solonchaks	100%
Degraded podzols clay and clayey soils	80%- 85%
Chestnut soils	65%- 70%
Clay and clayey chernozems of high fertility	40%- 50%
Sandy Soils	20%- 35%

Lower categories. The first sub-division of the Great Soil Group of Table A-1 is called a soil series. Series are then divided into types, and types are further divided into phases. A series is a group of soils developed from the same type of parent materials. Type is determined from the texture of the A-horizon. (See Appendix B for definition of the A-horizon.) Phase is determined by some deviation from the normal, such as erosion, slope, stoniness, or soluble salt content. In the United States, each series is given a name like Houston clay, Stony phase.

Engineering unified soil classification system

This system is not applicable to agronomic soils, but is intended for soil classification for foundations of hydraulic structures.

This system is a modification of the original Cesagrande Airfield classification system developed by Arthur Cesagrande of Harvard University for the Corps of Engineers during World War II. This classification is based on the characteristics of the soil which indicates how it will behave as a construction material. The original classification has been expanded and revised in cooperation with the U.S. Bureau of Reclamation so that it now applies to embankments and foundations as well as to roads and airfields.

In the unified system, soils are identified according to their texture and plasticity and are grouped according to their performance as engineering construction material. The following properties have been found most useful in predicting how a soil will behave as a construction material and consequently form the basis of the unified system:

a. Percentages of gravel, sand, and fines (fraction passing No. 200 sieve).
b. Shape of the grain-size distribution curve.
c. Plasticity and compressibility characteristics.

In the unified system, the soil is given a name which is intended to be a short description, and a letter symbol which consists of two letters indicating its principal characteristics. Table A-2 summarizes the system, giving the names, letter symbols, and general information about the soils. For more detailed description of each group, one may refer to Military Standard Unified Soil Classification System for Roads, Airfields, Embankments, and Foundations MIL-STD-619B. In the unified system, soils are divided into coarse-grained and fine-grained materials. For convenience, any soil having 50 percent or less passing the No. 200 U.S. standard series sieve size (0.074 mm) is termed coarse-grained, and any soil having more than 50 percent passing the No. 200 sieve is termed fine-grained.

Other engineering classification systems

Kirkham (1964) mentioned two other important engineering soil-classification systems. They are used by the American Association of State Highway Officials (AASHO) and U.S. Civil Aeronautics Administration. Both are similar to the unified system in which soil texture and plasticity are stressed. These systems have almost the same limitations as the unified system has as far as the infiltration aspect of soil property is concerned.

The AASHO system of classifying soils is an engineering property classification based on field performance of soils. It is the most widely known system used in highway construction. The following analyses and properties are used in the identification and classification of soils in this system: sieve analysis, mechanical analysis, liquid limit, plastic limit, and compaction.

Under this system, grouping soils of about the same general load-carrying capacity and service characteristics results in seven basic groups that were designated A-1 through A-7. The best soils for road subgrades are classified as A-1, the next A-2, and so on to class A-7, the poorest soils for subgrade. (For detail of this classification see AASHO "Standard Specifications for Highway Materials and Methods of Sampling and Testing," Part I, pp. 45-52.)

Table A-2. Categories and group symbols of engineering unified soil classification system.*

Category				Group symbols
Coarse-grained soils	Gravels	Clean gravel	Gravels, well graded Gravels, poorly graded	GW GP
		Gravels with fines	Gravels, mixed non-pl.** fines Gravels, clayey-pl. fines	GM GC
	Sands	Clean sands	Sands, well graded Sands, poorly graded	SW SP
		Sands with fines	Sands, mixed non-pl. fines Sands, clayey-pl. fines	SM SC
Fine-grained soils	Silts and clays	*** LL less than 50	Mineral silts, low pl. Clays (mineral), low pl. Organic silts, low pl.	ML CL OL
		LL greater than 50	Mineral silts, high pl. Clays (mineral), high pl. Organic clays, high pl.	MH CH OH
Highly organic soils			Organic soils as peat	Pt

*Adapted from "Earth Manual" (1960, pp. 1-23).

**pl. = plastic, or plasticity.

***The liquid limit (LL) is the ratio of weight of water to weight of dry soil, expressed in percent, for a soil-water mixture that just flows under the pull of gravity.

Comprehensive pedological system

This classification system has been under development by the Soil Survey staff of the USDA and other interested soil scientists since 1951 for the following reasons:

a. In the earlier, similar pedological classification, the profiles of virgin soils have been stressed. Few soils now are virgin (Kirkham, 1964).

b. Earlier pedological systems have been developed primarily for application to Russian and Western European soils, and to soils of the United States. Little provision has been given to tropical soils, for which data are now accumulating.

c. In the earlier pedological systems, soils were classified primarily into soil series with few relations, if any, shown between the series, even when the soils in the same series were only a few hundred miles apart.

d. In earlier systems, much of the work was done as an art. Physical and chemical measurement data were not widely taken or used.

e. Earlier systems have not had sufficiently descriptive and logical nomenclature for identifying soils and showing their interrelation. (The Comprehensive system has a radically and completely new nomenclature.)

f. Earlier pedological systems often stressed genetic factors of soil formation instead of giving emphasis to the soil properties as found. (The Comprehensive system places emphasis on soil properties rather than on genetic factors.)

The categories of this system are orders, suborders, subgroups, families, and series. The category soil type, such as loam, sandy loam, etc., is not included in the nomenclature. There are 10 orders, and their names all end in sols (soils). The names of the orders and their meanings are tabulated in Table A-3. For detail of the categories adopted in the system, see Tables A-4 through A-8.[1]

Although this system has overcome many of the difficulties of earlier pedological systems, the limitations of this classification are evident. It is too detailed and difficult to be used in the determination of the soil class or category for highways, with little work on site.

---

[1]Personal communication with Dr. A. Southard, Soils and Biometeorology Department, Utah State University, Logan, Utah.

Table A-3. Name of orders and their approximate meanings.

Name of Order	Approximate Meaning
1. Entisols	Recent soils.
2. Vertisols	Inverted soils, in the sense that surface soil has sloughed into cracks and subsoil has been pushed, by swelling action, to the surface. They crack markedly when dry.
3. Inceptisols	Young (inception) soils, as the ando soils, which are formed of young volcanic ash.
4. Aridisols	Arid soils, as desert soils.
5. Mollisols	Crumbly (soft) surface layer, as do the chernozems and prairie soils.
6. Spodosols	Soils that have a horizon at least 6" below the soil surface containing free sesquioxides (Al_2O_3, Fe_2O_3), and organic carbon which have leached from surface layer.
7. Alfisols	Do not, as the name suggests, (alfi: Al, Aluminum, f(e) iron) contain a subsurface layer rich in the sesquioxides; they have a clay-enriched subsoil, like spodosols, they often have an ashy-gray subsurface horizon.
8. Ultisols	Very old and hence are found only in humid (never post-glacial) climates.
9. Oxisols	Contain horizons rich in oxides of silica of iron and of aluminum. They are restricted to tropical and sub-tropical regions.
10. Histosols	Contain to a large extent, or actually are residues of plant tissues. They are organic soils such as peat and mulch.

Table A-4. Names of Orders, Suborders, and Great Groups.

Order	Suborder	Great Group
Entisols (1)	Aquents	Cryaquents
		Haplaquents
		Hydraquents
		Psammaquents
		Tropaquents
	Arents	
	Fluvents	Cryofluvents
		Torrifluvents
		Tropofluvents
		Udifluvents
		Ustifluvents
		Xerofluvents
	Orthents	Cryorthents
		Torriorthents
		Troporthents
		Udorthents
		Ustorthents
		Xerorthents
	Psamments	Cryopsamments
		Quartzipsamments
		Torripsamments
		Udipsamments
		Ustipsamments
		Xeropsamments
Vertisols (2)	Torrerts	
	Uderts	Chromuderts
		Pelluderts
	Usterts	Chromusterts
		Pellusterts
	Xererts	Chromoxererts
		Pelloxererts
Inceptisols (3)	Andepts	Cryandepts
		Durandepts
		Dystrandepts
		Eutrandepts
		Hydrandepts
		Vitrandepts
	Aquepts	Andaquepts
		Cryaquepts
Inceptisols (3)	Aquepts	Fragiaquepts
		Halaquepts
		Haplaquepts
		Humaquepts
		Plinthaquepts
		Tropaquepts
	Ochrepts	Cryochrepts
		Durochrepts
		Dystrochrepts
		Eutrochrepts
		Fragiochrepts
		Ustochrepts
		Xerochrepts
	Plaggepts	
	Tropepts	Dystropepts
		Eutropepts
		Humitropepts
		Ustropepts
	Umbrepts	Anthrumbrepts
		Cryumbrepts
		Fragiumbrepts
		Haplumbrepts
		Xerumbrepts
Aridisols (4)	Argids	Durargids
		Haplargids
		Nadurargids
		Natrargids
		Paleargids
	Orthids	Calciorthids
		Camborthids
		Durorthids
		Paleorthids
		Salorthids
Mollisols (5)	Albolls	Argialbolls
		Natralbolls
	Aquolls	Argiaquolls
		Calciaquolls
		Cryaquolls
		Duraquolls
		Haplaquolls
		Natraquolls

Table A-4. Continued.

Order	Suborder	Great Group	Order	Suborder	Great Group
Mollisols (5)	Borolls	Argiborolls	Alfisols (7)	Aqualfs	Albaqualfs
		Calciborolls			Fragiaqualfs
		Cryoborolls			Glossaqualfs
		Haploborolls			Natraqualfs
		Natriborolls			Ochraqualfs
		Paleborolls			Tropaqualfs
		Vermiborolls			Umbraqualfs
	Rendolls			Boralfs	Cryoboralfs
					Eutroboralfs
	Udolls	Arguidolls			Fragiboralfs
		Hapludolls			Glossoboralfs
		Paleudolls			Natriboralfs
		Vermudolls			Paleboralfs
	Ustolls	Arguistolls		Udalfs	Agrudalfs
		Calcuistolls			Ferrudalfs
		Durustolls			Fragiudalfs
		Haplustolls			Glossudalfs
		Natrustolls			Hapludalfs
		Paleustolls			Natrudalfs
		Vermustolls			Paleudalfs
					Tropudalfs
	Xerolls	Argixerolls			
		Calcixerolls		Ustalfs	Durustalfs
		Durixerolls			Haplustalfs
		Haploxerolls			Natrustalfs
		Natrixerolls			Paleustalfs
		Palexerolls			Plinthustalfs
					Rhodustalfs
Spodosols (6)	Aquods	Cryaquods			
		Duraquods		Xeralfs	Durixeralfs
		Fragiaquods			Haploxeralfs
		Haplaquods			Natrixeralfs
		Placaquods			Palexeralfs
		Sideraquods			Plinthoxeralfs
		Tropaquods			Rhodoxeralfs
	Ferrods		Ultisols (8)	Aquults	Fragiaquults
					Ochraquults
	Humods	Cryohumods			Plinthaquults
		Fragihumods			Tropaquults
		Haplohumods			Umbraquults
		Placohumods			
		Tropohumods		Humults	Haplohumults
					Palehumults
	Orthods	Cryorthods			Tropohumults
		Fragiorthods			
		Haplorthods			
		Placorthods			

Table A-4. Continued.

Order	Suborder	Great Group	Order	Suborder	Great Group
Ultisols (8)	Udults	Fragiudults	Oxisols (9)	Humox	Acrohumox
		Hapludults			Gibbsihumox
		Paleudults			Haplohumox
		Plinthudults			Sombrihumox
		Rhodudults			
		Tropudults		Orthox	Acrorthox
					Eutrorthox
	Ustults	Haplustults			Gibbsiorthox
		Paleustults			Haplorthox
		Plinthustults			Umbriorthox
		Rhodustults			
		Tropustults		Torrox	
	Xerults	Haploxerults		Ustox	Acrustox
		Palexerults			Eutrustox
					Haplustox
Oxisols (9)	Aquox	Gibbsiaquox			
		Ochraquox	Histosols (10)	Imcomplete	
		Plinthaquox			
		Umbraquox			

Table A-5. Present soil orders and approximate equivalents in revised classification of Baldwin et al. (1938).

Present order	Approximate equivalents
1. Entisols	Azonal soils, and some Low Humic Gley soils.
2. Vertisols	Grumusols.
3. Inceptisols	Ando, Sol Brun Acide, some Brown Forest, Low-Humic Gley, and Humic Gley soils.
4. Aridisols	Desert, Reddish Desert, Sierozen, Solonchak, some Brown and Reddish Brown soils, and associated Solonetz.
5. Mollisols	Chestnut, Chernozem, Brunizem (Prairie), Rendzinas, some Brown, Brown Forest, and associated Solonetz and Humic Gley soils.
6. Spodosol	Podzols, Brown Podzolic soils, and Ground-Water Podzols.
7. Alfisols	Gray-Brown Podzolic, Gray Wooded soils, Noncalcic Brown soils, Degraded Chernozem, and associated Planosols and some Half-Bog soils.
8. Ultisols	Red-Yellow Podzolic soils, Reddish-Brown Lateritic soils of the U.S., and associated Planosols and Half-Bog soils.
9. Oxisols	Laterite soils, Latosols.
10. Histosols	Bog soils.

Table A-6. Formative elements in names of soil Orders.

No. of order[1/]	Name of order	Formative element in name of order	Derivation of formative element	Mnemonicon and pronunciation of formative elements
1.	Entisol...	ent	Nonsense syllable.	recent.
2.	Vertisol..	ert	L. verto, turn.	invert.
3.	Inceptisol	ept	L. inceptum, beginning.	inception.
4.	Aridisol..	id	L. aridus, dry.	arid.
5.	Mollisol..	oll	L. mollis, soft.	mollify.
6.	Spodosol..	od	Gk. spodos, wood ash	Podzol; odd.
7.	Alfisol...	alf	Nonsense syllable.	Pedalfer.
8.	Ultisol...	ult	L. ultimus, last.	Ultimate.
9.	Oxisol....	ox	F. oxide, oxide.	oxide.
10.	Histosol..	ist	G. histos, tissue.	histology.

[1/] Numbers of the orders are listed here for the convenience of those who became familiar with them during development of the system of classification.

Table A-7. Formative elements in names of Suborders.

Formative elements	Derivation of formative element	Mnemonicon	Connotation of formative element
alb	L. albus, white.	albino	Presence of albic horizon (a bleached eluvial horizon).
and	Modified from Ando.	Ando	Ando-like.
aqu	L. aqua, water.	aquarium	Characteristics associated with wetness.
ar	L. arare, to plow	arable	Mixed horizons.
arg	Modified from argillic horizon; L. argilla, white clay.	argillite	Presence of argillic horizon (a horizon with illuvial clay).
bor	Gr. boreas, northern.	boreal	Cool.
ferr	L. ferrum, iron.	ferruginous	Presence of iron.
fibr	L. fibra, fiber.	fibrous	Least decomposed stage.
fluv	L. fluvius, river.	fluvial	Flood plains.
hem	Gr. hemi, half.	hemisphere	Intermediate stage of decomposition.
hum	L. humus, earth.	humus	Presence of organic matter.
lept.	Gr. leptos, thin.	leptometer	Thin horizon.
ochr	Gr. base of ochros, pale.	ocher	Presence of ochric epipedon (a light-colored surface).
orth	Gr. orthos, true.	orthophonic	The common ones.
plag	Modified from Ger. plaggen, sod.		Presence of plaggen epipedon.
psamm	Gr. psammos, sand.	psammite	Sand textures.
rend	Modified from Rendzina.	Rendzina	Rendzina-like.
sapr	Gr. sapros, rotten.	saprophyte	Most decomposed stage.
torr	L. torridus, hot and dry.	torrid	Usually dry.
trop	Modified from Gr. tropikos, of the solstice.	tropical	Continually warm.
ud	L. udus, humid.	udometer	Of humid climates.
umbr	L. umbra, shade.	umbrella	Presence of umbric epipedon (a dark-colored surface).
ust	L. ustus, burnt.	combustion	Of dry climates, usually hot in summer.
xer	Gr. xeros, dry.	xerophyte	Annual dry season.

Table A-8. Formative elements for names of Great Groups.

Formative element	Derivation of formative element	Mnemonicon	Connotation of formative element
acr	Modified from Gr. akros, at the end.	acrolith	Extreme weathering.
agr	L. ager, field.	agriculture	An agric horizon.
alb	L. albus, white.	albino	An albic horizon.
and	Modified from Ando.	Ando	Ando-like.
anthr	Gr. anthropos, man.	anthropology	An anthropic epipedon.
aqu	L. aqua, water.	aquarium	Characteristic associated with wetness.
arg	Modified from argillic horizon; L. argilla, white clay.	argillite	An argillic horizon.
calc	L. calcis, lime.	calcium	A calcic horizon.
camb	L. L. cambiare, to exchange.	change	A cambic horizon.
chrom	Gr. chroma, color.	chroma	High chroma.
cry	Gr. kryos, coldness.	crystal	Cold.
dur	L. durus, hard.	durable	A duripan.
dystr, dys	Modified from Gr. dys, ill; dystrophic, infertile.	dystrophic	Low base saturation.
eutr, eu	Modified from Gr. eu, good; eutrophic, fertile.	eutrophic	High base saturation.
ferr	L. ferrum, iron.	ferric	Presence of iron.
frag	Modified from L. fragilis, brittle.	fragile	Presence of fragipan.
fragloss	Compound of fra(g) and gloss.		See the formative elements frag and gloss.
gibbs	Modified from gibbsite.	gibbsite	Presence of gibbsite.
gloss	Gr. glossa, tongue.	glossary	Tongued.
hal	Gr. hals, salt.	halophyte	Salty.
hapl	Gr. haplous, simple.	haploid	Minimum horizon.
hum	L. humus, earth.		Presence of humus.
hydr	Gr. hydor, water.	hydrophobia	Presence of water.
hyp	Gr. hypnon, moss.	hypnum	Presence of hypnum moss.
luo, lu	Gr. louo, wash.	ablution	Illuvial.
moll	L. mollis, soft.	mollify	Presence of mollic epipedon.
nadur	Compound of na(tr), and dur.		
natr	Modified from natrium, sodium.		Presence of natric horizon.
ochr	Gr. base of ochros, pale.	ocher	Presence of ochric epipedon (a light-colored surface).
pale	Gr. paleos, old.	paleosol	Old development.
pell	Gr. pellos, dusky.		Low chroma.
plac	Gr. base of plax, flat stone.		Presence of a thin pan.

Table A-8. Continued.

Formative element	Derivation of formative element	Mnemonicon	Connotation of formative element
plag	Modified from Ger. plaggen, sod.		Presence of plaggen horizon.
plinth	Gr. plinthos, brick.		Presence of plinthite.
quartz	Ger. quarz, quartz.	quartz	High quartz content.
rend	Modified from Rendzina	Rendzina	Rendzina-like.
rhod	Gr. base of rhodon, rose.	rhododendron	Dark-red colors.
sal	L. base of sal, salt.	saline	Presence of salic horizon.
sider	Gr. sideros, iron.	siderite	Presence of free iron oxides.
sphagno	Gr. sphagnos, bog.	sphagnum-moss	Presence of sphagnum-moss.
torr	L. torridus, hot and dry.	torrid	Usually dry.
trop	Modified from Gr. tropikos, of the solstice.	tropical	Continually warm.
ud	L. udus, humid.	udometer	Of humid climates.
umbr	L. base of umbra, shade.	umbrella	Presence of umbric epipedon.
ust	L. base of ustus, burnt.	combustion	Dry climate, usually hot in summer.
verm	L. base of vermes, worm.	vermiform	Wormy, or mixed by animals.
vitr	L. vitrum, glass.	vitreous	Presence of glass.
xer	Gr. xeros, dry.	xerophyte	Annual dry season.
sombr	F. sombre, dark.	somber	A dark horizon.

European and forest soils classifications

The European soils classification is similar to the pedological classification. For details, see Franz (1961). The forest soils classification has only two main groups: the upland forest soils and the bottomland forest soils (hydromorphic). For details, see Wilde (1958).

Land capability classification system

Another soil classification system used by the U.S. Soil Conservation Service for in-farm surveys is the Land Capability groupings. The Land Capability groups are based on the needs and limitations of the soil, i.e., on the response of the groups to management required to keep them productive and to protect them from erosion and other hazards (Klingebiel and Montgomery, 1961). Soil characteristics considered in placing soils directly or indirectly into land capability groups include depth and texture of top soil, land slope, drainage (a function of the soil's internal permeability and topographic position), rockiness, salinity, and the productivity of the soil for plant growth. There are eight main classes which may be described briefly as follows.

Land suited for cultivation and other uses. There are four classes.

Class I Soils in this class have few limitations that restrict their use.

Class II Soils in this class can be cultivated regularly. They have some limitations that reduce the choice of plants or require moderate conservation practices.

Class III Soils in this class can be cropped regularly. They have severe limitations that reduce the choice of plants or require special conservation practices, or both.

Class IV Soils in this class should be cultiviated only occasionally. They have very severe limitations that restrict the choice of plants or require very careful management, or both.

Land limited in use. The following four classes are generally not suited to cultiviation.

Class V Soils in this class have little or no erosion hazard, usually flat, but have other limitations that limit their use largely to pasture, range, or woodland.

Class VI Soils in this class are steep and have severe limitations that make them generally unsuited to cultivation and limit their use largely to pasture, range, or woodland.

Class VII Soils in this class have very severe limitations that make them unsuited to cultivation and restrict their use largely to grazing, woodland, and wildlife.

Class VIII Soils and land forms in this class have limitations that preclude their use from commercial plant production and restrict their use to recreation, wildlife, water supply, or esthetic purposes.

Each of the aforementioned classes is subdivided into subclasses. Four limitations recognized at the subclass level are: (1) risks of erosion, (2) wetness, drainage, or overflow, (3) rooting-zone limitations, (4) climatic limitation. The subclass provides the map user with information about both degree and kind of limitation. Class I has no subclasses.

For detail of this classification system, see Klingebiel and Montgomery (1961). As mentioned by England (1970), this classification provides farm planning specialists with enough information to prepare alternate plans for cropping, fertilizer application, irrigation erosion control, and other management practices.

Moreover, England (1970) mentioned the possibility of use of this classification in hydrologic studies. He summarized his discussion on ''Land Capability: A hydrologic response unit in agricultural watersheds'' by:

> Land-capability classes are based on the same soil-land form criteria as those used in hydrologic soil groupings i.e., surface moisture capacities and position on the landscape. In addition, land-capability classes are intuitively unique in land use and provide a basis for futuristic estimates of land use as well as hydrologic performance. This concept is exploratory and is offered here as an inducement for discussion and, hopefully, further testing.

Classification based on land system

A ''land system'' is defined as an area or a group of areas throughout which there is a recurring pattern of topography, geology, soils, and vegetation (Christian and Stewart in Turner, 1963). This method was developed to predict the land capability of large areas in undeveloped regions. To map conjointly the four variables–topography, geology, soils, and vegetation–without designating a large number of independent zones on a map probably means that some overlapping sometimes takes place. The degree of overlapping depends on the surveyor and his scale of mapping (Turner, 1963). To use this system in infiltration studies a map showing the existing patterns of land use is needed.

Classification based on texture of surface soils

Earlier work on infiltration capacities, i.e., the ASCE Hydrology Handbook (1949) showed that infiltration rates were listed in relation to the texture of the surface soil. In this approach it is assumed that the texture of the surface soil is a fair indication of its structure, and that there is no change in texture with depth, or such changes are not significant as far as infiltration is concerned. This approach resulted in three soil groups, as shown in Table A-9.

There are limitations in this approach: (1) Surface texture is used as the sole criterion for a hydrologic classification of soil and other soil properties that can dominate the infiltration and water storage processes are ignored. These properties are structure, mineralogy, drainage characteristics, and depth. (2) Using the terms sands, loams, and clays for the whole profile, as obtained from the surface soil texture, implies the uniformity of texture for the whole profile. This is generally not true for mineral soils. (See Appendix B for soil horizons and layers.)

Classification based on topographic grouping of soils

England and Onstad (1968) and England and Holtan (1969) grouped soils by their upper layer porosity and their position on the landscape. Hydrologic response units in the watersheds studied vary from deep upland soils with high storage capacity through shallow eroded hillsides to very deep alluvial-colluvial zones. The three soil groups are: upland, hillside, and bottomland.

The authors gave the following advantages for grouping soils topographically by their surface soil porosity: (1) Elevation sequences of soil groups are compatible with, and in fact, are responsible for variations in the hydraulics of surface and subsurface flows. (2) The distribution of the soil groups defined as hydrologic response units is normally consistent with the distribution of the various land uses or of the native vegetation within the watersheds. Thus the roles of soils and land use can be considered simultaneously in a framework that is rationally consistent with the hydrologic performance of the landscape (England, 1970).

Table A-9. Infiltration rates for bare soil at the end of one hour.

Soil Groups	Infiltration Rate in./hour
High	0.50 to 1.00
Intermediate	0.10 to 0.50
Low	0.01 to 0.10

Noteworthy is a new land-use classification system which has been proposed by the U.S. Geological Survey (see Transactions, American Geophysical Union, Vol. 54, No. 2, p. 89, 1973). The system is based on a numerical code, describing only the generalized first and second levels of classification. The first level is numerically coded into nine categories (urban and built-up land, agricultural land, range and forest land, water, nonforested wetland, barren land, tundra, and permanent snow and icefields). The second level subdivides each first level category into more than 30 numerically coded categories.

Classification based on soil associations

Soil associations are defined as groups of individual soils often following repetitious patterns over a larger area. Miller and Cary (1966) hydrologically classified 210 soil associations in the Susquehanna River Basin by deriving weighted Soil Conservation Service (SCS) curve numbers for the associations and by assigning A, B, C, and D categories to them. From a 5-inch rainstorm, soil associations producing less than 1.0 inch of runoff were classified as 'A,' between 1.0 inch and 1.7 inches as 'B,' between 1.7 inches and 2.9 inches as 'C,' and higher than 2.9 inches as 'D.'

Miller and Cary specified that the following tools were necessary to formulate a hydrological soil grouping map: (1) soil association maps for the entire river basin, (2) several stream and rain gaged watersheds with sufficient lengths of record to provide a good estimate of rainfall and runoff amount, and (3) an evaluation of individual soils properties which can be used as a common denominator to relate hydrologically similar soil associations. This could be either: soils information showing depth and drainage characteristics of individual soils or the hydrological soil classification table of the SCS National Engineering Handbook, Section 4.

Soil Conservation Service of
USDA classification

Musgrave (1955) placed thousands of U.S. soil series into four groups based upon the soils final constant or minimum rate of infiltration, defined as the rate of intake after prolonged wetting.

The Soil Conservation Service (SCS) of the USDA subsequently placed over 6,000 soil series into Musgrave's grouping and adopted the groups as the basis for watershed planning. The groupings are used to derive soil-cover complex numbers in the rainfall-runoff relationship used in estimating maximum annual floods from agricultural watersheds.

The soils have been classified into four groups: A, B, C, and D. Soil properties that influence the final constant rate of infiltration for a bare soil were investigated. These properties are the depth of seasonally highwater table, permeability, and depth to very slowly

permeable layer. Each soil group has been described by SCS in 1972 as follows:

A. Low runoff potential. Soils in this group have high (rapid) infiltration rates even when thoroughly wetted and consist chiefly of deep, well to excessively drained sands or gravels. These soils have a high rate of water transmission. (Includes Psamments except those in Lithic, Aquic, or Aquodic subgroups; soils other than those in groups C or D in fragmental, sandy-skeletal, or sandy families; soils in Grossarenic subgroups of Udults and Udalfs; and soils in Arenic subgroups of Udults and Udalfs except those in clayey or fine families.)

B. Moderately low runoff potential. Soils in this group have moderate infiltration rates when thoroughly wetted and consist chiefly of moderately deep to deep, moderately well to well drained soils with moderately fine to moderately coarse textures and with moderately slow to moderately rapid permeability. These soils have a moderate rate of water transmission.

C. Moderately high runoff potential. Soils in this group have slow infiltration rates when thoroughly wetted and consist chiefly of soils with a layer that impedes downward movement of water, soils with moderately fine to fine texture, soils with slow infiltration due to salts or alkali, or soils with moderate water tables. These soils may be somewhat poorly drained, well and moderately well drained soils with slowly and very slowly permeable layers (fragipans, hardpans, hard bedrock, and the like) at moderate depth (20-40 inches). (Includes soils in Albic or Aquic subgroups; soils in Aeric subgroups of Aquents, Aquepts, Aquolls, Aqualfs, and Aquults in loamy families; soils other than those in group D that are in fine, very fine, or clayey families except those with kaolinitic, oxidic, or halloysitic mineralogy; Humods and Orthods; soils with fragipans or petrocalcic horizons; soils in shallow families that have permeable substrata; soils in Lithic subgroups that have rock which is pervious or cracked enough to allow water to penetrate.)

D. High runoff potential. Soils in this group have very slow infiltration rates when thoroughly wetted and consist chiefly of clay soils with a high swelling potential, soils with a permanent high water table, soils with a claypan or clay layer at or near the surface, soils with very slow infiltration due to salts or alkali, and shallow soils over nearly impervious material. These soils have a very slow rate of water transmission. (Includes all Vertisols; all Histosols; All Aquods; soils in Aquents, Aquepts, Aquolls, Aqualfs, and Aquults except for Aeric subgroups in loamy families; soils with natric horizons; soils in Lithic subgroups that have impermeable substrata; and soils in shallow families that have impermeable substrata.)

Classification based on catena concept

In order to supplement and refine the classification of the SCS, Chiang (1971) suggested a rating table using the catena concept. The

rating table allows for an intermediate class between each of the four groups classified by SCS.

A soil catena, by definition, is a group of soil series developed from similar parent material but differing in drainage. Five drainage classes as shown in Table A-10 are used and generally related to the relief position. The parent material of the soil is shown on the left-hand side of each soil catena. Table A-10 is part of typical soil catena diagram prepared by Matelski (Chiang, 1971). Each row is called a soil catena. The dashed line in Table 5 shows the possible overlaps with adjacent drainage classes or soil depth phases.

Table A-11 shows the rearranged runoff potential rating (RPR) after Chiang (1971). The rating is given according to internal drainage, depth, and texture of the soil, as well as subsurface soil conditions. Row 4 is used as the standard rating. Subsequent modification is then made based on the difference in soil texture and the condition underlying the soil. The runoff potential rating is first given according to drainage. The depth of the soil over bedrock becomes the controlling factor only if the soil is well drained. Then comes the texture of the soil which has a substantial effect on infiltration capacity and hence runoff potential, provided the soil is well drained or moderately well drained.

Whenever a detailed soil survey report is available, the grouping of the soil series into A, +B, B, +C, C, +D, or D is straightforward. In addition to the soil report, a soil catena diagram is required in order to have the drainage class, the depth-phase of the soil, and its parent material. But, in the absence of the soil catena diagrams, the drainage, the depth, the texture, and the underlying condition of the soil can be obtained from the soil report under the ''description of the soils.''

In case a soil survey report is not available, hydrologic soil groups at a lower resolution level may be delineated from air photo analysis. In preparation for use with the RPR table, the following map symbols are tentatively proposed for mapping units (Weeden, 1962):

a. Landform:
   Symbols shown in Table A-12 are recommended for landform description. The letter symbols were prepared by Lueder and modified by Weeden (1962).

b. Drainage:

Well-drained	e
Somewhat poorly-drained to moderately well-drained	m
Poorly to very poorly-drained	p

Table A-10. Typical catena diagrams for part of Pennsylvania.

Chief parent material	Well drained: Shallow (< 18")	Well drained: Moderately deep (18"-36")	Well drained: Deep (>36")	Moderately well drained	Somewhat poorly drained	Poorly drained	Very poorly drained
Chiefly ridge and valley							
56. Gray, brown acid sandstone, conglomerate and some shale	Ramsey	(----Dekalb*		Cookport----)		(----Nolo	Lickdale, Brinkerton, very wet
57. Gray acid coarse sandstone, conglomerate and quartzite		Leetonia					
58. Red acid sandstone with some red and gray shale		(----Lehew	Ungers	Amaranth----)			
59. Red acid siltstone, shale and some sandstone	Klinesville	----) Calvin, Calvin, neutral substratum	Ungers	Amaranth----)			
60. Gray brown acid shale, siltstone & some sandstone	Berks, ridges Weikert	----)	Lashley	Blairton-----)		(----Holton	
61. Red acid clay shale			(----Minora				
62. Gray yellow acid deep coarse sands over limestone or dolomite			Sandy Barrens Land				

* Soil Series

Table A-11. Runoff potential rating table using the soil catena diagram.

Soil Texture	I	II	III	IV	V	VI	VII
	well drained			moderately well drained	somewhat poorly drained	poorly drained	very poorly drained
	deep (>36")	moderately deep (18"-36")	shallow <18"				
1. Coarse-textured soil on vertically fractured rock.	A	+B	B	B	+C	+D	D
2. Coarse-texture	A**-(+B) (B)*	B	+C-(+D)**	B	+C	+D	D
3. Medium-textured soil on vertically fractured rock.	+B	B	+C	+C	C	+D	D
4. Medium texture or mixture of coarse to fine texture.	+B**-(B)	+C	C-(+D)***	+C	C	+D	D
5. Fine texture	B**-(+C)	C	C-(D)***	C	C	D	D

Revised rating for well-drained soils:

* if fragipans or clay pans exist in deep soil
** if the soil is deeper than 10 ft. and excessively well drained
*** if the soil is less than 9 in. deep.

After Chiang (1971).

Table A-12. Letter symbols for landforms.

		Residual soils			
Sedimentary	S	Igneous	I	Metamorphic	MM
Argillite	Sa	Granite	Ig	Gneiss	MMg
Shale	Sh	Gabbro	Ia	Schist	MMs
Sandstone	Ss	Diorite	Id	Slate	MMl
Limestone	Sl	Basalt	Ib	Quartzite	MMq
Conglomerate	Sc	Diabase	Is		
Interbedded	Ssh	Lava	Il		
Sandstone and Shale	etc.		etc.		

		Nonresidual Soils			
Alluvial	A	Glacial	G	Colluvial	C
Recent	AR	Ground Moraine	GM		
Old	AO	Terminal or	GMM	Windblown	W
Undifferentiated	A	Marginal Moraine			
		Outwash Plain	GO	Dunes	WD
Fan	AF	Lake Bed	GL	Loess	WL
Delta	AD	Drumlin	GD		
Undifferentiated	AM	Esker	GE		
mantle		Kame	GK	Marine	M
		Kame Group	GKG		
		Kame Terrace	GKT	Beach	MB
		Stratified Drift	GS	(not windblown)	
				Tidal Marsh	MTM
				Unsorted Drift	GU

Terrace T

Swamp Z Fill F

c. Depth to bedrock:

0-3'	Shallow-medium	1
3-10'	Deep	2
> 10'	Very deep	3

d. Slope:

0-4%	Flat	f
4-16%	Gently sloping	g
16-40%	Steep	s
> 40%	Very steep	v

The combination of a, b, c, and d specifies the RPR of the soil. Landform represents the parent material and hence the texture of the soil. Drainage class and depth to bedrock indicate the position of the soil within a soil catena diagram. The slope helps recognize the local landform.

The following examples illustrate the meaning of the symbols describing separate mapping units in terms of landform, drainage, soil depth, and slope: GO-e-3-f means glacial outwash, (coarse texture), well-drained, very deep, and flat. According to Table A-11, this soil unit should have an RPR of either A or +B. As another example, Ssh-m-2-g indicates the soil derived from interbedded sandstone and shale, (medium texture), moderately well to somewhat poorly-drained, deep, and gently sloping. This soil unit should be given an RPR of C or +C.

As can be seen from these examples, the RPR obtained from air photo analysis cannot be as accurate as that from a detailed soil survey report. Detailed explanation and additional references may be found in Weeden (1962).

Summary and conclusions

The different soil classification systems under review can be divided into two main groups:

a. Pedological grouping: This includes pedological system, engineering unified soil classification system, AASHO system, comprehensive pedological system, and European and forest soils classification.

b. Hydrological grouping: This includes land capability classification system, classification based on land system, classification based on texture of surface soils, classification based on topographic grouping of soils, classification based on soil associations, Soil Conservation Service of USDA classification, and classification based on catena concept.

For runoff study in the interstate highway system, a detailed soil survey such as used in the pedological grouping is unnecessary. A soil

classification system which refines the Soil Conservation Service (SCS) system under hydrological grouping is recommended. It appears that a system which divides soils into groups according to their final infiltration rates and takes into consideration other soil properties that affect the infiltration capacity of soil under rainstorms meets the needed requirements for practical purposes. The soil classification system followed by the SCS soil scientists and refined by Chiang (RPR System) is thus adequate for runoff study because:

a. Soils in the USA have already been classified by the SCS personnel into the four groups A, B, C, and D. Details about the classification and its use with soil-cover complex are available in the SCS National Engineering Handbook, Section 4, Hydrology.

b. If refinement on the SCS four groups is needed, the classification based on the catena concept is straightforward and usually available from landform maps, air photo maps, or soil survey maps.

c. The minimum infiltration rates by which the soil groups are classified could be used to estimate runoff from major events, such as maximum annual floods, provided that the precipitation was of long duration and that the soils were fully wet.

d. Field operations of soil classification on a national scale, such as that of the SCS and Highway Department, require the use of soil parameters that are universally applicable and for which values are either currently available, easily obtainable by simple and rapid techniques, or can be estimated from such known soil properties as soil texture, depth, drainage, soil moisture at the surface, and slope.

References

American Association of State Highway Officals. 1961. Standard Specifications for Highway Materials and Methods of Sampling and Testing, Part I, Specifications, 401 pp., Washington, D.C.

American Society of Civil Engineers. 1949. Hydrology Handbook, 184 pp., New York, N.Y.

Baldwin, M., C. E. Kellogg, and J. Thorp. 1938. Soil classification in soils and men, Handbook of Agriculture, USDA.

Chiang, S. L. 1971. A runoff potential rating table for soils, J. Hydrol. 13:54-62.

Chiang, S. L., and G. W. Petersen. 1970. Soil catena concept for hydrologic interpretations. J. Soil and Water Conserv. 25(6):225-227.

Earth Manual. 1960. U.S. Department of the Interior, Bureau of Reclamation.

England, C. B. 1970. Land capability: a hydrologic response unit in agricultural watersheds, USDA-ARS 41-172.

England, C. B., and H. N. Holtan. 1969. Geomorphic grouping of soils in watershed engineering, J. Hydrol. 7:217-225.

England, C. B., and C. A. Onstad. 1968. Isolation and characterization of hydrologic response units within agricultural watersheds, Water Resources Res., 4(1):73-77.

Franz, H. 1960. Feldbodenkunke, Verlag Georg. Fromme and Co., Vienna and Munich, (reviewed in Soil Sci. Soc. Am. Proc., August 1961).

Gibbons, F. R. 1961. Some misconceptions about what soil survey can do, J. Soil Sci. 12:96-100.

Kirkham, D. C. 1964. Soil physics, Handbook of Applied Hydrology, (ed. by V. T. Chow), McGraw-Hill Book Co., New York, N.Y.

Klingebiel, A. A., and P. H. Montgomery. 1961. Land capability classification, USDA-SCS Agriculture Handbook No. 210.

Macvicar, C. N. 1969. A basis for the classification of soil, J. Soil Sci. 20:141-152.

Miller, H. W., and J. B. Cary. 1966. Soil associations and Susquehanna River Basin hydrology, J. Soil and Water Conserv. 21:18-20.

Musgrave, G. W. 1955. How much of the rain enters the soil? USDA Yearbook 1955:151-159.

Soil Conservation Service. 1964. National Engineering Handbook, Part IV, Hydrology, USDA.

Soil Conservation Service. 1972. Soil survey of Utah County, Utah, Central Part. USDA.

Thorp, J., and G. D. Smith. 1949. Higher categories of soil classification: Order, Suborder and Great Soil Groups, Soil Sci., 67:117-126.

Turner, A. K. 1963. Infiltration, runoff and soil classifications, J. Hydrol. 1:129-143.

Weeden, H. A. 1962. Soil mapping for highway engineers, Eng. Res. Bull. B-82, The Pennsylvania State University, University Park, Pa.

Wilde, S. A. 1958. Forest Soils, The Ronald Press Co., New York, N.Y.

United States Department of Defense. 1968. Unified soil classification system for roads, airfields, embankments, and foundations, MIL-STD-619B, 30 pp.

Appendix B

Master Horizons and Layers of Mineral Soils

Mineral soils are composed of three organic horizons and 14 mineral horizons and layers.

Organic horizons

Horizon	Description
O	Organic horizons consisting of those: (1) formed or forming in the upper part of mineral soils above the mineral part; (2) dominated by fresh or partly decomposed organic material; and (3) containing more than 30 percent organic matter if the mineral fraction is more than 50 percent clay, or more than 20 percent organic matter if the mineral fraction has no clay. Intermediate clay content requires proportional organic matter content.
O1	Organic horizons in which essentially the original form of most vegetative matter is visible to the naked eye.
O2	Organic horizons in which the original form of most plant or animal matter cannot be recognized with the naked eye.

Mineral horizons and layers

Horizon	Description
A	Mineral horizons consisting of: (1) horizons of organic-matter accumulation formed or forming at or adjacent to the surface; (2) horizons that have lost clay, iron, or aluminum with resultant concentration of quartz or other resistant minerals of sand or silt size; or (3) horizons dominated by 1 or 2 above but transitional to an underlying B or C.
A1	Mineral horizons, formed or forming at or adjacent to the surface, in which the feature emphasized is an accumulation of humified organic matter intimately associated with the mineral fraction.
A2	Mineral horizons in which the feature emphasized is loss of clay, iron, or aluminum, with resultant concentration of quartz or other resistant minerals in sand and silt sizes.

A3 A transitional horizon between A and B, and dominated by properties characteristic of an overlying A1 or A2 but having some subordinate properties of an underlying B.

AB A horizon transitional between A and B, having an upper part dominated by properties of A and a lower part dominated by properties of B, and the two parts cannot conveniently be separated into A3 and B1.

A&B Horizons that would qualify for A2 except for included parts constituting less than 50 percent of the volume that would qualify as B.

AC A horizon transitional between A and C, having subordinate properties of both A and C, but not dominated by properties characteristic of either A or C.

B Horizon in which the dominant feature or features is one or more of the following: (1) an illuvial concentration of silicate clay, iron, aluminum, or humas, alone or in combination; (2) a residual concentration of sesquioxides of silicate clays, alone or mixed, that has formed by means other than solution and removal of carbonates or more soluble salts; (3) coating of sesquioxides adequate to give conspicuously darker, stronger, or redder colors than overlying and underlying horizons in the same sequum but without apparent illuviation of iron and not genetically related to B horizons that meet requirements of 1 or 2 in the same sequum; or (4) an alteration of material from its original condition of sequums lacking conditions defined in 1, 2, and 3 that obliterates original rock structure, that forms silicate clays, liberates oxides, or both, and that forms granulas, blocky, or prismatic structure of textures are such that volume changes accompany changes in moisture.

B1 A transitional horizon between B and A1 or between B and A2 in which the horizon is dominated by properties of an underlying B2 but has some subordinate properties of an overlying A1 or A2.

B&A Any horizon qualifying as B in more than 50 percent of its volume including parts that qualify as A2.

B2 That part of the B horizon where the properties on which the B is based are without clearly expressed subordinate characteristics indicating that the horizon is transitional to an adjacent overlying A or an adjacent underlying C or R.

B3 A transitional horizon between B and C or R in which the properties diagnostic of an overlying B2 are clearly expressed but are associated with clearly expressed properties characteristic of C or R.

C A mineral horizon or layer, excluding bedrock, that is either like or unlike the material from which the solum is presumed to have formed, relatively little affected by pedogenic processes, and lacking properties diagnostic of A or B but including materials modified by: (1) weathering outside the zone of major biological activity; (2) reversible cementation, development of brittleness, development of high bulk density, and other properties characteristic of fragipans; (3) gleying; (4) accumulation of calcium or magnesium carbonate or more soluble salts; (5) cementation by such accumulations as calcium or magnesium carbonate or more soluble salts; or (6) cementation by alkali-soluble siliceous material or by iron and silica.

R Underlying consolidated bedrock, such as granite, sandstone, or limestone. If presumed to be like the parent rock from which the adjacent overlying layer or horizon was formed, the symbol R is used alone. If presumed to be unlike the overlying material, the R is preceded by a Roman numeral denoting lithologic discontinuity as explained under the heading.

GPO 910-459

B121
11